2019-05-14

Investigating the Mechanism of Adherent-Invasive E. coli Induced Mitochondrial Fission in the Intestinal Epithelium

Mancini, Nicole

UNIVERSITY OF CALGARY

Investigating the Mechanism of Adherent-Invasive *E. coli* Induced Mitochondrial Fission in the Intestinal Epithelium

by

Nicole Mancini

A THESIS

SUBMITTED TO THE FACULTY OF GRADUATE STUDIES

IN PARTIAL FULFILMENT OF THE REQUIREMENTS FOR THE

DEGREE OF DOCTOR OF PHILOSOPHY

GRADUATE PROGRAM IN GASTROINTESTINAL SCIENCES

CALGARY, ALBERTA

MAY, 2019

Abstract

Mitochondrial dynamics, a field which encompasses the processes of mitochondrial fusion and fission, was first described in 1914 by Lewis & Lewis [1]. Since this original anecdotal depiction in chick embryos of mitochondria which formed extensive networks that dynamically and rapidly remodeled, the field has exploded to include reports of imbalanced mitochondrial dynamics in disease of almost any tissue in the body. Although many papers seek to understand the role of mitochondrial dynamics in inflammatory disease, the role for these processes in inflammatory bowel disease (IBD) has never been studied. My thesis seeks to provide preliminary data investigating this major gap in research of the role of mitochondrial dynamics in the gastrointestinal tract.

Furthermore, recent studies have shown that imbalances in mitochondrial dynamics are common features of intracellular infection with a diverse array of microbial agents. As the etiology of IBD is heavily influenced by microbes in the gastrointestinal tract, my thesis studied the Crohn's disease-associated pathobiont adherent-invasive *Escherichia coli* (AIEC), demonstrating the link between mitochondrial dynamics, host-microbe interactions, and potentially, IBD. Specifically, my thesis addressed the hypotheses that (1) AIEC drive mitochondrial fission in intestinal epithelial cells, and (2) AIEC-induced mitochondrial fission impacts intestinal epithelial function (e.g. cell viability, or barrier function).

Infection by AIEC in intestinal epithelial cell lines induced massive mitochondrial fragmentation, which was associated with mitochondrial dysfunction.

The mechanism of AIEC-induced mitochondrial fragmentation involved invasion of bacteria, and the host fission protein Drp1 (dynamin-related protein 1). Downstream of mitochondrial fission, apoptosis, loss of barrier function, and transcription of interleukin-8 occurred. Treatment with the Drp1 inhibitor Mdivi1 blocked the loss of barrier function that occurred in association with AIEC infection. This mechanistic work has laid the foundation to explore the role of AIEC-induced mitochondrial fission in the function of the gastrointestinal epithelium.

Preliminary data showed an imbalance in mitochondrial dynamics mediators by mRNA and protein expression in IBD patients and in murine models of colitis, demonstrating a link between mitochondrial dynamics and IBD for the first time, setting the stage for future studies thoroughly investigating the role for mitochondrial fission and fusion in the etiology of IBD.

Acknowledgements

To my supervisor Dr. Derek McKay, thank-you for the incredible opportunity to study in your lab. Based on my experience in your lab, I always give the following advice to students deciding in which lab to pursue research in. Although your research project may seem important, the number one consideration in choosing your Masters or PhD lab should be the potential mentorship with your supervisor. Your support through my program truly transformed my PhD experience from average to extraordinary. Your unwavering faith in me kept me going daily amid endless trials and tribulations. Your open-door policy to discuss data, study design, or personal issues was an opportunity not all graduate students are afforded to, which I was extremely grateful for. Your enthusiasm for my project, and science in general, kept me from giving up when I felt that all my efforts were for nothing. Thank-you for challenging me insistently every time I presented at lab meeting, giving me the confidence to respond to questions at seminars and in my candidacy exam. Thank-you for references year after year which were probably much more kind than I deserved. Studying to achieve my PhD changed the person I am today, giving me an array of skills and experiences that I will bring to all of my future pursuits – much of the personal characteristics which I now embody are thanks to your tremendous mentorship in the past 5 years – I cannot thank you enough.

To Dr. Jane Shearer, thank-you for your encouragement and enthusiasm throughout my studies, and for always reminding me of the big picture. To Dr. Kevin Rioux, thank-you for your clinical point-of-view on my research, and for

career advice as a successful clinician-scientist. To Dr. Tim Shutt, thank-you for providing your unrivaled expertise in mitochondrial dynamics which made a huge impact on my research directions, and for making time for me to drop by your office anytime to discuss methods. To Dr. Fernando Lopes, thank-you for your passion for my project, and your patience with helping me master lab techniques and answering endless questions.

To the Gastrointestinal Research Group, Inflammation Research Network, and Snyder Institute for Chronic Diseases, thank-you for the opportunity to be a part of a wonderful community where I met many mentors, colleagues, and friends.

To the past and present members of the McKay lab, thank-you for your advice on my project, your help with techniques, and most importantly, the unforgettable memories and laughs made inside the laboratory and out.

Thank-you to my friends who have supported me since year 1, providing me with a distraction from my studies when I needed it, and for always being proud of the path I was on. Thank-you to my brother Jason, and Sheena, for showing interest in my experiments at every stage, and even listening to a few presentations as I practiced to give seminars. Thank-you to my mom; without you I would have quit several times over in my first 2 years. You brought me back to see the end goal every time I lost all hope, and gave me the strength to push through the most difficult moments. Thank-you to my dad who worked a lifetime to provide me with opportunities to pursue any future I could dream of, showing by example a truly

extraordinary work ethic. Thank-you to Gill and Hubble who lifted me up with toothy grins and wagging tails every day when I came home from the lab.

Thank-you to Chris – my partner, and my rock. Your faith in me to achieve great things truly drove me to be better on a daily basis. You pushed me to take on new challenges on days when it was tough to step foot in the lab. You gave me perspective when I needed a much overdue break. Without your support through the more difficult times during my studies, I would not have achieved this tremendous feat. I am so proud to have you standing by my side as I finish my PhD and move to the next stage in my career.

Last but not least, thank-you to all the funding sources that made this work possible: the NSERC and CIHR agencies, the University of Calgary Eyes High program, and the Killam foundation.

Table of Contents

Chapter 3 Results

List of Tables

List of Figures

List of Abbreviations

AIEC	Adherent-Invasive *Escherichia coli*
AIF	Apoptosis-Inducing Factor
AMPK	AMP-Activated Protein Kinase
Arp2/3	Actin-Related Protein 2/3
ATG16L1	Autophagy Related Protein 16-1
ATP	Adenosine Triphosphate
AURKA	Aurora-A Kinase
BAK	Bcl-2 Homologous Antagonist Killer
BAX	Bcl-2 Associated X
CamK	Calcium-Calmodulin-Dependent Kinase
CCCP	Carbonyl Cyanide m-Cholorophenyl Hydrazone
CD	Crohn's Disease
CDK	Cyclin-Dependent Kinase
CEACAM6	Carcinoembryonic Antigen Related Cell Adhesion Molecule 6
DAMPs	Damage-Associated Molecular Patterns
DNP	2,4-dinitrophenol
Drp1	Dynamin-Related Protein 1
DSS	Dextran Sodium Sulfate
ER	Endoplasmic Reticulum
Erk2	Extracellular-Signal Regulated Kinase
$FADH_2$	Flavin Adenine Dinucleotide
Fis1	Mitochondrial Fission 1
GI	Gastrointestinal
GTP	Guanosine Triphosphate
HRP	Horseradish Peroxidase
IL	Interleukin
IBD	Inflammatory Bowel Disease
IMM	Inner Mitochondrial Membrane
INF	Inverted Formin-2
LPF	Long Polar Fimbriae
LPS	Lipopolysaccharide
MCU	Mitochondrial Calcium Uniporter
MEF	Mouse Embryonic Fibroblast
MFF	Mitochondrial Fission Factor
MFN1	Mitofusin 1
MFN2	Mitofusin 2
MiD49/51	Mitochondrial Dynamics Proteins 49/51
MOI	Multiplicity of Infection
MPP	Mitochondrial Processing Peptidase
NADH	Nicotinamide Adenine Dinucleotide
NSAIDS	Nonsteroidal Anti-Inflammatory Drugs

NOD2	Nucleotide-Binding Oligomerization Domain-Containing Protein 2
OMA-1	Overlapping With The M-AAA Protease 1 Homolog
OMV	Outer Membrane Vesicle
OPA1	Optic Atrophy Factor 1
PAMPs	Pathogen-Associated Molecular Patterns
PINK1	Parkin/PTEN-Induced Kinase 1
PKA	Protein Kinase A
ROS	Reactive Oxygen Species
SUMO	Small Ubiquitin-like Modifier
TCA	Tricarboxylic Acid Cycle
TER	Trans-Epithelial Resistance
TJ	Tight Junctions
TNBS	2,4,6,-trinitrobenzenesulfonic Acid
TNF	Tumor Necrosis Factor
TOM	Translocase of the Mitochondrial Outer Membrane
UC	Ulcerative Colitis
VDAC	Voltage Dependent Anion Channel
YME1L	Yeast Mitochondrial Escape Protein 1
ZO-1	Zona Occludens-1

Chapter 1: Introduction

1.1 Gastrointestinal Epithelial Cell Function

Within the gastrointestinal tract (GI), the small intestine and large intestine carry out the main functions of nutrient and electrolyte absorption, fluid balance, and waste storage [2]. These organs are composed of a mucosa and submucosa; the mucosa is made up of a single layer of epithelium resting upon the lamina propria for structural and immune support, and the muscularis mucosae [2,3]. The submucosa contains the main muscle layers mediating intestinal motility, nerves, and blood vessels [3]. The intestinal epithelium is made up of goblet cells, enteroendocrine cells, tuft cells, Paneth cells (found in the small intestine), and the nutrient-absorptive epithelial cells which form crypts and villi in the small intestine, and crypts without villi in the large intestine [2–4]. Stem cells are located at the base of crypts and function to replenish the epithelium [2]. Goblet cells function to produce mucus which protects the underlying epithelium from physical damage and immunological threats [4]. Enteroendocrine and tuft cells secrete factors that have various digestive and immune functions such as histamine, somatostatin, gastrin, serotonin, and IL-25 [2,5,6]. Paneth cells secrete antimicrobial peptides, limiting access of commensal or pathogenic bacteria to the mucosa [4]. Absorptive epithelial cells absorb nutrients derived from lipids, carbohydrates, and proteins, as well as vitamins, water, and bile salts [2,3].

As the first line of defense in the gastrointestinal tract separating internal structures from the external environment, epithelial cells interact extensively with

the great amounts of bacteria present in the gastrointestinal lumen. M cells, located within Peyer's patches in the small intestine, allow sampling of luminal antigens by adaptive immune cells, and allow entry of some bacteria into the mucosa [2,7,8]. Intestinal epithelial cells express toll-like receptors intracellularly and at their basolateral surface, transducing signals after interacting with damage-associated molecular patterns (DAMPs) or pathogen-associated molecular patterns (PAMPs). This interaction leads to various inflammatory responses [2,4]. Enterocytes also secrete IgA into the gastrointestinal lumen which coats luminal material, excluding it from internalization by the epithelium [2,3]. While invading pathogens are a threat to the host and therefore interact extensively with the host immune defenses, commensal bacteria take part in interactions with host cells that are beneficial to normal gastrointestinal function. Commensal bacteria thrive in a specific niche within the gastrointestinal environment, excluding potential pathogens from colonization [9]. Education of the mucosal immune system relies on the presence of commensal bacteria [4]. Commensal bacteria synthesize short chain fatty acids, a main energy source for epithelial cells, from dietary fiber that is otherwise indigestible [10]. The dysregulation of interactions between bacteria and the host, pathogenic or commensal, is a transformative research avenue in all tissues of the body.

1.2 Inflammatory Bowel Disease

Inflammatory Bowel Disease (IBD) is a life-altering chronic condition characterized by bowel symptoms such as diarrhea, abdominal pain, and bloating, and affects a significant portion of the western world including Canada [11]. Affecting 270,000 Canadians in 2018, IBD encompasses both ulcerative colitis (UC) and Crohn's disease (CD) (Crohn's Colitis Canada). This disease not only impacts daily quality of life of affected individuals due to gastrointestinal symptoms, but impacts patient and caregiver mental health, for example, by increasing levels of anxiety and stress [12,13]. Many factors that lead to altered GI tissue function contribute to the development of IBD, such as reduced barrier function of intestinal epithelial cells [14–16], dysregulated immune reactions [17], disruptions in autophagy of epithelial and immune cells [18], disruptions in endoplasmic reticulum (ER) stress pathways [19], and changes to the complex community of commensal bacteria present in the GI tract [20]. Many of these potential causes interact in some way, and are influenced by both genetic and environmental factors.

1.2.a Role of Bacteria in Inflammatory Bowel Disease

Alterations to the composition of the gut microbiota are linked to the development of IBD, specifically CD. Increased total numbers of bacteria have been shown to colonize the mucosal layer of the GI tract of patients with IBD compared to control subjects where bacteria primarily remain in the lumen [21]. The composition of microbial communities differ when comparing control to CD and UC

samples as a whole [22,23]. The microbial ecosystem of patients with CD is less diverse with fewer members of the Firmicutes phylum present compared to control subjects [24]. More specifically, Frank *et al.* [25] demonstrated that at the phylum level, Firmicutes and Bacteroidetes are depleted in UC and CD, whereas Proteobacteria are increased. Clinically, this altered microbial composition was associated with abscess development [25]. Within Firmicutes, the bacterium *Faecalibacterium prausnitzii* is reduced in abundance in patients with IBD compared to control [26,27].

Metabolites that are both essential for gastrointestinal cell function, and known to be metabolized directly by luminal bacteria (e.g. butyrate, the main energy source of epithelial cells) are reduced in the fecal material of CD and UC patients compared to controls [28]. These apparent abnormalities in the microbial metabolome could contribute to functional changes seen in the GI tract during disease such as reduced barrier function and immune dysregulation.

Considering the adaptive immunological response to the altered bacterial composition, there is increased proliferation of intestinal T cells isolated from areas of active disease compared to uninvolved areas in response to exposure to microbial antigens *in vitro* [11]. In a CD patient cohort, Mow *et al.* [29] demonstrated that patients with humoral immune responses to bacterial antigens were more likely to develop disease complications such as fibrostenosis, perforation, or the requirement for surgery. Prominent gene susceptibilities to CD result from mutations in NOD2 (nucleotide-binding oligomerization domain-containing protein 2) [30,31] and ATG16L1 (autophagy related protein 16-1) [32]. The NOD2 and ATG16L1 proteins mediate

control of invading intracellular bacteria, highlighting the role of the innate immune system in responding to dysregulation of host interactions with bacteria in CD. Due to the apparent role of bacteria in the pathogenesis of IBD, antibiotics have been suggested as viable therapeutics to control disease or maintain remission, but well-designed clinical studies have not been performed to back up these ideas [33].

Patients with ileal, ileal-colonic, or colonic CD have been shown to harbor an increased proportion of *Escherichia coli* strains in the ileal and colonic mucosa compared to other constituents of the microbiota [26,27,34–36]. Nazareth *et al.* [37] showed that 63% of patients in a cohort of CD with 142 individuals had increased levels of *E. coli* in the blood compared to no detectable *E. coli* in the blood in controls (disease location was not used to stratify patients). In a cohort of 96 patients, individuals experiencing active disease had a higher abundance of *E. coli* within their intestinal mucosa compared to inactive disease [27].

Dysregulation of the composition or activity of the microbiota may be associated with flares of inflammation in IBD patients, as with adherent-invasive *Escherichia coli* (AIEC), which is known to frequently colonize patients with CD [38]. AIEC represent a distinct type of pathogenic *E. coli*, differing genetically from organisms such as enterohemorrhagic *E. coli* [39,40]. Adherent-invasive *E. coli* is considered a pathobiont organism (an organism that is normally benign but gains characteristics that are harmful to health due to environmental stimuli), as subjects unaffected by intestinal disease have been shown to harbor AIEC [41–44]. AIEC may

take advantage of genetically susceptible hosts, as suggested by studies showing that ATG16L1 and NOD2 are important factors for clearing intracellular AIEC [45–47].

E. coli strain LF82 is the prototypical AIEC strain that was initially isolated from the ileal lesion of a CD patient [39], and many different AIEC strains with similar characteristics have since been isolated from both the ileum and colon of patients with CD and the colon of patients with UC [40,43,44,48–52]. Although there is a body of literature describing AIEC as a distinct group of *E. coli*, it is noteworthy that no consistent description by specific genes or virulence factors has been defined for AIEC, calling into question the impact of studies that seek to identify and characterize AIEC strains. Phenotypic criteria defining AIEC between studies also varies, but generally includes greater adhesion and invasion to human gastrointestinal epithelial cell lines compared to other *E. coli* isolates (from IBD or control tissues), or compared to reference non-invasive *E. coli* strains [34,38,42,50,52].

1.3 Role of Adherent-Invasive *Escherichia coli* in Inflammatory Bowel Disease

Although no known IBD-causing bacterium has been identified, AIEC have been studied as a factor that may contribute to the development or propagation of IBD [53] (Fig.1). Genetically, AIEC strains LF82, NRG857c, and other IBD isolates of the B2 phylogenetic group resemble uropathogenic and avian-pathogenic *E. coli* [54,55].

To date, no robust genetic defining feature has been identified to distinguish AIEC from commensal *E. coli* isolated from IBD patients that do not adhere and

invade epithelial cells. Some research has suggested that the FimH gene, encoding the pilus adhesin, is different between these two sub-groups of *E. coli* [56], explaining the ability of AIEC to invade, but this result is contested [57].

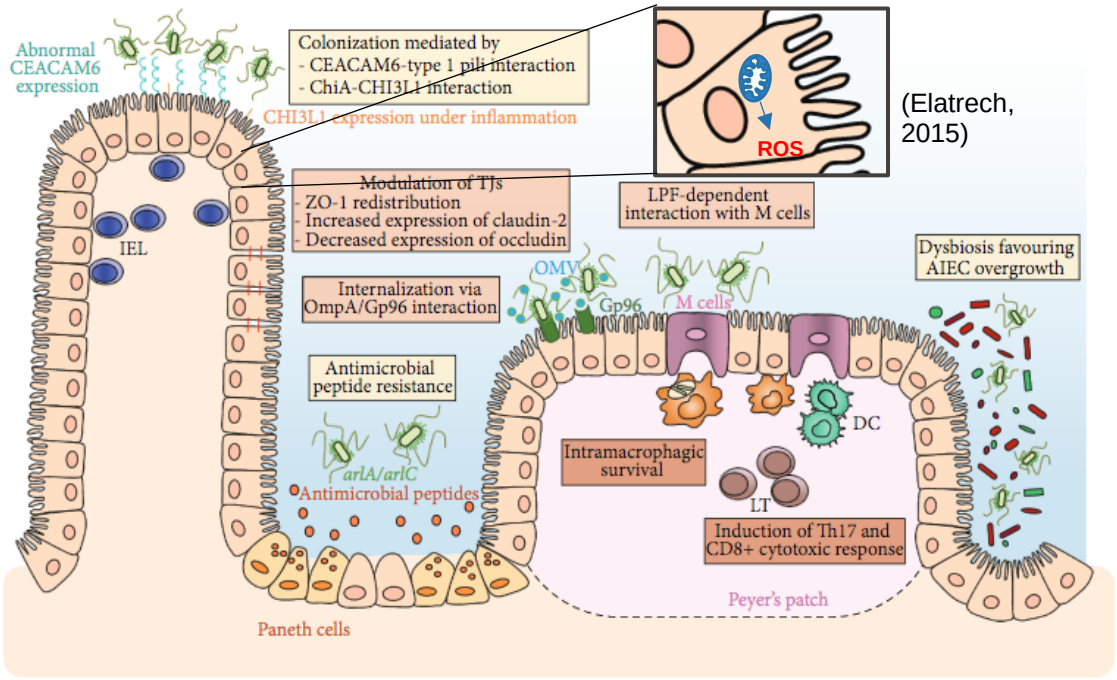

Figure 1. Strategies used by AIEC to trigger intestinal inflammation. (1) AIEC are able to strongly adhere to intestinal epithelial cells and colonize gut mucosa using type 1 pili that can bind to mannose residues of CEACAM6, which is overexpressed on the apical surface of ileal epithelial cells in patients with ileal CD. AIEC are also able to adhere to chitinase 3-like-1 receptor (CHI3L1) *via* the chitin-binding domain of ChiA bacterial protein. AIEC actively resists antimicrobial peptides secreted by Paneth cells. This mechanism involves two genes, *arlA*, which enodes a Mig-14 family protein implicated in defensin resistance, and *arlC*, an OmpT family outer membrane protease. (2) AIEC translocation through the epithelial barrier is increased following different mechanisms leading to exacerbation of intestinal inflammation. Modulation of tight junctions (TJs) by AIEC induces paracellular barrier permeability involving ZO-1 redistribution, increased expression of pore-forming claudin-2, and decreased expression of occludin. The endoplasmic reticulum (ER) stress response glycoprotein Gp96 is overexpressed at the apical membrane of ileal epithelial cells in CD patients and acts as a host-receptor for AIEC outer membrane vesicles (OMV) carrying OmpA protein promoting the invasion of the intestinal mucosa. AIEC bacteria interact with Peyer's patches and translocate across M cells *via* long polar fimbriae (LPF) expression to access lymphoid cells. (3) AIEC intramacrophagic replication is favored in the submucosal compartment of host cells. AIEC intramacrophagic survival could be due to host autophagy defects leading to increased bacterial replication and also enhancing inflammatory responses. AIEC can also induce Th17 and CD8+ cytotoxic responses. Elatrech *et al.* showed that AIEC infection is associated with increased Reactive Oxygen Species (ROS) production[91]. Figure adapted from [53].

AIEC features several different adhesin molecules such as type 1 pili [58], long polar fimbriae [59], and flagella [60] (Table. 1). Highlighting the characterization of AIEC as a pathobiont, environmental factors of the host impact AIEC invasion and effect on the host. Host immunological factors such as the presence of TNFα (which induces enterocyte CEACAM6 (Carcinoembryonic Antigen Related Cell Adhesion Molecule 6) expression [38]) promotes AIEC invasion through type I pilus interaction with intestinal epithelial cells [38]. Increasing bile acid availability (which occurs associated with microbial dysbiosis in IBD patients [26]) in an explant of murine Peyers patches increased association of *E. coli* LF82 with the epithelium and translocation of LF82 through M cells dependent on long polar fimbriae [61]. In the CEABAC10 transgenic model (mice that express the human CEACAM6 molecule in the epithelium [62]), Martinez-Medina [63] showed that bacterial load, tissue damage, and cytokine production (Table 2) during LF82 infection were exacerbated by a western diet. Small *et al.* [64] demonstrated that once AIEC had colonized the gastrointestinal tract, the host was more susceptible to disease induced by *Salmonella* typhimurium or *Citrobacter rodentium*, highlighting the role of environmental factors in the impact of AIEC on host disease. Use of IBD therapeutics such as the TNFα binding antibody infliximab reduces epithelial invasion of AIEC [65].

In vitro, AIEC has been shown to increase permeability through loss of transepithelial resistance in intestinal epithelial cells [48,52,66,67], suggesting that if

AIEC gain access to the epithelium, AIEC and other bacteria can reach immune cells that reside in the mucosa.

Table 1. Adherent-Invasive *E. coli* Virulence Factors				
Bacterial Factor	Role in Infection	Strain	Cell Type/Model	Ref
Adhesion & Invasion				
Type I pilli	Adhesion to CEACAM6 on intestinal epithelial cells.	LF82	HEp-2 (human laryngeal carcinoma), Intestine-407 (human small intestine epithelial)	58
Long polar fimbraie	Adhesion to M cells in Peyer's Patches. Host molecule not identified.	LF82	Murine small intestinal peyer's patches ex vivo & in vivo. Human small intestinal peyer's patches ex vivo. M like cells in vitro (Caco-2-cl1 and Raji B cell coculture)	59
Flagella	Invasion into intestinal epithelial cells, motility. Necessary to induce disease (weight loss, macroscopic disease activity).	LF82	HEp-2, Intestine-407, Caco-2 (human colorectal epithelial). Murine BALBc/J DSS colitis.	60,68
ChiA	Adhesion to CHI3L1 on intestinal epithelial cells. Necessary to induced disease (weight loss, macroscopic disease activity, histological damage, pro-inflammatory cytokine production, inflammatory infiltrate).	LF82	SW480 (human colonic epithelial), Caco-2, HEK293 (human kidney), HT29 (human colonic epithelial), T84 (human colonic epithelial). Murine C57Bl/6 DSS colitis.	69,70
OmpA (outer membrane vesicle)	Secreted from AIEC promoting invasion through Gp96 on intestinal epithelial cells.	LF82	Intestine-407, Caco-2	71,72
Nlpl lipoprotein	Adhesion and invasion inside intestinal epithelial cells and macrophages through unknown mechanism.	LF82	Intestine-407, J774-A1 (murine macrophage-like cell line)	60
Gene Regulation				

OmpC & OmpR	Promote adhesion and invasion of AIEC to intestinal epithelial cells through regulation of SigmaE.	LF82	Intestine-407, T84	[71,73]
SigmaE Factor	Promote adhesion and invasion of AIEC to intestinal epithelial cells through regulation of unknown factors.	LF82	Intestine-407, T84	[73]
Nlpl lipoprotein	Regulates type I pili and flagella expression through unknown mechanism. Does not impact type I pili biogenesis in membrane.	LF82	Intestine-407, J774-A1	[60]
FlhD, FliA, Yhjh	Regulatory pathway impacting adhesion and invasion through flagella and type I pilli synthesis and other unknown factors.	LF82	Intestine-407	[74]
QseC	Quorum sensing factor regulating adhesin expression in response to host metabolites.	LF82	None	[75]
Persistence in Host				
HtrA	Replication and/or persistence within macrophages, possibly through resistance to conditions within phagolysosome.	LF82	J774-A1	[76]
DsbA	Replication and/or persistence within macrophages, possibly through resistance to conditions within phagolysosome. Regulates flagella and type I pilli expression.	LF82	J774-A1, Intestine-407	[77]

When AIEC invades inside macrophages they are incorporated into a phagosome, which matures into a phagolysosome, and acidification of the vesicle is necessary for bacterial replication [78]. AIEC invade phagocytic cells and replicate inside them [42,52], inducing pro-inflammatory cytokine production such as TNFα [79–81], suggesting that AIEC provoke inflammation in the mucosal surfaces to which they gain access. In fact, AIEC have been shown to induce cytokine transcription and translation in a variety of cell types (macrophages, neutrophils, dendritic cells, and epithelial cells) and *in vivo* in several different models (Table 2), supporting the idea that AIEC has the ability to induce inflammation in the host.

AIEC persist inside macrophages by inhibiting apoptosis [82,83], and upregulating stress responses through the stress sensing protein HtrA [76], and protein synthesis protein DsbA [77]. Although the cellular response of the epithelium to AIEC has been less well studied compared to macrophages, limited data suggests that AIEC strain LF82 induced cell death, defined by cell membrane disruption or caspase-3 activation, in Caco-2 intestinal epithelial cells and human colonic mucosal explants at high bacterial loads (MOI 1000, 20h) [80,84]. The mechanism of cell death induced by AIEC has not been studied in epithelial cells.

Table 2. Regulation of Host Cytokines by Adherent-Invasive *E. coli*			
Finding	**Strain**	**Cell Type/Model**	**Ref**
Increased TNFα protein secretion	LF82, NRG857c	Murine macrophage-like cell line J774, THP-1 cell line (human monocyte), Human monocyte-derived dendritic cells, human colonic mucosa explant, C57/Bl6 mice treated with antibiotics, DSS colitis model in C57/Bl6 mice treated with antibiotics, CEABAC10 mice with westernized diet, infected CD1 and C57Bl/6 mice treated with antibiotics	46,79,80,84–87
Unchanged TNFα protein secretion	LF82	DSS colitis model in C57/Bl6 mice	70
Increased TNFα mRNA content	LF82, EC10, EC15, EC23, 06362	Caco-2 (human colorectal epithelium), human mucosal explants	52
Increased IL-8 protein secretion	LF82, *E. coli* O83:H1	PLB-985 human myeloid cell line differentiated into neutrophils, T84 cell line (human colonic epithelium), Caco-2, Caco-2BBE, DSS colitis model in C57/Bl6 mice	49,69,80,81,88,89
Increased IL-8 mRNA content	LF82	PLB-985 human myeloid cell line differentiated into neutrophils, T84, Caco-2, HT29 (human colonic epithelium), human mucosal explants	47,52,81,89–93
Increased IL-1β protein secretion	LF82	Human monocyte-derived dendritic cells, DSS colitis model in C57/Bl6 mice	69,80
Increased IL-1β mRNA content	LF82	CEABAC10 transgenic mice	94
Increased IL-6 protein secretion	LF82	Human monocyte-derived dendritic cells, THP-1 cell line, DSS colitis model in C57/Bl6 mice	46,69,70,80
Increased IL-6 mRNA content	LF82	CEABAC10 transgenic mice	94
Increased IL-23 protein secretion	LF82	Human monocyte-derived dendritic cells	80
Increased IL-23 protein secretion	LF82	Human monocyte-derived dendritic cells	80
Increased IL-12p70 protein	LF82	Human monocyte-derived dendritic cells	80
Increased IL-10 protein secretion	LF82	Human monocyte-derived dendritic cells	80

Reduced IL-10 mRNA content	LF82	CEABAC10 transgenic mice	94
Increased IL-18 protein secretion	LF82	Human monocyte-derived dendritic cells	80
No change in IL-18 protein	LF82	Human colonic mucosa explant	84
Increased CCL20 protein secretion	LF82	T84, Caco-2BBe	49
Increased IFNβ mRNA content	LF82	HEK293 (human embryonic kidney cell)	69
Increased IFNβ protein secretion	LF82	HEK293 (human embryonic kidney cell)	69
Increased IFNγ protein secretion	NRG857c	infected CD1 and C57Bl/6 mice treated with antibiotics	86
Increased IL-22 protein secretion	LF82	DSS colitis model in C57/Bl6 mice	70,95
Increased IL-17 protein secretion	NRG857c	CD1, DBA/2, 129e, C3H, and C57BL/6 mice treated with antibiotics	86
Increased IL-17 mRNA content	LF82	CEABAC10 transgenic mice	94,95
Increased MCP1 protein secretion	NRG857c	CD1, DBA/2, C3H, and C57BL/6 mice treated with antibiotics	86

After invasion of LF82 occurs in a host, nucleotide-binding oligomerization domain-containing protein 2, or NOD2, is necessary in epithelial cells to mount an immune response against LF82 [59,85]. AIEC inside epithelial cells and phagocytic cells are cleared by autophagy, a process that is known to be disrupted in some genetically susceptible hosts (e.g. individuals with a mutation in the ATG16L1 gene), highlighting the importance of both genetic and environmental factors that contribute to the development of CD [46,47,81,96,97].

AIEC have the ability to form biofilms *in vitro*, potentially acting as a strategy allowing AIEC to establish a persistent infection *in vivo* [41,98,99]. Some strains have increased resistance against host antimicrobial peptides, which could be a mechanism through which AIEC persist in the host intestine compared to commensal *E. coli* that cannot resist anti-microbial peptides [100].

Extensive work characterizing the interaction of AIEC with epithelial cells and phagocytic cells has been performed *in vitro*. The following studies aim to link AIEC infection with disease *in vivo*, to determine if AIEC could be a contributor to disease in humans. Several models exist for studying AIEC *in vivo*, which allow mice that do not express the epithelial CEACAM6 receptor to gain susceptibility to AIEC colonization. These models take advantage of the CEABAC10 mouse, which is a transgenic mouse expressing the human CEACAM6 receptor, or antibiotic pre-treatment of mice which increases susceptibility to infection.

Using the CEABAC10 model, AIEC was convincingly shown to induce increased permeability in the GI tract by FITC-dextran flux from the

gastrointestinal tract to the serum, and accumulation of a biotin-tracer within the mucosa from the lumen [101]. This increase in permeability was attributed to an increased expression of the tight junction protein claudin-2 shown in one representative image, but was not quantified across all animals [101]. Disease signified by weight loss, histopathology, increased permeability, blood in the stool and stool consistency was induced by AIEC infection, which was associated with pro-inflammatory cytokine production (Table 2) [94,102].

After antibiotic treatment, C57BL/6 and CD1 mice are susceptible to colonization by AIEC and penetration of AIEC within the mucosa, resulting in histopathology [86,103], and worsening the outcome of dextran sodium sulphate (DSS)-induced colitis as measured by permeability, weight loss, histology, and macroscopic disease score [85,94].

In the context of DSS colitis alone, without antibiotic treatment, AIEC drives weight loss, macroscopic disease, tissue damage and infiltration of immune cells [68–70]. Together these studies strongly show that AIEC have the ability to establish an infection *in vivo*, reducing barrier function in the GI tract, and propagating inflammation in the context of existing GI damage.

These studies set the precedent for a model of AIEC pathogenesis in Crohn's disease whereby AIEC can provoke intestinal inflammation in a host with previous damage to the gastrointestinal system. The next step in this field is to understand the genetic or environmental elements that drive AIEC to have the phenotype that

it takes on *in vitro* and *in vivo*, and determine if the presence of AIEC in patients correlates to worsening disease outcomes.

1.4 Mitochondria: Form and Function

Structurally, mitochondria are formed by an outer mitochondrial membrane (containing proteins such as the voltage dependent ion channel, VDAC [104], and the translocase of the mitochondrial outer membrane, TOM [105]) which encases an inner mitochondrial membrane (IMM) forming an intermembrane space within the organelle (Fig.2). The innermost compartment of the mitochondria is the matrix, which contains mitochondrial DNA (mtDNA), ATP, and proteins such as metabolic enzymes and heat shock proteins [106].

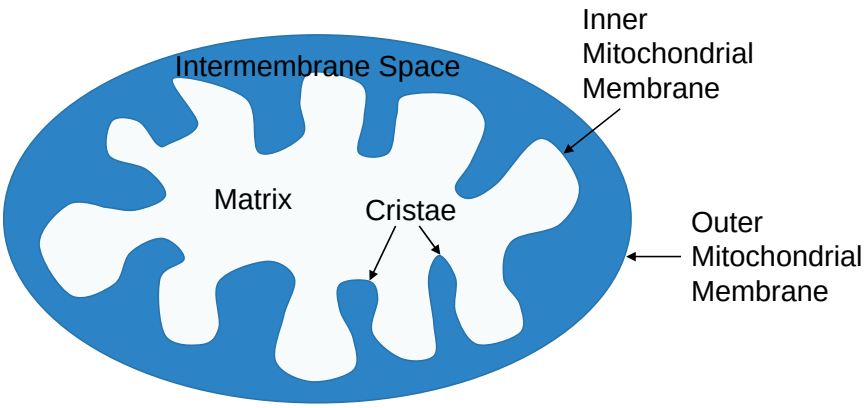

Figure 2. Structural organization of the mitochondria in schematic form.

Within the IMM is the electron transport chain formed by integral proteins and electron carriers that allow transport of hydrogen ions across the IMM, forming a membrane potential, or electrochemical gradient. This inner membrane contains regions of extensive folding referred to as cristae which are highly concentrated in enzymes involved in oxidative phosphorylation, compared to unfolded areas where these enzymes are fewer [107]. Mitochondria serve a variety of functions within the cell, the most characterized function being ATP production. The citric acid cycle, or the tricarboxylic acid (TCA) cycle, in the mitochondrial matrix functions to produce the substrates NADH and $FADH_2$ that donate electrons to fuel oxidative phosphorylation, the process through which ATP is produced. Another function includes the production of reactive oxygen species (ROS), which have been classically viewed as damaging agents to cellular proteins, lipids, and DNA, but have emerged more recently as important mediators of cell signaling pathways related to cell viability and inflammation [108,109]. Although ROS produced from oxidative phosphorylation are the main contributors to oxidative stress in the cell, ROS can also be produced through NADPH oxidase activity in phagocytic cells [110].

Mitochondrial calcium plays a role in cellular calcium buffering and signaling within the mitochondria with regards to oxidative phosphorylation and cell death [111].

1.5 The Role of Mitochondria in Apoptosis

Mitochondria play a governing role in the intrinsic pathway of apoptosis (Fig.3) [112]. This apoptotic pathway is initiated by activation of the BAX (Bcl-2 Associated X) and BAK (Bcl-2 Homologous Antagonist Killer) proteins, which together physically form the mitochondrial permeability transition pore, allowing cytochrome c from the electron transport chain housed in the IMM to be released into the cytosol [113,114]. After cytochrome c release occurs, cleavage of caspase-3 and -7 can be initiated, which act directly to fragment nuclear DNA [113]. Caspase-independent apoptosis is also possible through the mitochondrial pathway due to release of Apoptosis-Inducing Factor (AIF) through the mitochondrial transition pore, which itself travels to the nucleus, initiating DNA fragmentation [115]. Because of the role mitochondria play in metabolism and cell death, a large area of research on mitochondria presently focuses on aging and cellular senescence [116].

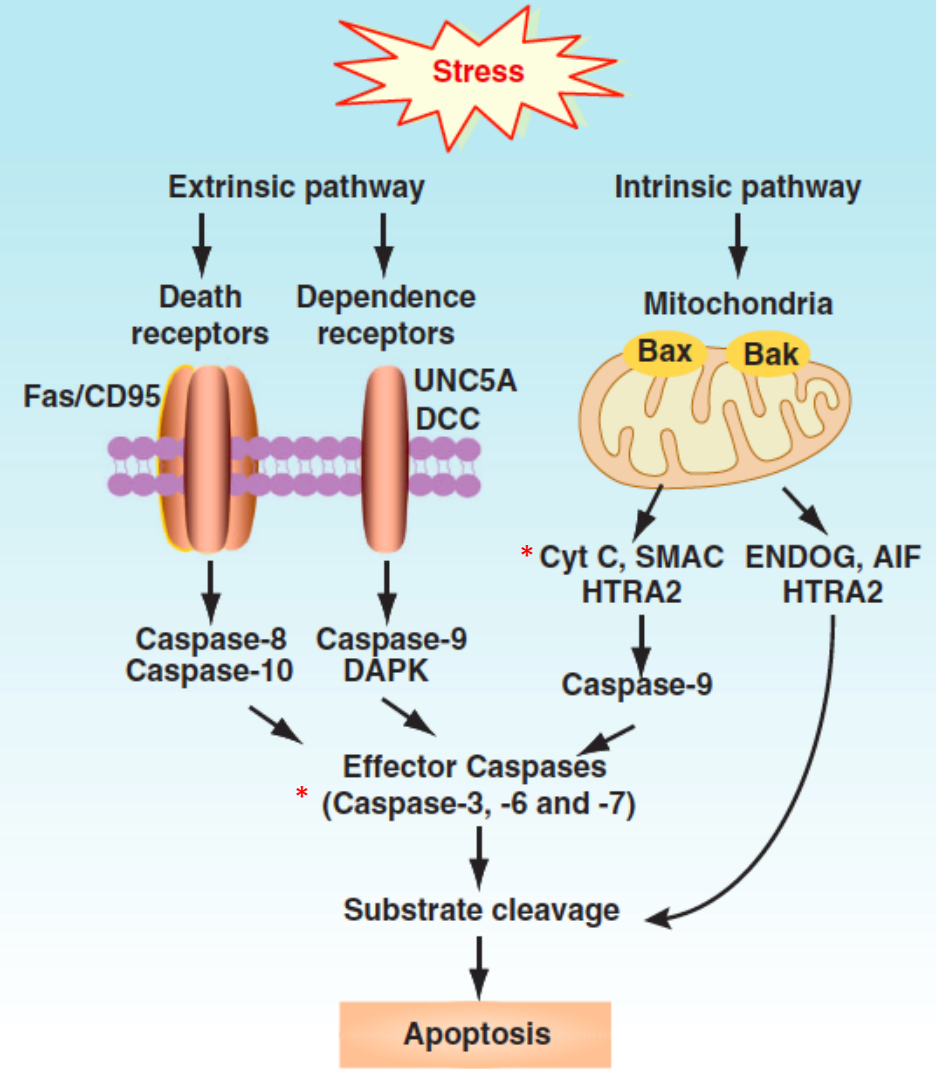

Figure 3. Extrinsic and intrinsic apoptosis. There are two intracellular pathways to control apoptosis. A third pathway, mediated by cytolytic effectors including T and NK cells, delivers pro-apoptotic granzymes through perforin-mediated pores, culling the least fit cells, and promoting survival of the remaining cells through autophagy. The extrinsic pathway is mediated by DRs including tumor necrosis factor family members such as Fas/CD95 and dependence receptors like deleted in colorectal carcinoma or unc-5 homolog A. The intrinsic mitochondrial pathway is controlled by Bcl-2 family proteins such as Bax and Bak. When lethal signals prevail, mitochondrial outer membrane permeabilization occurs and leads to release of the mitochondrial proteins such as CytC, SMAC, HTRA2, endonuclease G (ENDOG), apoptosis-inducing factor (AIF), and HTRA2. Along these, Cyt C, SMAC, and HTRA2 contribute to caspase-dependent apoptosis, whereas ENDOG, AIF, and HTRA2 contributed to caspase-independent apoptosis. Components that are measured in my study are highlighted with a red star. Modified from [112].

1.6 Mitochondrial Dynamics

An aspect of mitochondria that contributes dominantly to the maintenance of cellular homeostasis is the highly dynamic nature of these organelles within the cell. Mitochondria actively take part in events referred to as fusion – the joining of two distinct mitochondria into one organelle, resulting in a mitochondrial network – and fission – the separation of mitochondria from the network, forming punctate, individual organelles (Fig.4). These processes are in a dynamic balance that is related to the overall health status of the cell and tissue. The consequences of these morphological changes in the mitochondria, and the stimuli that provoke these changes, are an ongoing area of research.

1.6a Mitochondrial Fusion

Outer mitochondrial membrane fusion is mediated by Mitofusin (MFN) 1 and 2 proteins, which contain 2 C-terminal heptad repeat subunits HR1 and HR2 separated by 2 transmembrane subunits [117]. The mechanism through which these proteins cooperate to induce membrane fusion is unclear. Brandt *et al.* [118] observed that the mitofusins are involved in formation of a protein rich interaction point between adjacent mitochondrial membranes, which transitions to form a protein-rich ring, allowing membrane fusion to occur at the periphery of the ring. This process requires GTP hydrolysis [118]. Preliminary research on the mitofusins showed that the interaction between HR1 and HR2 maintained MFN2 in an inactive state [119].

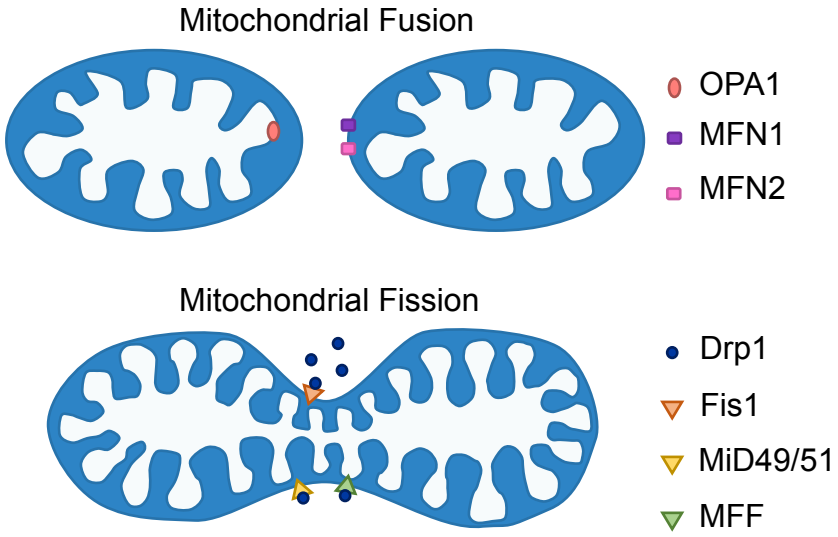

Figure 4. Mitochondrial dynamics processes mitochondrial fusion and fission and their associated effectors. Mitochondrial fusion refers to the fusion of inner and outer mitochondrial membrane, which is mediated by OPA1 (Optic Atrophy Factor 1) and MFN1 and MFN2 (Mitofusin 1 and 2). Mitochondrial fission refers to the scission of the inner and outer mitochondrial membranes. Drp1 (Dynamin-Related Protein 1) mediates mitochondrial fragmentation after binding to one of the mitochondrial adaptors: Fis1 (Fission-1), MiD49/51 (Mitochondrial Dynamics Proteins 49/51), or MFF (Mitochondrial Fission Factor).

Before 2018 it was thought that, prior to fusion, homotypic or heterotypic interactions of HR1 and HR2 domains on dimerized mitofusin proteins must occur on adjacent mitochondria [117,120,121]. GTP binding and hydrolysis is essential for mitofusin C-terminal interactions and resulting membrane fusion [118,121,122]. The G domain of MFN1 may also be involved in dimerization of mitofusins on opposing mitochondrial membranes, dependent on GTP binding [122]. Although these studies all suggest a role of HR1 and HR2 interacting with mitofusins on the adjacent mitochondria by the same domains, Mattie *et al.* [123], made the unexpected finding that the mitofusins contain 1 transmembrane domain only, with the C terminus containing the HR2 domain existing in the intermembrane space. This finding made it necessary to reconsider the mechanism of mitochondrial fusion to accommodate the hypothesis that mitofusin N terminal domains carry out the task of tethering adjacent mitochondrial membrane, while the mitofusin C terminal domain regulates mitochondrial fusion through dimerization of mitofusins by redox-regulated disulfide linkage within the intermembrane space [124]. Previous studies suggesting that mitofusins from adjacent mitochondria must interact to mediate fusion may have not considered the redox conditions of the experiment, which could limit dimerization of mitofusins on the same mitochondria within intramembrane space, blocking mitochondria fusion through other proteins on the adjacent mitochondria. The half-lives of MFN1 and MFN2 are regulated by ubiquitination [125]. Mitofusin 2 also plays a role in mitochondria-endoplasmic reticulum tethering, which is important for maintaining cellular calcium homeostasis [126,127].

Optic Atrophy Factor 1 (OPA1) mediates inner mitochondrial membrane fusion [128]. OPA1 mRNA is extensively alternatively spliced forming 8 isoforms which differ within a region encoding 50 amino acids after translation to the OPA1 protein [129]. These mRNA products are further proteolytically processed to produce short and long OPA1 isoforms, which govern the location of OPA1 in the inner mitochondrial membrane, dictating function [129,130]. Native OPA1 protein is cleaved by Mitochondrial Processing Peptidase (MPP) to remove a leader sequence, producing the long and short protein isoforms [131].

Following cleavage by MPP, OPA1 is cleaved further at different sites within the protein depending on which mRNA isoform is expressed [131]. In general, high molecular weight protein isoforms of OPA1 are necessary for fusion of the inner mitochondrial membrane, a reaction that is energized by GTP hydrolysis, and requires OPA1 binding of cardiolipin on the adjacent inner mitochondrial membrane [132–134]. The protease Yeast Mitochondrial Escape Protein 1 (YME1L) contributes to cleavage of OPA1 at the S2 cleavage site in Mouse Embryonic Fibroblasts (MEFs) [135], while the protease Overlapping With The M-AAA Protease 1 Homolog (OMA-1) mediates cleavage of OPA1 at the S1 cleavage site which is inducible by loss of membrane potential by carbonyl cyanide m-cholorophenyl hydrazone (CCCP) in HeLa cells and MEFs, or loss of Dynamin-related protein 1 (Drp1) in HeLa cells [136–138]. In both cases, cleavage of high molecular weight protein isoforms of OPA1 to produce low molecular weight protein isoforms drove mitochondrial fission [135,136]. Controversy exists over the necessity of OPA1 short

protein isoforms in mitochondrial fusion, with some studies showing that the long protein isoforms alone are necessary [131], while others suggest that both long and short isoforms need to be present [135,139].

The overall effect of mitochondrial fusion is to allow mixing of mitochondrial matrix and membrane contents between individual mitochondria [140,141]. This has been shown to allow gene complementation of damaged mtDNA found in individual mitochondria by wild-type genes found in other mitochondria, reducing the chance of translating these mutations into a cell phenotype. The function of matrix mixing has been highlighted by experiments by Yang *et al.* [142] showing isolated mtDNA-depleted mitochondria regain respiratory function after fusing with neighboring mitochondria, independent of transcription or translation. Ono *et al.* [143] also demonstrated this phenomenon by reporting restoration of growth following mitochondrial fusion between two cell lines harboring different mutations in genes involved in mtDNA replication and protein translation. Fusion also allows mixing of matrix proteins and distributes hydrogen and calcium ions between mitochondria, conveying an increase in health of the overall mitochondrial network by equalizing membrane potential between mitochondria, and consequently, distant areas of the cell [144–146]. Fusion of membranes allows mixing of membrane protein and lipid composition between mitochondria, such as fatty acids, which contributes to regulation of metabolism [141]. Sharing material between all mitochondria of the cell through the process of fusion plays a major role in maintaining overall mitochondrial homeostasis with respect to all functions of the mitochondria [147].

When mitochondrial homeostasis is disrupted by stressful environmental conditions, fusion can promote increased energy production and protect mitochondria from being inducted into the mitophagy pathway when energy is scarce [148,149].

1.6b Mitochondrial Fission

The opposite process to fusion is mitochondrial fission, referring to the separation of fused mitochondria (Fig.4). The most important protein to mediate fission is Dynamin-Related Protein 1 (Drp1), which is a GTPase that forms oligomers surrounding mitochondrial membranes, and utilizes GTP hydrolysis to carry out the fission reaction [128,150,151]. Dynamin-2, another GTPase, works in association with Drp1 to induce mitochondrial fission [152]. Drp1 is regulated by phosphorylation, ubiquitination, and SUMOylation [153]. Phosphorylation occurs by the following kinases and phosphatases: Cyclin-dependent kinase I (CDK1), Cyclin-dependent kinase 5 (CDK5), Extracellular-signal regulated kinase 2 (Erk2), Aurora-A kinase (AURKA), Calcium-calmodulin-dependent kinase (CamK), Protein kinase A (PKA), AMP-activated protein kinase (AMPK), Calcineuron, and PGAM Family Member 5 (PGAM5) at the Ser616 or Ser637 amino acids sites [154]. SUMOylation promotes pro-fission Drp1 activity via the SUMO E3 ligase MAPL [155]. MITOL/MARCH-V, a ubiquitin ligase found on the outer mitochondrial membrane, can act on Drp1 leading to degradation, negatively regulating mitochondrial fission [156,157]. Karbowski *et al.* [158] and Park *et al.* [159] found that MITOL/MARCH-V

promotes mitochondrial fission by regulating Drp1 localization at the outer mitochondrial membrane, with no evidence of Drp1 degradation, and by degradation of MFN1. The cell cycle regulator APC/C^{Cdh1} (Anaphase Promoting Complex) promotes mitochondrial fusion at the mitosis-G1 cell cycle transition by signaling Drp1 degradation by tagging Drp1 for ubiquitination [160].

Drp1 has several adaptor molecules that it can interact with at the mitochondrial membrane to anchor in the correct position to carry out fission. These proteins include Mitochondrial Fission Factor (MFF), Fission-1 (Fis1), and Mitochondrial Dynamics Proteins 49 and 51 (MiD49/51) [161]. Data from Otera *et al.* [162] and Osellame *et al.* [163] suggest that the adaptor of greatest importance to fission is MFF, as knock down of MFF protein expression drastically reduces the capacity of mitochondria to become fragmented, which is not observed with knock down of Fis1. Both MiD49/51 and MFF have been shown to recruit Drp1 to the mitochondria independently of Fis1 [161,162,164]. Drp1 targeting by MFF and MiD49/51 is dependent on the oligomerization state of Drp1, and GTP availability, potentially allowing for a fine-tuned regulation of fission dependent on the local microenvironment and status of Drp1-adaptor interactions, rather than simply the presence of a single adaptor molecule [165–167]. MiD49/51 dissociate from Drp1 prior to the fission event, suggesting that they prepare Drp1 for fission without participating in fission itself [167].

In addition to these Drp1 adaptor molecules, De Vos *et al.* [168] demonstrated in 2005 that blocking actin polymerization blocked mitochondrial fission, and Drp1

and actin are known to interact, regulating Drp1 GTP hydrolysis [169]. In 2011, Friedman *et al.* [170] observed that mitochondrial constriction occurs at points of endoplasmic reticulum-mitochondria contact in kidney epithelial cells. The endoplasmic reticulum protein Inverted formin-2 (INF2) promotes accumulation of oligomerized Drp1 at the mitochondria and fission, dependent on actin polymerization, myosin II, and Actin-related protein 2/3 (Arp2/3) [171–174]. Chakrabarti *et al.* [175] demonstrated that in response to the ionophore ionomycin, ER calcium stores are transferred to the mitochondrial matrix through the mitochondrial calcium uniporter (MCU), inducing mitochondrial fission. This was dependent on INF2-actin polymerization which promoted physical interaction between the ER and mitochondria, facilitating calcium transfer [175]. Mitochondrial constrictions dependent on MCU induced by ionomycin were thought to be Drp1-independent IMM fission. Li *et al.* [176] also showed that actin polymerization is essential for the induction of fission, independent of Drp1. Further studies are necessary to elucidate if actin alone can drive fission, or actin in combination with an unknown factor can drive fission, independent of Drp1. Other cytoskeletal proteins such as Spire1C, Sept2, and cofilin are necessary to promote Drp1 localization to the mitochondria in response to CCCP [177–179].

Cardiolipin, a phospholipid within the inner and outer mitochondrial membranes, allows activation and oligomerization of Drp1 [180–183]. Drp1 is negatively regulated by phosphatidic acid (a component necessary for the synthesis of cardiolipin, found in the mitochondrial membrane) [184], and synthesis of cardiolipin

within the mitochondrial membrane is necessary for mitochondrial fusion [185]. From this literature, cardiolipin plays a role in regulating mitochondrial dynamics, but the mechanism is unclear.

Research focused on investigating inner mitochondrial membrane fission is sparse. Drp1 knock down in cell culture where mitochondrial fragmentation can occur suggests that other fission mediators must exist [186]. Cho *et al.* [187] demonstrated that constrictions of the inner mitochondrial membrane are independent of Drp1, and may be mediated by short-form OPA1. Anand *et al.* [188] demonstrated that short OPA1 protein isoforms co-localize with Drp1 and ER contacts during mitochondrial fission, and that over-expression of short OPA1 protein isoforms induces mitochondrial fragmentation. This study did not eliminate the possibility that overexpression of OPA1 impacted Drp1 activity, leading to Drp1-dependent mitochondrial fragmentation. In the context of Drp1 knock-down by siRNA in HeLa cells, mitochondrial networks are fused, although OPA1 long isoforms are lost, suggesting that short forms of OPA1 alone cannot drive mitochondrial fission [138]. Otera *et al.* [189] showed that when the Drp1 adaptor molecules MiD49/51 are absent, OPA1 cleavage is associated with mitochondrial fission, but this does not exclude the possibility that other Drp1 adaptors (e.g. MFF) could be responsible for recruiting Drp1 in this case. A number of papers report mitochondrial fission associated with cleavage of OPA1 in different cells (HT22 (mouse neuronal cell line), HeLa, MEFs) without evidence of an increase in total Drp1, or an increase in Drp1 in the mitochondrial protein fraction, suggesting that

OPA1 can drive fission alone [190–192]. These observations do not exclude the role of Drp1, as a single measure of Drp1 recruitment to the mitochondria could miss subtle changes in Drp1 localization or post-translational modifications that regulate Drp1 activity. Jones *et al.* [193] described OPA1 cleavage in response to CCCP-induced membrane potential loss in the absence of Drp1, which was not associated with mitochondrial fission, suggesting that OPA1 alone does not have the capacity to drive fission. Overall, the role for short-form OPA1 as a mediator of inner mitochondrial membrane fission is not well supported by the above reports (although not disputed), leaving a gap in the explanation of the mitochondrial fission mechanism to be filled by further study on OPA1, or other unidentified proteins.

Fission is important for mitophagy, – the process of recycling old and/or damaged mitochondria. Mitochondria that are unhealthy, indicated by loss of mitochondrial membrane potential, must separate from the mitochondrial network to be inducted into the mitophagy pathway [194]. This pathway begins with the activation of mitophagy receptors Parkin/PTEN-Induced Kinase 1 (PINK1), BCL2 Interacting Protein 3-Like (NIX)/Bcl-2 and Adenovirus E1B 19-kDa-Interacting Protein 3 (BNIP3), FUN 14 Domain-Containing Protein 1 (FUNDC1), or BCL2L13 [195], initiating the recruitment of downstream effectors such as LC3 on autophagosomes. Removal of these mitochondria maintains the health of the mitochondrial network as a whole [194].

Fission allows for mobility of mitochondria, contributing to migration of mitochondria to other areas of the cell [196,197], as well as segregation of mitochondria into daughter cells following cell division [198]. The relative distribution of healthy mitochondria between cells following mitosis may play a role in determining the destined phenotype of daughter cells after division, such as with epithelial stem cell regeneration [199]. In mesenchymal stem cells, cells of varying states of differentiation display a wide range of mitochondrial network morphologies, and expression patterns of mitochondrial dynamics mediator genes, highlighting the potential importance of mitochondrial dynamics in differentiation [200]. In the drosophila gastrointestinal tract, mitochondrial fission was necessary to maintain stem cell function, while mitochondrial fusion promoted differentiation [201].

Fission plays a role in apoptosis, or programmed cell death. Pro-apoptotic stimuli have been shown to induce fission, dependent on the activity of Drp1 [202]. Since the first papers suggesting that the induction of fission may lead to apoptosis, the role of fission has been studied extensively in many different models. The literature described in Table 3, while not an exhaustive list, highlight the idea that apoptosis is dependent on fission in some cases (green shading), but not others (red shading). This may reflect differences in the pathway of different stimuli used (pharmacological agents, disease models), the cell type or tissue, and the developmental stage of the tissue.

Table 3. Role of Mitochondrial Fission in Apoptosis		
Finding	**Cell Type/Model**	**Ref**
Apoptosis-inducing stimuli (staurosporine, BAX overexpression, etoposide) induced fission, dependent on Drp1 activity.	COS-7 cells (monkey kidney fibroblast), HeLa cells (human cervix epithelium)	202
Apoptosis (activated caspase-3) during embryonic development occurred dependent on Drp1.	Murine embryos	203
Apoptosis measured by annexin V positivity is dependent on Drp1 in response to oxidative stress, short term thapsigargin treatment, but not staurosporine or long term thapsigargin treatment. Apoptosis measured by cytochrome c release is dependent on Drp1 in response to tBID overexpression, oxidative stress, and thapsigargin treatment, but not staurosporine.	MEFs (mouse embryonic fibroblasts)	204
Apoptosis (caspase-3 cleavage, cytochrome c release) induced by ischemia-reperfusion injury was dependent on Drp1.	Ischemia-reperfusion model in HL-1 cells (mouse cardiomyocyte cell line)	205
Apoptosis (cytochrome c release, caspase activation) induced by overexpression of p20 is dependent on Drp1 activity.	Rat fibroblasts, H1299 cells (human lung epithelium)	206
Dominant active MFN2 prevented apoptosis (BAX activation, cytochrome c release) induced by apoptosis.	COS-7 cells	207
Mdivi1 reduces mitochondrial fission and apoptosis (caspase-3 and -9 cleavage, annexin V positivity) induced by amyloid B.	SK-N-MC, SK-N-SH, and SHSY-5Y cells (human neuroblastoma	208
Knock-down of Fis1 or Drp1 decreased apoptosis (nuclei morphology, PARP cleavage, Bax translocation, cytochrome c release) induced by staurosporine, actinomycin D, etoposide, anti-Fas antibody. Knock-down of OPA1 increased apoptosis in response to the same stimuli.	HeLa cells	209

Apoptosis (annexin V positivity, cytochrome c release, TUNEL staining) is dependent on Drp1 activity.	Glycochenodeoxycholate (GCDC) liver injury model in murine	210
Mdivi-1 reduces apoptosis (TUNEL staining) during embryogenesis.	Porcine embryonic fibroblasts	211
Apoptosis (propidium iodide exclusion, caspase activity, cytochrome c release) is induced by staurosporine, etoposide, UV light, and TNFα independent of Drp1.	MEFs	203
Knock-down of Drp1 enhances apoptosis (TUNEL staining, annexin V positivity, caspase-3 activity) in response to hypoxia or at basal conditions.	Primary bovine pulmonary arterial endothelial cells	212
Long term induction of fission by FCCP, which induced mitochondrial fission, did not lead to induction of apoptosis (nuclear morphology, annexin V staining).	HeLa	213
Knock-down of Drp1 induced apoptosis (cytochrome c release).	HCT116 (human colon epithelium) and SW480 cells (human colon epithelium)	214
Knock-down of Drp1 induced apoptosis (annexin V positivity).	Brain Tumor Initiating Cells (BITC) isolated from human glioblastoma tissues	215

When apoptosis is dependent on Drp1, the mechanism has been described as follows. In response to staurosporine, sumoylated Drp1 accumulates at the mitochondria dependent on the BAX (BCL2 Associated X) and BAK (BCL2 Homologous Antagonist/Killer) proteins [216]. Xu *et al.* [217] showed that BAX activation is initiated by PGAM5 (Mitochondrial Serine/threonine protein phosphatase PGAM5), in response to staurosporine (a protein kinase inhibitor) and arenobufagin (a mTOR pathway inhibitor), and the resulting apoptosis is dependent on Drp1 in HCT116 epithelial cells. Prudent *et al.* [155] studied the mechanism of how Drp1 contributes to cytochrome c release, showing that Drp1 is SUMOylated by MAPL in response to staurosporine treatment downstream of BAX activation (substantiating the earlier report by Wasiak *et al.* [216] of Drp1 SUMOylation), allowing Drp1 oligomerization at the mitochondria. MAPL also allowed ER-mitochondrial contact to occur, allowing transfer of calcium to the mitochondria, dysregulation of cristae structures, and, ultimately, release of cytochrome c release [155]. Grosse *et al.* [218] demonstrated that Drp1 was necessary to allow cytochrome c release following assembly of BAX on the outer mitochondrial membrane in response to actinomycin D treatment (inhibits protein synthesis), further supporting the idea that Drp1 is necessary to allow cytochrome c release to occur. Consistent with the idea that mitochondrial fission is a pre-requisite to the induction of apoptosis, mitochondrial fusion mediators have been shown to be largely anti-apoptotic [204,207], although exceptions exist [219].

1.6c Mitochondrial Dynamics in Genetic Disorders

The importance of mitochondrial dynamics in cell and tissue function has been suggested through evidence of the dysregulation of fusion-fission balance in many diseases. Mutations in the fusion-mediating proteins are known to cause conditions such as Charcot-Marie-Tooth disease (a peripheral neuropathy effecting the legs, caused by mutations in MFN2) [220], and autosomal dominant optic atrophy (associated with blindness, caused by mutations in OPA1) [221]. Recently, mutations in Drp1 have also been linked to severe neurological disease encompassing optic atrophy, developmental delay, and epilepsy [222–224]. Disruptions in the signaling pathways known to regulate mitophagy (e.g. mutations in PINK1 and Parkin proteins) are implicated in some forms of Parkinson's disease [225].

1.7 The Role of Mitochondrial Dysfunction in Inflammatory Disease

As mitochondria are major regulators of oxidative stress and apoptosis – factors tightly linked to cell survival – these organelles have been the subject of directed research in many disease models and as a potential therapeutic target for these conditions. Although several rare and severe mitochondrial diseases have been identified that originate from genetic alterations in mitochondrial proteins, most inflammatory-type diseases that are associated with mitochondrial dysfunction are chronic age-associated conditions such as cardiac disease and diabetes.

Chronic heart disease is a major contributor to worldwide death, and leads to ischemia reperfusion injury in the heart in some circumstances. This condition induces drastic increases in reactive oxygen species production and apoptosis of cardiac myocytes, causing tissue damage and reducing heart function of the host [226]. Asthma, another common pulmonary condition, is characterized by features of inflammation [227,228], mitochondrial dysfunction [229], and oxidative stress [230]. Many neurodegenerative diseases including Alzheimer's disease and Huntington's disease are associated with dysregulated levels of ROS and metabolic precursors in the brain, which correlate with altered regulation of metabolic pathways, causing neuronal dysfunction [231]. Development of type II diabetes coincides with mitochondrial dysfunction – decreased ATP production and increased ROS production specifically – that leads to dysregulated sugar metabolism [232]. Related to type II diabetes is metabolic syndrome which is highly influenced by oxidative stress [233]. Mitochondria have been linked to the pathophysiology of Non-Alcoholic Fatty Liver Disease (NAFLD) by the mitochondria's role in metabolism of fatty acids, and reduced ATP production has been reported in the context of NAFLD [234]. Progression of certain cancers has also been linked to increased ROS production by the mitochondria which effects both cell cycle signaling directly and genome stability by reactions between DNA and ROS [232]. A new trend in research on these conditions has been to determine if mitochondrial dynamics play a role in the oxidative stress seen in many of these well-characterized inflammatory diseases [235,236].

Literature describing a direct effect of pro-inflammatory mediators impacting the processes of mitochondrial dynamics is consistent with the idea that mitochondrial dynamics may propagate inflammation in disease [109,237–245]. In fact, there is ample evidence to suggest that imbalances in mitochondrial dynamics are a feature of, or contribute to, the development of inflammatory conditions in a variety of tissues (Table 4). These studies show that there is an imbalance in the fission and fusion processes, and some conditions can be treated in animal models with agents that restore homeostatic mitochondrial dynamics such as P110 [244,246–250], and Mdivi1 [240,251–254]. P110 is a linear peptide which was designed to target the site of protein interaction between Fis1 and Drp1 to reduce mitochondrial fission [255]. Mdivi1 is a quinazolinone derivative which targets the GTPase domain of Drp1 to prevent mitochondrial fission [256].

Disease of the GI tract is commonly caused by inflammation, but these tissues have been assessed only superficially in relation to mitochondrial dynamics compared to the heart, lungs, muscle, and brain, and most focus on gastric or colorectal cancer [257–265]; this represents a gap in our knowledge about GI physiology – a gap that my research addresses, with specific reference to adherent-invasive *E. coli* and the epithelium.

Table 4. Role of Mitochondrial Dynamics in Inflammatory Disease			
Disease in Humans	**Disease Model**	**Major Finding**	**Ref**
Pulmonary Arterial Hypertension (PAH)	Human PAH isolated pulmonary arterial smooth muscle cells. Rat cobalt-induced PAH. Rat chronic hypoxia model.	Induction of mitochondrial fission associated with decreased MFN2 mRNA expression, increased Drp1 mRNA and protein expression, and decreased Fis1 mRNA expression. Drp1-dependent fission drives hyper-proliferation. Drp1 inhibition reduces disease severity.	252
	Rat monocrotaline PAH. Rat chronic hypoxia+Sugen-5416 PAH.	Induction of mitochondrial fission associated with reduced MFN2 mRNA and protein expression. MFN2 overexpression promotes mitochondrial fusion, controls hyper-proliferation, and reduces disease severity.	266
Asthma	Linoleic acid metabolite 13-S-HODE treatment of human bronchial epithelial cells	Induction of mitochondrial fission.	229
Cardiac Ischemic-Reperfusion (IR) Injury or Myocardial Infarction	IR in isolated murine ventricular cardiomyocytes. Rat langendorff IR model.	Induction of fission associated with increased protein Drp1 expression. Inhibition of Drp1 reduces severity of disease.	267
	IR in murine atrial cardiomyocyte cell line. Murine IRI model.	Induction of fission. Inhibition of Drp1 reduced myocardial infarct size.	251
	Murine coronary artery suture myocardial infarction model	MFN2 protein expression is decreased. MFN2 knock-down increases severity of disease.	254
	Murine coronary artery occlusion IR model	MFN1 & MFN2 knock-down reduced severity of disease.	268
Metabolic Disease (diabetes, obesity)	Isolated patient skeletal muscle biopsies	Reduced MFN2 mRNA.	269
	Isolated patient leukocytes	Reduced MFN1, MFN2, and OPA1 protein expression, increased Fis1 protein expression.	270
	Cybrid patient cells expressing diabetes susceptibility risk factor	Drp1 inhibition reduces oxidative stress and improves insulin resistance.	254
Kidney Disease	Renal ischemia-reperfusion injury and cisplatin-induced nephrotoxicity	Drp1 inhibition reduces acute kidney injury.	253

Liver Disease	Concanavalin A induced acute livery injury	Drp1 inhibition reduced liver damage.	240
Cancer	Human thyroid cancer cell lines	Drp1 inhibition reduced cell migration.	271
	Human lung cancer cell lines, human lung tumor tissue	Increased Drp1 gene expression, mitochondrial fission, Drp1 inhibition promotes cancer cell death.	272
	Human primary glioblastoma brain tumor initiating cells	Increased mitochondrial fission, Drp1 inhibition promotes tumor cell death.	215
Neurodegenerative Disease	Amyotrophic lateral sclerosis patient fibroblasts. Transgenic mice expressing patient mutations	Increased mitochondrial fission and mitochondrial dysfunction. Drp1 inhibition reduces disease severity in murine model.	244
	Multiple sclerosis experimental autoimmune encephalomyelitis murine model	Increased phosphorylation of Drp1 (Ser616). Drp1 inhibition reduces severity of disease.	249
	MPTP (1-methyl-4-phenyl-1,2,3,6-tetrahydropyridine) murine model of Parkinson's disease	Increased translocation of Drp1 to the mitochondria, Drp1 inhibition reduces severity of disease.	247

1.8 Mitochondrial Dysfunction in the Gastrointestinal Tract

A limited number of studies have shown that mitochondrial dysfunction is a feature of gastrointestinal mucosal cells during inflammation. Animal studies show that mice harboring mutations resulting in increased ATP production are protected from dextran sulfate sodium (DSS) and 2,4,6,-trinitrobenzenesulfonic acid (TNBS) colitis [273], and that agents reducing mitochondrial ROS production and inflammasome activation, or increasing antioxidant expression, also reduce severity of DSS colitis [274–276]. DSS treatment of colon epithelial cells *in vitro* induces ultrastructural disruptions of the mitochondria measured by electron microscopy [264]. These animal studies suggest that mitochondrial derived oxidative stress plays a role in inflammation, and could contribute to human disease.

Fragmented data from a limited number of studies with small numbers of patients support a role for mitochondrial dysfunction in IBD. Reduced levels of ATP synthase, the enzyme essential for producing ATP in mitochondria, have been reported in patients with UC and CD when compared to control subjects [277]. Reduced levels of antioxidants, mitochondrial heat shock proteins, and enzymes involved in metabolism, such as malate dehydrogenase, have been reported [278]. Elevated levels of reactive oxygen species have also been reported in tissues of both patients with UC and CD [279]. Stimuli that are thought to reactivate colitis in humans (stress, infection, smoking, NSAIDS) can also disrupt mitochondrial function [280–284]. Patients with genetic mitochondrial disease experience symptoms and diagnostic criteria resembling that of patients with Crohn's disease [285].

Research on the relationship between mitochondria and IBD is not part of an established field, but these studies suggest that a link may exist.

The McKay lab has previously established that *in vitro*, colon-derived epithelial cells under metabolic stress exhibit enhanced permeability [286] after treatment with DNP (2,4-dinitrophenol, a mitochondrial uncoupler of oxidative phosphorylation) and commensal bacteria (*E. coli* HB101); human colonic epithelial T84 cells show decreased trans-epithelial resistance (TER), increased flux of horseradish peroxidase (HRP), changes in actin cytoskeleton structure, and increased bacterial internalization [286]. These changes in epithelial barrier function were shown to be independent of apoptosis at the experimental time point for TER and bacterial internalization, but dependent on the cytoskeleton for bacterial internalization, and protein synthesis by the commensal bacteria [287]. Decreased occludin and zona occludens-1 (ZO-1) tight junction protein levels were also reported in conjunction with changes in permeability [287]. Disruptions in barrier function induced by DNP and commensal *E. coli* were exacerbated by TNF-α treatment [288]. Butyrate, which is one component of the bacterial metabolome that could be affected when dysbiosis of the microbiome occurs [28], ameliorates the effect of DNP and commensal *E. coli* on epithelial cells in terms of barrier function [289]. These findings were complemented by data showing that after induction of DSS colitis in mice, the mitochondrial reactive oxygen species scavenger MitoTempo showed therapeutic benefits [290]. DSS administration in mice produces inflammation by inducing epithelial cell death, enhanced GI permeability, and elevated immune

reactions by GI immune cells [291]. These data implicate mitochondria in gastrointestinal epithelial cell function in the context of inflammation, as mitochondria are the main target of metabolic stress induced by DNP, and disease severity is affected by the presence of mitochondria-derived reactive oxygen species.

1.9 The Role of Pathogens in Influencing Mitochondrial Fusion & Fission

Data exist highlighting the potential for LF82 *E. coli* to influence mitochondrial function in infected cells; Elatrech *et al.* [91] and Jensen *et al.* [80] showed that *in vitro*, LF82 infection of colonic epithelial cells (T84 and Caco-2 cells) induced increased production of overall cellular ROS and several studies reported loss of trans-epithelial resistance, a measure of barrier function that is maintained in an ATP-dependent manner, of intestinal epithelial cells upon treatment with AIEC [52,65,67].

Emerging data supports the notion that alteration in the mitochondrial fusion-fission balance is a feature of infection with diverse pathogens – bacterial, viral, and parasitic (Table 5). Even LPS alone can drive increases in mitochondrial fission in endothelial cells, microglia, and myoblasts [292–295]. Interestingly, induction of fusion or fission during infection is shown to be of benefit to either the host or invading organism in the context of single cell-type culture models, depending on the situation, thereby influencing the fundamental host-microbe interaction.

These examples of mitochondrial dynamics impacting pathogen load or host cell viability reveal a new contribution of the mitochondria as a key regulator of

host-microbe interactions, and innate immunity. Although this field has begun to describe how fission and fusion induced by infection can alter the infection itself, the functional consequences of the regulation of mitochondrial dynamics in an infection has yet to be shown in an organism, making it difficult to decide if regulation of mitochondria is beneficial for the host or the microbe.

Table 5 – Evidence of Altered Mitochondrial Dynamics in Infection		
Organism	**Major Finding Associated with Infection**	**Ref**
	Bacteria	
Listeria monocytogenes	Induction of fission dependent on LLO toxin, independent of Drp1. Previous fragmentation of mitochondrial networks restrict invasion of bacteria.	296,297
Shigella flexneri	Induction of fission increasing bacterial load (by blocking induction into xenophagy pathway) and host cell death, dependent on Drp1.	298,299
Helicobacter pylori	Induction of fission associated with Drp1 recruitment.	300
Chlamydia trachomatis	Induces fusion short term (associated with increased bacterial growth, reduced cell death, dependent on OPA1 and MFN1/2, associated with increased p-Drp1 Ser637 and reduced colocalization of Drp1 and mitochondria), fission long term infection.	301,302
Legionella pneuomophila	Induction fission dependent on type IV secretion system and Drp1, promoting bacterial replication.	303
Brucella abortus	Induction of fission independent of Drp1, associated with reduced MFN1/2 protein expression. No impact of fission on bacterial replication, host cell apoptosis.	304
	Viruses	
Hepatitis B	Induction of fission associated with increased p-Drp1 Ser616 and Drp1 recruitment to mitochondria.	305
Human Immunodeficiency	Induction of fission associated with increased Drp1 protein expression and Drp1 recruitment to mitochondria. Decreased Drp1 in and increased fusion in neurons from patients with HIV-associated neurocognitive disorder.	306–308
Rotavirus	Induction of fission associated with increased p-Drp1 Ser616, decreased p-Drp1 Ser637 expression, increased recruitment to mitochondria, dependent on NS4 protein. Fission promotes host cell death and viral replication.	309
Coxsackie B	Induction of fission associated with increased Drp1 gene and protein expression, worsens cardiac disease severity.	310

Dengue	Induction of fission, associated with decreased MFN1/2 protein expression. Induction of fusion by NS4B viral protein, associated with reduction in p-Drp1 Ser616 and recruitment of Drp1 to the mitochondria increases viral titer and host interfon production. Induction of fusion associated with reduced MFN2 increased Drp1 and p-Drp Ser616, increases viral load.	311–313
Severe Acute Respiratory	Induction of fusion associated with decreased Drp1 protein expression.	314
Parasites		
Schistosoma mansoni	Induction of fission associated with reduced MFN2 and increased p-Drp1 (Ser616) protein expression.	315
Toxoplasma gondii	Short term infection – induction of fission, long term infection – mitochondrial morphology returned to basal state. Fission increases parasite burden.	316,317

1.10 Hypothesis and Aims

Hypothesis – Adherent-invasive *E. coli* induce mitochondrial dysfunction and mitochondrial fission, promoting epithelial cell apoptosis and loss of barrier function.

Aim 1 – Characterize the process of AIEC-induced mitochondrial fission

A. Image mitochondrial network morphology in T84, HT29, and Caco-2 cells in response to AIEC using spinning disk confocal microscopy

B. Assess changes in fission and fusion protein levels (OPA1, Drp1) in the human colonic epithelial T84 cell line in response to AIEC (strain LF82, NRG857c, commensal *E. coli* strain HB101 or F18 used as a negative control) over time and as the dose increases. Carbonyl cyanide 3-chlorophenylhydrazone (CCCP) is a mitochondrial ionophore and is used as an inducer of fission.

C. Assess parameters of mitochondrial health such as mitochondrial membrane potential, ATP concentration, and mitochondrial ultrastructure.

Aim 2 – Characterize the mechanism leading from AIEC infection to AIEC-induced fission from the perspective of the bacteria and the host cell

A. Assess the role of soluble mediators produced in the AIEC culture medium in inducing mitochondrial fission by treating cells with AIEC spent medium

B. Assess the necessity of bacterial invasion on AIEC-induced fission by comparing invasion of different AIEC strains and resulting mitochondrial fission. Measure mitochondrial fragmentation induced by FimH mutant LF82.

C. Determine role of reactive oxygen species in AIEC-induced fission by quenching ROS with antioxidants Vitamin C and Mito-TEMPO and measuring mitochondrial fission.

D. Determine role of Drp1 by measuring AIEC-induced fission during treatment with P110, Mdivi1, and Leflunomide, and after siRNA knock-down of Drp1.

Aim 3 – Determine the consequence of AIEC-induced mitochondrial fission on epithelial cell function (e.g. apoptosis, barrier function, bacterial load, cytokine production)

A. Measure apoptosis in response to AIEC infection by cytochrome c release from mitochondria and cleavage of caspase 3. If apoptosis is induced, determine if the induction is dependent on fission.

B. Measure epithelial barrier function in response to AIEC infection by trans-epithelial resistance, FITC-Dextran flux, and translocation of bacteria. If barrier function is disrupted, determine if this is dependent on fission.

C. Measure bacterial persistence inside epithelial cells and the impact of blocking mitochondrial fission.

D. Measure cytokine production in response to AIEC infection (IL-8). If cytokines are enhanced, determine if induction is dependent on fission.

Real-time PCR of Human, Mouse Tissue Samples, and T84 Cells

Experiments with human samples were conducted under a protocol approved by the University of Calgary Conjoint Health Research Ethics Board (REB 17-20941). Patient characteristics are described in Table 6. Animal experiments adhered to the Canadian guidelines on animal welfare as administered by the University of Calgary Animal Care Committee protocol AC13-0015.

Human colonic punch biopsies were collected in RNAlater (750μL, Life Technologies), and murine colonic tissue was collected in Ribozol (VWR, Radnor, PA, U.S), and stored at -80°C. Human tissues were transferred to Ribozol (1 mL, VWR) prior to processing. Tissues were transferred from storage tubes into 12 x 75 mm glass tubes (VWR, 47729-570) and homogenized using the Polytron PT-MR1200 homogenizer 3 times for 5 seconds at setting 19.

For human biopsies, RNA was extracted using the organic extraction method [318,319]. Two hundred μL of chloroform was added per mL of Ribozol, and samples were shaken vigorously until the solution was homogenous and incubated at room temperature (RT) for 3 min. Samples were centrifuged for 15 minutes at 4°C, 12,000 *g*. The aqueous solution (upper, clear) was collected and transferred to a fresh RNAse free tube. Five hundred μL of isopropyl alcohol was added per mL of original sample, mixed by inverting the tube, incubated for 10 min. at RT, followed by centrifugation for 10 min. at 4°C, 12,000 *g*. The supernatant was removed to leave a clear pellet, which was re-suspended in 75% ethanol (1 mL per 1 mL original Ribozol solution),

and spun down for 5 min. at 4°C, 7,500 *g*. The supernatant was removed and the pellet left to try in the fume hood until almost all the ethanol was gone. Pellets were dissolved in 50 μL of RNAse free water and RNA concentration was measured using the ND-1000 NanoDrop Spectrophotometer (ThermoFisher Scientific, MA, U.S.).

For the murine samples from DSS-treated mice, lithium chloride (Ambion, 9480) was added to the RNA at a final concentration of 2.5 M, incubated for 30 min. at -20°C, and spun for 15 min. at 4°C, 16,000 *g*. The supernatant was removed and the pellet re-suspended in 1 mL of ice cold 70% ethanol, then spun for 15 min at 4°C, 16,000 *g*. This wash step was repeated, and pellets were dried to remove residual ethanol, and then re-suspended in RNAse free water (50 μL).

Table 6 – Patient Characteristics	CD – Crohn's disease, UC – ulcerative colitis				
Condition	**Sex**	**Age**	**Disease Location**	**Disease State**	**Biopsy Location**
Healthy	M	50	na	control	ascending colon
Healthy	M	51	na	control	descending colon
Healthy	F	58	na	control	descending colon
Healthy	F	52	na	control	ascending colon
Healthy	M	59	na	control	ascending colon
Healthy	F	53	na	control	ascending colon
Healthy	M	65	na	control	ascending colon
Healthy	M	72	na	control	ascending colon
Healthy	F	51	na	control	ascending colon
Healthy	M	70	na	control	ascending colon
Healthy	F	44	na	control	descending colon
Healthy	F	28	na	control	descending colon
Healthy	F	19	na	control	descending colon
Healthy	F	63	na	control	ascending colon
Healthy	F	43	na	control	ascending colon
UC	F	34	rectum	inflamed	rectum
UC	F	32	unknown	non-inflamed	ascending colon
UC	F	32	unknown	inflamed	ascending colon
UC	F	23	unknown	non-inflamed	ascending colon
UC	M	36	pancolitis	inflamed	colon
UC	M	49	rectum	non-inflamed	ascending colon
UC	M	49	rectum	inflamed	ascending colon
UC	F	22	pancolitis	inflamed	rectum
UC	F	34	unknown	non-inflamed	descending colon
UC	F	34	unknown	inflamed	descending colon

UC	M	20	unknown	inflamed	descending colon
UC	F	31	unknown	non-inflamed	ascending colon
UC	F	31	unknown	inflamed	ascending colon
UC	M	32	rectum	non-inflamed	descending colon
UC	M	32	rectum	inflamed	descending colon
CD	F	47	ileocolonic	non-inflamed	not noted
CD	F	47	ileocolonic	inflamed	not noted
CD	F	25	ileocolonic	non-inflamed	not noted
CD	F	62	ileocolonic	non-inflamed	not noted
CD	F	39	ileocolonic	inflamed	descending colon
CD	F	39	ileocolonic	non-inflamed	descending colon
CD	M	64	colonic	non-inflamed	transverse colon
CD	F	31	ileal	inflamed	neo-terminal
CD	M	50	colonic	inflamed	sigmoid colon
CD	M	50	Colonic	non-inflamed	sigmoid colon
CD	M	28	ileal	inflamed	neo-terminal
CD	F	33	ileocolonic	inflamed	descending colon
CD	F	61	unknown	non-inflamed	not noted
CD	M	46	ileocolonic	inflamed	not noted
CD	F	50	ileocolonic	non-inflamed	descending colon

RNA was isolated from T84 epithelial cells using the Aurum Total RNA Mini Kit (Bio-Rad, Mississauga, ON, Canada, 7326820). Cells were seeded at 500,000 cells/well in 12-well plates, cultured for 24-48h, and treated. Cells were washed with PBS once and collected in the kit lysis solution. Cells within lysis solution were stored at -80°C until processing. After thawing, an equal volume of 70% ethanol was mixed with the lysis buffer and loaded into the RNA binding column. This column was spun for 30 sec. at 16,000 *g* (all later spins had the same conditions), and the filtrate discarded. The column was washed with low stringency wash solution (from kit) and spun to discard the solution. The column was treated with DNAse I (80 μL, 5 μL of DNase I reconstituted in 10mM Tris, pH 7.5, diluted in 75 μL of DNase dilution solution provided with the kit) for 15 min. at RT, and washed with high stringency wash solution. RNA was eluted from the column in 50 μL of elution buffer.

cDNA synthesis was performed using an iScript kit (Bio-Rad, 1778890). Samples were prepared by diluting 4 μL of the iScript Reaction Mix (containing oligo(dT) and hexamer primers) per 20 μL of total volume in RNAse free water, 500 ng of RNA, and 1 μL of iScript Reverse Transcriptase.

Assessment of Drp1 (Dynamin-Related Protein 1), Fis1 (Fission 1), MFN1 (Mitofusin 1), MFN2 (Mitofusin 2), and OPA1 (Optic Atrophy Factor 1), mttRNA-leu (mitochondrial tRNA), and RPL27 (ribosomal protein L27) for human tissue, mtND1 (mitochondrial NADH dehydrogenase subunit 1) and 18S for mouse tissue, mRNA expression by qPCR was performed using the Realplex Eppendorf Mastercycler or StepOnePlus Real-Time PCR system using the iQSYBER Green Supermix (Bio-Rad)

with 6.25 ng of RNA and the primers shown in Table 7. A master mix was created containing 10 μL iQSYBR Green Mix (2x concentrated solution), 4.2 μL RNAse free water, and 0.8 μL primer mix (contains forward and reverse primers taken from a 10 μM stock solution) per sample (scaled up to cover number of samples in plate). Fifteen μL of this master mix was loaded into each well of the qPCR plate (Twin.tec real-time PCR plate, skirted, Eppendorf, 951022003 for the Eppendorf Mastercycler, MicroAmp Fast Optical 96-Well Reaction Plate with Barcode, Applied Biosystems, Life Technologies, 4346906 for StepOnePlus system). Five μL of diluted cDNA was added to each well of the qPCR plate in triplicate. The qPCR program was run as follows: (1) 94°C, 3min., 45 cycles of steps 2-4: (2) 95°C, 15sec., (3) T_m of primer e.g. 60°C, 30sec., (4) 72°C, 30sec., (5) 95°C, 15sec., (6) 60°C, 30sec. Resulting values were computed to SYBR green expression based on a standard curve, and were normalized to RPL27 or 18S expression. Control values normalized to a housekeeping gene were averaged, and all samples were normalized to this averaged value to calculate the relative expression of each sample (making the average of control values equal 1). No-template and a no-reverse transcription negative controls were used which showed no amplification. Melting curves were performed which showed 1 peak. Efficiency of primers as determined by standard curves all exceeded an R^2 value of 0.9.

Table 7. Primer Sequences for Quantitative PCR		
Human		
Gene	**Forward**	**Reverse**
RPL27	ATCGCCAAGAGATCAAAGATAA	TCTGAAGACATCCTTATTGACG
mttRNA-leu	CACCCAAGAACAGGGTTTGT	TGGCCATGGGTATGTTGTTA
Drp1	ACCCGGAGACCTCTCATTCT	TGACAACGTTGGGTGAAAAA
Fis1	GACATCCGTAAAGGCATCCGT	GAAGACGTAATCCCGCTGTT
OPA1	TCCCGCTTTATGACAGAACC	AAATAGCTGCATCCCATTGC
IL-8	CAAGGAAAACTGGGTGCAGA	CTGGCAACCCTACAACAGAC
Mouse		
18s	ACGCGCGCTACACTGACTGG	CGATCCGAGGGCCTCACTAAACC
mtND1	AATCGCCATAGCCTTCCTAACAT	GGCGTCTGCAAATGGTTGTAA
Drp1	CTGGATCACGGGACAAGG	GTTGCCTGTTGTTGGTTCCT
Fis1	CCTGATTGATAAGGCCATGAA	ACAGCCAGTCCAATGAGTCC
OPA1	TGACAAACTTAAGGAGGCTGTG	CATTGTGCTGAATAACCCTCAA
MFN1	GTGAGCTTCACCAGTGCAAAA	CACAGTCGAGCAAAAGTAGTGG
MFN2	CATTCTTGTGGTCGGAGGAG	AAGGAGAGGGCGATGAGTCT

Cell Culture

T84 colonic epithelial cells were maintained in 10% fetal bovine serum (FBS; Sigma MO, USA) 1:1 Dulbecco's Modified Eagle's Medium (DMEM)/F12 Ham medium (Sigma) containing HEPES (2 mM, Sigma), L-glutamine (2.68 mM, Gibco by Life Technologies, ThermFisher), sodium pyruvate (0.6 mM, Sigma), sodium bicarbonate (0.015%, Gibco, ThermoFisher), and penicillin-streptomycin (120 units/mL penicillin, 0.12 mg/mL streptomycin, Sigma) [320,321]. HT29 colonic epithelial cells were maintained in 5% FBS DMEM containing L-glutamine (2.16 mM), non-essential amino acids (1x, Sigma), and penicillin-streptomycin (108 units/mL penicillin, 0.11 mg/mL streptomycin, Sigma). Caco-2 colonic epithelial cells were maintained in 5% FBS DMEM containing L-glutamine (2.16 mM), non-essential amino acids (1x), and penicillin-streptomycin (108 units/mL penicillin, 0.11 mg/mL streptomycin). T84 cells were a kind gift from Dr. Kim Barrett (UCSD), and HT29 and Caco-2 cell were purchased from ATCC (Manassas, VA, U.S.). Penicillin-streptomycin was excluded from the medium preparation during infection conditions.

For sub-culture or seeding, cells were dissociated from tissue culture flasks by Trypsin-EDTA (5 mL for T75 flasks, 12 mL for T175 flasks, 0.25%, Gibco, ThermoFisher), for 30 min. at 37°C. Following dissociation, warmed medium (37°C) was added to the trypsin (double the volume of trypsin), cells were pipetted up and down to promote further dissociation, and spun down for 5 min. at 367 *g*. Cells were re-suspended in medium and redistributed in new flasks or counted, and plated on

appropriate tissue culture vessels (described below for each assay).

Commensal *E. coli* (strains HB101 and F18) were maintained on Luria-Bertani (LB) agar (VWR, J104-1KG) and cultured in LB broth (Becton Dickinson, Franklin Lakes, NJ, U.S., 244620) overnight at 37°C. AIEC strain LF82 (from Dr. P. Sherman (Univ. Toronto)) was maintained on columbia sheep blood agar (BBL, 221263) and cultured in penassay broth ([66], Fluka Analytical, ThermoFisher, 70184). LF82 GFP$^{\Delta FimH}$ and LF82-GFP (a kind gift from J. Söderholm, Linköping University) (were maintained on LB (100 μg/mL ampicillen) and cultured in LB broth (100 μg/ml ampicillen)). NRG857c *E. coli* was maintained on LB and cultured in LB broth (a kind gift from Dr. Coombes (McMaster Univ.)). All bacteria were streaked onto agar plates and grown at 37°C overnight. One colony from the agar plate was inoculated into 10 mL of broth and grown on a shaker at 37°C overnight. *E. coli* LF82 spent medium was prepared by incubating T84 cells (500,000 cells/well) with LF82 (10^4 CFU/mL, 16h), collecting medium containing LF82, spinning down LF82 (10 min., 1258 *g*) and filtering the supernatant (0.2 μm filter). Fresh T84 cells were treated with LF82 spent medium. Dead LF82 were prepared by incubating T84 cells with LF82 (10^4 CFU/mL, 16h), collecting supernatant containing LF82, spinning down LF82 (10 min., 1258 *g*), re-suspending LF82 in 2.5% glutaraldehyde (Sigma, G-6257), incubating for 2h and rinsing fixed LF82 with PBS twice [322]. Bacterial death was confirmed by plating fixed bacteria on blood agar plates, growing at 37°C overnight, and checking for colonies. Fresh T84 cells were treated with dead LF82, which were not enumerated but should be in similar numbers to

live LF82 after treatment with T84 cells for 16h (the bacterial concentration was 10^4 CFU/mL at the incubation start time with T84 cells, and were grown for 16h and collected before fixation).

P110 (a gift from Dr. D. Mochly-Rosen) treatments consisted of a 30 min. pre-treatment, and co-treatment supplemented every 2 hours at 10 μM [255]. Mdivi1 (Sigma, M0199) co-treatment 5 μM [256]. Mdivi1 is a Drp1-dependent inhibitor of mitochondrial fission and has no impact on the actin cytoskeleton or endoplasmic reticulum morphology [256]. Leflunomide co-treatment 50 μM (Cayman Chemical Company, Ann Arbor, MI, U.S., 14860, [323]).

Bacterial Growth Curves

E. coli HB101 or *E. coli* LF82 were inoculated at 10^4 CFU/mL in antibiotic-free T84 cell medium ± P110 (10 μM), Mdivi1 (5 μM), or Leflunomide (50 μM), and grown at 37°C in the cell culture incubator, and optical density (O.D.) was measured at each time point.

Isolation of Epithelial Cells from Murine Colonic Tissue

Whole colonic tissue was isolated from mice (male balb/c, 8-10 weeks old, Charles River Laboratories, strain code 028) and transferred to a tube with HBSS (Hanks' balanced salt solution) containing 1 mM EDTA (Ethylenediaminetetraacetic acid) for 10 min. at 37°C. Dislodged crypts were collected, and the remaining tissue was collected for the next step. Colonic tissue

was cut into small pieces and step 1 was repeated with fresh HBSS with EDTA, followed by 10 vigorous shakes of the container to dislodge crypts. Both solutions were passed through a 70 μm filter (VWR, 732-2758). The filter was inverted and DMEM was used to wash the filter out to collect crypts in a 50 mL falcon tube. Crypts were centrifuged at 400 *g* for 5 min., re-suspended in HBSS + EDTA and pipetted up and down to obtain single cells, and centrifuged again for 5 min. 400 *g*. Cells were then re-suspended in Ribozol for RNA extraction or RIPA/protein lysis buffer for western blot.

Immunofluorescence of *E. coli* LF82 and *E. coli* HB101 Infection

T84 cells were seeded on sterile coverslips in 24 well plates (500,000 cells/well, Thermo Fisher Scientific, 12-545-81, #1.5) and grown for 24-48h, then infected with *E. coli* LF82 or *E. coli* HB101 for 4h, 10^8 CFU/mL. Cells were fixed with pre-warmed (37 °C) 4% paraformaldehyde (Acros Organics, Thermo Fisher Scientific, 41678-5000, 10 min.), washed and permeabilized with 0.1% TX100 in PBS (2x 5 min.) before blocking. Samples were blocked with 10% donkey serum (Stemcell Technologies, diluted in 0.1% TX100 RT 30 min.), labelled with anti-*E. coli* antibody (abcam, Cambridge, UK, ab13627, diluted in 0.1% TX100, 1:50, 37°C, 30 min.), washed 2x 5min., labelled with donkey anti-goat secondary (Alexa Fluor 488 antibody A11055, Invitrogen, Thermo Fisher Scientific, diluted in 0.1% TX100, 1:1000, RT, 30 min.), washed 2x 5min., and stained with DAPI (1:1000, RT, 5 min.). After 2 washes (5 min. each), coverslips were mounted on slides with Dako

Fluorescent Mounting Medium (Dako North America, Inc., Agilent Technologies, CA, USA, S3023), and imaged on an Olympus BX41 widefield microscope.

Reactive Oxygen Species Measurement

Reactive oxygen species were measured using the DCFDA/H2DCFDA Cellular Reactive Oxygen Species Detection Assay Kit (abcam, ab11385) and by fluorescence imaging of MitoSOX dye (ThermoFisher, M36008). For the DCFDA assay, T84 cells were seeded at 250,000 cells per well in a 96 well plate and grown for 24-48h (Optical Btm Plt PolymerBase Black w/Lid Cell Culture Sterile, ThermoFisher Scientific, 165305), washed and incubated with the DCFDA dye (25 μM, diluted in kit buffer) for 30 min. at 37°C. After staining cells were infected with *E. coli* HB101 or *E. coli* LF82 at 10^6 CFU/mL, or treated with rotenone (40 μM, positive control) for 4h, 6h, or 16h, and dye fluorescence was read by a spectrophotometer at excitation/emission 485/535 nm. Treatments were diluted in phenol red-free T84 cell culture medium (Sigma).

For MitoSOX staining, T84 cells were seeded into a 96-well plate at 100,000 cells/well and cultured for 72h. Cells were washed 1x with PBS and stained with MitoSOX (5 μM, diluted in HBSS) for 30 min. at 37 °C. Cells were washed 2x 5 min. each with PBS, and then treated with rotenone (40 μM) by itself, or with Vitamin C (0.25 mM), or with MitoTEMPO (10 μM) for 16h in phenol red-free T84 cell culture medium. The plate was incubated in the IncuCyte ZOOM microscope and imaged every 2h (20x magnification, Essen Biosiences, Sartorius). Analysis was performed

using pre-set analysis programs on the IncuCyte ZOOM software; masks were chosen which highlight positive staining and quantify the percent of the cell monolayer with positive staining.

Western blot

Protein isolation and western blot follows a similar protocol as Ceponis *et al.* [324]. 500,000 to 1 million cells were seeded in 6-well plates and grown for 24-48h, then treated. Following treatment, whole cell lysate proteins were isolated by rinsing cell culture plates with 1 mL of PBS and adding RIPA/protein lysis buffer (25 μL/well), scraping cells and collecting them in a microcentrifuge tube. Samples were frozen at -80ºC, thawed, and spun down for 5 min. at 16,000 *g* to remove cell debris (supernatant contains protein). Mitochondria were isolated from epithelial cells with the Mitochondria Isolation Kit For Tissue and Cultured Cells (BioChain, Newark, CA, U.S., KC010100). For mitochondrial isolation, 15 million cells were grown on 145 mm x 20 mm petri dishes (Grenier Bio-one, Cellstar, 639160) for 72h. Following treatment (*E. coli* LF82, 4h 10^8 CFU/mL or 16h 10^4 CFU/mL), cells were rinsed with PBS and harvested in 500 μL of Mitochondrial Isolation Buffer (from manufacturer) by scraping, and frozen at -80ºC. Thawed samples were spin down at 600 *g* for 10 min. to remove cell debris. The supernatant was spun down at 12,000 *g* for 15 min. to pellet mitochondria. Pellets were washed with Mitochondrial Isolation Buffer, and spun down at 12,000 *g* for 15 min., re-suspended in RIPA/protein lysis buffer. Mitochondrial protein samples were sonicated 3 times for 3 sec. prior to

protein quantification (Microson Ultrasonic Cell Disruptor). Protein was quantified by Bradford assay (Bio-Rad). Protein (20-50 μg) was run on acrylamide gels (8% for OPA1, 12% for all others) for 30 min. at 80 volts followed by 2h at 100 volts, transferred to 0.2 μm PVDF membranes (Bio-Rad), blocked (5% TBST milk), and probed. Primary antibodies used were Actin (SantaCruz, sc-1616, 1:1000), p-Drp1 Ser 616 (Cell signaling, D9A1, 1:1000), Drp1 (abcam, ab56788, 1:2000), OPA1 (abcam, ab42364, 1:1000), Caspase-3 (Cell signaling, 9662 1:1000), Cleaved caspase-3 (Cell signaling, 9661, 1:1000). Densitometry was performed using ImageJ software by inverting the image, drawing a box around the bands (keeping the same sized box for each protein within each gel), and using the measure function.

Bacterial Internalization Assay

Bacterial internalization assays were performed using T84 cells at 50-70% confluence as described in Nazli *et al.* [286]. Cells were seeded in 6-well plates (Greiner bio-one, 657 160) and grown for 24-48h prior to treatment (0.5 – 1 million cells/well). After treatment with *E. coli* (1 mL/well, 2h/4h/8h at 10^8 CFU/mL, 16h at 10^4 CFU/mL, strain HB101, LF82, or NRG857c), the number of bacteria in the medium was quantified by collecting 200 μL of media in a 96-well plate, serial diluting in PBS by 10, and plated on blood agar plates (plated 5 dilutions, generally 10^6-10^{10} dilution was plated). After aspirating culture medium, cells were washed with 1 mL of PBS and treated with gentamicin (100 μg/mL, 1mL/well, Sigma) for 1 h to kill extracellular bacteria. Epithelial cells were washed with PBS, then treated

with Triton X-100 (5 min. on shaker, 1% in PBS, 1mL/well, Sigma) to induce cell lysis. The resulting internal cell lysate was vortexed and collected in a 96-well plate (200 μL). Lysates were serially diluted in PBS by 10, and the 10^0-10^5 dilutions were plated on agar plates and grown at 37°C overnight. Colony-forming units per mL were compared to external colony-forming units per mL, counted in the first step, to derive percent invasion of bacteria.

Transmission Electron Microscopy

T84 cells were seeded on 12-well plates (500,000 cells/well) and grown for 24-48h prior to treatment. After treatment, cells were rinsed once with PBS and fixed in glutaraldehyde, dehydrated, embedded, sectioned, collected on a grid, and imaged on the Hitachi H-7650 TEM at 5000x magnification. For each condition, 5 epithelial cell layers were examined.

Mitochondrial Membrane Potential

T84 cells were seeded on 96-well plates ($1x10^5$/well) and grown for 24-48h. Cells were stained with Tetramethylrhodamine Ethyl Ester dye (TMRE, ThermoFisher Scientific, 30 min., 75 nM, diluted in HBSS), washed, and treated with experimental conditions (CCCP 4 μM, *E. coli* LF82 or *E. coli* HB101 10^4 or 10^8 CFU/mL for 16h, imaged every 30 min.). Fields of view were chosen using pre-formatted imaging patterns on the IncuCyte ZOOM software (3 fields of view (FOV) per well, evenly spaced vertically), and imaged on the IncuCyte ZOOM microscope

(20x magnification, 1 image/FOV/30min., Essen Biosiences, Sartorius, Gottingen, Germany). Analysis was performed using pre-set analysis programs on the IncuCyte ZOOM software, masks were chosen which highlight positive staining and quantify the degree of staining by fluorescence intensity.

ATP Assay

T84 cells were seeded on 12-well plates (500,000 cells/well) and intracellular ATP was measured using the CellTiter-Glo Luminescent Cell Viability Assay (Promega, WI, USA, G7571). Treatments consisted of *E. coli* F18 or *E. coli* LF82 at 4h (10^8 CFU/mL) or 16h (10^4 CFU/mL). Cells were rinsed with PBS following treatments, CellTiter-Glo Reagent was added to cells (300 μL), cells were collected and the amount of light produced in each sample due to luciferase activity in the CellTiter-Glo Reagent was recorded using the Victor3V 1420 Multilabel Counter (PerkinElmer, Waltham, MA, U.S.) in a white walled 96-well plate (Griener bio-one, 655083). Luciferase values were compared to a ATP standard curve (diluted in CellTiter-Glo Reagent, 5 point standard curve diluted by 10, top concentration was 50 μM) and normalized to protein content in samples (measured by Bradford assay (Bio-Rad).

Quantification of Mitochondrial Morphology

T84 cells were seeded on 8 well chamber slides (250,000 cells/well, ThermoFisher Scientific, Lab-Tek, 155409) and grown for 24-48h. Cells were stained using MitoTracker Red CMXRos probe (50 nM, Invitrogen Detection Technologies, Molecular Probes, M7512, diluted in HBSS) for 30 min. at 37°C, washed (3x, 5 min. in pre-warmed PBS), stained with Hoescht dye (1 mg/mL, ThermoFisher Scientific, H3570, diluted in PBS), washed (2x 5 min. in pre-warmed PBS), and treated. Treatments were diluted in phenol red-free T84 medium. Live cells were imaged on the Leica DMI6000B Diskovery Flex spinning disk confocal microscope (Wetzlar, Germany). Quantification was performed by imaging nuclei, choosing a cell, switching fluorescent channels to image MitoTracker, and rated as "fused", "intermediate", or "fragmented" (Fig.5) [312,325]. "Fused" was defined as cells with the majority of mitochondria forming interconnecting networks usually spanning more than half the size of the cell. "Fragmented" was defined as cells with >80% spherical mitochondria. "Intermediate" was defined as cells containing a combination of "fused" and "fragmented" mitochondria, or short tubules not interconnected with each other. Twenty separate fields of view spanning most of each epithelial monolayer were selected, 1 cell rated per field of view. Image brightness and contrast were adjusted in powerpoint to display equal background between images within a figure and to allow visualization of dim mitochondria (entire image was manipulated equally).

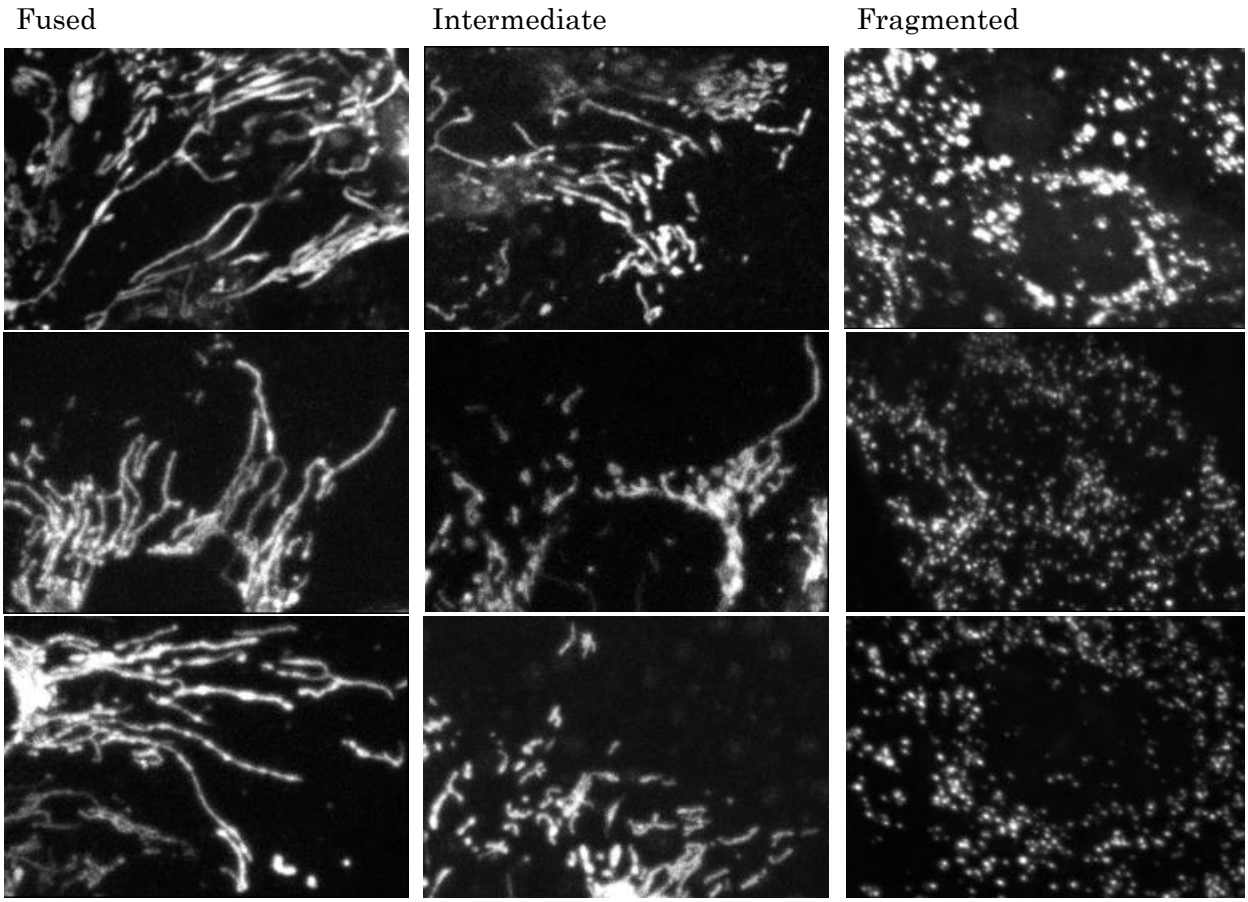

Figure 5. Examples of mitochondrial morphology in T84 cells. Mitochondrial networks were stained live with mitotracker red dye and imaged by confocal microscopy at 63X magnification. Examples of "fused", "intermediate", and "fragmented" mitochondria are given.

Drp1 siRNA Transfection

T84 cells were trypsinized (Gibco) for 1 h at 37°C, trypsin was neutralized using antibiotic-free T84 medium, cells were spun down (367 *g*, 5 min.) and re-suspended in antibiotic-free T84 medium. Separate diluted solutions of Lipofectamine 2000 (2 μL/well, ThermoFisher Scientific) and Drp1 siRNA (Santa Cruz Biotechnology, sc-43732, 30 nM) or control non-targeting siRNA (Santa Cruz Biotechnology, sc-37007, 30 nM) were prepared, each with enough of each to account for all of the wells needed in the experiment, diluted in Opti-MEM medium (Gibco, 31985-070). The diluted siRNA mixture was added to the lipofectamine mixture tube, incubated for 5 minutes, and transferred to a 50 mL falcon tube. Cells were added to the lipofectamine-siRNA solution and transferred to 8 well chamber slide at 100,000 cells/well (ThermoFisher Scientific, Lab-Tek, 155409). Media was changed no later than 16h after seeding to remove lipofectamine. Cells were stained (see mitochondrial morphology section) 72h following transfection, and treated with bacteria (2h, 10^8 CFU/mL).

Epithelial Barrier Function

Transepithelial resistance (TER), the flux of FITC-dextran and transepithelial passage of *E. coli* across filter (3 μm pore)-grown (Greiner-BioOne) T84 cell monolayers (starting TER ≥1000 Ohms/cm^2) were performed as previously described [286,288]. Cells were seeded at 1 million cells/well and grown for a minimum of 7 days or until starting TER was reached. Bacteria were loaded on the apical side of filters at

10^8 CFU/mL. TER was measured every 2h using a voltohmeter. FITC-dextran was added to the apical chamber at 4h (70 kDa, 200 μg/mL) and collected in the basolateral chamber at 6 hours. FITC-dextran containing-medium was transferred to a white walled 96-well plate (Griener bio-one, 655083) and quantified by spectrophotometry at excitation of 485 nm and emission of 535 nm. Medium containing bacteria was collected in the basolateral chamber at 6 hours, centrifuged (1258 *g*, 5 min), and re-suspended in 100 μL PBS. Bacteria were plated on columbia sheep blood agar plates (BBL) and grown overnight at 37°C to enumerate colony-forming units.

Ussing Chamber Studies

Macro- and microscopically normal colonic specimens were collected from 6 patients during surgery for colonic cancer at the University Hospital, Linköping. The patients, 4 men and 2 women, median age of 75 years (range 60-89), had no generalized disease and none had received preoperative chemotherapy or radiotherapy. The study was approved by the Regional Ethical Review Board, and all subjects had given their written informed consent. The external muscle and myenteric plexus were stripped off the colonic specimens, and mucosal sections were mounted on Ussing chambers (Harvard apparatus Inc., Holliston, MA, USA) as previously described [326]. Transepithelial resistance (TER) was monitored throughout the experiment to ensure tissue viability. Chambers were equilibrated for 30 min to achieve steady state conditions and then live GFP-labelled *E. coli* LF82 was added to

the mucosal sides of 3 separate chambers at a final concentration of 10^8 CFU/ml. Three chambers added Krebs buffer only served as controls. After 2h, tissues were removed and put in Protein Lysis/RIPA buffer (1mL, 10mM Tris-Cl pH 7.4, 1mM EDTA, 1% Triton X-100, 0.1% sodium deoxycholate, 0.1% SDS, 140mM NaCl, 1% NP-40, 0.05M NaF), RNA-later (mRNA extraction) or TEM-fixative (2% paraformaldehyde, 2.5% glutaraldehyde in 0.1M phosphate buffer, pH 7.4), respectively and shipped to Calgary. Serosal buffers were collected and directly frozen at -70°C. Studies were performed by Asa Keita, principal research engineer, Linköping University.

Cytokine Production

Interleukin-8 was measured in conditioned medium by ELISA using paired antibodies from R&D Systems Inc. (Minneapolis, USA). ELISA plates were coated with 100 μL/well of the capture antibody diluted 1:120 in filtered PBS overnight at room temperature. The capture antibody was washed 3x (0.05% Tween-PBS). Plates were blocked using 300 μL/well of blocking buffer (1% bovine serum albumin (BSA) in PBS) for 1h at RT. A seven-point standard curve was created starting at 1000 pg/mL human IL-8 diluted in reagent diluent (0.1% BSA, 0.05% Tween 20 in PBS). The standard curve samples and experimental samples were loaded into the plate in duplicate (100 μL/well) after washing 3x (samples were diluted 1:4 with reagent diluent) and incubated overnight at 4°C. Plates were washed 3x and 100 μL/well of the detection antibody was loaded diluted 1:60 in reagent diluent. The detection

antibody was incubated for 2h at RT. The detection antibody was washed 3x. Horseradish peroxidase (HRP) was added diluted 1:40 in reagent diluent (100 µL/well) to plates and incubated for 20 min. at RT. HRP was washed 3x followed by the addition of TMB substrate (100 µL/well, 3,3',5,5'-Tetramethylbenzidine, Sigma). The TMB reaction was stopped using 100 µL/well of 2N sulfuric acid. Optical density was recorded by spectrophotometry at 450nm.

Cytochrome C Release Immunofluorescence

Cells were seeded on coverslips (ThermoFisher Scientific, 12-545-81, #1.5) in 24 well plates at 500,000 cells/well. After 24-48h, cells were treated with *E. coli* LF82 at 10^8 CFU/mL. At desired time points, cells were rinsed with pre-warmed (37°C water bath) PBS 2x, and fixed with pre-warmed (37°C water bath) 4% paraformaldehyde in PBS (Acros Organics, Thermo Fisher Scientific, 41678-5000, 15min., 37°C). Cells were washed 3x with PBS followed by quenching with NH_4Cl (Sigma, 50 mM, 15 min., RT). Cells were washed 1x with PBS and permeabilized with triton X-100 (Sigma, 0.2%, 15 min., RT). Cells were washed 3x 2 min. with PBS (RT, on shaker). Samples were blocked with 10% goat serum in PBS (Cedarlane, 30 min., RT, on rocker). Samples were incubated with primary antibodies targeting TOM20 (rabbit, Santa Cruz, FL-145, 1:100 diluted in 5% goat serum in PBS, 1h, 37°C) and cytochrome c (mouse, BD Pharminogen, 560263, Alexa Fluor 488, 1:50 diluted in 5% goat serum in PBS, 1h, 37°C). Samples were washed 3x 5 min. with PBS (RT, on shaker), followed by incubation with a secondary

antibody (goat anti-rabbit, ThermoFisher Scientific, Alexa Fluor 568, A11011, 1:1000 diluted in 5% goat serum in PBS, 1h, RT). Samples were washed 3x 5 min. with PBS (RT, on shaker), followed by staining with DAPI (4',6-diamidino-2-phenylindole, 1:1000 in PBS, 5 min., RT, on rocker). Samples were washed 2x 5 min. with PBS (RT, on shaker), coverslips were retrieved from wells using forceps (before removal of PBS from well) and mounted on slides with Dako Fluorescent Mounting Medium, cells facing down on the slide (Dako North America, Inc., Agilent Technologies, CA, USA, S3023), and imaged on Olympus IX83 Confocal Microscope.

Data Presentation and Analysis

Data are presented as mean ± SEM, statistical significance was accepted at $P < 0.05$, where n values represent the number of epithelial preparations. Experiments were repeated 2-5 times. When comparing two groups, Student's t test was performed. When multiple groups were compared, a One Way ANOVA followed by either a Dunnett's Multiple Comparison or Tukey's Multiple Comparison post-test was performed. For non-parametric data, a Kruskal-Wallis followed by Dunn's multiple comparison post-test was performed. For mitochondrial morphology data, differences were recorded if statistical significance was reached comparing percentages of fused or fragmented morphologies. Analyses were conducted by Prism software version 6.0.

RESULTS I: Mitochondrial Dynamics in IBD Patients & Murine Colitis

Patients with IBD have increased expression of genes regulating mitochondrial fusion and fission, suggesting hyper-active processes of mitochondrial dynamics

With no previous data available investigating possible imbalances in mitochondrial dynamics in the context of IBD, qPCR was performed on biopsies isolated from patients with ulcerative colitis and Crohn's disease. Patient groups were separated by inflamed and non-inflamed samples, which were defined by endoscopic appearance at the time of biopsy. Mitochondrial copy number, a measure of overall mitochondrial health by the ratio of mtDNA content to nuclear DNA content [327], was unchanged in patients with IBD (Fig.1A). Inflamed Crohn's disease samples had similar fission mRNA expression to control samples, while OPA1 and MFN1 was increased (Fig.1B,C). Rather than an imbalance in mitochondrial dynamics favoring fission or fusion, non-inflamed CD samples showed increased Drp1, MFN1, and OPA1 gene expression (Fig.1B,C). Patients with ulcerative colitis showed a trend towards reduced mitochondrial copy number (Fig.1A), and inflamed samples had increased mRNA expression of Drp1, Fis1, and MFN1 (Fig.1B).

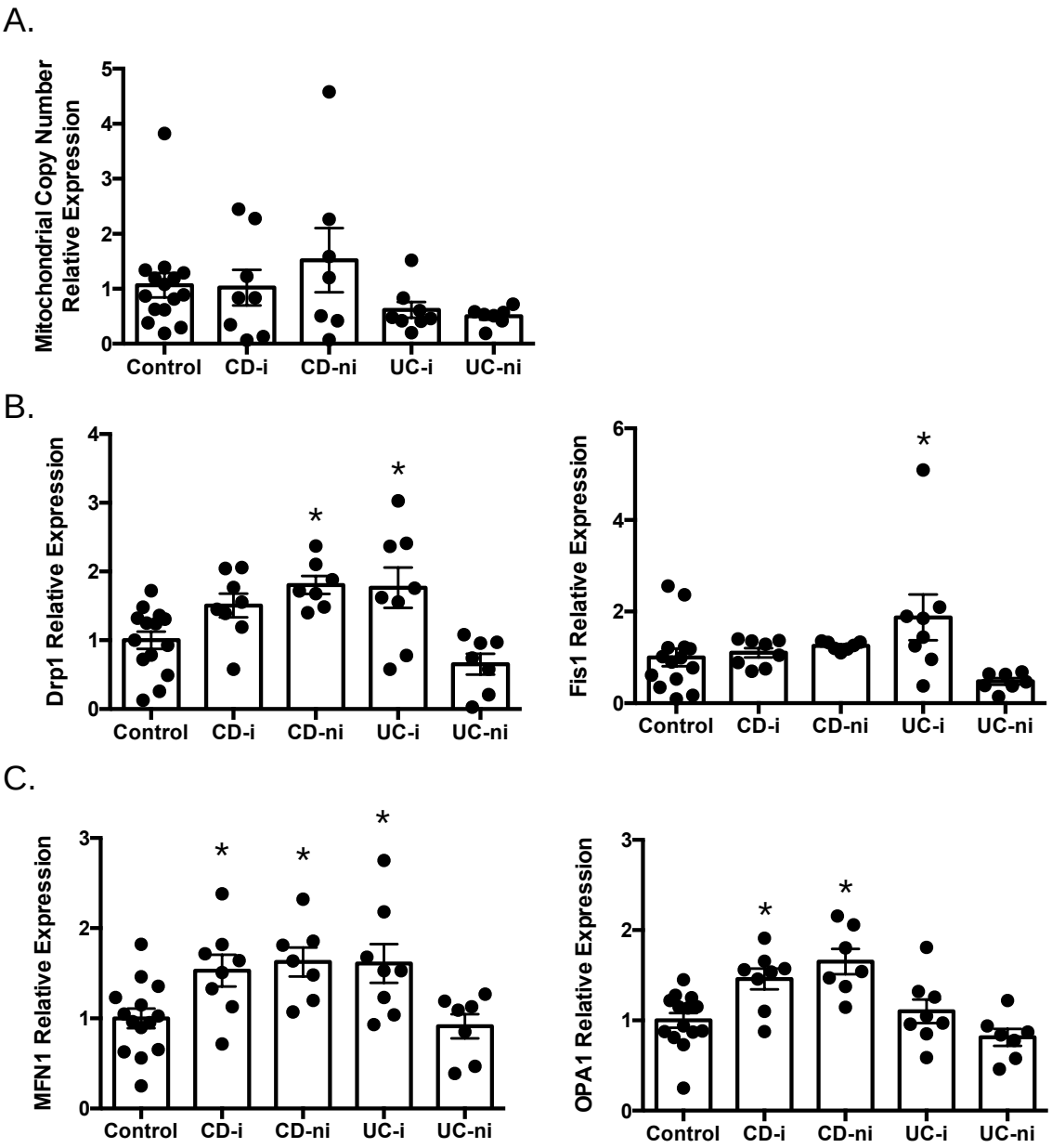

Figure 1. Mitochondrial fission and fusion genes are increased in patients with inflammatory bowel disease. Quantitative PCR analysis of biopsies from an inflamed (i) or non-inflamed (ni) region of the intestine (mostly colon) of patients with Crohn's disease (CD) or ulcerative colitis (UC). Biopsies from control subjects were collected during colon cancer screening. **(A)** Mitochondrial copy number (mitochondrial tRNA-leucine gene expression normalized to ribosomal protein L27 gene expression), **(B)** Mitochondrial fission genes Dynamin-Related Protein 1 (Drp1) and Fission-1 (Fis1), **(C)** Mitochondrial fusion genes Mitofusin 1 (MFN1) and Optic Atrophy Factor 1 (OPA1). Gene of interest is normalized to the housekeeping gene Ribosomal Protein L27 (RPL27), then normalized to the average expression of control, mean ± SEM, *$p<0.05$, One Way ANOVA, Dunnett's multiple comparisons test compared to control.

Markers of increased mitochondrial fission and fusion are apparent in a murine model of colitis

Looking next at a murine model recapitulating some features of IBD, DSS colitis, no differences were seen in mitochondrial copy number or MFF mRNA expression in total colon tissue (Fig.2A,B). Mirroring the results in IBD tissues, Drp1 mRNA expression was elevated at day 5 of DSS-induced colitis, and Fis1 expression was elevated at day 3 and day 5 of colitis in total colon tissue (Fig.2B). The fusion genes MFN1, MFN2, and OPA1 were also elevated at day 5 DSS in total colon tissue (Fig.2C).

Looking more specifically at the epithelial cell compartment of DSS colons, changes were not observed in mitochondrial copy number in the epithelium (Fig.3A). A trend towards increased Drp1 (day 5) and Fis1 (day 5) expression was observed, and an increased expression of MFF occurred at day 1 and day 3 DSS (Fig.3B). Similar to total colon tissue, a trend was seen towards higher expression of fusion genes in epithelial cells at day 5 DSS (Fig.3C).

Considering the increase in Drp1 gene expression in total colon tissue during DSS colitis, phosphorylation of Drp1 at the protein level was determined (Ser616 site – recruits Drp1 to the mitochondria), which was increased at day 5 (Fig.4A,B). This increase in p-Drp1 (Ser616) was not recapitulated in the epithelial cell fraction of DSS colons (Fig.5A,B)

Overall, an upregulation of mitochondrial dynamics genes in IBD patients and murine colitis tissues was observed compared to control. Gene changes

observed were consistent with increases in p-Drp1 (Ser616) in murine colitis tissues.

A. Total colon

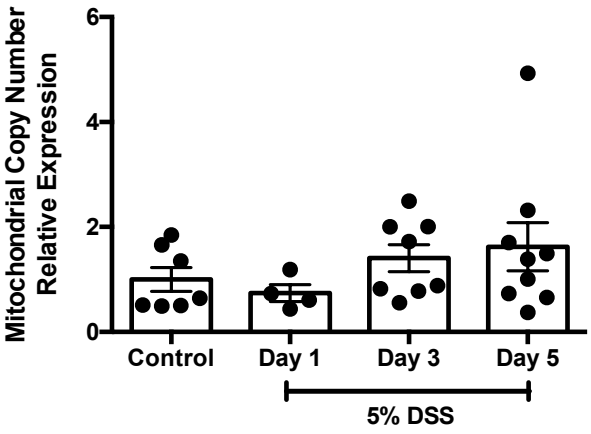

B. Total colon

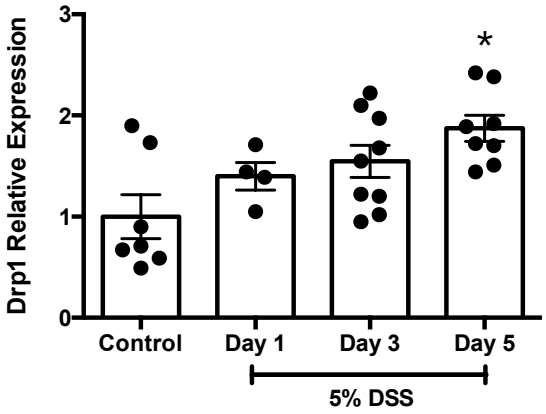

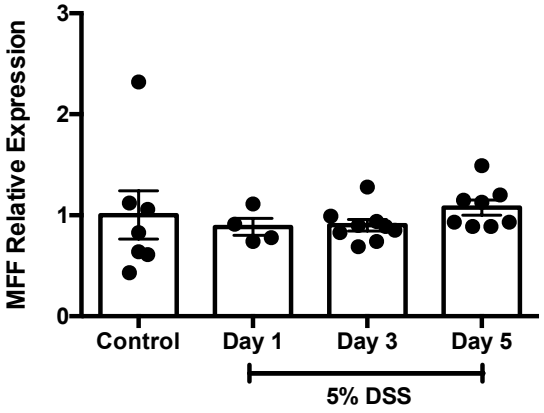

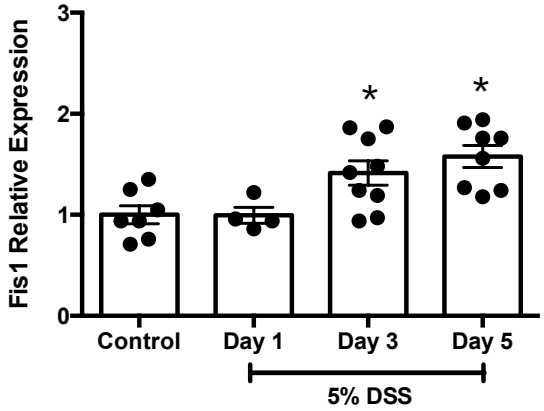

C. Total colon

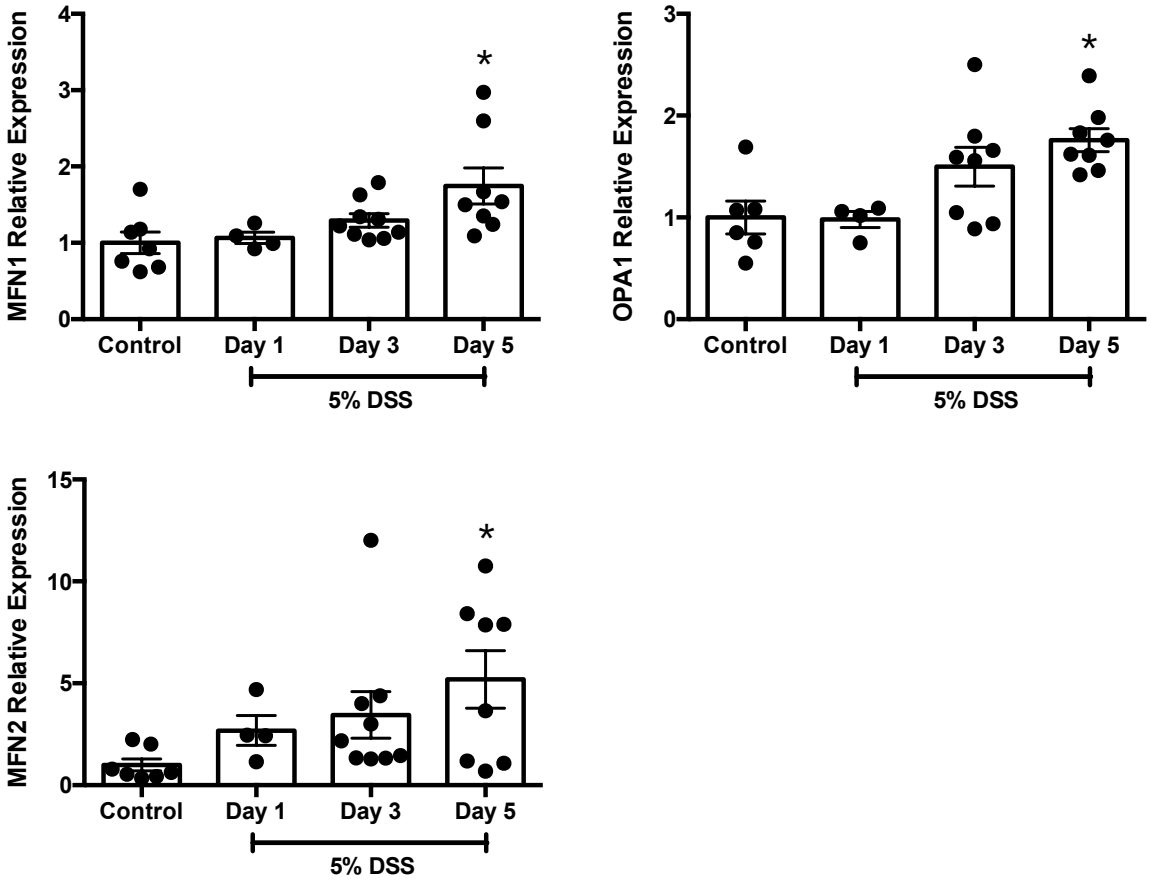

Figure 2. Mitochondrial fission and fusion gene expression is increased in the Dextran Sodium Sulfate (DSS) murine model of colitis in the colon. Male Balb/c mice were treated with 5% DSS drinking water and at necropsy a portion of mid-colon was excised and homogenized in Ribozol for RNA extraction. Quantitative PCR analysis in the total colon tissue of: **(A)** Mitochondrial copy number (Mitochondrial NADH dehydrogenase subunit 1 gene expression normalized to 18S gene expression), **(B)** Dynamin-related protein 1 (Drp1), Mitochondrial fission factor (MFF), and Fission-1 (Fis1), **(C)** Mitofusin 1 (MFN1), Mitofusin 2 (MFN2), and Optic Atrophy Factor 1 (OPA). Gene of interest is normalized to a housekeeping gene (18S), then normalized to the average expression of control, mean ± SEM, *$p<0.05$, One Way ANOVA, Dunnett's multiple comparisons test compared to control.

A. Epithelial cells

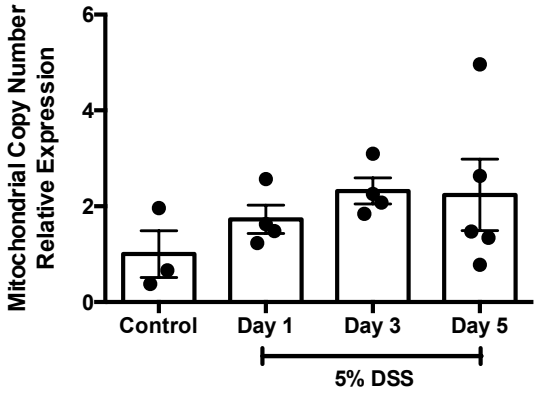

B. Epithelial cells

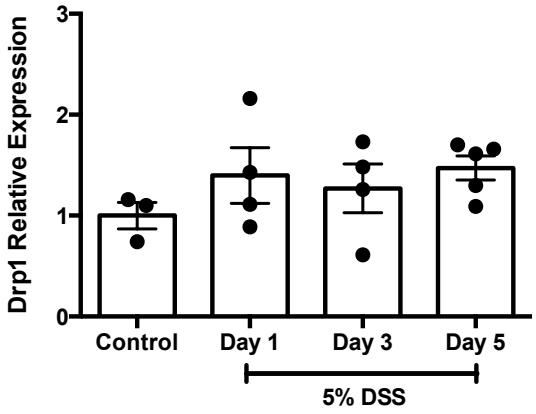

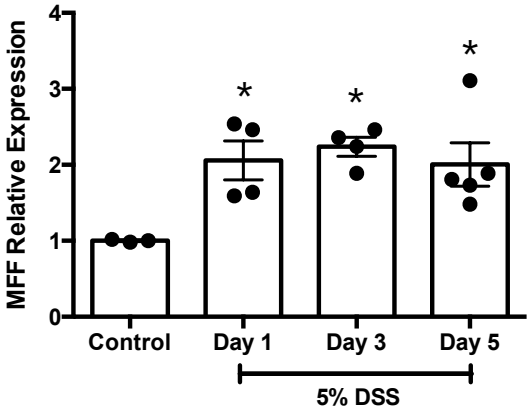

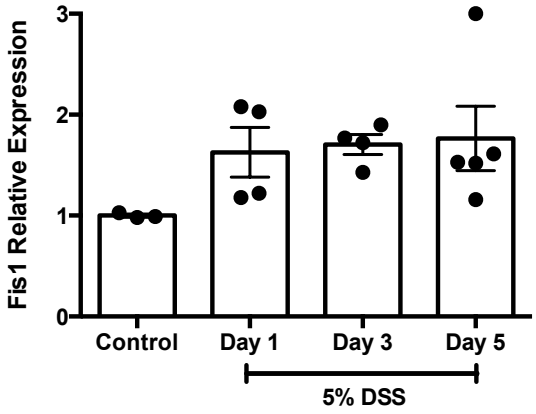

C. Epithelial

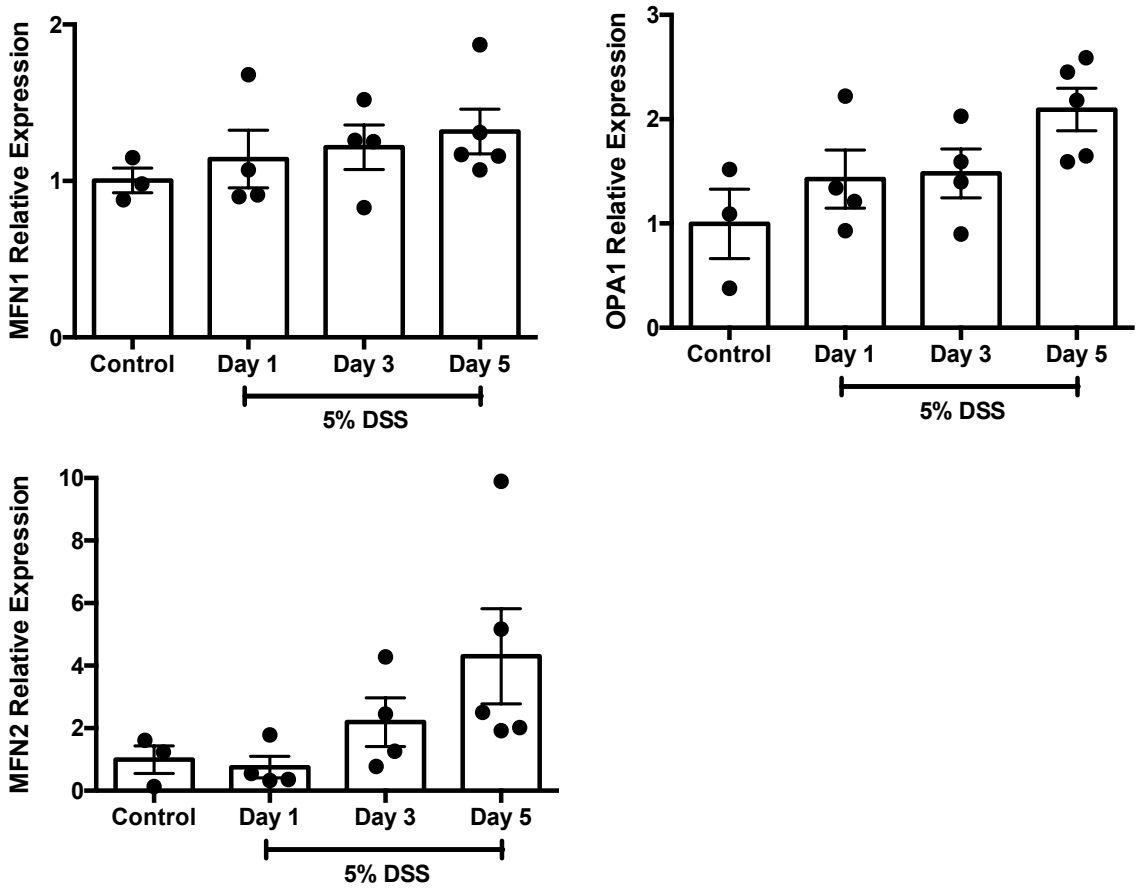

Figure 3. Mitochondrial fission gene expression is increased in the Dextran Sodium Sulfate (DSS) murine model of colitis in epithelial cells. Male Balb/c mice were treated with 5% DSS drinking water and at necropsy the entire colon was excised, epithelial cells dissociated from colon tissue and isolated, and were collected in Ribozol for RNA extraction. Quantitative PCR analysis in the total colon tissue of: **(A)** Mitochondrial copy number (Mitochondrial NADH dehydrogenase subunit 1 gene expression normalized to 18S gene expression), **(B)** Dynamin-related protein 1 (Drp1), Mitochondrial fission factor (MFF), and Fission-1 (Fis1), **(C)** Mitofusin 1 (MFN1), Mitofusin 2 (MFN2), and Optic Atrophy Factor 1 (OPA). Gene of interest is normalized to a housekeeping gene (18S), then normalized to the average expression of control, mean ± SEM, *$p<0.05$, One Way ANOVA, Dunnett's multiple comparisons test compared to control.

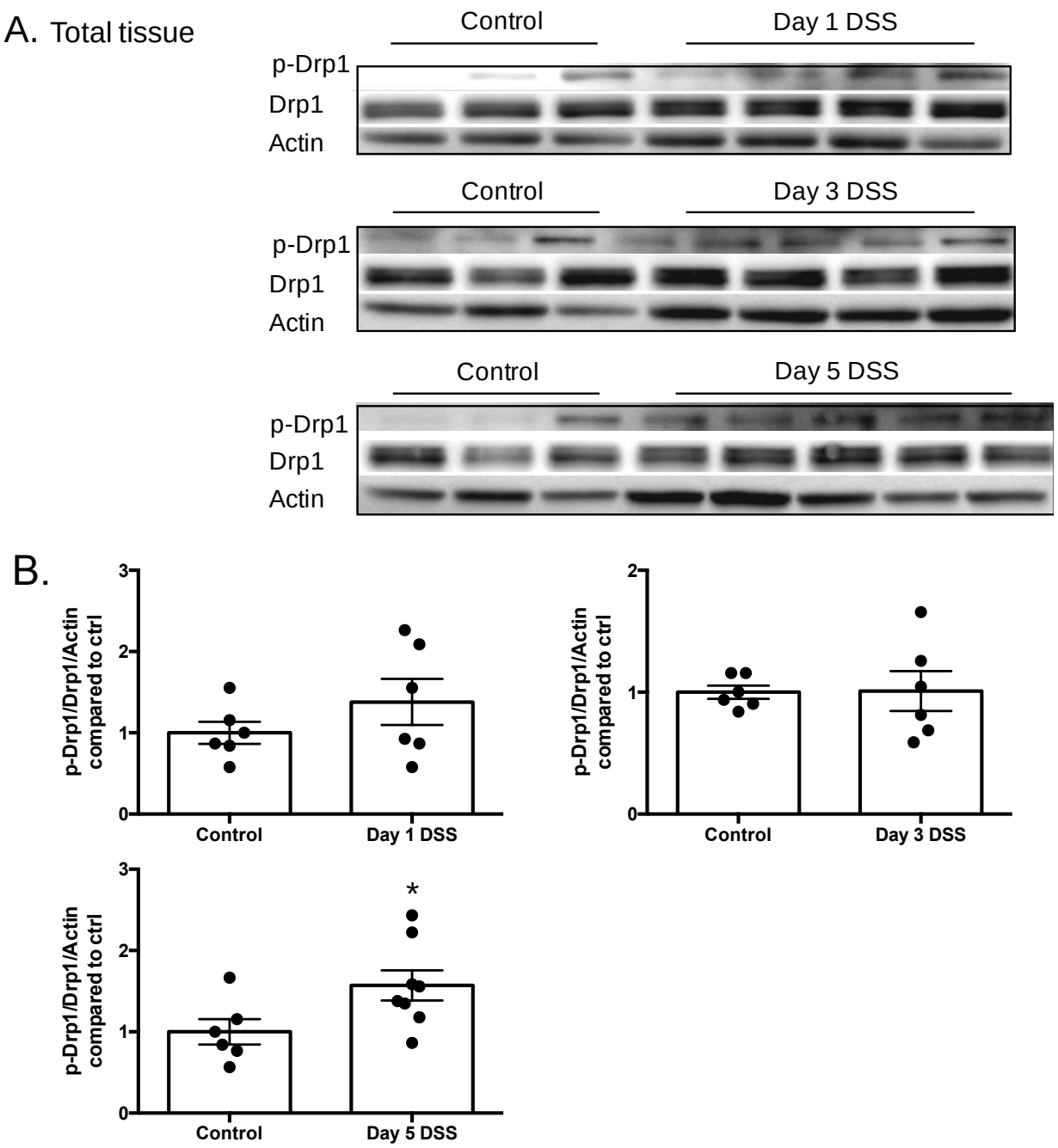

Figure 4. p-Drp1 (Ser616) protein expression is increased at Day 5 in the Dextran Sodium Sulfate colitis model in the colon. Male Balb/c mice were treated with 5% DSS drinking water and at necropsy a portion of mid-colon was excised and homogenized in protein lysis buffer for protein extraction. **(A)** Representative images of western blots of p-Drp1 (Ser616), total Drp1, and actin at Day 1, 3, and 5 5% DSS colitis, **(B)** Densitometry of p-Drp1 (Ser616) expression normalized to total Drp1, normalized to total protein content (actin) using ImageJ software. Mean ± SEM, *p<0.05, t-test.

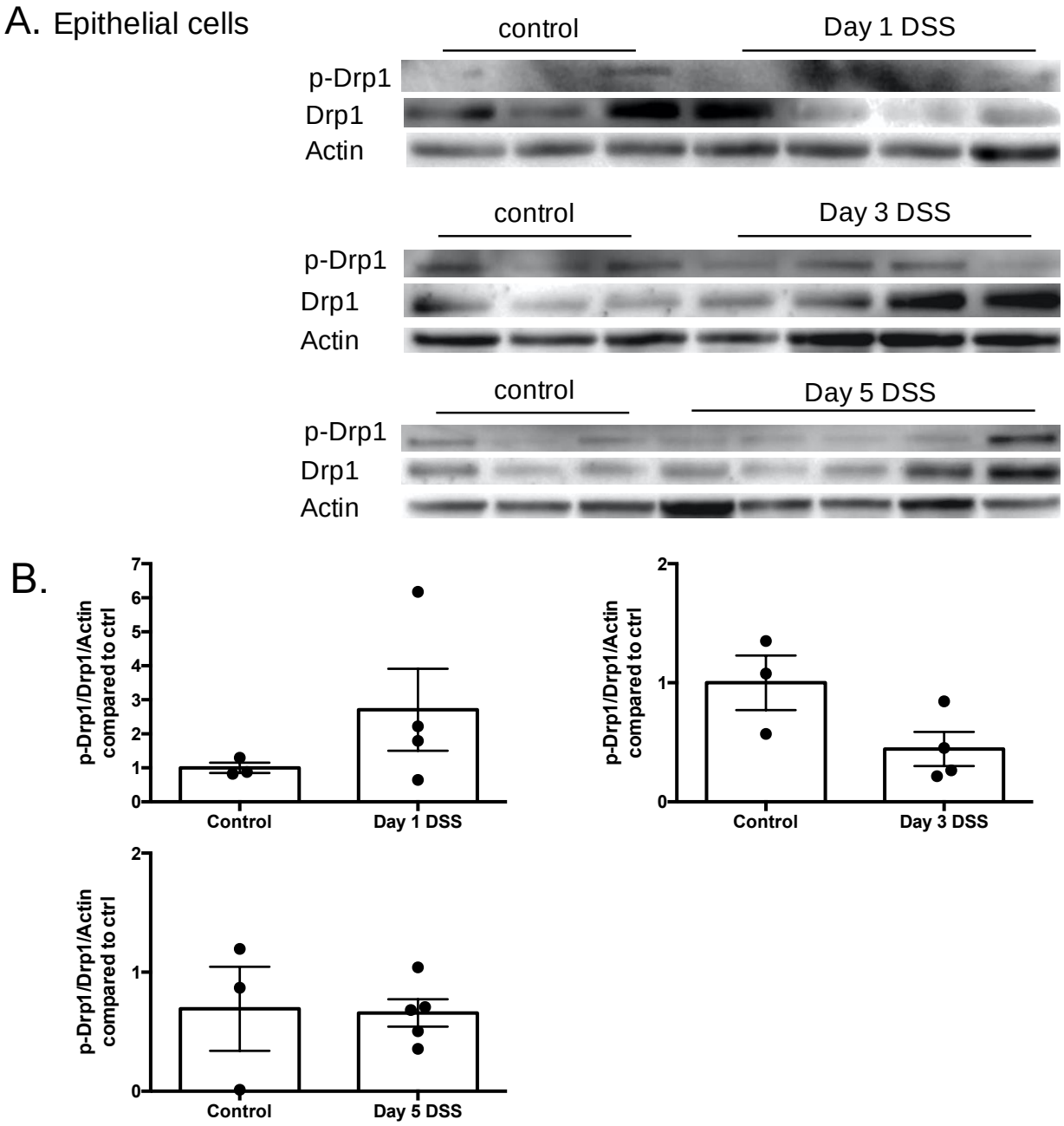

Figure 5. p-Drp1 (Ser616) protein expression is unchanged in the Dextran Sodium Sulfate (DSS) colitis model in epithelial cells. Male Balb/c mice were treated with 5% DSS drinking water and at necropsy the entire colon was excised, epithelial cells dissociated from colon tissue and isolated, which were collected in protein lysis buffer for protein extraction. **(A)** Representative images of western blots of p-Drp1 (Ser616), total Drp1, and actin at Day 1, 3, and 5 5% DSS colitis, **(B)** Densitometry of p-Drp1 (Ser616) expression normalized to total Drp1, normalized to total protein content (actin). Mean ± SEM, *p<0.05, t-test.

RESULTS II: AIEC-Induced Mitochondrial Dysfunction & Fission

AIEC strain LF82 adheres to, and invades inside, T84 human colonic epithelial cells

The T84 human colonic epithelial cell line was used as an *in vitro* model of the gastrointestinal epithelium. The prototypical AIEC strain LF82, which is the most studied AIEC strain [34,39], was used to investigate mitochondrial dynamics in the intestinal epithelium. A commensal laboratory strain *E. coli* HB101, without invasive properties, was used as a negative control. Adhesive and invasive properties of *E. coli* HB101 and *E. coli* LF82 were assessed to define the T84 cell infection model. *E. coli* HB101 and *E. coli* LF82 did not have significantly different growth between 6h and 16h of infection (Fig.6A). After a 4h infection at 10^8 CFU/mL, *E. coli* LF82 adhered to most of the T84 cell monolayer, while *E. coli* HB101 was non-adherent (Fig.6B). *E. coli* LF82 invaded inside T84 cells to a greater degree than *E. coli* HB101 at 2h and 16h (Fig.6C). *E. coli* NRG857c, another strain of AIEC, had reduced invasion compared to *E. coli* LF82 (Fig.6C).

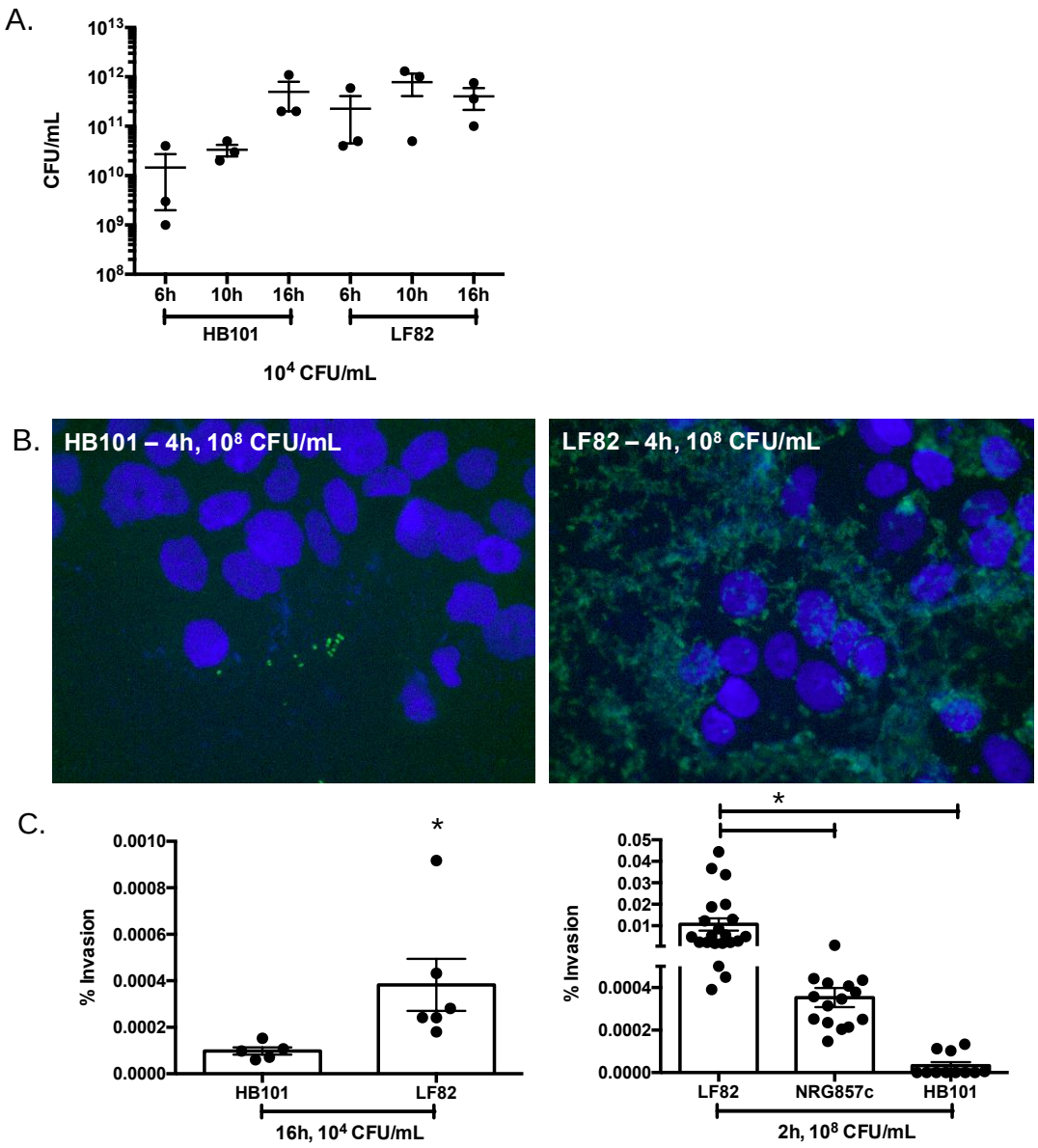

Figure 6. Adherent-invasive *E. coli* LF82 has greater adherence and invasion into T84 cells than *E. coli* HB101. (A) Bacterial growth of *E. coli* HB101 and *E. coli* LF82 at 6h, 10h, and 16h (10^4 CFU/mL) was quantified by growing bacteria in T84 medium at 37°C, serially diluting this bacteria in PBS, and plating on LB (for *E. coli* HB101) or blood agar (for *E. coli* LF82) plates. Plates were grown overnight at 37°C and colonies were counted, Mean ± SEM, *p<0.05, One Way ANOVA, Tukey's Multiple Comparison Test, **(B)** Immunofluorescent staining of T84 cells infection with *E. coli* HB101 or *E. coli* LF82 (green) after washing and fixation. The nucleus was stained by DAPI (blue). Imaged at 20X magnification. **(C)** Bacterial internalization assays of *E. coli* HB101, *E. coli* LF82, and *E. coli* NRG857c in T84 cells performed at 2h (10^8 CFU/mL) and 16h (10^4 CFU/mL), Mean ± SEM, *p<0.05, t-test or One Way ANOVA, Tukey's Multiple Comparison Test.

E. coli LF82 induces mitochondrial dysfunction in T84 cells

Elatrech *et al.* [91] and Jensen *et al.* [80] found that *E. coli* LF82 induce reactive oxygen species production in T84 human colonic epithelial cells, suggesting that *E. coli* LF82 alter mitochondrial function in the gastrointestinal epithelium. In my research, mitochondrial ultrastructure, mitochondrial membrane potential, ATP content, and ROS production were studied as measures of mitochondrial function. At 4h post-infection (10^8 CFU/mL), mitochondrial ultrastructural characteristics such as cristae structure were disrupted as shown by transmission electron microscopy (Fig.7). Mitochondria appear swollen, with few cristae (Fig.7). At 16h post-infection (10^4 CFU/mL), mitochondria are mostly depleted within T84 cells, and those that remain are swollen with few cristae (Fig.7).

At a short time point (3.5h, 10^8 CFU/mL), and a long time point (8.5h, 10^4 CFU/mL), *E. coli* LF82 infection of T84 cells led to depolarization of the mitochondrial membrane, similar to the mitochondrial uncoupler CCCP (Carbonyl cyanide m-chlorophenyl hydrazone), which was used as a positive control (Fig.8A,B). At 8.5h, *E. coli* HB101 infection did not reduce mitochondrial membrane potential significantly below control levels (Fig.8A,B). Loss of membrane potential suggests that these mitochondria are unable to produce ATP through oxidative phosphorylation. This notion was supported by reduced ATP content within T84 cells at 4h (10^8 CFU/mL) or 16h (10^4 CFU/mL) post-infection with *E. coli* LF82 (Fig.9B). A non-invasive *E. coli*, strain F18, had similar levels of ATP to control cells (Fig.9A).

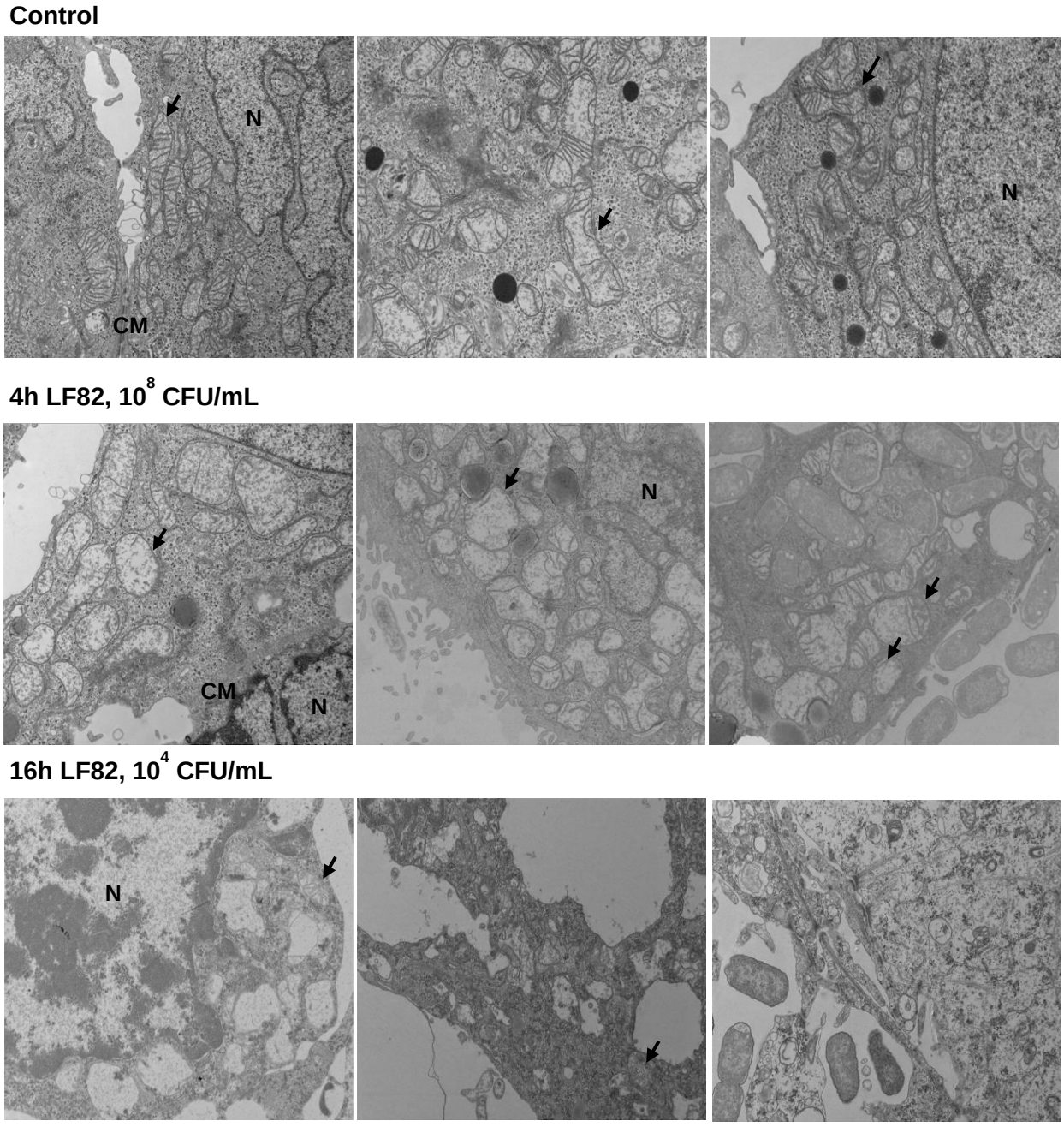

Figure 7. Mitochondrial ultrastructure is disrupted in T84 cells by *E. coli* LF82 infection. Transmission electron microscopy of T84 cells infected with *E. coli* LF82 (4h, 10^8 CFU/mL or 16h, 10^4 CFU/mL). T84 cells were seeded at 500,000 cells/well in a 6-well plate and cultured for 24-48h before treatment. Three representative images per treatment group are shown, each from a different experiment. Arrows indicate mitochondria, N indicates a nucleus, and CM indicates a cell membrane. 5000x magnification. n=4-5 from 3 experiments.

A.

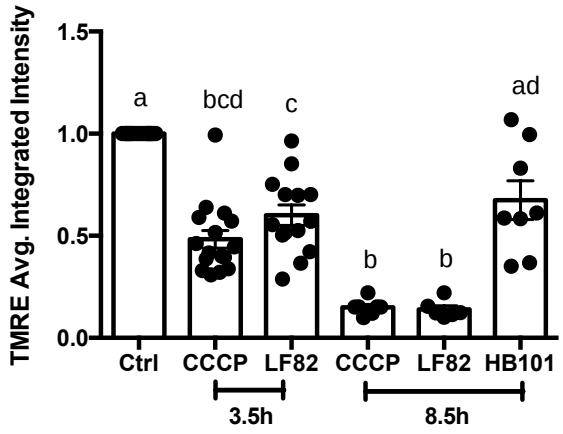

B.

Control

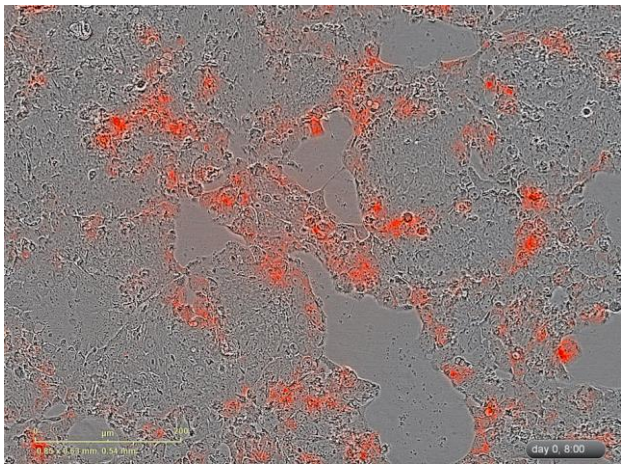

CCCP – 8.5h, 4 μM

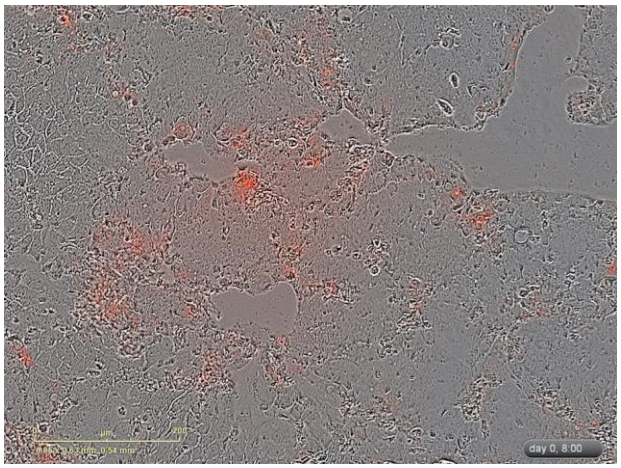

E. coli HB101 – 8.5h, 10^4 CFU/mL

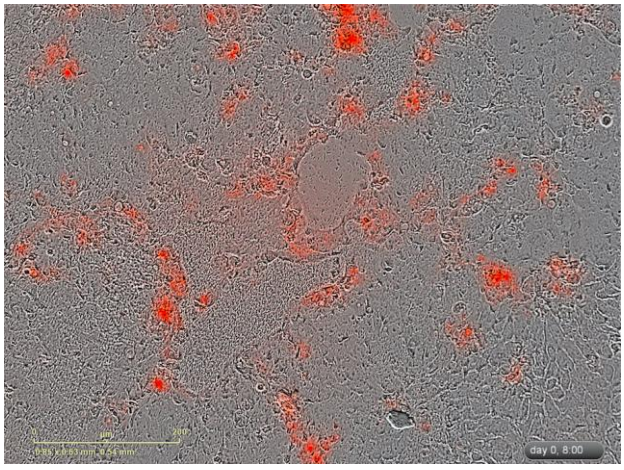

E. coli LF82 – 8.5h, 10^4 CFU/mL

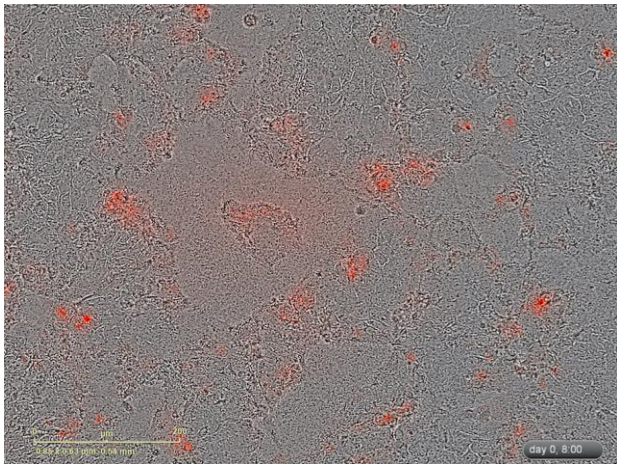

Figure 8. Mitochondrial membrane potential is reduced during *E. coli* LF82 infection. Mitochondrial membrane potential was measured by fluorescence of TMRE (tetramethylrhodamine ethyl ester perchorlate) dye by microscopy. Loss of dye fluorescence indicates loss of mitochondrial membrane potential. T84 cells were seeded at 100,000 cells/well in a 96-well plate and cultured for 24-48h before treatment. **(A)** Quantification of TMRE average integrated fluorescence intensity. Ctrl – control. CCCP (carbonyl cyanide 3-chlorophenylhydrazone) is a mitochondrial uncoupler (3.5h or 8.5h, 4μM). Mean ± SEM, $p<0.05$, different letters indicate statistically significant differences between groups, Kruskal-Wallis, Dunn's multiple comparison test. **(B)** Representative images of TMRE staining of T84 cells.

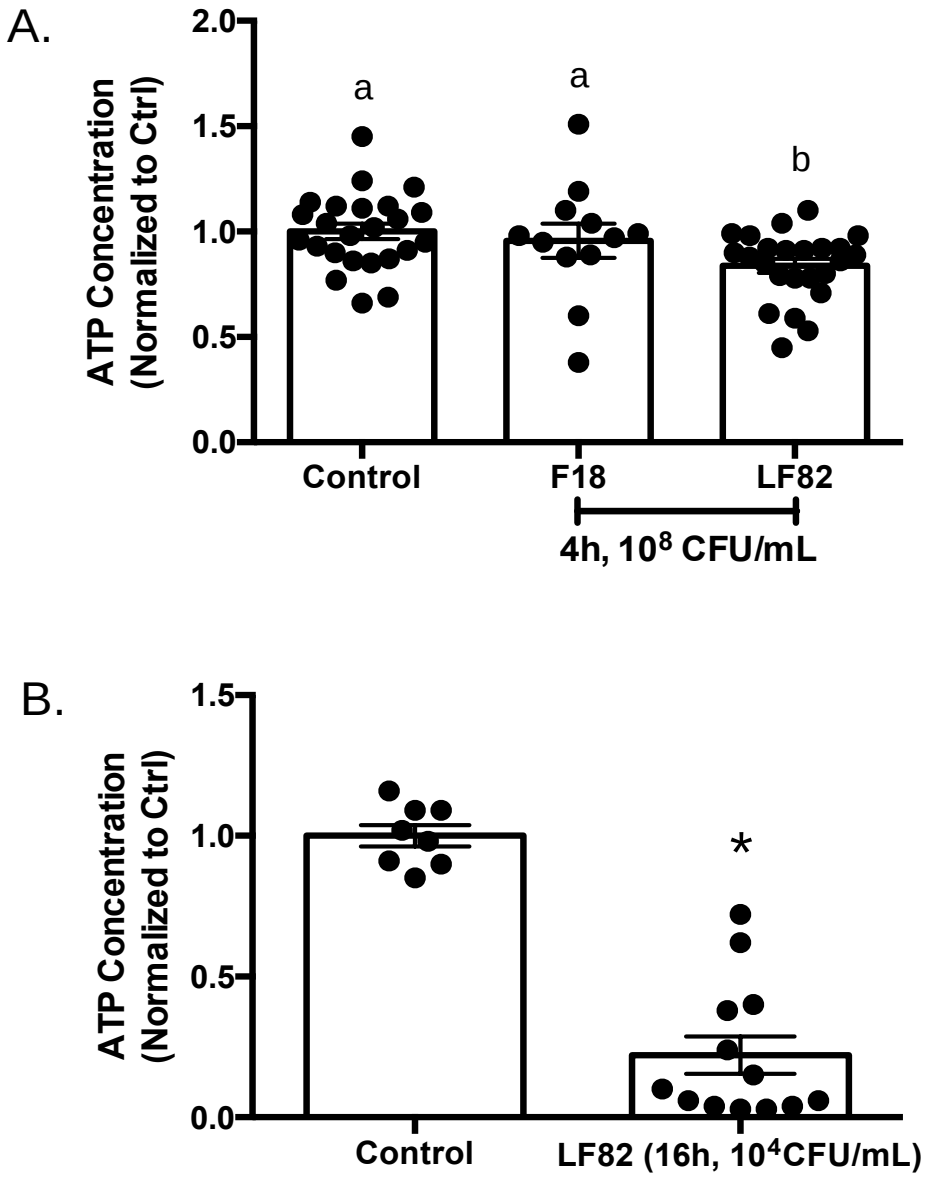

Figure 9. ATP concentration in T84 cells is reduced during *E. coli* LF82 infection. ATP concentration was measured using the Promega CellTiter-Glo Luminescent Cell Viability Assay from T84 cell monolayers infected for **(A)** 4h, 10^8 CFU/mL. F18 is a non-invasive *E. coli* strain. Mean ± SEM, $p<0.05$, different letters indicate statistically significant differences between groups, One Way ANOVA, Tukey's Multiple Comparison test or **(B)** 16h, 10^4 CFU/mL, Mean ± SEM, *$p<0.05$, t-test. T84 cells were seeded at 500,000 cells/well in a 12-well plate and cultured for 24-48h before treatment. ATP concentrations were normalized to 100 μg of protein as measured by the Bradford assay.

Reactive oxygen species were assessed by the DCFDA (2′,7′-Dichlorodihydrofluorescein diacetate) fluorescent dye which binds to most cellular ROS [328]. At 4h, 6h, and 16h post-infection, T84 cells infected with neither *E. coli* LF82 or *E. coli* HB101 had increased ROS compared to uninfected cells (Fig.10). The positive control rotenone, an inhibitor of the electron transport chain complex I, induced a statistically significant increase in ROS at all time points (Fig.10).

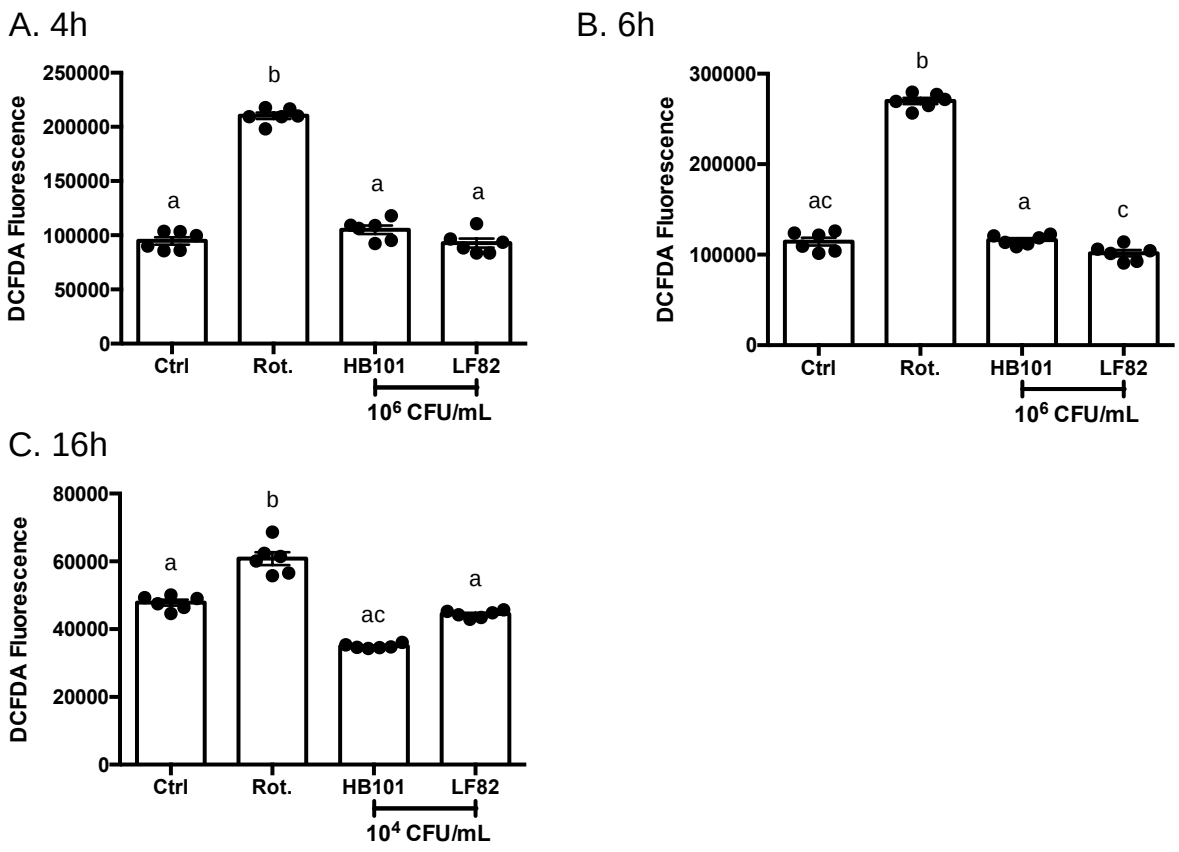

Figure 10. ROS production is not induced by *E. coli* LF82 infection in T84 cells. ROS was measured by DCFDA (2',7'-dichlorodihydrofluorescein diacetate, stained for 30min., 25 μM, prior to treatment) fluorescence, read by a spectrophotometer (excitation/emission = 485/535 nm) at **(A)** 4h, **(B)** 6h, and **(C)** 16h. T84 cells were seeded at 250,000 cells/well in a 96-well plate and cultured for 24-48h before treatment. Ctrl – Control. Rot - Roteneone (40 μM), an electron transport chain complex I inhibitor, was used a positive control. *E. coli* HB101 is a non-invasive, laboratory *E. coli* strain. $p<0.05$, different letters indicate statistically significant differences between groups, One Way ANOVA, Tukey's Multiple Comparison Test.

Mitochondrial fragmentation is associated with E. coli LF82 infection of T84 cells

Considering the literature suggesting that intracellular pathogens often induce imbalances in the processes of mitochondrial dynamics, ultimately leading to altered mitochondrial network structure (Table 5), I imaged mitochondrial networks in T84 cells infected with *E. coli* LF82 at several time points by confocal microscopy. Control T84 cells displayed mostly fused and intermediate mitochondrial network morphology, while CCCP (a positive control) induced complete fragmentation of the mitochondrial network at 4h or 16h (Fig.11A,B). *E. coli* LF82 also induced fragmentation of the mitochondrial network at short time points (2h, 4h, 10^8 CFU/mL), and a long time point (16h, 10^4 CFU/mL) to a degree that was statistically different from uninfected cells (Fig.11A,B). *E. coli* HB101 induced an intermediate mitochondrial network phenotype with more fragmented cells and less fused cells compared to control, without the complete fission observed in *E. coli* LF82 treated cells (16h, 10^4 CFU/mL) (Fig.11A,B). *E. coli* LF82 induced fission occurred in Caco-2 and HT29 cells as well (Fig.12).

In summary, *E. coli* LF82 infection induced mitochondrial dysfunction and mitochondrial fission at short and long time points, which was not observed with the non-invasive strains of *E. coli*, HB101 and F18.

A. **Control** **CCCP 16h, 4μM** **HB101 16h, 10^4 CFU/mL**

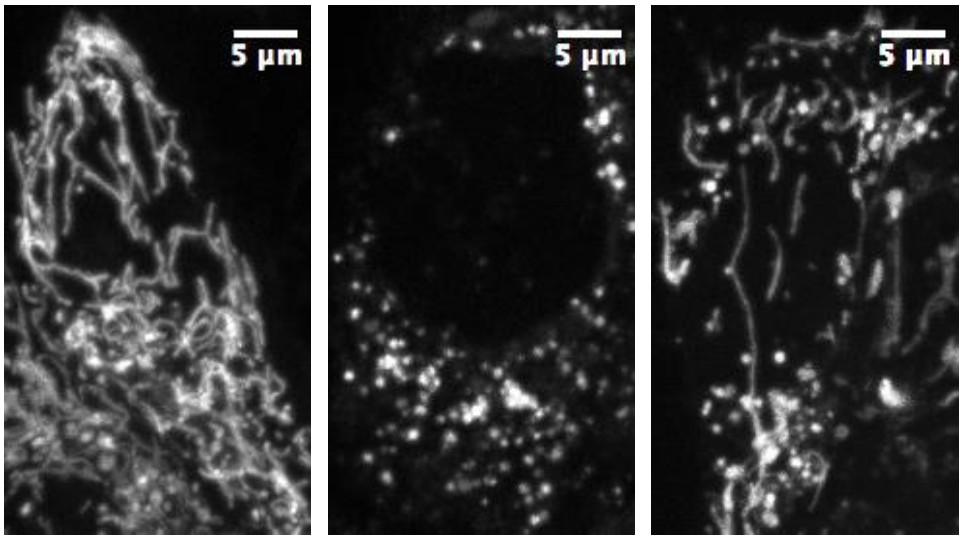

LF82 2h, 10^8 CFU/mL **LF82 4h, 10^8 CFU/mL** **LF82 16h, 10^4 CFU/mL**

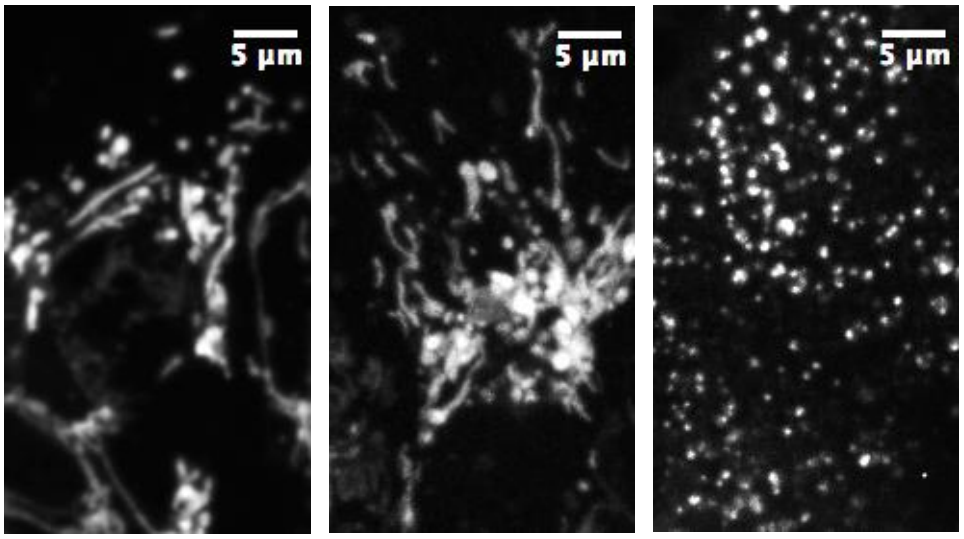

B.

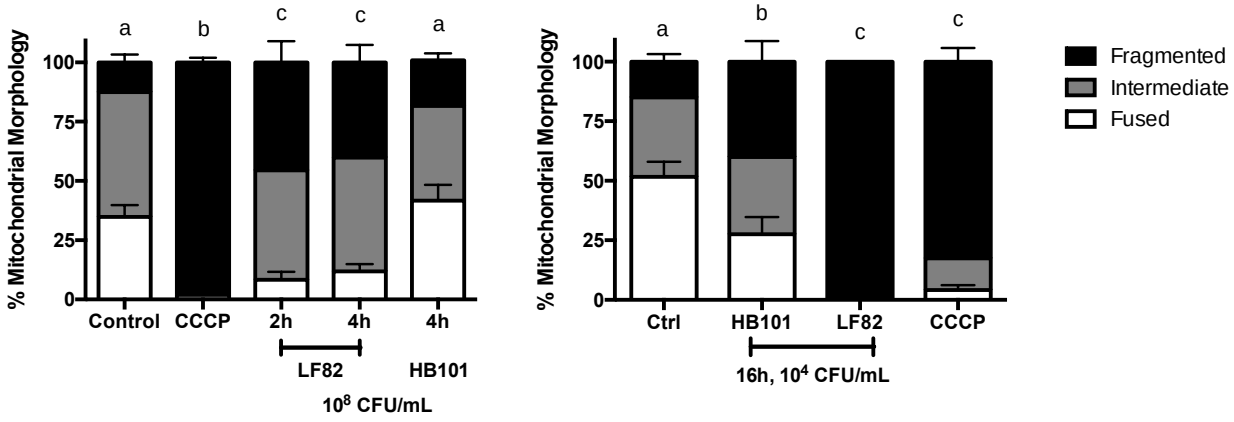

Figure 11. Infection with *E. coli* LF82 induces mitochondrial fragmentation. Mitochondrial networks were stained live with mitotracker red dye and imaged by confocal microscopy at 63X magnification. T84 cells were seeded at 250,000 cells/well in an 8-well chamber slide and cultured for 24-48h before staining and treatment. **(A)** Representative images, **(B)** Quantification of mitochondrial networks performed by choosing 1 cell within a field of view by nuclear staining (Hoescht), and rating that cell as "fragmented", "intermediate", or "fused". Twenty fields of view (20 cells total) were rated per monolayer. Ctrl – control. CCCP (carbonyl cyanide 3-chlorophenylhydrazone) is a mitochondrial uncoupler used as a positive control for fragmented mitochondrial morphology (4h or 16h, 4μM). *E. coli* HB101 is a non-invasive, laboratory strain of *E. coli*. The bacterial inoculum at 2h and 4h was 10^8 CFU/mL, at 16h it was 10^4 CFU/mL. Mean ± SEM, $p<0.05$, different letters indicate statistically significant differences between groups, Two Way ANOVA, Tukey's Multiple Comparison Test, n=6 from 3 experiments.

A.

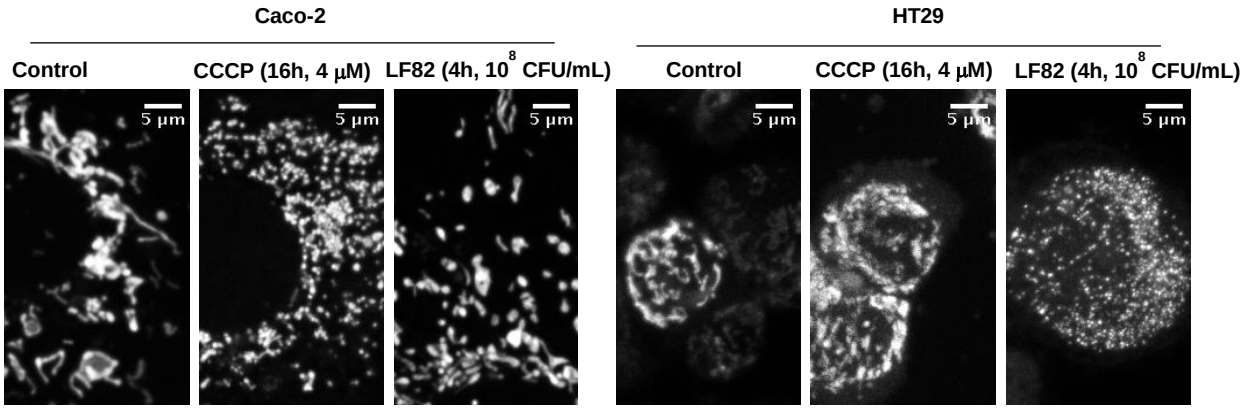

B. Caco-2

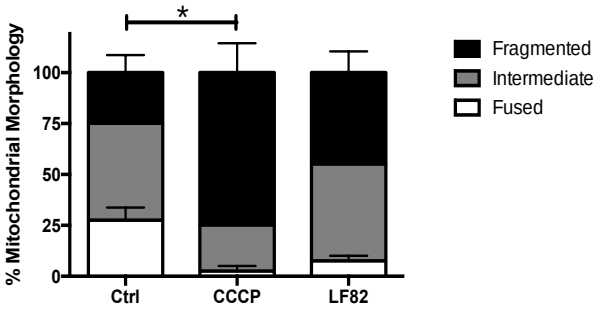

Figure 12. *E. coli* LF82 induces mitochondrial fragmentation in Caco-2 and HT29 cell lines. Mitochondrial networks were stained live with mitotracker red dye and imaged by confocal microscopy at 63X magnification. Caco-2 and HT29 cells were seeded at 250,000 cells/well in an 8-well chamber slide and cultured for 24-48h before staining and treatment. **(A)** Representative images, **(B)** Quantification of mitochondrial networks in Caco-2 cells was performed by choosing 1 cell within a field of view by nuclear staining (Hoescht), and rating that cell as "fragmented", "intermediate", or "fused". Twenty fields of view (20 cells total) were rated per monolayer. CCCP (carbonyl cyanide 3-chlorophenylhydrazone) is a mitochondrial uncoupler used as a positive control for fragmented mitochondrial morphology (4h or 16h, 4μM). Ctrl – control. Mean ± SEM, *$p<0.05$, One Way ANOVA, Dunnett's Multiple Comparison Test, compared to control n=4 from 2 experiments.

RESULTS III: Mechanisms of AIEC-Induced Fission

E. coli LF82-induced fission is dependent on live bacteria and adherence to T84 cells

After observing that *E. coli* LF82 induced mitochondrial fission in 3 human intestinal epithelial cell lines, it was of interest to interrogate the mechanism through which the bacteria has the capacity to impact mitochondria. In order to test the role of soluble mediators in the T84 cell *E. coli* LF82 co-culture, spent medium from this co-culture was prepared to determine if spent medium alone would induce mitochondrial fission in the absence of bacteria. Spent medium was isolated by co-culturing *E. coli* LF82 with T84 cells (as in a regular infection regimen), collecting the media at 16h (containing LF82), centrifuging this media to obtain only the supernatant (leaving LF82 behind in the pellet), and filtering this supernatant to ensure exclusion of any bacteria. Naïve epithelial cells were treated with this spent medium preparation. Spent medium-treated T84 cells had a similar mitochondrial morphology profile to untreated cells (Fig.13A,B), while CCCP and *E. coli* LF82 (positive controls) had fragmented mitochondrial morphology.

To determine if live bacteria were necessary for this effect, *E. coli* LF82 were treated with 2.5% glutaraldehyde, resulting in fixation of the bacteria; cells treated with dead bacteria had primarily fused and intermediate mitochondrial morphologies, similar to control (Fig.13A,B). Fixed bacteria that were plated on blood agar plates resulted in no colonies.

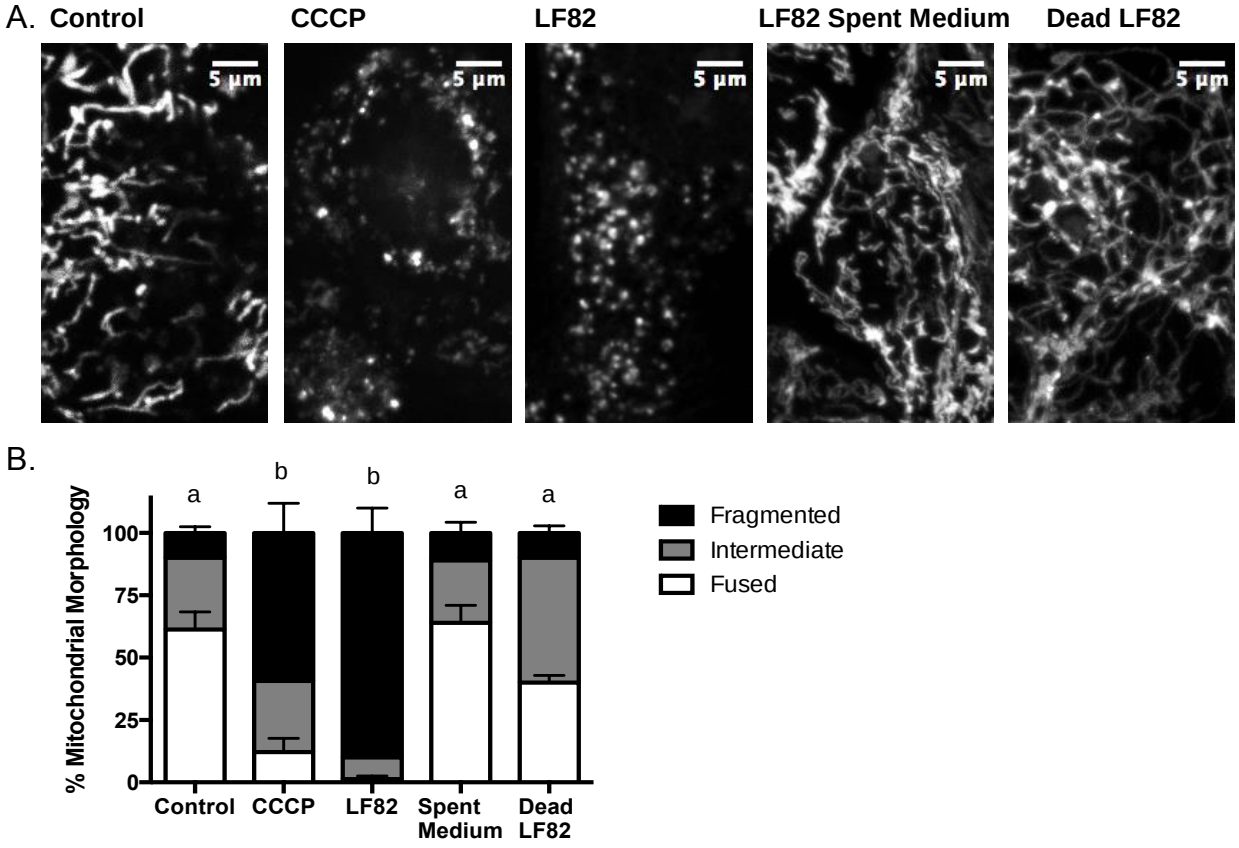

Figure 13. *E. coli* LF82-induced mitochondrial fragmentation is dependent on adherence of live bacteria. Mitochondrial networks were stained live with mitotracker red dye and imaged by confocal microscopy at 63X magnification. T84 cells were seeded at 250,000 cells/well in an 8-well chamber slide and cultured for 24-48h before staining and treatment. **(A)** Representative images, **(B)** Quantification of mitochondrial networks performed by choosing 1 cell within a field of view by nuclear staining, and rating that cell as "fragmented", "intermediate", or "fused". Twenty fields of view (20 cells total) were rated per cell monolayer. CCCP (carbonyl cyanide 3-chlorophenylhydrazone) is a mitochondrial uncoupler used as a positive control for fragmented mitochondrial morphology (4h, 4 µM). The *E. coli* LF82 inoculum was 10^4 CFU/mL for 16h. Spent medium was prepared by growing *E. coli* LF82 with cells for 16h (10^4 CFU/mL), collecting the medium at 16h, spinning down the bacteria (10 min., 1258 *g*), collecting the supernatant and filtering it (0.2 µM filter). Naïve T84 cells were treated with this spent medium to assess mitochondrial morphology. Dead *E. coli* LF82 were prepared by fixing live *E. coli* LF82 after a 16h co-culture period with T84 cells (10^4 CFU/mL) using 2.5% glutaraldehyde. Mean ± SEM, $p<0.05$, different letters indicate statistically significant differences between groups, Two Way ANOVA, Tukey's Multiple Comparison Test, n=3-8 from 4 experiments.

Invasion drives E. coli LF82-induced mitochondrial fission

As *E. coli* LF82 is an invasive bacterium, I was interested to determine if AIEC-induced mitochondrial fission was dependent on invasion into T84 cells. Another AIEC strain, *E. coli* NRG857c, had reduced invasion inside T84 cells compared to *E. coli* LF82 at 2h (Fig.6C). Reduced invasion by *E. coli* NRG857c correlated with a reduction in fragmentation and an increase in fused mitochondrial networks compared to *E. coli* LF82 (Fig.14A,B). As invasion correlated with the degree of mitochondrial fragmentation, I investigated the role of invasion further using an *E. coli* LF82 strain containing a mutation in the FimH gene encoding the bacterial pilus. This strain had reduced invasion inside T84 cells (Fig.15A), and cells treated with the mutant strain displayed a similar mitochondrial morphology profile to untreated cells (Fig.15B,C), although the wild-type counterpart of this mutant strain induced increased mitochondrial fragmentation compared to control (Fig.15B,C).

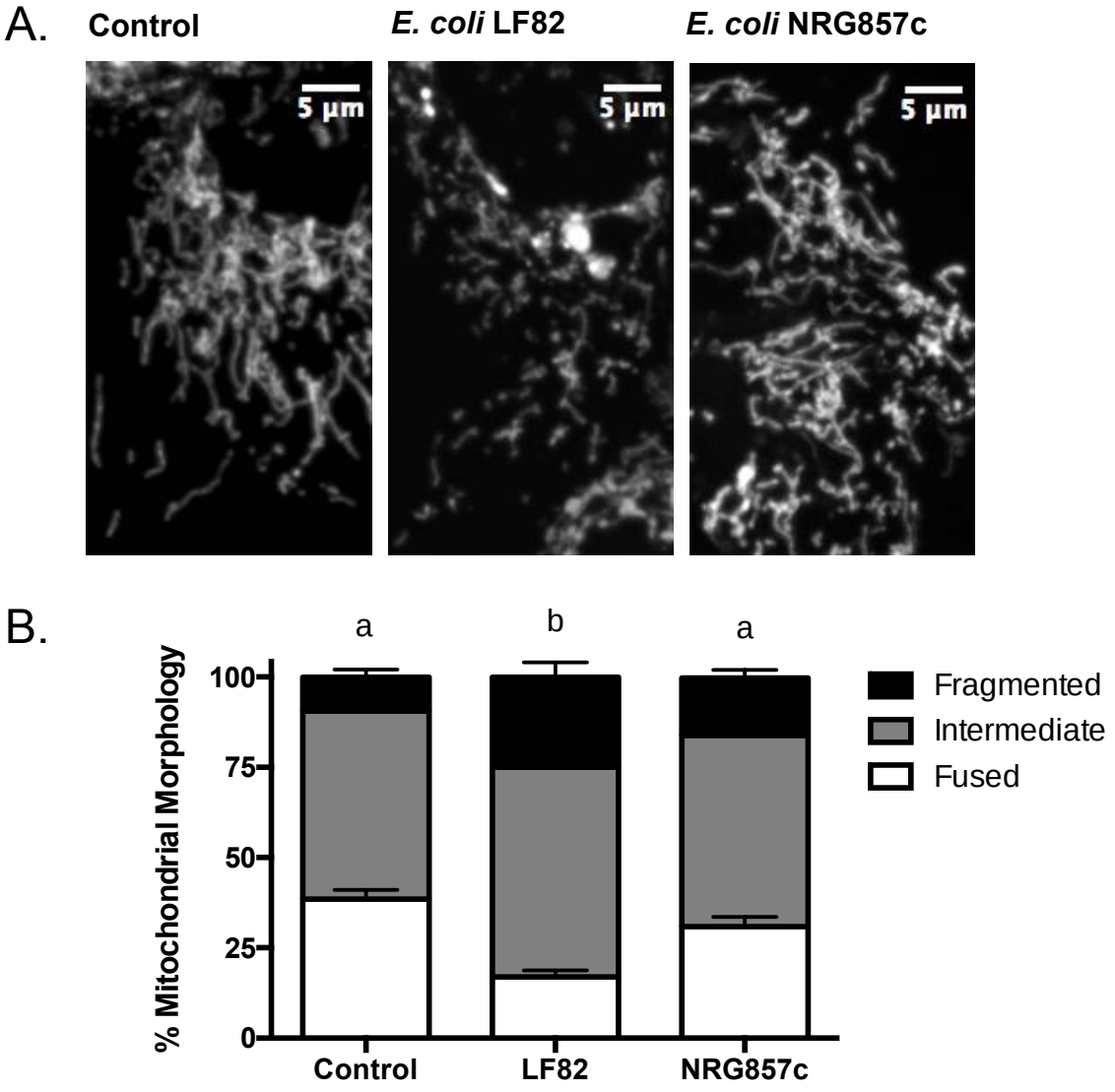

Figure 14. Mitochondrial fragmentation induced by adherent-invasive *E. coli* is correlated with invasion into epithelial cells. Mitochondrial networks were stained live with mitotracker red dye and imaged by confocal microscopy at 63X magnification. T84 cells were seeded at 250,000 cells/well in an 8-well chamber slide and cultured for 24-48h before staining and treatment. **(A)** Representative images, **(B)** Quantification of mitochondrial networks performed by choosing 1 cell within a field of view by nuclear staining, and rating that cell as "fragmented", "intermediate", or "fused". 20 fields of view (20 cells total) were rated per cell monolayer. T84 cells were treated for 2h with 10^8 CFU/mL of *E. coli* LF82 or *E. coli* NRG857c. Mean ± SEM, $p<0.05$, different letters indicate statistically significant differences between groups, Two Way ANOVA, Tukey's Multiple Comparison Test, n=17-18 from 9 experiments.

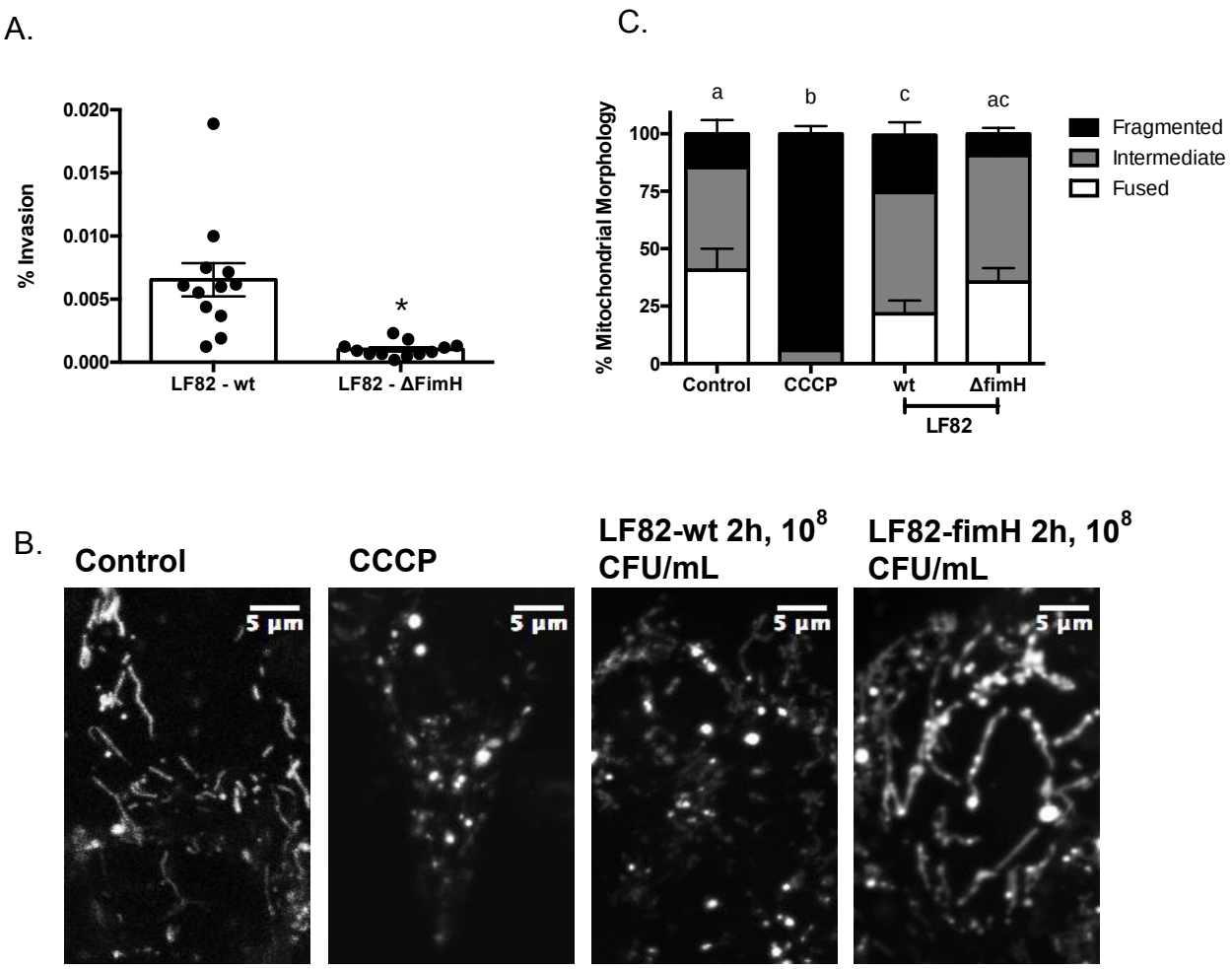

Figure 15. Mitochondrial fragmentation induced by *E. coli* LF82 is dependent on invasion. (A) Numbers of intracellular bacteria 2h post-infection (10^8 CFU/mL) with wild type (wt) and FimH mutant *E. coli* LF82 (ΔfimH), mean ± SEM, *p<0.05, t-test. T84 cells were seeded at 500,000 cells to 1 million cells/well and cultured for 24-48h before treatment. **(B)** Representative images of mitochondrial networks were stained live with mitotracker red dye and imaged by confocal microscopy at 63X magnification. T84 cells were seeded at 250,000 cells/well in an 8-well chamber slide and cultured for 24-48h before staining and treatment. **(C)** Quantification of mitochondrial networks performed by choosing 1 cell within a field of view by nuclear staining, and rating that cell as "fragmented", "intermediate", or "fused". Twenty fields of view (20 cells total) were rated per cell monolayer. CCCP (carbonyl cyanide 3-chlorophenylhydrazone) is a mitochondrial uncoupler used as a positive control for fragmented mitochondrial morphology (2h, 4 µM). Mean ± SEM, p<0.05, different letters indicate statistically significant differences between groups, Two Way ANOVA, Tukey's Multiple Comparison Test, n=8-10 from 5 experiments.

Reactive oxygen species do not drive E. coli LF82-induced fission

After investigating the bacterial characteristics that were necessary to induce mitochondrial fission, I next questioned which host factors played a role in driving mitochondrial fission. Although elevated ROS in response to *E. coli* LF82 was not observed in T84 cells by DCFDA staining (Fig.10), there is evidence that ROS can propagate mitochondrial fragmentation in the literature [329–333]. Considering this, it is possible that even small amounts of ROS that are under the level of detection by the DCFDA assay used to measure ROS in my study could impact mitochondrial dynamics. *E. coli* LF82-induced fission was still observed 16h post-infection (10^4 CFU/mL) (Fig.16A,B) after confirming that vitamin C (targets total cellular ROS) and Mito-TEMPO (targets mitochondrial-derived ROS) reduced ROS production induced by rotenone (a complex I inhibitor) (Fig.16C).

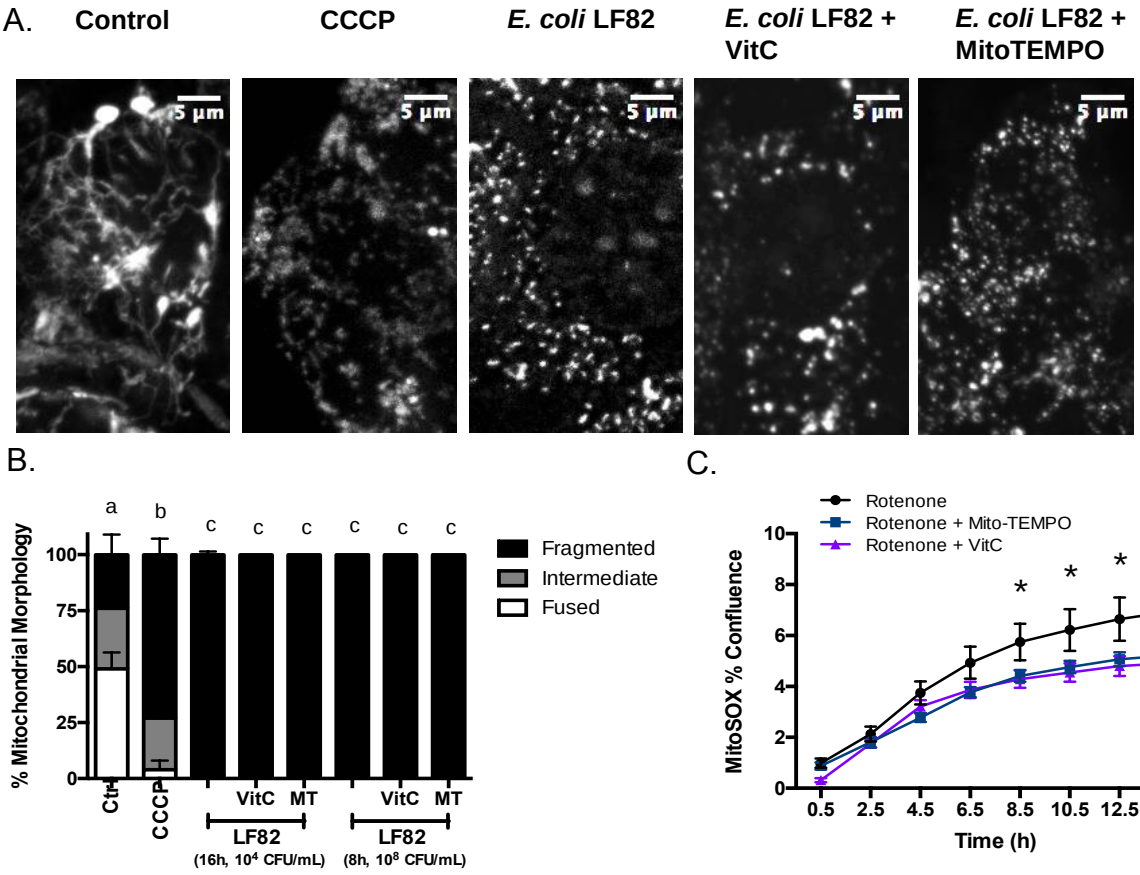

Figure 16. Use of antioxidants did not block *E. coli* LF82-induced epithelial mitochondrial fragmentation. Mitochondrial networks were stained live with mitotracker red dye and imaged by confocal microscopy at 63X magnification. T84 cells were seeded at 250,000 cells/well in an 8-well chamber slide and cultured for 24-48h before staining and treatment. **(A)** Representative images, **(B)** Quantification of mitochondrial networks performed by choosing 1 cell within a field of view by nuclear staining, and rating that cell as "fragmented", "intermediate", or "fused". Twenty fields of view (20 cells total) were rated per cell monolayer. CCCP (carbonyl cyanide 3-chlorophenylhydrazone) is a mitochondrial uncoupler used as a positive control for fragmented mitochondrial morphology (16h, 4 µM). Vitamin C (16h, 0.25 mM), and MitoTEMPO (16h, 10 µM) are antioxidants. Mean ± SEM, $p<0.05$, different letters indicate statistically significant differences between groups, Two Way ANOVA, Tukey's Multiple Comparison Test. n=5-7 from 3 experiments. **(C)** Cells were stained with MitoSOX dye to detect whole cellular ROS, and imaged every 2h, and the confluence of well with positive staining was quantified. Mean ± SEM, *$p<0.05$, Two Way ANOVA, Dunnett's Multiple Comparison Test compared to rotenone. Rotenone, an electron transport chain complex I inhibitor, was used a positive control (40 µM).

Protein levels of fission mediators are not increased in association with LF82-induced fission

Within the host cell, many mitochondrial proteins play a role in regulating mitochondrial network morphology [219]. Drp1, the main mediator of mitochondrial fission, was measured as the most likely candidate driving *E. coli* LF82-induced fission. The role of Drp1 was assessed first by measuring protein levels of p-Drp1 (Ser616), which is a form of Drp1 that is recruited to the mitochondria, allowing activation of the Drp1 GTPase and resulting in fission [154]. Unexpectedly, increased p-Drp1 (Ser616) was not apparent at 2-4h post-infection (10^8 CFU/mL) (Fig.17A,B).

In some experiments the ratio between p-Drp1 to Drp1 seemed to be increased (red star), whereas some experiments showed a reduced level of p-Drp1 compared to Drp1 (red pound symbol) (Fig.17A). Over longer time periods at a lower dose (10^6 CFU/mL), changes in p-Drp1 seem to occur but were inconsistent between experiments (indicated with the red star) (Fig.18A). Overall, there was no statistically significant difference over time in p-Drp1 at a single time point (Fig.18C). At several bacterial inoculums at 8h or 16h, p-Drp1 (Ser616) in T84 cells remained unchanged overall (Fig.18A,B), although increases or decreases in p-Drp1 were observed in isolated experiments (indicated with red stars).

As Drp1 undergoes many post-translational modifications that effect its location or degradation [154], recruitment of Drp1 to the mitochondria was measured by fractionating cytosolic and mitochondrial protein lysates, the purity of which was assessed by measuring tubulin and VDAC in the cytosolic and mitochondrial lysates

(Fig.19). At a short-term time point (2-4h, 10^8 CFU/mL), increases in Drp1 in the mitochondrial protein fraction were observed in some experiments that were not replicated in others (indicated by red stars) (Fig.20A). Overall, no consistent changes in Drp1 content within the mitochondrial protein fraction were observed short term (2-4h, 10^8 CFU/mL) (Fig.20A,B).

At a lower dose (10^6 CFU/mL) over a time course, increases or decreases in Drp1 in the mitochondrial protein fraction were observed at different time points that were inconsistent between experiments (indicated by red stars), with no change overall (Fig.21A,C). Similar results were observed at 8h or 16h at a variety of bacterial inoculums where differences were observed in specific conditions that were not replicated throughout all experiments, therefore no change overall was apparent (Fig.21B,D).

A. Short time point

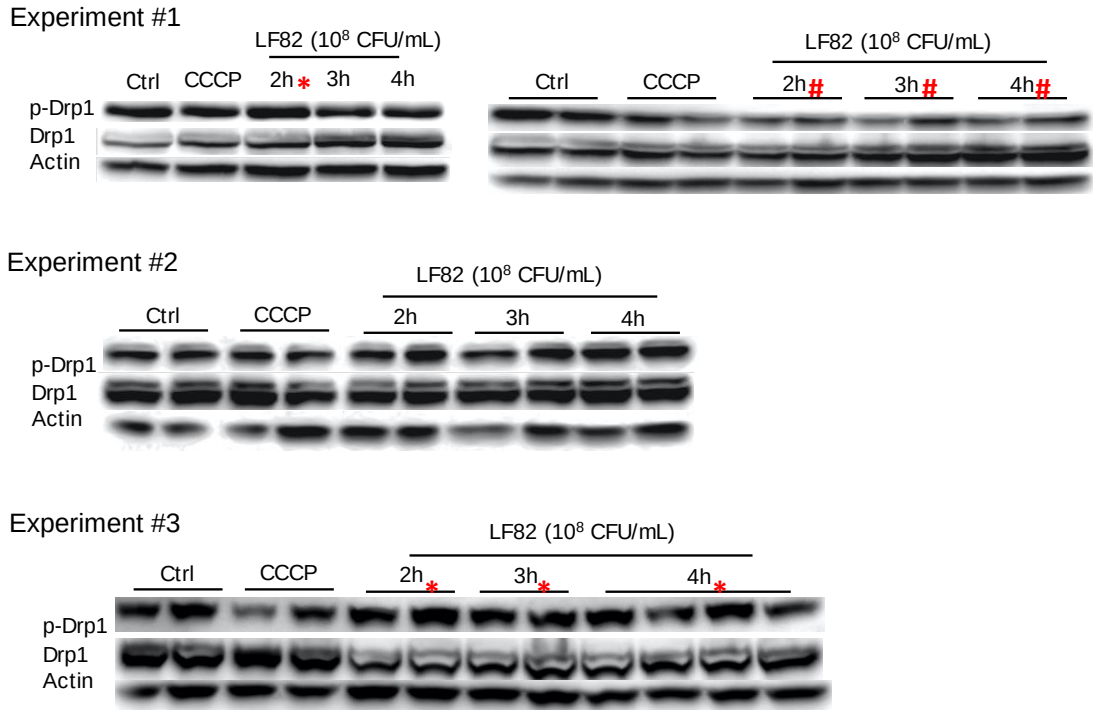

B.

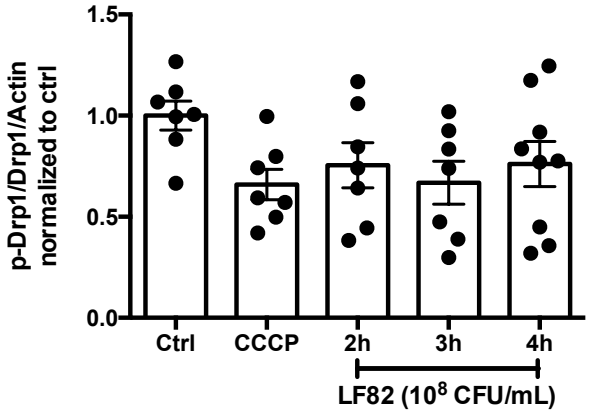

Figure 17. Changes in Drp1 phosphorylation at the Ser616 site are not observed in association with *E. coli* LF82 infection at 2-4h. (A) Representative western blots of p-Drp1, Drp1, and Actin at 2h, 3h, and 4h post-infection (10^8 CFU/mL). CCCP (carbonyl cyanide 3-chlorophenylhydrazone) is a mitochondrial uncoupler (4h, 4 μM). T84 cells were seeded at 0.5-1 million cells/well and cultured for 24-48h before treatment. Red star – increase in p-Drp1 expression. Red pound – decrease in p-Drp1 expression. **(B)** Densitometry was performed by the Measure function on ImageJ software normalizing p-Drp1 expression to Drp1 expression, normalized to total protein content (actin), Mean ± SEM, $p<0.05$, One Way ANOVA, Tukey's Multiple Comparison Test.

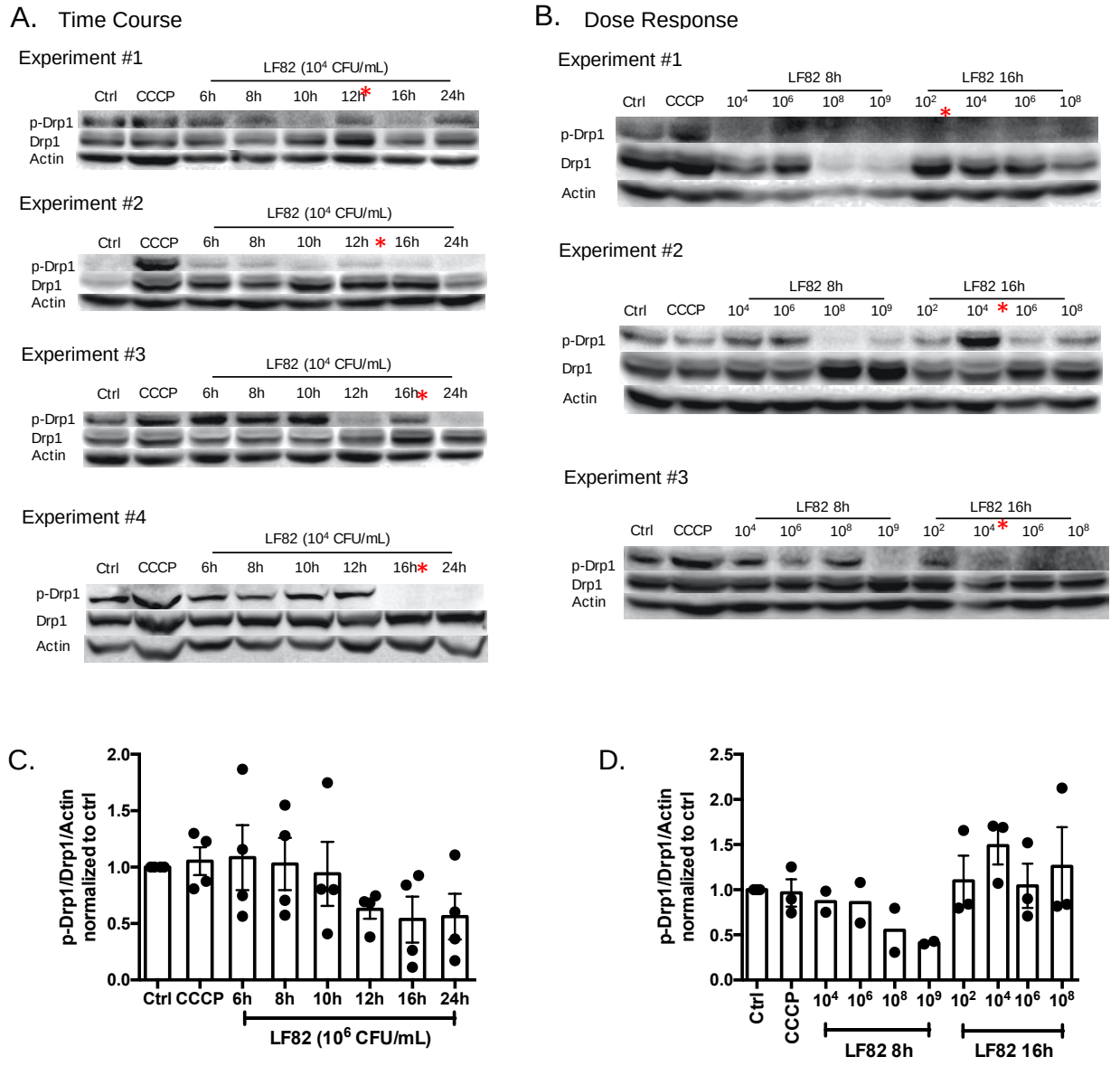

Figure 18. Changes in Drp1 phosphorylation at the Ser616 site are not associated with *E. coli* LF82 infection over a time course or dose response. (A) Representative western blots of p-Drp1, Drp1, and Actin over a time course of *E. coli* LF82 infection (10^6 CFU/mL). T84 cells were seeded at 0.5-1 million cells/well and cultured for 24-48h before treatment. Red star – increases or decreases in p-Drp1 expression. **(B)** Representative western blots of p-Drp1, Drp1, and Actin in an *E. coli* LF82 dose response at 8h and 16h. CCCP (carbonyl cyanide 3-chlorophenylhydrazone) is a mitochondrial uncoupler (4h, 4 μM). **(C)** Densitometry, Mean ± SEM, $p<0.05$, Kruskal-Wallis, Dunn's Multiple Comparison Test. **(D)** Densitometry, Mean ± SEM, $p<0.05$, Kruskal-Wallis, Dunn's Multiple Comparison Test.

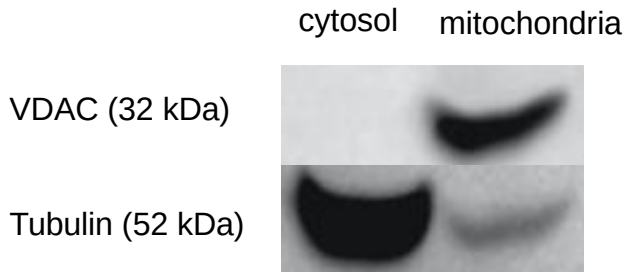

Figure 19. Mitochondrial protein isolates contain low levels of cytosolic contamination. Western blot of VDAC (Voltage Dependant Anion Channel, a mitochondrial protein) and tubulin (a cytosolic protein) in protein extracts from the mitochondrial and cytosolic fractions of cell lysates.

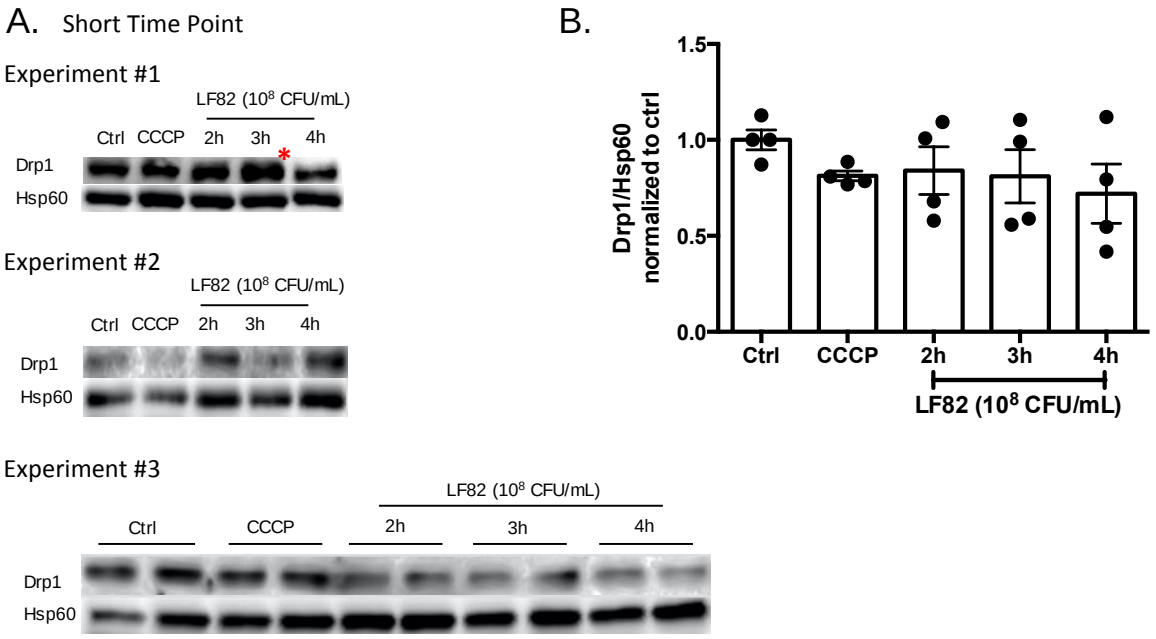

Figure 20. Changes in Drp1 in the mitochondrial protein fraction are not observed in association with *E. coli* LF82 infection at 2-4h. (A) Representative western blots of Drp1 and Hsp60 (Heat shock protein 60) at 2h, 3h, and 4h post-infection with *E. coli* LF82 (10^8 CFU/mL). T84 cells were seeded at 15 million cells/petri dish (145 mm x 20 mm) and cultured for 72h before treatment. Ctrl – Control. CCCP (carbonyl cyanide 3-chlorophenylhydrazone) is a mitochondrial uncoupler (4h, 4 μM). Red stars – increases in Drp1 expression. **(B)** Densitometry, Mean ± SEM, $p<0.05$, One Way ANOVA, Tukey's Multiple Comparison Test.

A. Time Course

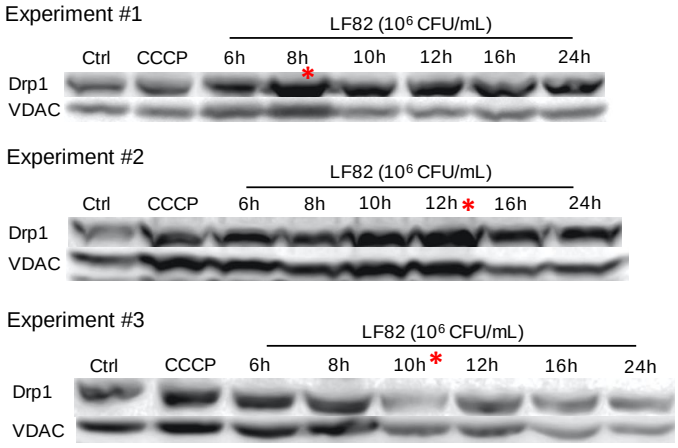

B. Dose Response

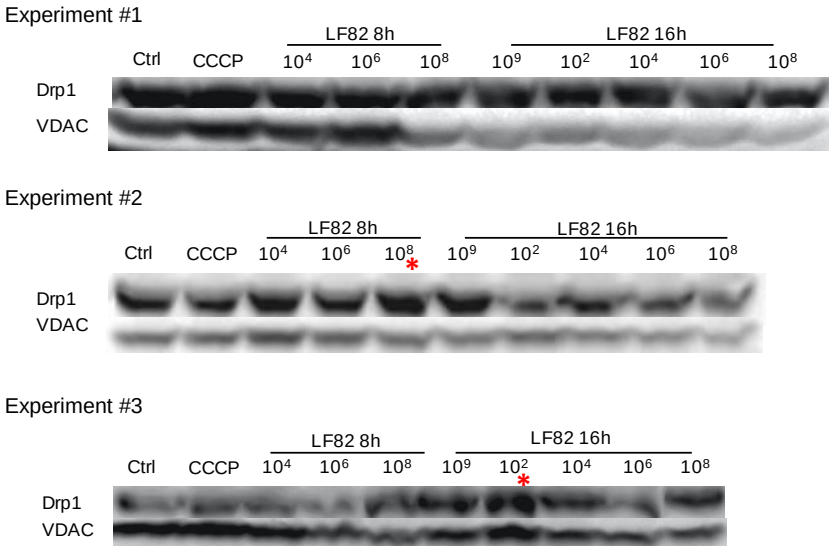

C.

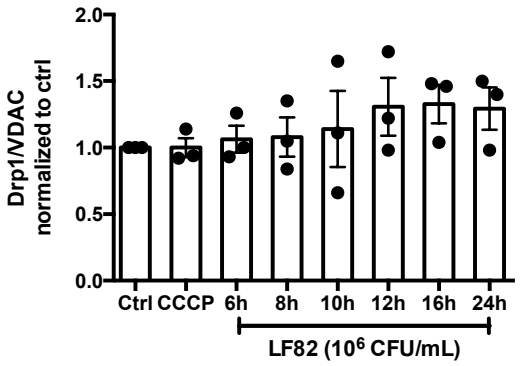

D.

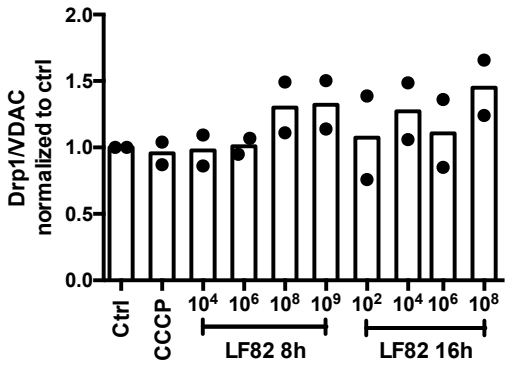

Figure 21. Changes in Drp1 in the mitochondrial protein fraction are not associated with *E. coli* LF82 infection over a time course or dose response. (A) Representative western blots of Drp1 and VDAC (Voltage Dependent Anion Channel) over a time course of *E. coli* LF82 infection (10^6 CFU/mL). T84 cells were seeded at 15 million cells/petri dish (145 mm x 20 mm) and cultured for 72h before treatment. Red stars – increase or decrease in Drp1 expression. **(B)** Representative western blots of Drp1 and VDAC in a *E. coli* LF82 dose response at 8h and 16h. CCCP (carbonyl cyanide 3-chlorophenylhydrazone) is a mitochondrial uncoupler (4h, 4 μM). **(C)** Densitometry, Mean ± SEM, $p<0.05$, Kruskal-Wallis, Dunn's Multiple Comparison Test. **(D)** Densitometry, Mean.

Long term E. coli LF82 infection is associated with OPA1 cleavage

As mitochondrial fusion mediators can also play a role in shaping overall mitochondrial network structures [153], cleavage of OPA1 was measured by western blot. CCCP, a mitochondrial uncoupler that is known to induce cleavage of OPA1 by activation of the inner mitochondrial membrane metallopeptidase OMA-1 [136–138], was used as a positive control. At short term infection time points (2-4h, 10^8 CFU/mL), OPA1 cleavage is not found in association with the induction of mitochondrial fragmentation (Fig.22A,B). Cleavage of OPA1 is apparent at 10^8 CFU/mL at 8h (Fig.23B,D). At 12h (10^6 CFU/mL) or 16h (10^4 CFU/mL) post-infection, OPA1 long isoforms are cleaved to favor short isoforms (Fig.23A-D).

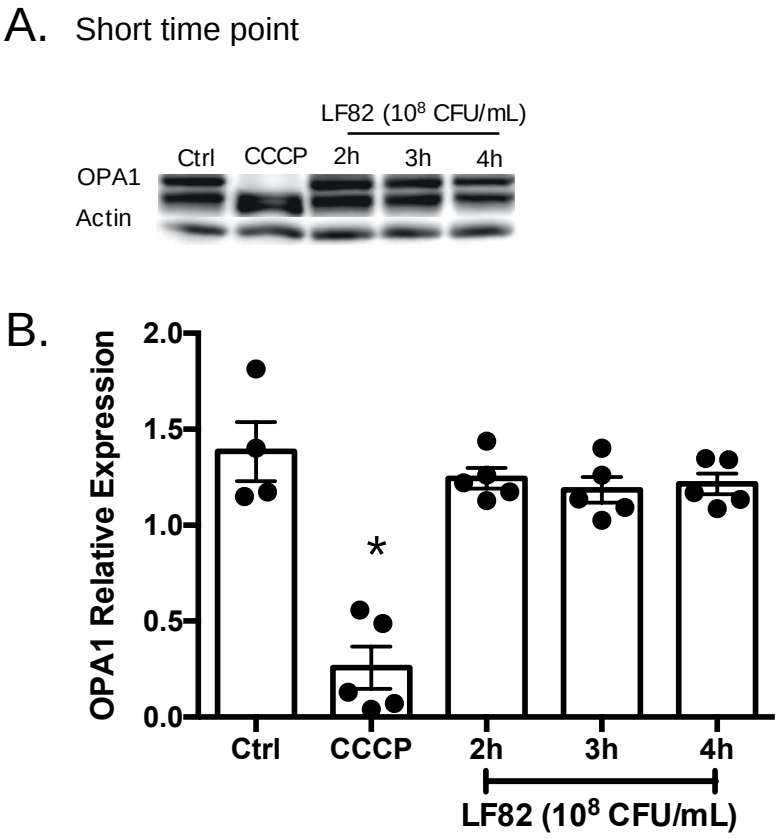

Figure 22. Cleavage of OPA1 is not associated with *E. coli* LF82 infection at 2-4h. **(A)** Representative western blot of OPA1 and Actin at 2h, 3h, and 4h post-infection with *E. coli* LF82 (10^8 CFU/mL). T84 cells were seeded at 0.5-1 million cells/well and cultured for 24-48h before treatment. CCCP (carbonyl cyanide 3-chlorophenylhydrazone) is a mitochondrial uncoupler (4h, 4 μM). **(B)** Densitometry of OPA1 upper band normalized to OPA1 lower band, Mean ± SEM, *$p<0.05$, One Way ANOVA, Dunnett's Multiple Comparison Test, compared to Ctrl (Control).

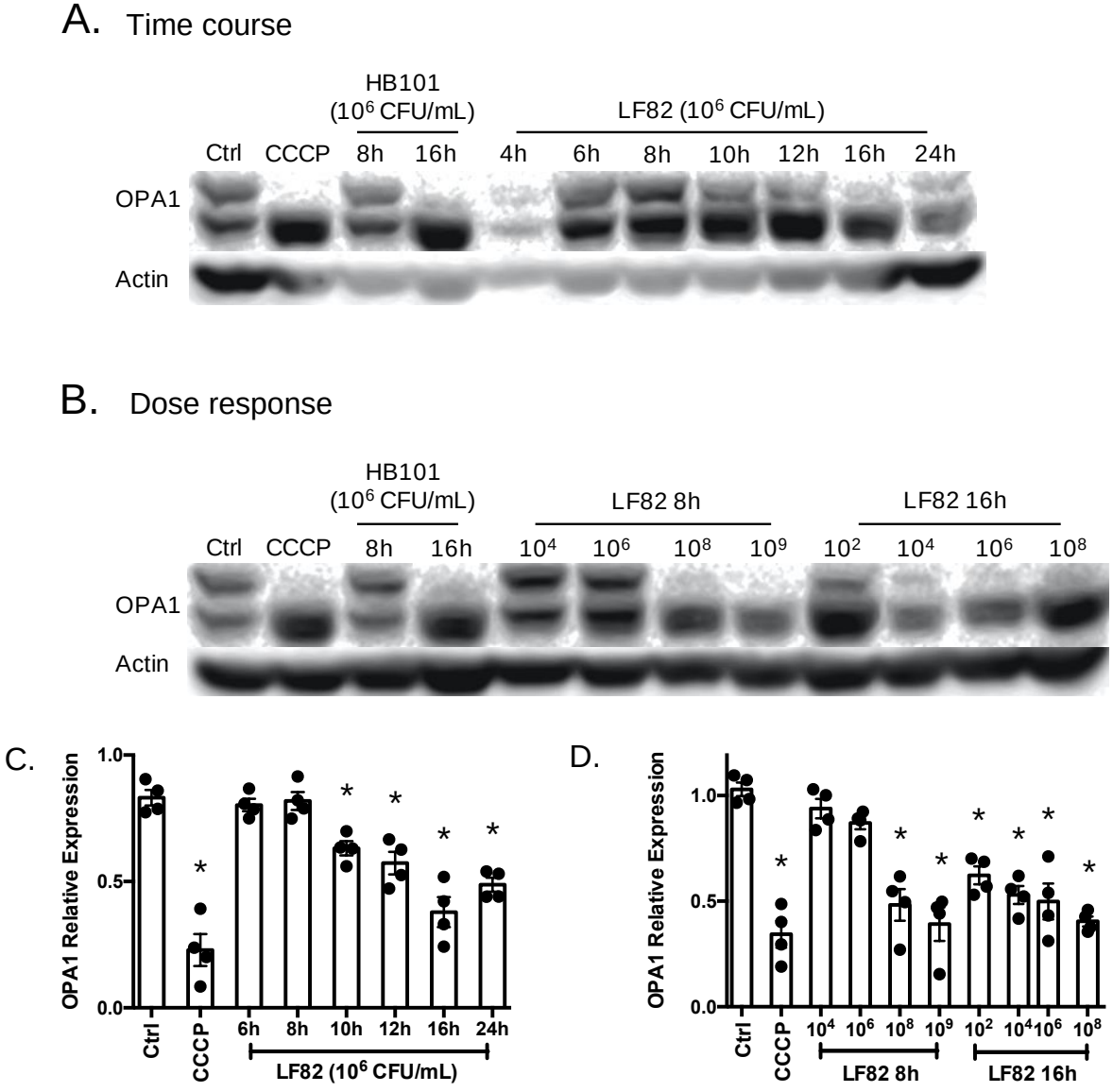

Figure 23. Cleavage of OPA1 is observed with *E. coli* LF82 infection over a time course or dose response. (A) Representative western blots of OPA1 and Actin over a time course of *E. coli* LF82 infection (10^6 CFU/mL). T84 cells were seeded at 0.5-1 million cells/well and cultured for 24-48h before treatment. CCCP (carbonyl cyanide 3-chlorophenylhydrazone) is a mitochondrial uncoupler (4h, 4 μM). Ctrl - Control **(B)** Representative western blots of OPA1 and Actin in an *E. coli* LF82 dose response at 8h and 16h. **(C)** Densitometry of OPA1 upper band normalized to OPA1 lower band, Mean ± SEM, *p<0.05, One Way ANOVA, Dunnett's Multiple Comparison Test, compared to control. **(D)** Densitometry, Mean ± SEM, *p<0.05, One Way ANOVA, Dunnett's Multiple Comparison Test, compared to control.

LF82-induced fission is dependent on interaction of Drp1 with Fis1

As Drp1 is the putative inducer of mitochondrial fission, and the fusion mediator OPA1 was not altered during the short-term infection, Drp1 was interrogated further as the driver of LF82-induced fission. The pharmacological inhibitors P110 and Mdivi1 were used to target Drp1. P110 binds Drp1 in the region that it interacts with the mitochondrial receptor Fis1, preventing recruitment of Drp1 to the mitochondria during stress-induced mitochondrial fission [255]. P110 (10 μM) and Mdivi1 (5 μM) reduced BAPTA-AM (a calcium chelator inducing fission at 2h and 4h [152,170]) and CCCP induced fission at 16h various time points (Fig.24). CCCP-induced fission was blocked by P110 up to 10h after P110 was added to culture (Fig.25).

P110, Mdivi1, and Leflunomide (a fusion inducer used in later studies) did not impact *E. coli* LF82 replication or survival in culture (Fig.26).

P110 and Mdivi1 reduced the degree of *E. coli* LF82-induced fission at 4h (10^8 CFU/mL) (Fig.27A,B), but not at 16h (10^4 CFU/mL) (Fig.27C).

Leflunomide had variable effects depending on the experiment with either a trend towards reduced *E. coli* LF82-induced fission at 4h (Fig.28A), or no effect on *E. coli* LF82-induced fission at 4h (Fig.28B).

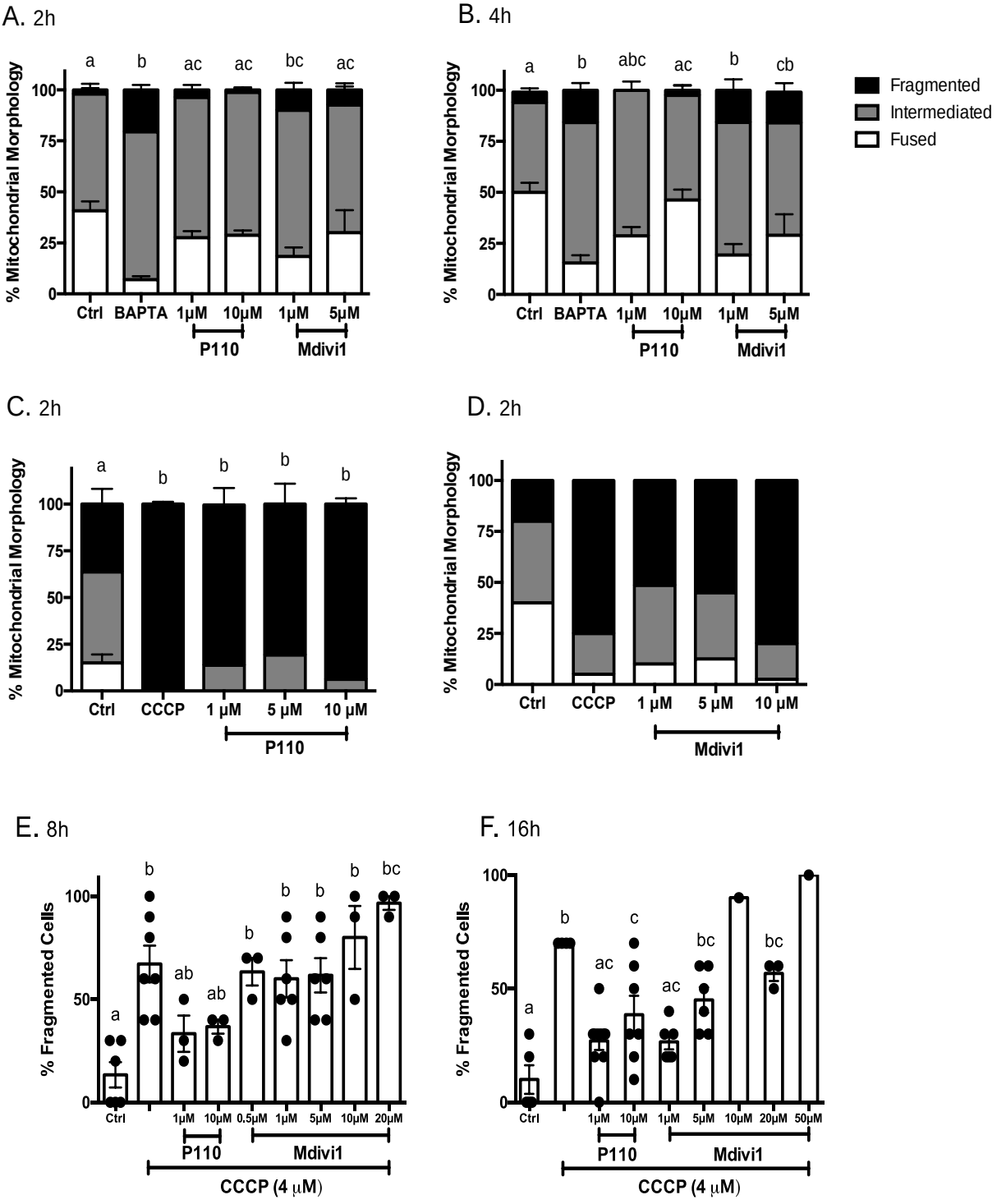
A. 2h
B. 4h
C. 2h
D. 2h
E. 8h
F. 16h
% Mitochondrial Morphology
% Fragmented Cells
Fragmented
Intermediated
Fused
Ctrl
BAPTA
1µM
10µM
5µM
P110
Mdivi1
CCCP
1 µM
5 µM
10 µM
0.5µM
20µM
50µM
CCCP (4 µM)

Figure 24. P110 and Mdivi1 block BAPTA and CCCP-induced mitochondrial fission. Mitochondrial networks were stained live with mitotracker red dye and imaged by confocal microscopy at 63X magnification. T84 cells were seeded at 250,000 cells/well in an 8-well chamber slide and cultured for 24-48h before staining and treatment. **(A)** 2h, **(B)** 4h, Quantification of mitochondrial networks performed by choosing 1 cell within a field of view by nuclear staining, and rating that cell as "fragmented", "intermediate", or "fused". Twenty fields of view (20 cells total) were rated per cell monolayer. BAPTA-AM is used as a positive control for Drp1-dependent mitochondrial fission (5 μM). Mean ± SEM, $p<0.05$, Two Way ANOVA, Tukey's Multiple Comparison Test. **(C)** 2h P110, **(D)** 2h Mdivi1, Quantification of mitochondria performed in the same way excluding the "intermediate" category, shown as % fragmented cells only. CCCP (carbonyl cyanide 3-chlorophenylhydrazone) is a mitochondrial uncoupler used as a positive control for fragmented mitochondrial morphology (16h, 4 μM). **(E)** 8h, **(F)** 16h. Mean ± SEM, $p<0.05$, different letters indicate statistically significant differences between groups, One Way ANOVA, Tukey's Multiple Comparison Test.

A.

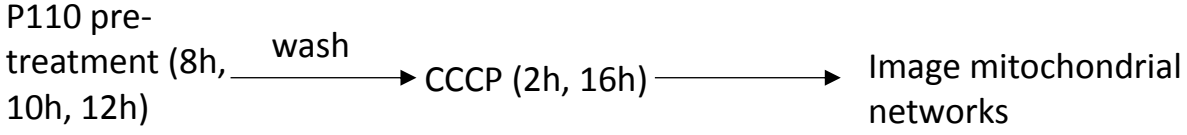

B.

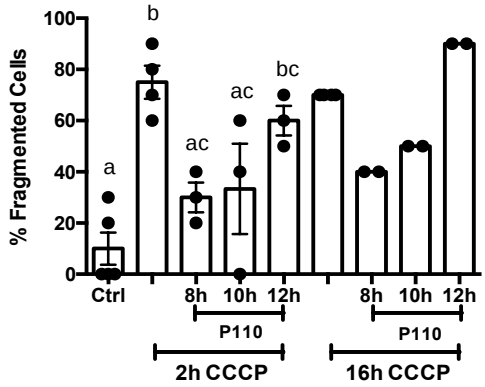

Figure 25. P110 is bioavailable at 10h in cell culture conditions. (A) Flow chart describing treatment protocol. Cells are pre-treated with P110 at 8h, 10h, or 12h, washed, then treated with CCCP for 2h or 16h, after which mitochondrial networks are stained and imaged by confocal microscopy. **(B)** Quantification of mitochondrial networks performed by choosing 1 cell within a field of view by nuclear staining, and rating that cell as "fragmented" or "fused". Twenty fields of view (20 cells total) were rated per cell monolayer. T84 cells were seeded at 250,000 cells/well in an 8-well chamber slide and cultured for 24-48h before staining and treatment. CCCP (carbonyl cyanide 3-chlorophenylhydrazone) is a mitochondrial uncoupler used as a positive control for fragmented mitochondrial morphology (2h or 16h, 4 μM). P110 – 1 μM. Mean ± SEM, $p<0.05$, different letters indicate statistically significant differences between groups, One Way ANOVA, Tukey's Multiple Comparison Test.

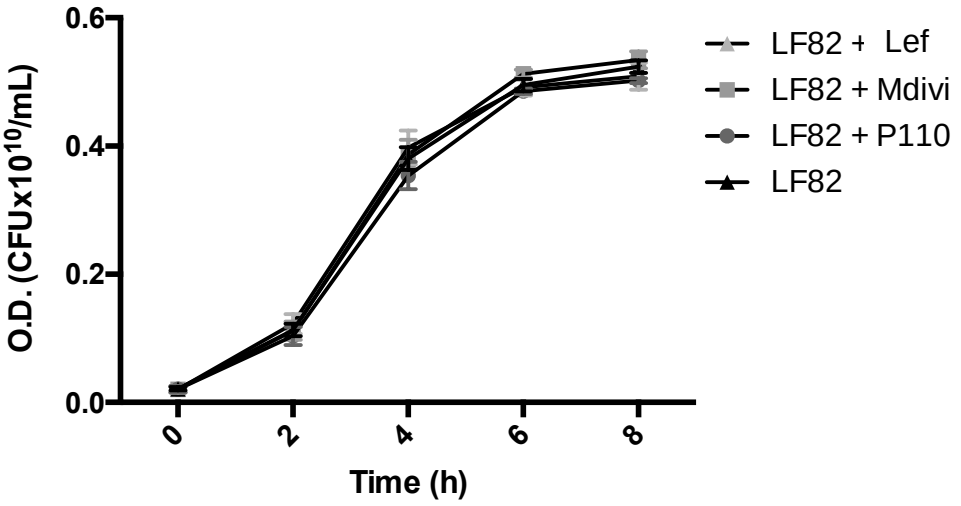

Figure 26. P110, Mdivi1, and Leflunomide do not impact growth of *E. coli* LF82. *E. coli* LF82 (10^8 CFU/mL) were grown in the presence of fission inhibitors P110 (10 μM), Mdivi1 (5 μM), or Leflunomide (50 μM) in T84 medium at 37°C and Optical Density (O.D.) was measured every 2 hours by spectrophotometry. Mean ± SEM, $p<0.05$, Two Way ANOVA, Dunnett's Multiple Comparison Test.

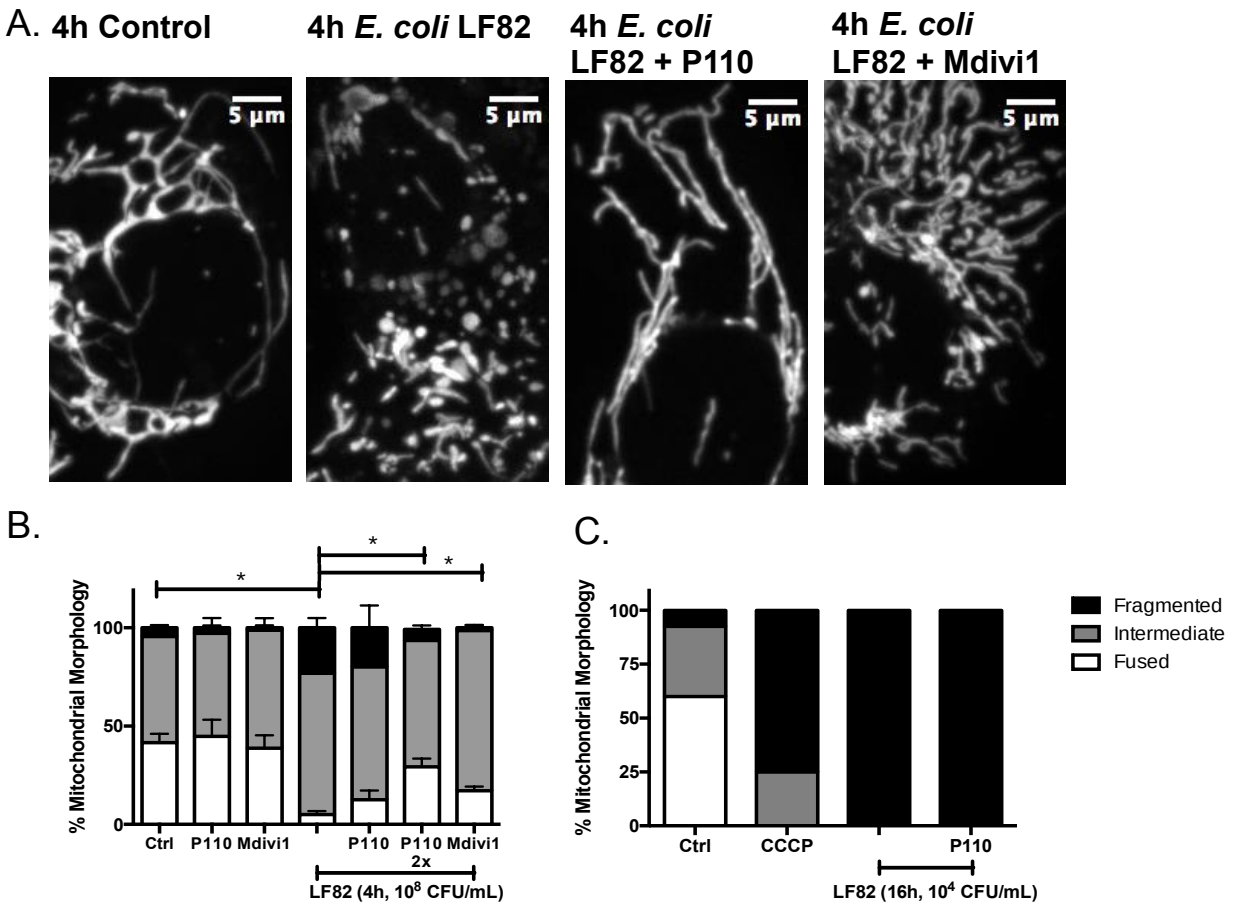

Figure 27. P110 and Mdivi1 reduced *E. coli* LF82 induced mitochondrial fragmentation at 4h. Mitochondrial networks were stained live with mitotracker red dye and imaged by confocal microscopy at 63X magnification. T84 cells were seeded at 250,000 cells/well in an 8-well chamber slide and cultured for 24-48h before staining and treatment. **(A)** Representative images, **(B)** Quantification of mitochondrial networks performed by choosing 1 cell within a field of view by nuclear staining, and rating that cell as "fragmented", "intermediate", or "fused". Twenty fields of view (20 cells total) were rated per cell monolayer. T84 cells were pre-treated with P110 for 30 min. (10 µM) followed by co-treatment with *E. coli* LF82 (10 µM). 2x – P110 was added every 2h into culture. T84 cells were co-treated with Mdivi1 once (5 µM). Mean ± SEM, *$p<0.05$, Two Way ANOVA, Tukey's Multiple Comparison Test, n=4-11 from 5 experiments. **(C)** 16h LF82 ± P110 (1 µM, co-treatment), n=2-3 from 1 experiment.

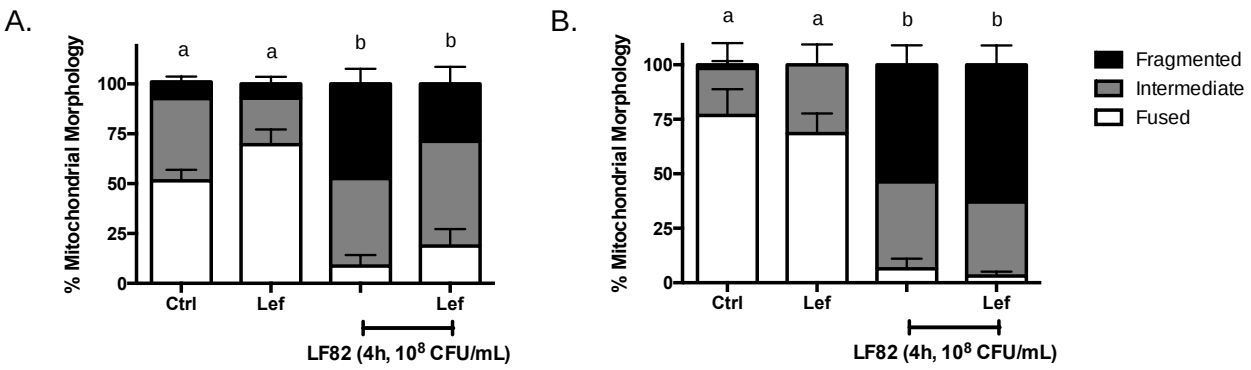

Figure 28. Leflunomide has variable effects on *E. coli* LF82-induced mitochondrial fission. Mitochondrial networks were stained live with mitotracker red dye and imaged by confocal microscopy at 63X magnification. T84 cells were seeded at 250,000 cells/well in an 8-well chamber slide and cultured for 24-48h before staining and treatment. Quantification of mitochondrial networks performed by choosing 1 cell within a field of view by nuclear staining, and rating that cell as "fragmented", "intermediate", or "fused". Twenty fields of view (20 cells total) were rated per cell monolayer. Ctrl – control. Lef – Leflunomide (50 μM). **(A)** Experiments showing a trend toward a response in *E. coli* LF82-induced mitochondrial fragmentation to Leflunomide, Mean ± SEM, $p<0.05$, different letters indicate statistically significant differences between groups, Two Way ANOVA, Tukey's Multiple Comparison Test, n=4-5 from 3 experiments. **(B)** Experiments showing no response in *E. coli* LF82-induced mitochondrial fragmentation to Leflunomide, Mean ± SEM, $p<0.05$, different letters indicate statistically significant differences between groups, Two Way ANOVA, Tukey's Multiple Comparison Test, n=3-5 from 2 experiments.

To further test the role of Drp1 in LF82-induced fission, Drp1 was targeted with siRNA to knock down (KD) protein expression. Drp1 protein was reduced to 71% ± 32% of mock transfected Drp1 protein with siRNA (Fig.29). Compared to mock transfected cells, Drp1 siRNA KD prevented *E. coli* LF82-induced mitochondrial fission (Fig.30A,B). Control siRNA (csiRNA), non-targeting siRNA used as a negative control, did not impact mitochondrial morphology (Fig.30A,B).

Overall, it was observed that AIEC-induced fission at 16h (10^4 CFU/mL) was not promoted by spent medium, or dead bacteria. Blocking invasion of *E. coli* LF82 blocked subsequent mitochondrial fission at 2h (10^8 CFU/mL). With regards to host factors, antioxidants did not block AIEC-induced fission (16h, 10^4 CFU/mL), and blocking Drp1 pharmacologically or genetically reduced AIEC-induced fission (2h, 4h, 10^8 CFU/mL). OPA1 cleavage was observed at late time points post-infection with *E. coli* LF82 (8h, 10^8 CFU/mL, 16h, 10^4 CFU/mL).

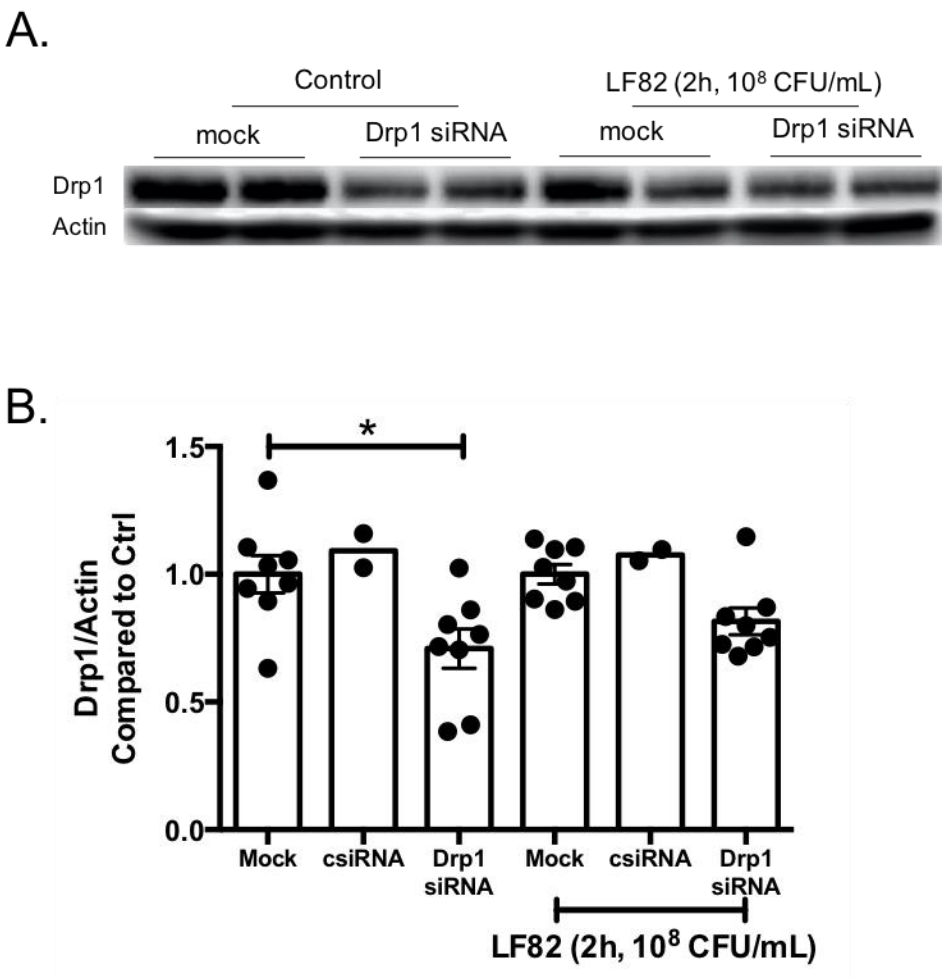

Figure 29. Drp1 protein expression was reduced in T84 cells by transfection with Drp1 siRNA. T84 cells (100,000 cells/well, 8 well chamber slide) were transfected with Drp1 siRNA (30nM) by lipofectamine and protein was collected 80h later (following 72h in culture after transfection, staining, treatment, and imaging). **(A)** Representative western blots of Drp1 and Actin, **(B)** Densitometry of western blots. csiRNA – control siRNA. Mean ± SEM, *p<0.05, One Way ANOVA, Tukey's Multiple Comparison Test.

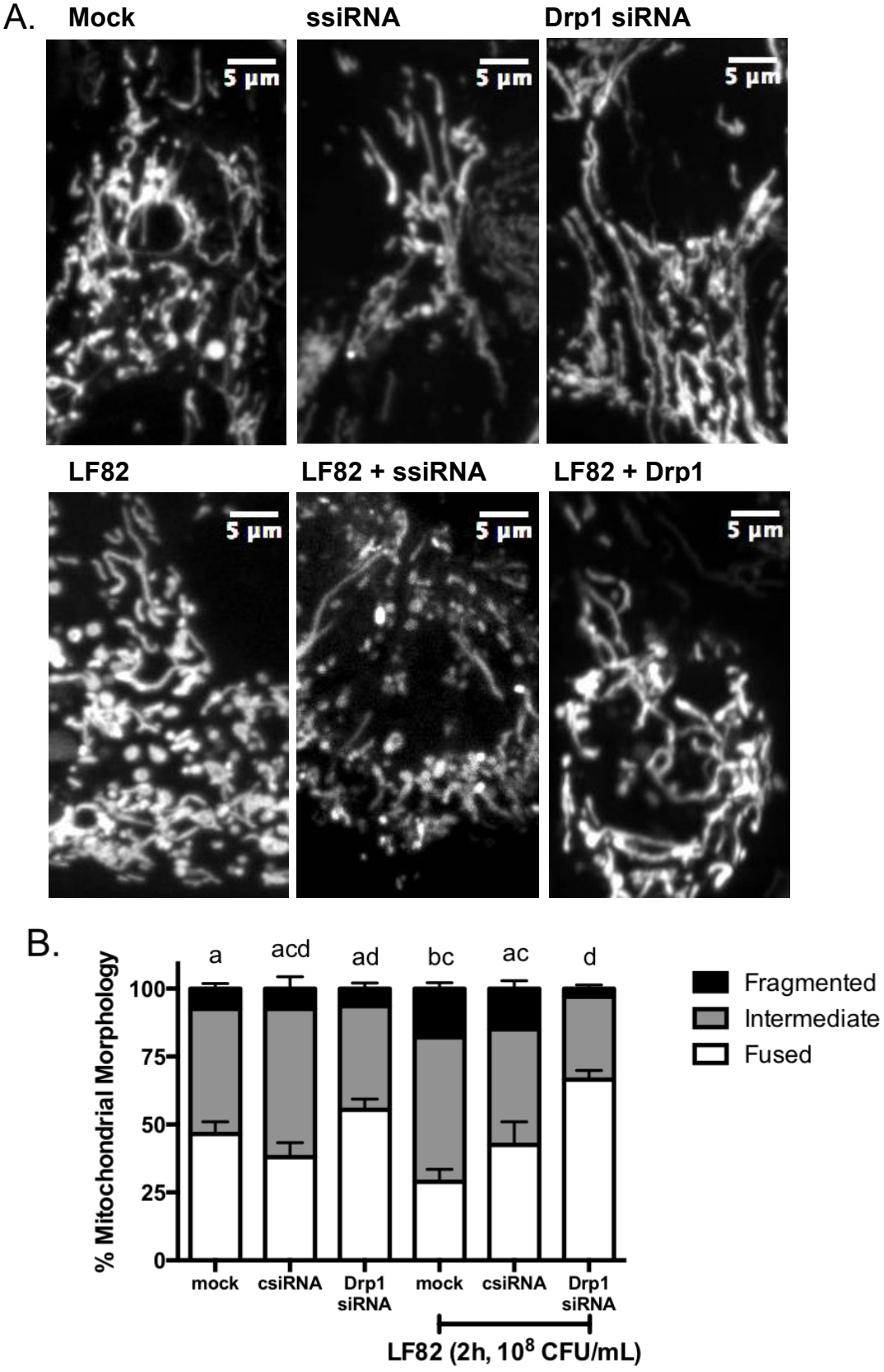
A.
Mock
ssiRNA
Drp1 siRNA
5 µm
LF82
LF82 + ssiRNA
LF82 + Drp1
B.
% Mitochondrial Morphology
100
75
50
25
0
a
acd
ad
bc
ac
d
Fragmented
Intermediate
Fused
mock
csiRNA
Drp1 siRNA
mock
csiRNA
Drp1 siRNA
LF82 (2h, 10^8 CFU/mL)

Figure 30. *E. coli* LF82 induced mitochondrial fragmentation is reduced by Drp1 knock-down. T84 cells (100,000 cells/well, 8-well chamber slide) were transfected with Drp1 siRNA (30nM) by lipofectamine and cells were stained 72h later. Mock transfected cells received lipofectamine with no siRNA. csiRNA – control siRNA. Mitochondrial networks were stained live with mitotracker red dye and imaged by confocal microscopy at 63X magnification. **(A)** Representative images, **(B)** Quantification of mitochondrial networks performed by choosing 1 cell within a field of view by nuclear staining, and rating that cell as "fragmented", "intermediate", or "fused". Twenty fields of view (20 cells total) were rated per cell monolayer. Mean ± SEM, $p<0.05$, different letters indicate statistically significant differences between groups, Two Way ANOVA, Tukey's Multiple Comparison Test, n=4-10 from 5 experiments.

RESULTS IV: Consequences of AIEC-Induced Fission

E. coli LF82 infection leads to cell death in T84 cells

The observation of vast mitochondrial fission in response to *E. coli* LF82 infection of gastrointestinal epithelial cells prompted the following question – what are the downstream consequences of mitochondrial fission? Investigating these functional consequences could allow generation of a hypothesis of how AIEC may impact disease state of infected individuals.

As mitochondrial fission-induced apoptosis is well described in the literature [219], I measured cytochrome c release from the mitochondria in response to *E. coli* LF82 infection. Staurosporine (an apoptosis inducer by inhibition of tyrosine kinases [334]) induced cytochrome c release in 46% of cells after 6h (Fig.31A,B). At 6h post-infection (10^8 CFU/mL), cytochrome c release was not apparent (Fig.31A,B). At 8h post-infection, 40% of cells had released cytochrome c from the mitochondria into the cytosol (Fig.31A,B). Targeting the enhanced mitochondrial fission starting at 2h (10^8 CFU/mL) with P110, Mdivi1, and Leflunomide did not abrogate LF82-induced cytochrome c release at 8h post-infection (Fig.31A,B).

Of note, although P110, Mdivi1, and Leflunomide blocked LF82-induced mitochondrial fission at 4h (Fig.27), the effect of these inhibitors was lost at 6h post-infection (Fig.31C), ultimately leading to enhanced cytochrome c release compared to control at 8h post-infection. It was concluded that short term blockade of LF82-induced mitochondrial fission was not protective with regards to LF82-induced programmed cell death long term (Fig.31).

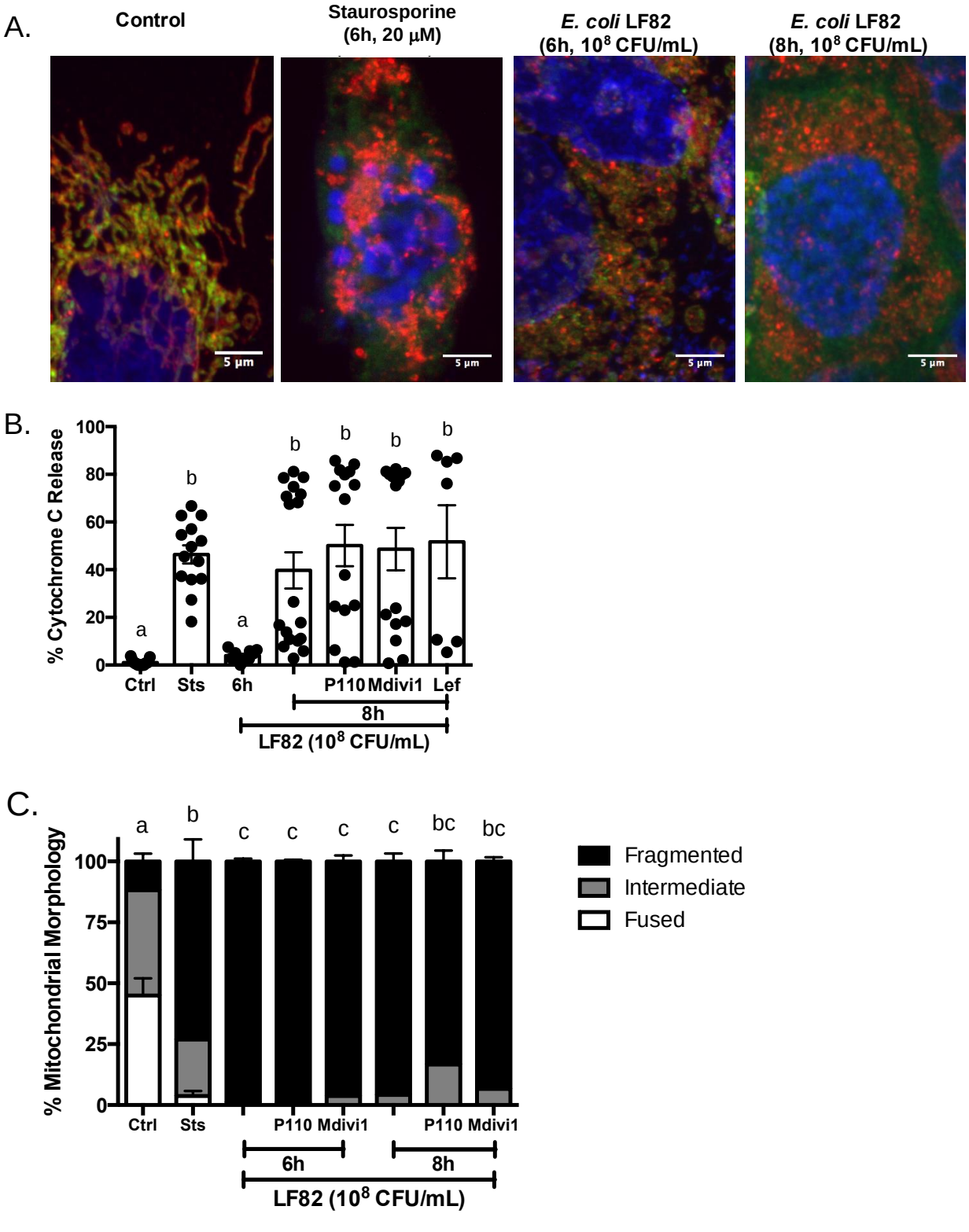
A.
Control
Staurosporine (6h, 20 μM)
E. coli LF82 (6h, 10^8 CFU/mL)
E. coli LF82 (8h, 10^8 CFU/mL)
5 μm
B.
% Cytochrome C Release
100
80
60
40
20
0
a
b
a
b
b
b
b
Ctrl
Sts
6h
P110
Mdivi1
Lef
8h
LF82 (10^8 CFU/mL)
C.
% Mitochondrial Morphology
a
b
c
c
c
c
bc
bc
100
75
50
25
0
Ctrl
Sts
P110
Mdivi1
P110
Mdivi1
6h
8h
LF82 (10^8 CFU/mL)
Fragmented
Intermediate
Fused

Figure 31. Cytochrome c release from mitochondria is induced by *E. coli* LF82 at 8h. (A) Representative images of immunofluorescent staining of mitochondria (red, TOM20), cytochrome c (green), and nuclei (blue, DAPI). Imaged at 100x magnification by confocal microscopy. T84 cells were seeded at 500,000 cells/well in an 24-well plate and cultured for 24-48h before staining and treatment. **(B)** Quantification of cytochrome c release from the mitochondria into the cytosol. The number of cells (enumerated by number of nuclei) displaying cytochrome c release per field of view was expressed as a percent of cells in the field of view. The % of cells with this phenotype from five images spread throughout each cell monolayer or well was averaged to give a single value for each cell monolayer (n). Ctrl – Control. Staurosporine (Sts, 6h, 20 μM) was used as a positive control. P110 – 30 min. pre-treatment followed by co-treatment with *E. coli* LF82 (10 μM). Mdivi1 – 5 μM co-treatment. Leflunomide (Lef) – 50 μM, co-treatment). Mean ± SEM, $p<0.05$, different letters indicate statistically significant differences between groups, One Way ANOVA, Tukey's Multiple Comparison Test. **(C)** Quantification of mitochondrial networks performed by choosing 1 cell within a field of view by nuclear staining, and rating that cell as "fragmented", "intermediate", or "fused". Twenty fields of view (20 cells total) were rated per cell monolayer. T84 cells were seeded at 250,000 cells/well in an 8-well chamber slide and cultured for 24-48h before staining and treatment. Mean ± SEM, $p<0.05$, different letters indicate statistically significant differences between groups, Two Way ANOVA, Tukey's Multiple Comparison Test, n=3-10 from 3 experiments.

Removing extracellular E. coli LF82 after the induction of mitochondrial fission reduces the degree of cytochrome c release induced by infection

The mitochondrial fission inhibitors P110, Mdivi1, and Leflunomide did not block *E. coli* LF82 induced cytochrome c release at 8h (10^8 CFU/mL), potentially due to an over-abundance of extracellular bacteria leading to T84 cell stress. To target the role of intracellular bacteria in inducing cytochrome c release, I treated T84 cells with *E. coli* LF82 for 4h (10^8 CFU/mL, a time point when intracellular bacteria are known to drive mitochondrial fission (Fig.11, 15)), washed the cells with PBS, treated the cells with gentamicin for 1h to kill extracellular bacteria, and fixed the cells 3h later to analyze cytochrome c release at 8h. Although without the gentamicin treatment, *E. coli* LF82 at 8h increased cytochrome c release compared to uninfected cells (Fig.32A), removing extracellular bacteria reduced the cytochrome c release at 8h to control levels (Fig.32A).

Surprisingly, after gentamicin treatment, analyzing cytochrome c release at 12h post-infection resulted in cell death that was statistically similar to uninfected cells, although it was also statistically similar to 8h *E. coli* LF82 infection without gentamicin. In order to correlate these results with levels of bacterial invasion, intracellular CFUs were enumerated with or without gentamicin treatment at 8h, showing that numbers of intracellular *E. coli* LF82 were the same (Fig.32B). Imaging the mitochondrial networks shows that cells treated with gentamicin after *E. coli* LF82 treatment have similar levels of mitochondrial fusion compared to uninfected cells, but at 12h mitochondrial fission is induced (Fig.32C).

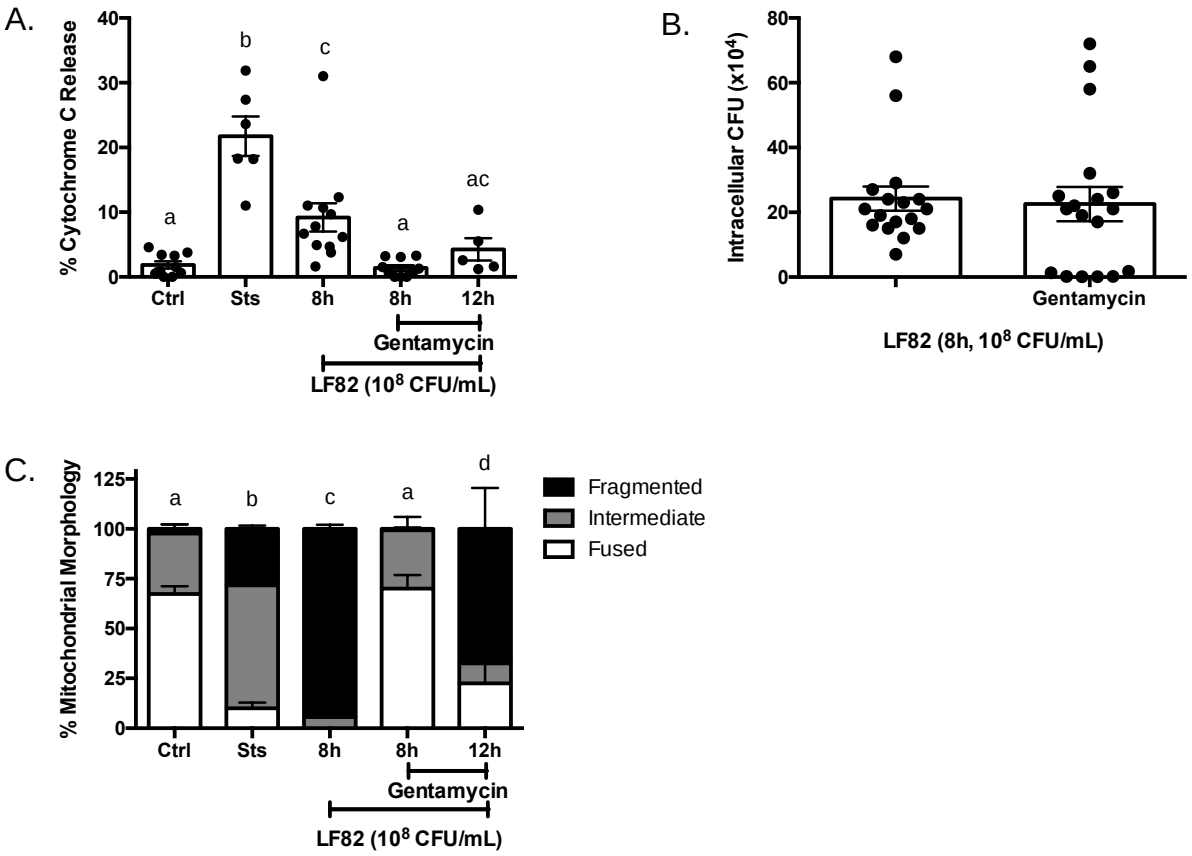
A.
% Cytochrome C Release
40
30
20
10
0
a
b
c
a
ac
Ctrl
Sts
8h
8h
12h
Gentamycin
LF82 (10^8 CFU/mL)
B.
Intracellular CFU (x10^4)
80
60
40
20
0
Gentamycin
LF82 (8h, 10^8 CFU/mL)
C.
% Mitochondrial Morphology
125
100
75
50
25
0
a
b
c
a
d
Ctrl
Sts
8h
8h
12h
Gentamycin
LF82 (10^8 CFU/mL)
Fragmented
Intermediate
Fused

Figure 32. Gentamicin treatment reduces degree of *E. coli* LF82-induced cytochrome c release. (A) Quantification of cytochrome c release from the mitochondria into the cytosol. The number of cells displaying cytochrome c release per field of view was expressed as a percent of cells in the field of view, enumerated by number of nuclei. The % of cells with this phenotype from five images spread throughout each cell monolayer or well was averaged to give a single value for each cell monolayer (n). T84 cells were seeded at 500,000 cells/well in a 24-well plate and cultured for 24-48h before staining and treatment. Ctrl – control. Staurosporine (Sts, 6h, 20 μM) was used as a positive control. Gentamicin-treated cells were treated with *E. coli* LF82 for 4h (10^8 CFU/mL), rinsed with PBS, treated with gentamicin for 1h (100 μg/mL), washed with PBS, and incubated with antibiotic-free T84 medium until a total treatment time (including 4h incubation with bacteria and 1h incubation with gentamicin) of 8h or 12h. Mean ± SEM, $p<0.05$, different letters indicate statistically significant differences between groups, One Way ANOVA, Tukey's Multiple Comparison Test. **(B)** Intracellular CFU's (colony forming units) after either 8h treatment with *E. coli* LF82 (10^8 CFU/mL), or 4h treatment with *E. coli* LF82 (10^8 CFU/mL), a PBS wash, a 1hr gentamicin treatment (100 μg/mL), a PBS wash, and incubation with antibiotic-free T84 medium for 3h. Cells were then washed and lysed with Triton X-100 (1%) for 5 min., cell lysates were collected in a 96-well plate, serial diluted in PBS, and bacteria were plated on blood agar, grown overnight at 37°C, and colonies were counted. T84 cells were seeded in 6-well plates (0.5-1 million cells/well) 24-48h before treatment. Mean ± SEM, $*p<0.05$, t-test. **(C)** Quantification of mitochondrial networks performed by choosing 1 cell within a field of view by nuclear staining, and rating that cell as "fragmented", "intermediate", or "fused". 20 fields of view (20 cells total) were rated per cell monolayer. T84 cells were seeded at 250,000 cells/well in an 8-well chamber slide and cultured for 24-48h before staining and treatment. Mean ± SEM, $p<0.05$, different letters indicate statistically significant differences between groups, Two Way ANOVA, Tukey's Multiple Comparison Test, n=3-9 from 3 experiments.

E. coli LF82-induced cell death is caspase-independent

As the intrinsic apoptotic pathway can activate caspases, which mediate cleavage leading to cell death, or can follow a caspase-independent cell death pathway [112], I measured caspase-3 cleavage by western blot to determine which pathway *E. coli* LF82-induced cell death follows. Staurosporine at 8h, 10h, 12h, or 24h (20 μM) induced cleavage of caspase-3 (Fig.33). Cytochrome c cleavage, a step upstream in the apoptotic pathway to caspase activation, occurs at 8h (10^8 CFU/mL) (Fig.31). At 8h, 10h, and 12h post-infection (10^8 CFU/ml) cleavage of caspase-3 was not observed by western blot, although staurosporine, the positive control, did lead to cleavage of caspase-3 (Fig.33A-C). Caspase-3 cleavage was also measured in a time course (Fig.33B) and dose response (Fig.33C) at intermediate (10^6 CFU/mL) and low (10^4 CFU/mL) infection inoculums, which revealed no consistent evidence of caspase-3 cleavage in response to LF82 infection, even at high doses for long treatment periods.

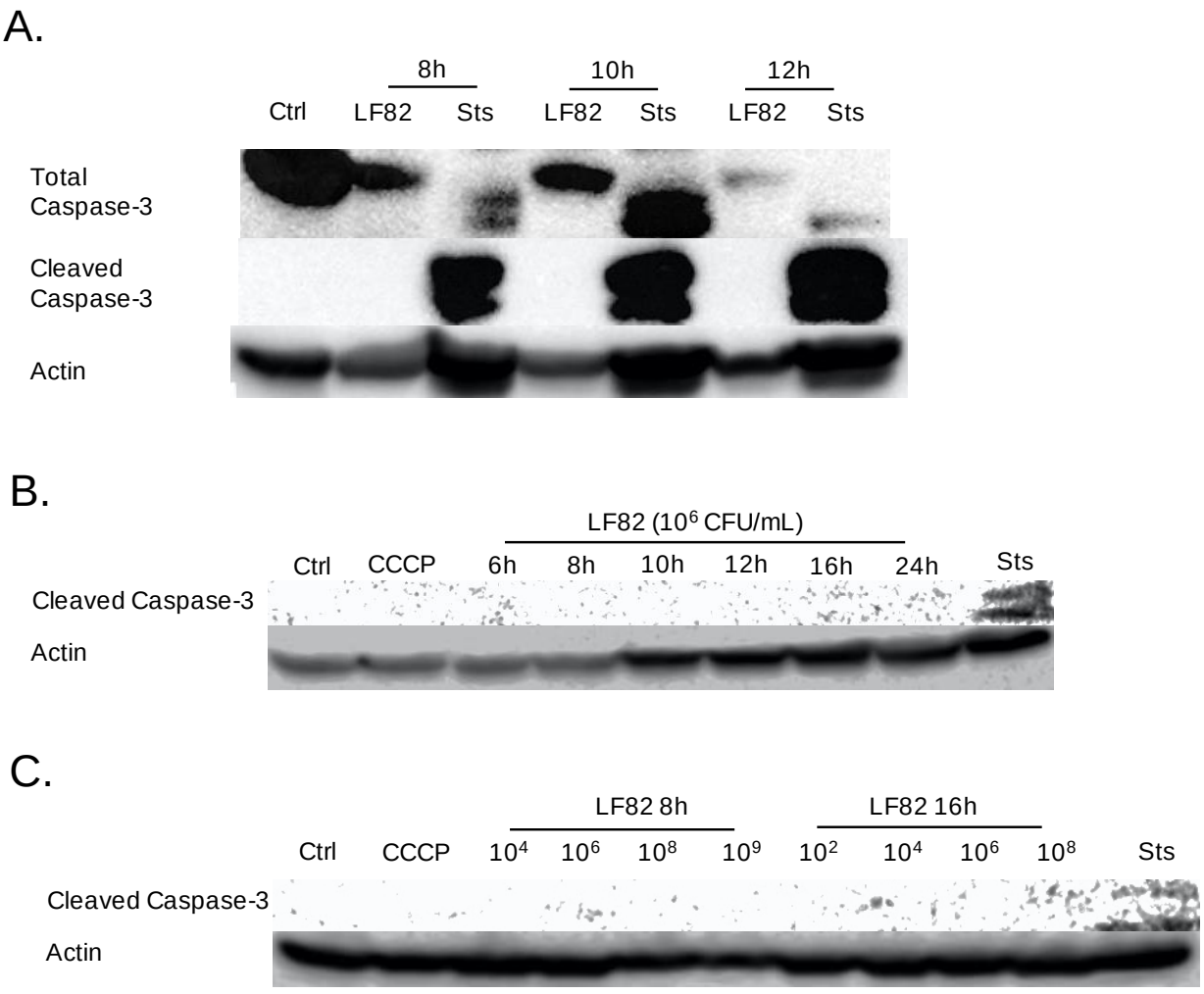

Figure 33. *E. coli* LF82 infection of T84 cells in not associated with caspase-3 cleavage. Western blot of cleavage caspase-3, total caspase-3, and actin. T84 cells were seeded at 0.5-1 million cells/well and cultured for 24-48h before treatment. CCCP (carbonyl cyanide 3-chlorophenylhydrazone) is a mitochondrial uncoupler (4h, 4 μM). Sts – Staurosporine (apoptosis inducer, positive control, 20 μM, 48h for (B) and (C)) **(A)** High dose *E. coli* LF82 (10^8 CFU/mL) at 8h, 10h, and 12, **(B)** *E. coli* LF82 time course at 10^6 CFU/mL, **(C)** *E. coli* LF82 dose response at 8h and 16h.

Short term Mdivi1 treatment blocked induction of epithelial cell permeability by E. coli LF82 infection

It is reported in the literature that different strains of AIEC, including LF82, promote loss of barrier function in the intestinal epithelium [48,52,66,67]. In this study, it was also observed that LF82 induced a drop in trans-epithelial resistance in polarized T84 cells grown on trans-well filters (starting TER = avg. 2000 ohms·cm^2) (Fig.34A), and in human colon tissues mounted in Ussing chambers (Fig.34A). FITC-dextran flux from the apical to basolateral side of T84 cell monolayers was increased at 6h post-infection (Fig.34B,C).

Blocking mitochondrial fission up to 4h post-infection (Fig.27) did not impact the drop in TER observed at 6h post-infection. (Fig.34A). FITC-dextran flux and translocation of *E. coli* LF82 from the apical to basolateral side of cells was also measured which, when considering all inhibitors of mitochondrial fission (P110, Mdivi1, and Leflunomide), was not impacted by short term inhibition of fission (Fig.34B,D). Focusing on the effect of Mdivi1, in 3 experiments, flux of FITC-dextran was reduced to control levels in all experiments (Fig.34C-left). After normalizing FITC-dextran flux to control levels in the same 3 experiments, there is a reduction in FITC-dextran flux comparing Mdivi1 + *E. coli* LF82 treatment to the *E. coli* LF82 infected group that is statistically different (Fig.34C-right). Focusing on the same 3 experiments as with FITC-dextran flux, bacterial translocation was reduced in the Mdivi1 + *E. coli* LF82 group compared to the *E. coli* LF82 infected group (Fig.34E). Although all data points are shown in Fig.34B and D, 1 experiment

was excluded for analysis in Fig.34C and E as the increases in permeability that were induced by *E. coli* LF82 were substantially higher than all other experiments, obscuring the changes in the other 3 experiments (enhanced permeability by *E. coli* LF82 was again blocked by Mdivi1). P110 and Leflunomide were excluded as they had no effect on FITC-dextran flux and bacterial translocation in preliminary experiments (Fig.34B,D).

A.

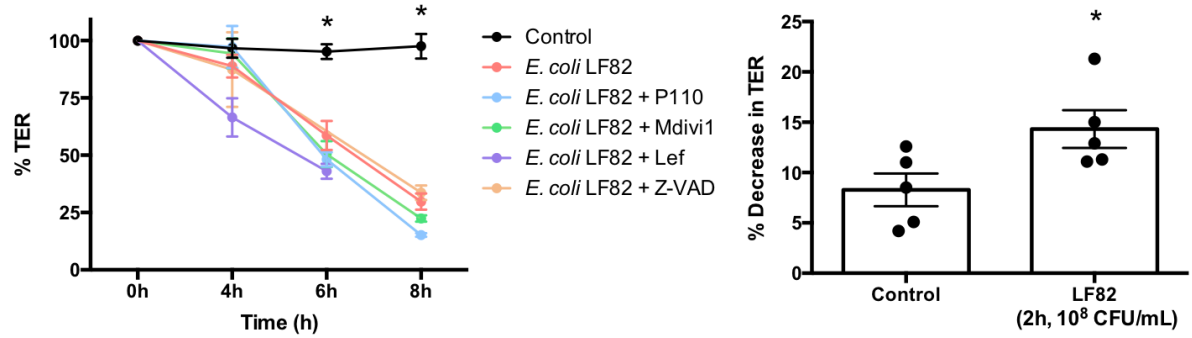
% TER
100
75
50
25
0
0h
4h
6h
8h
Time (h)
*
*
Control
E. coli LF82
E. coli LF82 + P110
E. coli LF82 + Mdivi1
E. coli LF82 + Lef
E. coli LF82 + Z-VAD
% Decrease in TER
25
20
15
10
5
0
*
Control
LF82
(2h, 10^8 CFU/mL)

B.

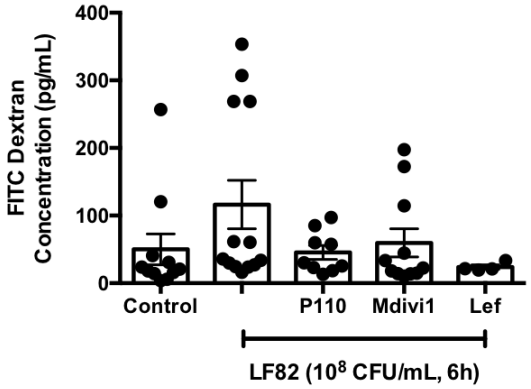
FITC Dextran
Concentration (pg/mL)
400
300
200
100
0
Control
P110
Mdivi1
Lef
LF82 (10^8 CFU/mL, 6h)

C.

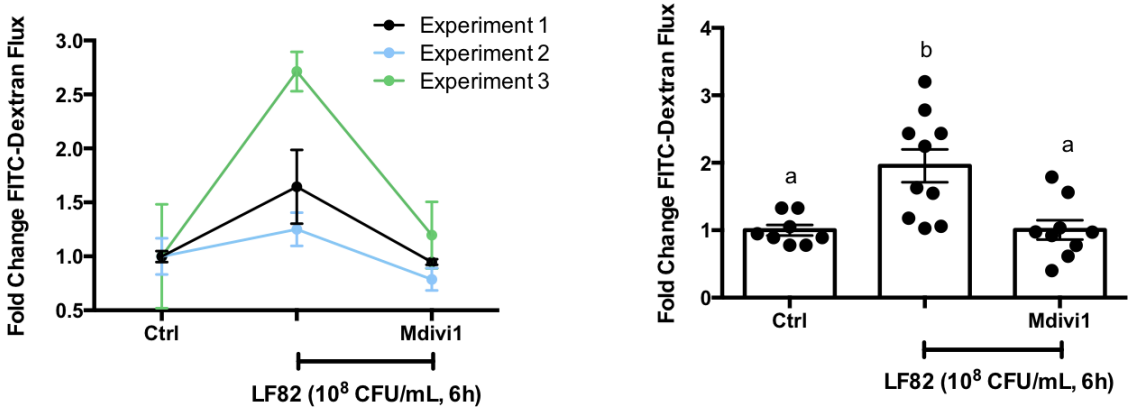
Fold Change FITC-Dextran Flux
3.0
2.5
2.0
1.5
1.0
0.5
Ctrl
Mdivi1
LF82 (10^8 CFU/mL, 6h)
Experiment 1
Experiment 2
Experiment 3
Fold Change FITC-Dextran Flux
4
3
2
1
0
a
b
a
Ctrl
Mdivi1
LF82 (10^8 CFU/mL, 6h)

D.

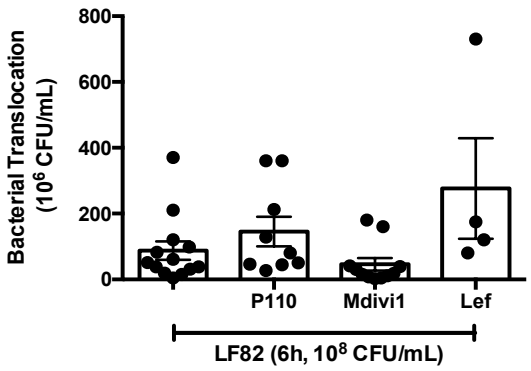
Bacterial Translocation
(10^6 CFU/mL)
800
600
400
200
0
P110
Mdivi1
Lef
LF82 (6h, 10^8 CFU/mL)

E.

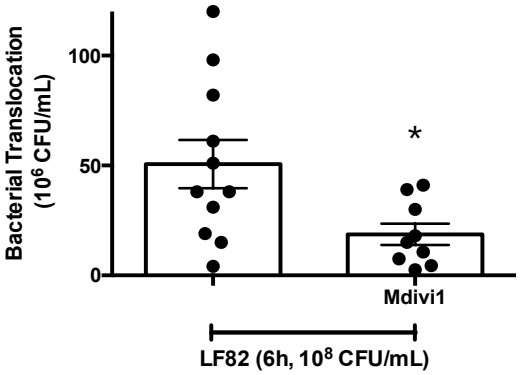
Bacterial Translocation
(10^6 CFU/mL)
100
50
0
*
Mdivi1
LF82 (6h, 10^8 CFU/mL)

Figure 34. Mdivi1 treatment reduces impact of *E. coli* LF82 infection on barrier function in T84 cells. (A) Left - Transepithelial resistance (TER) was measured of T84 cells. Cells were seeded into transwells (3 μM filters) placed into 12-well plates (1 million cells/transwell) and cultured for 7 days. Experiments were performed when cells reached a minimum of 1000 ohms·cm^2. Cells were infected with *E. coli* LF82 for 6h or 8h (depending on the experiment) at 10^8 CFU/mL, and TER was measured every 2h. P110 – 10 μM, 30 min. pre-treatment followed by co-treatment. Mdivi1 - 5 μM co-treatment. Lef – Leflunomide, 50 μM co-treatment. Z-VAD – 100 μM co-treatment. h – hours. % TER is the TER in 1000 ohms·cm^2 at each time point normalized to time 0. Mean ± SEM, *p<0.05 all groups compared to control, Two Way ANOVA, Tukey's Multiple Comparison Test, n=3-30 from 8 experiments (n=3/4 is *E. coli* LF82 + Lef and *E. coli* LF82 + Z-VAD groups). **Right** - Macro- and microscopically normal colonic specimens were collected from 5 patients during surgery for colonic cancer. The external muscle and myenteric plexus were stripped off the colonic specimens, and mucosal sections were mounted on Ussing chambers. Transepithelial resistance (TER) was monitored throughout the experiment to ensure tissue viability. Chambers were equilibrated for 30 min to achieve steady state conditions and then live GFP-labelled *E. coli* LF82 was added to the mucosal sides of 3 separate chambers at a final concentration of 10^8 CFU/ml. Three chambers added Krebs buffer only served as controls. Mean ± SEM, *p<0.05, t-test, n=5 from 1 experiment. **(B)** FITC-dextran flux across the T84 cell monolayer was measured by adding FITC-dextran to the apical side of transwells at 4h (70 kDa, 200 μg/mL), collecting the basolateral medium at 6h, and reading FITC fluorescence by a spectrophotometer. Mean ± SEM, p<0.05, One Way ANOVA, Tukey's Multiple Comparison Test, 4 experiments. **(C) Left** - FITC-dextran flux data from 3 experiments excluding P110 and Leflunomide data, normalized to control. No statistical analysis performed. n=2-4 per experiment, total n=9-10. **Right** - FITC-dextran flux data from 3 experiments excluding P110 and Leflunomide data, normalized to control. Mean ± SEM, p<0.05, different letters indicate statistically significant differences between groups, One Way ANOVA, Tukey's Multiple Comparison Test. **(D)** Bacterial translocation was measured by collecting *E. coli* LF82 in the basolateral chamber of transwells at 6h and plating on columbia sheep blood agar. Mean ± SEM, p<0.05, One Way ANOVA, Tukey's Multiple Comparison Test, 4 experiments. **(E)** Bacterial translocation from 3 experiments (same experiments as in FITC-Dextran data) excluding P110 and Leflunomide data. Mean ± SEM, *p<0.05, t-test. 4 data points (2 from *E. coli* LF82, 2 from *E. coli* LF82 + Mdivi1) were excluded which were 3 standard deviations away from the mean.

Leflunomide limits intracellular bacterial persistence

In the literature, it has been reported that an increase or decrease in mitochondrial fission in response to infection can be associated with altered replication of intracellular pathogens or an altered ability of the host to clear intracellular pathogens (Table 5). I measured numbers of intracellular *E. coli* LF82 normalized to extracellular bacteria at 2h (10^8 CFU/mL) in the presence of P110, Mdivi1, and Leflunomide, to determine if blocking fission would affect persistence of intracellular LF82. P110 and Mdivi1 did not reduce numbers of intracellular *E. coli* LF82 (Fig.35). Interestingly, the fusion inducer Leflunomide reduced numbers of intracellular LF82 (Fig.35). Of note, Leflunomide is known to alter pyrimidine synthesis metabolism [323], which could have an impact on bacterial replication intracellularly.

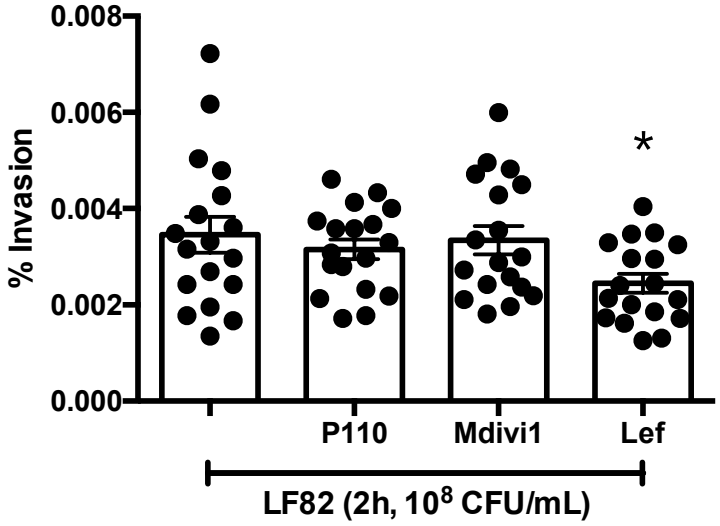

Figure 35. Leflunomide reduces numbers of intracellular *E. coli* LF82. Bacterial internalization assay in T84 cells with *E. coli* LF82 (10^8 CFU/mL, 2h) with or with P110 (30 min. pre-treatment followed by co-treatment with bacteria, 10 μM), Mdivi1 (5 μM), or Leflunomide (Lef, 50 μM). T84 cells were seeded in 6-well plates (0.5-1 million cells/well) 24-48h before treatment. Mean ± SEM, *$p<0.05$, One Way ANOVA, Dunnett's Multiple Comparison Test compared to LF82.

Interleukin-8 gene expression is increased by E. coli LF82 infection of T84 cells without an increase in interleukin-8 protein translation

Interleukin-8 transcription has been shown to be upregulated by adherent-invasive *E. coli* infection in a variety of gastrointestinal epithelial cell types (Caco-2 [47,52,90,92], T84 [89,91], and HT29 [92]). During a bacterial infection, bacterial products such as LPS or flagellin are recognized by the host Toll Like Receptors (TLRs) on epithelial cells, leading to production of pro-inflammatory cytokines such as IL-8 [335,336]. Although many papers demonstrate an induction of IL-8 gene expression in response to AIEC, only a minority showed an increase in IL-8 protein [49,80,88], and only 1 report measured both gene transcription and protein translation to correlate the two readouts [89].

As our lab has demonstrated that mitochondrial dysfunction can drive IL-8 secretion from T84 cells in response to intracellular bacteria [337], I measured IL-8 gene expression and protein secretion from T84 cells to determine if *E. coli* LF82 promotes a pro-inflammatory response in my model, and if blocking mitochondrial fragmentation would reduce this response. IL-8 gene expression was increased in response to *E. coli* LF82 infection of T84 cells at 4h (Fig.36A) and 8h (Fig.36B). P110 and Mdivi1 did not block or induce IL-8 gene expression compared to *E. coli* LF82 alone.

This increase in IL-8 gene expression did not correlate with an increase in IL-8 protein secretion from *E. coli* LF82-infected T84 cells, surprisingly (Fig.37B,C), although T84 cells did respond to TNFα treatment, a positive control, by secreting

IL-8 (Fig.37A). P110, Mdivi1, and Leflunomide did not alter IL-8 protein secretion compared to *E. coli* LF82 infection alone (Fig.37B,C).

In summary, *E. coli* LF82 was shown to induce cytochrome c release at 8h post-infection (10^8 CFU/mL), which was not impacted by P110, Mdivi1, and Leflunomide. Loss of barrier function was not impacted by P110 and Leflunomide. Mdivi1 blocked the loss of barrier function induced by *E. coli* LF82 at 6h (10^8 CFU/mL). Numbers of intracellular bacteria and IL-8 secretion were not impacted by P110, Mdivi1, or Leflunomide.

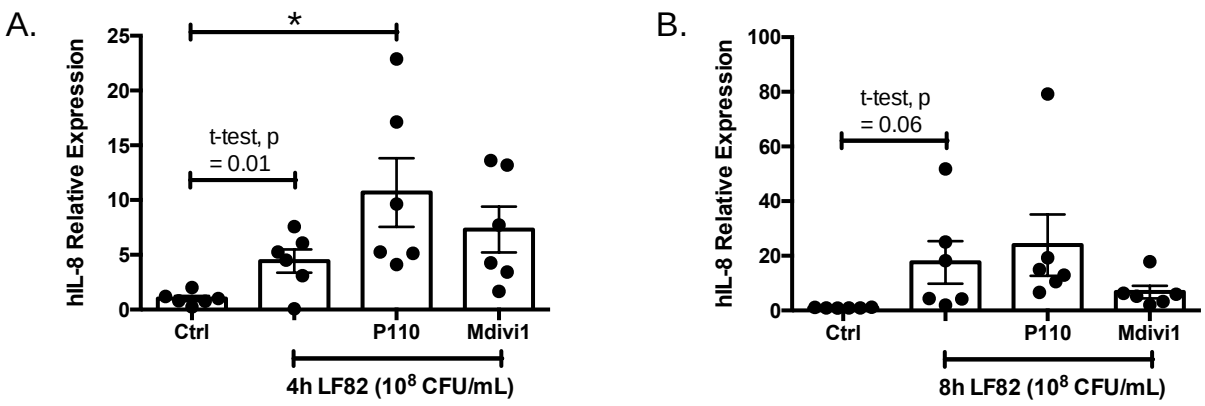

Figure 36. Interleukin-8 gene expression is increased in response to *E. coli* LF82 infection at 4h and 8h. Quantitative PCR analysis on T84 cells infected with *E. coli* LF82 at **(A)** 4h and **(B)** 8h (10^8 CFU/mL). P110 – 30 minute pre-treatment, followed by co-treatment with *E. coli* LF82 (10 μM). Mdivi1 – co-treatment with *E. coli* LF82 (5 μM). Ctrl – control. Relative expression was calculated by normalized IL-8 gene expression to 18S gene expression, and normalizing each sample to the average of the control group. Mean ± SEM, *$p<0.05$, One Way ANOVA, Tukey's Multiple Comparison Test. A t-test between control and *E. coli* LF82 alone gives a p-value of 0.01 and 0.06 for 4h and 8h treatment time respectively.

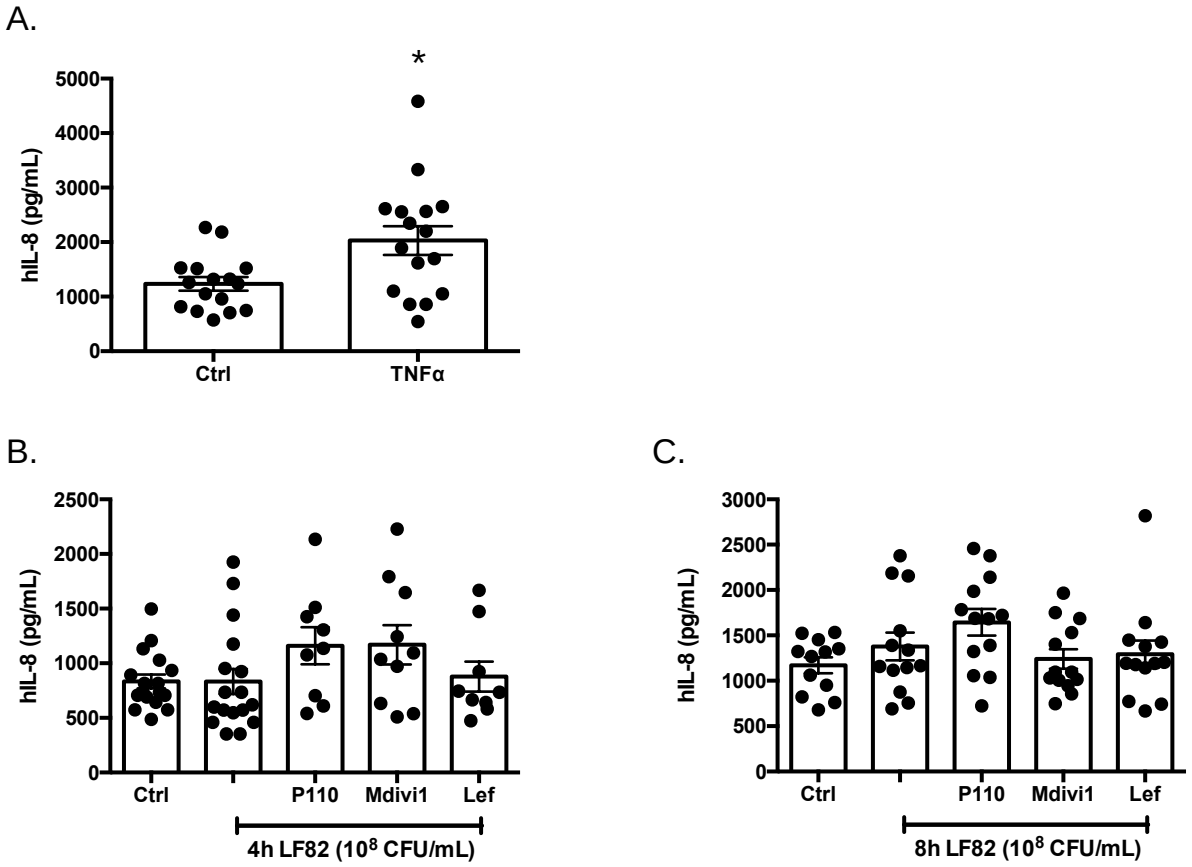

Figure 37. Interleukin-8 protein secretion is not induced by *E. coli* LF82 infection of T84 cells. Interleukin-8 protein secretion was measured in supernatants of T84 cells by Enzyme-linked Immunosorbent Assay **(A)** Tumour Necrosis Factor α was used as a positive control to induce IL-8 secretion from T84 cells (16h, 10 ng/mL), Mean ± SEM, *p<0.05, t-test. **(B)** 4h *E. coli* LF82 infection of T84 cells (10^8 CFU/mL), **(C)** 8h *E. coli* LF82 infection of T84 cells (10^8 CFU/mL). P110 – 30 minute pre-treatment, followed by co-treatment with *E. coli* LF82 (10 μM). Mdivi1 – co-treatment with *E. coli* LF82 (5 μM). Mean ± SEM, p<0.05, One Way ANOVA, Tukey's Multiple Comparison Test.

Table 8. Summary Table						
Time Point & Dose of *E. coli* LF82	**2h (10^8 CFU/mL)**	**4h (10^8 CFU/mL)**	**6h (10^8 CFU/mL)**	**8h (10^8 CFU/mL)**	**12h (10^8 CFU/mL)**	**16h (10^4 CFU/mL)**
Mitochondrial Morphology	50% fission	50% fission	100% fission	100% fission		100% fission
Mechanism	Fission dependent on invasion & Drp1	Fission dependent on Drp1. Loss of membrane potential.	P110 & Mdivi1 do not block fission	P110 & Mdivi1 do not block fission. OPA1 cleavage occurs.		Spent medium & dead bacteria do not induce fission. OPA1 cleavage occurs. Loss of membrane potential.
Consequences (no gentamicin treatment)			~10% cytochrome c release. Loss of barrier function (blocked by Mdivi1)	~50% cytochrome c release (not blocked by P110 & Mdivi1). Loss of barrier function.		
Consequences (gentamicin treatment)				0% fission. <10% cytochrome c release. Similar intracellular CFU's as no gentamicin	75% fission. ~5% cytochrome c release.	

Chapter 4: Discussion

The field of mitochondrial dynamics has been burgeoning with evidence showing that fission and fusion are dysregulated in inflammatory disease. This evidence has been coupled with examples of interventions targeting excessive fission which reduces severity of disease in animal models [270,338,339]. Inflammatory bowel disease is a chronic, debilitating disease that is increasing in prevalence [340]. It is also a disease that has diverse characteristics depending on the individual, highlighting the importance of exploring new ideas for treatments which may be effective in certain patients [341]. Targeting mitochondria in IBD has not been attempted in the clinic, but in parallel studies done to my thesis work, blocking excessive mitochondrial fission by P110 in the DSS and DNBS colitis models reduced disease severity (Appendix I).

The development and propagation of IBD is thought to be tightly connected to microbial dysbiosis of the gastrointestinal tract. In the last decade, many papers have emerged demonstrating how infection with microorganisms disrupts the balance of mitochondrial dynamics, sometimes impacting host cell viability or pathogen load (Table 5). No consensus exists in this field as to whether this regulation benefits the host or microbe, but in the future targeting changes in mitochondrial dynamics in response to infection could be a way to manipulate the host-microbe interaction. My thesis seeks to explore the basic biology of mitochondrial fragmentation induced by Adherent-invasive *E. coli*, which is

considered an IBD pathobiont organism, making it possible to explore targeting mitochondrial fragmentation in patients harboring AIEC in the future.

Measurement of markers of fission and fusion show evidence that mitochondrial dynamics is disrupted in humans with IBD and in an animal model of colitis

Quantitative PCR on genes regulating mitochondrial fusion and fission revealed that mitochondrial dynamics processes were upregulated in the context of disease, suggesting that remodeling of mitochondrial networks may play a role in the development or propagation of IBD. The link between IBD and mitochondrial dynamics has never been considered, so my study supports the advance of a new approach to understanding the biology of IBD, and the development of therapeutics.

As the mitochondrial fusion and fission proteins are highly post-translationally regulated, increases in mRNA expression of these factors does not directly show that protein activity is increased. As both fusion and fission genes are increased (opposite processes with regards to mitochondrial network morphology), a conclusion cannot be made from these data regarding the overall mitochondrial network morphology of cells in the gastrointestinal tract within these tissues. It is possible that the net results of hyperactive processes of mitochondrial dynamics would effect overall mitochondrial network structure within these tissues and therefore mitochondrial network function in IBD compared to control subjects.

Mitochondrial network structure of patient intestinal biopsies could be assessed by performing immunofluorescence on outer membrane mitochondrial

proteins in fixed tissue [342,343], although to my knowledge this method has not been attempted with gastrointestinal tissue, or human tissue sections from any organ. Future studies may benefit from assessing patients with certain disease characteristics (e.g. disease location, disease severity) as with the limited numbers of patients in this study, the patients could not be stratified by stringent parameters that may impact disease substantially.

The fact that patients with IBD vary greatly in responses to treatment [341] suggests that diverse disease phenotypes exist, making the processes of mitochondrial dynamics potentially relevant in certain individuals but not others. As my study focuses on AIEC, it would be interesting to perform a study stratifying individuals by the isolation of AIEC to see if AIEC infection correlated with the gene expression of fission and fusion mediators. Even after conducting this study, it would be impossible to draw clear conclusions about cause-and-effect; if AIEC expansion is promoted within the context of inflammation, which may have altered processes of mitochondrial dynamics due to other factors, or if AIEC induces changes in mitochondrial dynamics in human tissue by itself.

The increases in mitochondrial fusion and fission gene expression shown in human IBD tissue were mirrored in a murine model of colitis, suggesting a link between mitochondrial dynamics and inflammatory processes (Fig.2). Cell types other than epithelial cells may display altered fission and fusion as the epithelial cell changes in mitochondrial dynamics mediators were less striking than those in the total tissue. The increases in gene and protein expression of fission and fusion

genes observed in this study suggests that the processes of mitochondrial dynamics could be dysregulated in the context of inflammation in general and in IBD. Consistent with these data, studies parallel to my thesis work showed that systemic administration of P110, targeting Drp1, reduced severity of DSS and DNBS colitis (Appendix I). The idea that mitochondrial dynamics are disrupted in animal models of colitis is unexplored, and unsurprising considering the literature showing a link between mitochondrial dysfunction and inflammation in these models described in the introduction [264,273–276,290]. Both the DSS and DNBS colitis models utilize chemical injury of the colon to study inflammation. Although these models recapitulate some features of human disease, other animal models of colitis should be used to study the role of mitochondrial dynamics in inflammation more thoroughly (such as the T cell transfer model and IL-10 KO model [344]), in addition to more expansive human studies.

Considering these caveats, these data showing increases in fusion and fission gene and protein expression in IBD tissues and murine models of colitis fit cohesively with the vast literature that is emerging linking mitochondrial dynamics with inflammatory processes across a wide variety of tissues (Table 4). Considering the role of microbes in the etiology of IBD, the AIEC pathobiont has been studied as a possible contributor to inflammation in the context of a genetically or environmentally susceptible host [345]. Murine infection with AIEC, in the context of antibiotic treatment or chemical colitis, for example, have been used as models to study how commensal bacteria could become pathobionts under environmental

conditions within the host that provoke inflammation. My study sought to understand the molecular biology of the induction of severe mitochondrial fragmentation in intestinal epithelial cells in response to AIEC infection, and if this excessive fission could stimulate inflammation initiated by the epithelium.

Mitochondrial dysfunction and mitochondrial fragmentation are features of E. coli LF82 infection

Human colonic epithelial cells lines (T84, HT29, and Caco-2) were used as a model of the gastrointestinal epithelium in this study, which were infected by the LF82 strain of adherent-invasive *E. coli*. *E. coli* LF82 was compared to another AIEC strain *E. coli* NRG857c, and a non-invasive, laboratory strain *E. coli* HB101. Characterization of *E. coli* LF82 and *E. coli* HB101 in my model showed that differences between these strains were likely due to adherent and invasive capabilities of *E. coli* LF82 (which are frequently reported in the literature [34,38,42,50,52]), rather than differences in growth in culture alone (Fig.6).

The small difference in invasion between *E. coli* HB101 and *E. coli* NRG857c was unexpected due to the literature noting that compared to the non-adherent *E. coli* strain HS, *E. coli* NRG857c had similar invasion compared as *E. coli* LF82 in T84 and Caco-2 cells with a similar bacterial inoculum and length of infection as in my study [49]. Differences that could account for this discrepancy could be cell culture media serum content, confluency of epithelial monolayers or differences in the non-invasive *E. coli* strains used.

Crosstalk between intracellular bacteria and mitochondria has been reported in the literature [346]. With respect to AIEC, *E. coli* LF82 has been shown to induce ROS production from T84 cells [80,91], and infection is associated with dysregulated appearance of mitochondria by electron microscopy (although this observation was not recorded or followed up on in this publication or others)[42]. The observation of mitochondrial dysfunction in association with AIEC infection of intestinal epithelial cells *in vitro*, which has not been addressed further in the literature, was recapitulated and expanded by my data. Although mitochondria in infected cells looked rounder and less elongated than control cells by electron microscopy, and electron microscopy is considered the gold standard for assessing mitochondrial ultrastructure, it is not an accurate measurement of mitochondrial network structure due to its 2-dimensional nature [347]. As the differences in mitochondrial ultrastructure were remarkable between infected and control groups in both the short term and long term infection, quantification of the images was deemed unnecessary.

Based on mitochondrial ultrastructure, it was hypothesized that overt mitochondrial dysfunction was occurring in AIEC-infected epithelial cells. Measurement of mitochondrial membrane potential supported this hypothesis, as it is a widely used pertinent indicator of mitochondrial function [348–350]. Considering the ultrastructural deformities, loss of membrane potential (similar to the mitochondrial uncoupler CCCP [349]), and reduction in ATP content, intestinal epithelial cells infected with AIEC were considered to be under metabolic stress,

leading to an interest in studying mitochondrial dynamics as a factor tightly linked to mitochondrial dysfunction. The effect of *E. coli* HB101 infection on mitochondrial membrane potential was not statistically different from control, suggesting that unique characteristics of *E. coli* LF82 (such as adherence and invasion) led to these mitochondrial deficiencies.

To increase the specificity of conclusions regarding loss of ATP concentration attributed to mitochondrial function, the role of glycolysis in ATP production in T84 cells infected with *E. coli* LF82 could be explored by inhibiting glycolysis with 2-deoxyglucose [351]. These findings complement data from others showing that intracellular bacteria can impact mitochondrial function, such as *Brucella abortus* or *Mycobacterium tuberculosis* inhibiting aerobic metabolism to favor anaerobic glycolysis [352,353].

Mitochondrial dysfunction is associated with increased oxidative stress [354]. Reactive oxygen species (mostly superoxide anions) were shown to be produced by T84 cells in response to *E. coli* LF82 (3h, 10^7 CFU/mL) [91]. Jensen *et al.* [80] also reported an induction of ROS production (measured by DCFDA dye) by *E. coli* LF82 in Caco-2 cells 18h post-infection (1h exposure of bacteria, gentamicin treatment, followed by a 17h incubation), at high multiplicities of infection (MOI, 500 and 1000). At an MOI similar to my studies, 100, no ROS production was observed [80]. Elevated levels of ROS were not detected in my experiments at 4h, 6h, or 16h (10^8 CFU/mL) (Fig.10). Variability in timing between the experiment done by Elatrech *et al.* [91] and my experiment could contribute to the discrepancy observed if ROS

production occurred during a critical window of time and was quenched rapidly. It is possible that differences in culture conditions and passaging of bacteria could also contribute to differences in phenotype between the *E. coli* LF82 strain that was used in my study compared to that of Elatrech *et al.* [91].

Methodology used to measure ROS could have also impacted these results as the methods used in Elatrech *et al.* [91] primarily measures superoxide anions, while the DCFDA assay used in my experiments is less selective, measuring all types of ROS [328]. In this case, if different types of ROS were regulated differentially by *E. coli* LF82 in my model, there may be no difference at the endpoint in the presence of total ROS. ROS levels in T84 cells infected with *E. coli* LF82 could be measured more thoroughly by measuring the amount of ROS in each cell by flow cytometry of DCFDA dye [355], or by using dyes that are more specific to mitochondrial ROS such as MitoSOX. The hypothesis that differences in methodology between my study and Elatrech *et al.* [91] explain the differences in results is supported by similarities in observations between Jensen *et al.* [80] and my study both using DCFDA dye.

Mitochondrial network structure is closely tied to minute changes in mitochondrial activity or function [356]. Mitochondrial fragmentation was observed in the human colonic cell lines HT29 and Caco-2 infected with *E. coli* LF82, in addition to T84 cell monolayers, showing that this response is common between most epithelial cells, rather than an isolated response contributed to by unique T84 cell genetics.

Mitochondrial network structure was quantified by rating a single cell per field of view, pre-chosen based on nuclear staining, as fused, intermediate, or fragmented. Although this method has been used in the literature to quantify mitochondrial networks [312,325], new methods in the field have been developed since I have began my studies to quantify mitochondrial networks in an objective fashion using computer algorithms [350,357–359]. Fields of view were chosen in my study based on nuclear staining to increase objectivity of quantification, but this method has several disadvantages including subjectivity of ratings, reduced consistency between experiments and users, and inability to detect subtle changes between groups. If computational quantification was not possible, having a colleague treat the cells before I performed the quantification, to blind myself to the groups, would increase rigor of this method in the future. Although measuring mitochondrial morphology by computation analysis would allow statistical analysis of subtle changes in mitochondrial morphology that are difficult to interpret by eye, high standards for image quality are necessary to use these programs, and cells, or certain cell regions, with highly overlapping mitochondria can be impossible to analyze, although advancing technology is beginning to address this drawback [359].

Overall, the time- and dose- dependent disruption in mitochondrial function and dynamics observed in association with AIEC infection suggests that cell functions influenced by mitochondria (e.g. cell survival, barrier function) may be impacted. The observation that dramatic mitochondrial fragmentation occurs in response to *E. coli* LF82 infection of gastrointestinal epithelial cells supports the

literature showing that a variety of intracellular pathogens (bacterial, viral, and parasitic) drive imbalances in mitochondrial dynamics (Table 5). As this observation is a novel characteristic of AIEC infection, and could contribute to the impact of AIEC infection in humans, the question regarding the mechanism through which AIEC-induced mitochondrial fragmentation occurs arose.

E. coli LF82-induced mitochondrial fragmentation is dependent on adherence and invasion of live bacteria to intestinal epithelial cells

Spent medium exposed to naïve T84 cells, prepared from *E. coli* LF82 co-cultured with T84 cells, did not drive mitochondrial fragmentation (Fig.12A,B). Spent medium prepared in this way would contain any soluble mediators produced or released from *E. coli* LF82. Although adherent-invasive *E. coli* have not been shown to produce toxins found in prototypical pathogenic bacteria [49], the pore-forming alpha hemolysin molecule has been found in some strains [34,67]. Darfeuille-Michaud *et al.* [34] did not find that *E. coli* strain LF82 expressed the gene encoding the alpha hemolysin toxin, so it is assumed that toxins could not have made up a constituent of the spent medium.

Lipopolysaccharide, which could interact with epithelial cells by TLR4 to induce downstream signaling cascades, such as the MyD88/NFKB pathway [360], could be released from *E. coli* LF82 in culture and remain in spent medium to act on T84 cells. LPS alone is known to drive mitochondrial fragmentation, which is mediated by activation of TLR4, and dependent on ROS and Drp1 in pancreatic

cells and microglia [361–365]. As spent medium did not drive mitochondrial fragmentation in T84 cells, released LPS is not thought to play a role in driving *E. coli* LF82-induced fission. This experiment does not exclude the possibility that *E. coli* LF82 LPS activates intracellular TLR4 signaling.

Bacteria in culture, due to production of metabolites through metabolism of media constituents, reduce the pH of cell culture medium [366]. Spent medium prepared from *E. coli* LF82 had reduced pH compared to normal T84 cell medium (inferred by change of colour from red to orange/yellow due to phenol red in medium), but did not drive mitochondrial fragmentation, suggesting that changes in pH of the cell culture medium do not drive mitochondrial fragmentation in T84 cells alone.

This medium could also include any factors produced by T84 cells in response to *E. coli* LF82 infection that have the potential to act in an autocrine mechanism. One example could be cytokines that are upregulated by NFKB in response to TLR signaling such as TNFα and IL-6 which are also found to drive mitochondrial fission in adipocytes and murine gastrocnemius muscle, respectively [237,367], so could be acting in an autocrine fashion to promote fragmentation in T84 cells in response to *E. coli* LF82 spent medium. As these potential constituents of the spent medium did not recapitulate the mitochondrial fission with *E. coli* LF82 bacterial cells, the fission is assumed to be driven by interaction by *E. coli* LF82 physically with T84 cells. Only one bacterium, *Listeria monocytogenes*, was shown to drive mitochondrial fission by a soluble mediator (the LLO toxin, which functions to allow

the bacteria to escape the phagosome after internalization) [296] (Table 5). Other studies did not test the role of bacterial factors in driving mitochondrial fission.

It is important to note the possibility that constituents within the spent medium preparation are labile, therefore could have degraded during the preparation and application of the spent medium. One way to address this possibility, and increase confidence of the conclusion that soluble mediators do not contribute to AIEC-induced fission, would be to measure possible constituents of the spent medium (described above – e.g. LPS, cytokines) at the time of treatment to ensure that they have not been degraded.

After determining that secreted factors were not promoting mitochondrial fission in T84 cells in response to *E. coli* LF82 (suggesting that bacterial cells must physically contact epithelial cells), the question arose; is contact by *E. coli* LF82 with epithelial cells alone sufficient to drive mitochondrial fission? After measuring mitochondrial fragmentation in response to T84 cell culture with dead *E. coli* LF82, it was found that live *E. coli* LF82 were necessary for the induction of mitochondrial fragmentation (Fig.12A,B). *E. coli* LF82 were killed by glutaraldehyde fixation, which should preserve bacterial appendages used to interact with the host cell, allowing physical contact to occur between bacteria and epithelial cells [322]. In my study I confirmed that *E. coli* LF82 prepared this way were non-viable by plating them on blood agar, but did not confirm that these cells have the ability to adhere to intestinal epithelial cells. An option to test this in the future would be to fix epithelial cells exposed to glutaraldehyde-treated *E. coli* LF82 after washing to

determine if bacterial cells remained in association with epithelial cells, compared to a live infection.

Most studies measuring the role of live bacteria in driving a biological response use heat-killed bacteria, rather than fixed bacteria. For this study, fixed bacteria were used as a more measured method in killing bacteria (e.g heated bacteria could lose structural architecture depending on the severity of treatment). These data suggest that mitochondrial fragmentation is not instigated by a host response to the detection of extracellular *E. coli*. Other studies investigating the mechanism of pathogen-induced mitochondrial fission or fusion did not test dead pathogens, ignoring the possible contribution of host responses to extracellular stimulation by pathogens in changes to mitochondrial network structure (Table 5).

Interestingly, *E. coli* NRG857c had reduced invasion into T84 cells compared to *E. coli* LF82 (Fig.6C), which correlated with lack of mitochondrial fragmentation (Fig.13A), suggesting that invasion may play a role in *E. coli* LF82-induced mitochondrial fission. *E. coli* LF82 lacking the fimH-encoded pilus adhesin, which had reduced invasion into T84 cells, induced similar mitochondrial morphologies in T84 cells as uninfected cells (Fig.14). These data support the conclusion that AIEC-induced mitochondrial fission is dependent on invasion. The phenotype of mitochondrial networks in T84 cells infected with fimH mutated *E. coli* LF82 was in-between that of wild-type *E. coli* LF82 infected cells and uninfected cells statistically, most likely due to a small reduction in the proportion of fused mitochondrial networks in the cells infected the fimH mutated *E. coli* LF82

compared to untreated cells. This could be explained by contributions to invasion by other *E. coli* LF82 adhesins such as long polar fimbriae, flagella, or chitinase (ChiA) (Table 1).

E. coli LF82 invasion into T84 cells is low (0.0004%-0.01% of extracellular bacteria invade (Fig.6C)) compared to prototypical pathogens such as *Salmonella typhimurium*, which can reach 1-2% invasion into kidney, cervix, or colonic epithelial cell lines [368,369]. Due to this low level of invasion, it is hypothesized that not all T84 cells in a cell monolayer are infected by *E. coli* LF82. Future experiments would be interesting to determine if cells that contain bacteria have more fragmented mitochondria, and if the number of bacteria inside cells correlated with the degree of fragmentation observed. Interestingly, during infection at 16h (10^4 CFU/mL) of T84 cells with *E. coli* LF82, almost every single cell has fragmented mitochondrial morphology (Fig.11B; Fig.12B), although it is unlikely that every cell is infected with *E. coli* LF82 due to the low level of invasion (Fig.6C). Although at short time points (2h), mitochondrial fragmentation is dependent on invasion, further studies would need to be carried out to explain what component of *E. coli* LF82 infection contributes to mitochondrial fragmentation with low levels of *E. coli* LF82 invasion in cell monolayers that have complete induction of mitochondrial fission. As this mitochondrial fragmentation is not induced by spent medium or dead cells (Fig.13B), perhaps cells are all infected with low numbers of *E. coli* LF82 which have the capacity to drive mitochondrial fission, or cells engage

in intercellular communication which drives mitochondrial fission in uninfected cells.

E. coli LF82-induced mitochondrial fragmentation is not driven by reactive oxygen species

It well known that ROS production is enhanced in mitochondria that display fragmented mitochondrial morphology, and that ROS feed forward to promote mitochondrial fission [329–333]. By utilizing the ROS quenchers vitamin C and mitoTEMPO, which target cellular and mitochondrial ROS respectively, it was observed that reducing levels of ROS in T84 cells did not prevent AIEC-induced mitochondrial fragmentation (Fig.15A,B). As ROS is not completely eliminated by ROS quenchers (Fig.15C), this result does not disqualify the possibility that very small amounts of ROS are able to drive mitochondrial fission. Although ROS was reduced to a statistically significant degree in rotenone (used as a positive control, a complex I inhibitor) treated cells, it is impossible to conclude if the degree of ROS quenching would have a biological effect.

LF82-induced mitochondrial fragmentation is not associated with increased Drp1 phosphorylation or translocation to the mitochondria

Increased phosphorylation at the Ser616 site of Drp1, or recruitment to the mitochondria, surprisingly, were not consistently observed in association with mitochondrial fragmentation at the short or long infection regimens

(Fig.16,17,19,20). Differences in Drp1 were observed at isolated time points or bacterial doses that were not replicated throughout all experiments, potentially reflecting T84 cell passage effects or differences in bacterial invasion between experiments. As invasion was shown to be necessary to induce mitochondrial fission, varying degrees of invasion (potentially due to minute changes in cell confluency between experiments or bacterial phenotype) could lead to varying degrees of Drp1 activation processes that are reflected by phosphorylation of Drp1 or recruitment to the mitochondria.

The signaling pathways that lead to the activation of Drp1 in AIEC-induced fission are unknown. Possible candidate pathways that lead to post-translational modification of Drp1 are described below which could be targeted in the future to fill in the gap between bacterial invasion and the induction of mitochondrial fragmentation.

CCCP was used throughout this study as a mitochondrial fission inducer, as a positive control. CCCP is widely used for this purpose, and is known to lead to mitochondrial membrane depolarization leading to cleavage of OPA1. In some studies, CCCP was shown to induce fission dependent on Drp1 [140,193], and Drp1 recruitment to the mitochondria by western blot of the mitochondrial protein fraction was increased [255,370].

Due to these previous reports, I expected CCCP to induce phosphorylation of Drp1 and recruitment of Drp1 to the mitochondria. Although CCCP is an appropriate positive control to induce mitochondrial fragmentation, it was found

that Drp1 phosphorylation was not altered by CCCP treatment, which is consistent with other studies showing that CCCP-induced fission is independent of Drp1 [168], and that Drp1 recruitment to the mitochondria is not apparent by western blot of the mitochondrial fraction [130,161,371]. This difference could have been due to differences in timing, and cell type. A more appropriate positive control for western blots of Drp1 phosphorylation and recruitment may have been BAPTA-AM, a calcium chelator that induces mitochondrial fission dependent on Drp1 without other effects on mitochondrial membrane potential [152,170].

My data showing no consistent changes in Drp1 by western blot do not dismiss the possibility that Drp1 drives *E. coli* LF82-induced fission. Phosphorylation at the Ser616 site of Drp1 is a modification promoting Drp1 translocation to the mitochondria, regulated by upstream signaling mediators such as CDKI/cyclin B [372], CDK5 [373], Erk2 [374], and AURKA [375] depending on the cellular context. Other phosphorylation sites exist at the Ser637 (modified by PKA [372], AMPK [376] , Calcineurin [372], PGAM5 [377]) and Ser579 (modified by Erk1/2 [378]). SUMOylation of Drp1 is regulated by MAPL [155], DJ-1 [379], and SenP5 [380], promoting fission or fusion depending on the modification and cellular context. Drp1 can also be ubiquitinated by APC/CCdh1 [380] and MITOL/MARCH5 [156–159], effecting mitochondrial network structure.

Complex interplay between these many post-translational modifications could ultimately determine the fate of Drp1 proteins, meaning that the existence of one pro-fission modification supports the possibility of Drp1 driving fission, but the

absence of a single pro-fission modification does not preclude the presence of other modifications which could be regulating Drp1 in *E. coli* LF82-induced fission. Most studies do not resort to measuring every post-translational modification of Drp1 in this case, but rather focus on spatial location of Drp1 in the cell as an indirect measure of Drp1 activity.

Recruitment of Drp1 to the mitochondria was analyzed by western blotting in the mitochondrial protein lysate fraction, and a difference in association with *E. coli* LF82 infection was not observed. Although purity of the mitochondrial fraction was very high (Fig.18), these results could be skewed by small amounts of cytosolic protein contamination, which could contain large numbers of Drp1 molecules (as Drp1 exists primarily in the cytosol when not inducing fission). Due to this reason, western blotting is a less sensitive approach compared to immunofluorescence imaging of Drp1 localization with mitochondria, which could be carried out in the future to further analyze Drp1 translocation in association with AIEC-induced fission.

The presence of Drp1 at the mitochondria is not the only factor that contributes to Drp1-dependent shaping of the mitochondrial network. Multiple lines of evidence showed that the oligomerization state of Drp1 and GTPase activity regulates its competency to become activated at the mitochondria to induce fission. Liu *et al.* [165] and Clinton *et al.* [166] found that Drp1 binding to MFF is sensitive to the oligomerization state of Drp1. MFF and MiD49/51 have been shown to regulate Drp1 GTPase activity differently if interacting with Drp1 in isolation compared to

when they are both present [163]. I opted to target Drp1 pharmacologically and genetically to address the possibility that Drp1 is involved in *E. coli* LF82-induced fission although no evidence of Drp1 phosphorylation (at site Ser616) or recruitment to the mitochondria was observed.

Long term AIEC infection is associated with OPA1 cleavage

As the overall structure of the mitochondrial network is regulated by the balance between fusion and fission mediators, cleavage of OPA1 was measured as an indication of de-activation of OPA1, which would tip the balance towards mitochondrial fragmentation. At the high dose of *E. coli* LF82 (10^8 CFU/mL), OPA1 cleavage was not observed at 2-4 h (Fig.22), but was evident at 8h (Fig. 23B,D). OPA1 cleavage was also observed starting at 10h, 10^6 CFU/mL, and at 16h, 10^2 CFU/mL. Quantification of OPA1 cleavage in the field by densitometry is diverse with some studies showing representative images only and no quantification [136,137,381], the ratio of OPA1 long isoforms to total OPA1 protein levels [382,383], or the ratio of OPA1 short isoforms to OPA1 long isoforms [135].

The latter option was chosen in my study as it most accurately represented the drastic changes in cleavage observed in the majority of experiments, especially when accumulation of short isoforms was observed without complete extinction of long isoforms. As shown in Figure 38, measuring long isoform expression compared to total OPA1 expression underestimates the degree of change compared to control (the ratios are 0.3 and 0.5 respectively), although biologically the increase in short

isoforms even with the same expression of long isoform may be significant. The ratio of long to short isoform expression was not normalized to total protein content (actin), as the total amount of OPA1 between groups was not of interest in this particular study, which is consistent with other methods in the literature [135,382,383].

At early time points when fission is induced (2h, 10^8 CFU/mL), there is no evidence of OPA1 cleavage, while at the longer time points (8h, 10^8 CFU/mL, 16h, 10^4 CFU/mL), OPA1 cleavage occurs, suggesting that OPA1 may play a role in the mechanism of fission induction at later time points. This could be studied further by siRNA knock-down of OMA1, the protease that cleaves OPA1 in response to loss of mitochondrial membrane potential [136–138], or by genetic over-expression of the long isoform of OPA1 that is cleavage resistant [131]. While most studies investigating pathogen-induced imbalances in mitochondrial dynamics focus on the role of Drp1 (described in later sections), during *Chlamydia trachomatis* infection of HeLa cells, OPA1 was shown to be necessary in the induction of mitochondrial fusion and resulting increased bacterial replication [302]. Observing OPA1 cleavage in association with *E. coli* LF82-induced mitochondrial fission, which was not shown in any other studies investigating fission induced by a pathogen, may be a new mechanism through which a microbe-host interaction can occur at the level of the mitochondria.

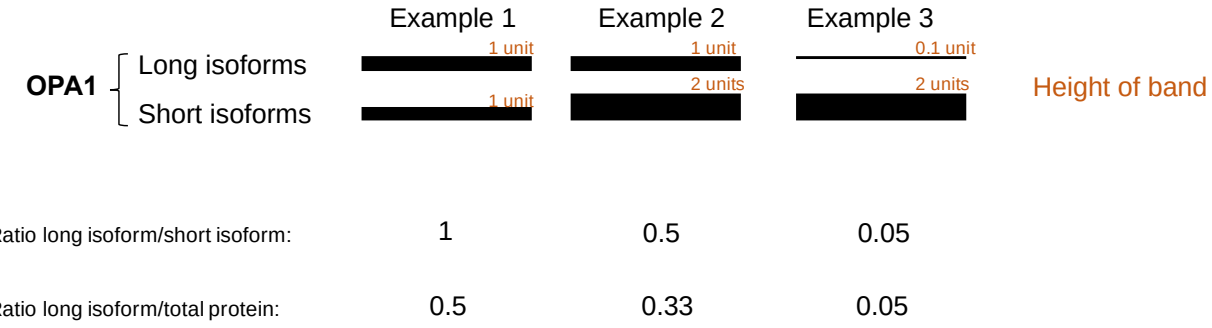

Figure 38. Examples of OPA1 densitometry measurement

E. coli LF82-induced fission is dependent on Drp1

Although Drp1 phosphorylation and recruitment was unchanged as measured by western blot (Fig.17,18,20,21), the role of Drp1 was explored further in *E. coli* LF82-induced mitochondrial fission due to the possibility of Drp1 activation that was missed with the previous methods, as explained above.

P110 and Mdivi1, inhibitors of Drp1-dependent fission, were found to block BAPTA-AM and CCCP induced mitochondrial fission (Fig.24A,B,E,F). Surprisingly, P110 and Mdivi1 did not block CCCP at short time points (2-4h) (Fig.24C,D). This could reflect the fast onset of CCCP induced mitochondrial membrane depolarization (loss of TMRE fluorescence occurs as early as 30 min.), leading to fission. This effect could be reduced as time goes on, as CCCP-induced fission is reversible [193], which could make mitochondrial networks more vulnerable to the effect of P110 and Mdivi1 at the later time points (8h, 16h), allowing the CCCP-

induced fission to be blocked by P110 and Mdivi1 (Fig.23E,F). At higher concentrations of Mdivi1 at 8h and 16h, the number of fragmented cells was increased higher than CCCP, which could result from Mdivi1-induced cytotoxicity, which has been reported in the literature in cancer cell lines from a variety of tissues such as ovary, melanoma, glioblastoma, breast, lung and kidney [384]. From these data I concluded that P110 and Mdivi1 could be used to determine if *E. coli* LF82-induced fission was Drp1-dependent.

One disadvantage of testing these inhibitors in blocking CCCP-induced fission is that during the 16h time point, fission is induced by CCCP within a few hours of treatment, whereas LF82-induced fission at 16h may occur closer to the end of the time point, as the bacterial load increases over time. P110 is a short linear peptide [255], making it vulnerable to metabolism within the cell or in culture [385], compared to Mdivi1, which has a more complex, non-linear structure [256]. By pre-treating T84 cells with P110 for specified periods of time, followed by CCCP treatment, it was observed that P110 has an effect at 10h in culture, whereas at 12h it's CCCP-induced fission blocking effect is lost (Fig.25).

It is necessary to note that P110, Mdivi1, and Leflunomide do not impact growth of *E. coli* LF82 for later experiments when these inhibitors are tested in T84 cells and *E. coli* LF82 co-cultures (Fig.26).

At 4h, P110 and Mdivi1 reduced the degree mitochondrial fragmentation induced by *E. coli* LF82, suggesting that the fission is dependent on Drp1, and that the interaction between Fis1 and Drp1 specifically, is important (Fig.27). P110 had

the greatest effect on the mitochondrial morphology when added every 2 hours into culture (Fig.27). This may be explained by bioavailability of P110 in cell culture in the presence of *E. coli* LF82, or turnover of Fis1 or Drp1 proteins. At 16h post-infection with *E. coli* LF82 (10^4 CFU/mL), P110 co-treatment did not block mitochondrial fragmentation (Fig.27C). This may be due to the reduced effect of P110 past 10h in cell culture conditions (Fig.25). This result may also suggest that Drp1 is no longer responsible for driving *E. coli* LF82-induced mitochondrial fragmentation at long times points, but this conclusion cannot be confirmed as the ability of P110 to block Drp1 at this time point is called into question. Further experiments boosting cell culture concentrations of P110 at different time points over 16h may have clarified this result further. As P110 and Mdivi1 can be used to manipulate *E. coli* LF82-induced mitochondrial fragmentation, they can be used to interrogate the potential downstream events in T84 cells.

Leflunomide treatment was used as another approach to target *E. coli* LF82-induced mitochondrial fragmentation in an attempt to repurpose an FDA approved therapeutic. The variability in the ability of leflunomide to block mitochondrial fragmentation in this model limited its use in investigating downstream consequences of *E. coli* LF82-induced fission (Fig.28).

To further test the role of Drp1 by a different method, Drp1 was knocked out genetically by siRNA (Fig.29). Knock down in basal conditions did not promote a statistically significant difference in mitochondrial morphology compared to control, although fused mitochondria were increased slightly (Fig.30). Control non-targeting

siRNA had no effect on mitochondrial morphology, suggesting that signaling processes induced by siRNA alone did not impact mitochondrial fission and fusion (Fig.28). To further test that the Drp1 siRNA used targets Drp1 specifically, Drp1 could be expressed separately to complement the knocked-down gene, and mitochondrial morphology measured to see if the effects are reversed. Using a second Drp1 siRNA sequence in parallel and observing similar results would also increase confidence that the results are due to Drp1 inhibition rather than off-target effects.

Drp1 siRNA promoted mitochondrial fusion in the context of *E. coli* LF82 infection, which was statistically different than mock transfected infected cells (Fig.30), suggesting that Drp1 is necessary for AIEC-induced fission during a short term, high dose infection (2h, 10^8 CFU/mL). It is noteworthy that only 30% Drp1 protein knock-down was achieved with this protocol, which could explain why inhibition of mitochondrial fission was not greater in the Drp1 siRNA groups. *E. coli* LF82-induced mitochondrial fragmentation was not blocked longer than 4h in this model, which is attributed to the low level of knock-down achieved and the transient nature of siRNA experiments in general. For future studies, the role of Drp1 at later time points of *E. coli* LF82 infection could be interrogated if a knock-down cell line was created through shRNA technology [386–388].

These data are congruent with the literature showing that mitochondrial fragmentation induced by other infectious agents is most often Drp1-dependent, or associated with changes in Drp1 modifications or recruitment to the mitochondria

(Table 5). Exceptions do exist for some organisms, where other possible mechanisms of fission are suggested as contributors to the mitochondrial morphology independent of Drp1 such as constriction of mitochondria by the endoplasmic reticulum [297], or by downregulation of mitochondrial fusion mediators [304,311] (Table 5). Having found that *E. coli* LF82 drives mitochondrial fragmentation, associated with loss of mitochondrial function, a series of assays to assess the impact of this perturbed mitochondrial function on epithelial cell biology were performed.

LF82 infection leads to intestinal epithelial cell death

Cytochrome c release was observed during the later time points of a high dose infection (8h, 10^8 CFU/mL), showing that downstream of the induction of fission (2h), cell death pathways are initiated (Fig.31). Cytochrome c release is considered an irreversible stimuli leading to activation of downstream cell death pathways [155], so is defined as a marker of imminent cell death in my study. Although this is the case in the majority of scenarios, exceptions do exist whereby suppression of apoptotic pathways following cytochrome c release can occur [389]. Further studies would need to be done to confirm if cytochrome c release in this model truly leads to nuclear fragmentation, such as TUNEL (terminal-deoxynucleotidyl-mediated dUTP nick end-labeling) staining, DNA laddering, or chromatin condensation by electron microscopy [390–392].

Although blockade of mitochondrial fission has been shown to reduce cytochrome c release in other experimental systems [204–206,209], P110, Mdivi1, and

Leflunomide did not block AIEC-induced cytochrome c release at 8h (Fig.31B). Of note, although these pharmacological agents reduced AIEC-induced fission at 4h (Fig.27), at 6h and 8h they cease to block mitochondrial fragmentation (Fig.31C). As the bacterial load continues to expand throughout the experiment, extracellular bacteria (which most likely translocate within T84 cells) may reach a point at 6h that drives an excessive level of fission, preventing P110 and Mdivi1 from having an effect. The conclusion that can be drawn from the data showing the P110 and Mdivi1 do not have an effect on *E. coli* LF82 induced cytochrome c release at 8h is that short term inhibition of mitochondrial fragmentation (up to 4h) does not block cell death induced by *E. coli* LF82 at 8h post-infection.

As another possible explanation, OPA1 is cleaved at 8h post-infection (10^8 CFU/mL) with *E. coli* LF82 (Fig.22B), which could be driving AIEC-induced fission at this later time point, whereas AIEC-induced fission at 4h is driven by enhanced Drp1 activity. As P110 and Mdivi1 do not target OPA1, they would not have an effect on cytochrome c release if cytochrome c release is being driven by OPA1 at 8h. This could be due to an imbalance in the mitochondrial dynamics processes; if OPA1, a pro-fusion mediator, has reduced activity due to cleavage, a smaller amount of Drp1 may be necessary to drive fission. A small amount of active Drp1 could act even in the presence of P110 and Mdivi1, as they do not completely block all fission processes (Fig.27). OPA1 has also been described in a limited number of studies as a pro-fission mediator in the cleaved form [187,188], which could also impact

the mitochondrial morphology in my model at 8h, but this idea is not widely accepted in the literature [393].

The induction of cell death in association with mitochondrial fission has been reported in the literature by some intracellular pathogens; *Shigella flexneri*, another intracellular bacteria, induced host cell death (measured by lactate dehydrogenase release from the cell) which was dependent on Drp1 [298]. Rotavirus induced cell death (measured by cytochrome c release and caspase-3 and caspase-9 cleavage) in kidney epithelial cells which was dependent on Drp1 [309]. In contrast, *Chlamydia trachomatis* suppressed host cell death, which was dependent on OPA1 and MFN1/2 [302]. The induction of fission in association with *Brucella abortus* did not impact host cell death [304]. Based on the diverse results of these studies, it cannot be said that cell death universally follows the induction of mitochondrial fission by intracellular pathogens. The observation that *E. coli* LF82 infection is associated with cell death, which is not dependent on mitochondrial fission at early time points, adds to the limited amount of research studying the possible downstream effects of imbalances in mitochondrial dynamics in the context of infection.

One hypothesis to explain why P110, Mdivi1, and Leflunomide did not block cytochrome c release associated with *E. coli* LF82 infection is that great numbers of extracellular bacteria drove increased numbers of intracellular bacteria, to a point that the system was overloaded with fission-inducing stimuli that could not be overcome by the effect of the fission inhibitors. The effect of the intracellular

bacteria that translocate inside T84 cells after 4h of *E. coli* LF82 treatment on cytochrome c release was measured at 8h and 12h following initial infection (using a treatment regimen whereby extracellular bacteria are killed by gentamicin at 4h). Surprisingly, cytochrome c release was not observed 12 h post-infection with this protocol, meaning that the numbers of intracellular bacteria acquired within T84 cells over 4h were not enough to drive cell death (Fig.32A).

Alternatively, the discrepancy at 8h between gentamicin and non-gentamicin treated cells in cytochrome c release could be explained by the massive numbers of extracellular bacteria that exist at 8h (10^{12} CFU/mL), which could drive fission alone. The observation that numbers of intracellular *E. coli* LF82 were the same with or without gentamicin treatment suggests that intracellular bacteria alone were not driving cell death (Fig.32B), supporting the hypothesis that at 8h, extracellular *E. coli* LF82 drove cell death.

Although intracellular bacteria drive mitochondrial fragmentation at 4h, depleting extracellular bacteria blocks the mitochondrial fragmentation observed at 8h, suggesting that this process is reversible (Fig.33C). This result also suggests that past the 4h time point, mitochondrial fragmentation is driven by extracellular bacteria rather than intracellular bacteria, as fission is lost when extracellular bacteria are removed at 4h (Fig.32C).

All of these conclusions rely on the hypothesis that cell death induced by *E. coli* LF82 is dependent on mitochondrial fragmentation, which could not be tested in this model due to the inefficacy of P110 and Mdivi1 in blocking mitochondrial

fission past 4h. It is also possible that epithelial cell death in response to *E. coli* LF82 is unrelated to mitochondrial fragmentation. This hypothesis could be tested by creating a stable knock-down of Drp1 by shRNA [386–388].

As AIEC-induced cell death in epithelial cells is scarcely studied, I measured cleavage of caspase-3 to determine if cell death occurs through the prototypical apoptotic pathway through activation of the apoptosome which targets cleavage of caspase 3 and caspase 7 [394]. At 12h post-infection (10^8 CFU/mL), and 24h post-infection (10^6 CFU/mL) no evidence of cleaved caspase-3 was observed (Fig.31), suggesting that AIEC-induced cell death is independent of caspase 3, one pathway that can be activated by intrinsic apoptosis. This is consistent with a report describing infection with *brucella arbortus* where cell death is induced without activation of caspase-3 [304]. AIEC-induced cell death could be through AIF (apoptosis inducing factor)-dependent apoptosis, as AIF is also released from the mitochondrial matrix similar to cytochrome c release to initiate this pathway, independent of caspases [115].

The observation of cytochrome c release in association with *E. coli* LF82 infection without caspase-3 cleavage does not exclude the possibility that necrosis, rather than apoptosis, may be occurring in response to *E. coli* LF82 infection of T84 cells [395,396]. The release of cytosolic contents, such as lactate dehydrogenase (LDH) from cells infected with *E. coli* LF82 could be measured to determine if necrosis is a possible pathway occurring in this model, but as cellular membrane permeability

can occur in late stage apoptosis *in vitro* [394], apoptosis and necrosis cannot be definitively differentiated this way.

Within the category of necrosis, cell death can occur via an unregulated pathway, or by necroptosis, which is a pathway regulated by the activation of RIPK1/3 (Receptor interacting serine/threonine kinase 1) and MLKL (Mixed lineage kinase domain like pseudokinase) [394,397]. To determine if necroptosis is occurring, RIPK1 or MLKKL could be measured by western blot or downstream cell death could be measured after necrostatin treatment, which targets RIPK1. Necroptosis has been linked to the induction of mitochondrial fission in some studies, whereas others show that these processes are unrelated [219].

Barrier function is lost in association with E. coli LF82 infection of T84 cells, which is blocked by Mdivi1

As different strains of adherent-invasive *E. coli* have been previously reported to disrupt barrier function in the literature [48,52,66,67], barrier function in response to *E. coli* LF82 infection was measured by TER in T84 monolayers and in human biopsies mounted in Ussing chambers (Fig.34A). Transepithelial resistance is a measure of ion conductance between cells, so is mostly a measure of paracellular permeability mediated by tight junction characteristics. Transepithelial resistence will also be effected by larger barrier defects other than loosening of tight junctions, so loss of TER in this model does not indicate the size of the barrier function induced by *E. coli* LF82. The observation that translocation of

70 kDa FITC-dextran from the apical to basolateral side of T84 cell monolayers indicates that larger paracellular barrier defects are present than subtle loosening of tight junctions (Fig.34B,C). The ability of *E. coli* LF82 to translocate through T84 cells supports the existence of a paracellular gap at least the size of bacteria (which are greater in size than a 70kDa FITC-dextran molecule [398]), but could also be attributed to transcellular translocation of bacteria (Fig.34B,C).

The main aim of this experiment was to determine if barrier dysfunction induced by *E. coli* LF82 was dependent on mitochondrial fragmentation. The fission inhibitors P110, Mdivi1 and Leflunomide did not block the loss of TER at 6h (Fig.34A), suggesting that the loss of barrier function was not dependent on mitochondrial fragmentation up to 4h. As P110 did not block mitochondrial fragmentation past 4h (Fig.27), it is possible that the fission proceeding after this time point lead to barrier losses at 6h that are dependent on mitochondrial fission. This question could be addressed by creating a stable knock-down of Drp1 by shRNA [386–388]. P110 and Leflunomide did not block FITC-dextran flux (Fig.34B) or translocation of bacteria through the cell monolayer (Fig.34D) at 6h, suggesting that loss of barrier function at this time point was not dependent on mitochondrial fragmentation mediated by the Drp1-Fis1 interaction (which is targeted by P110) at 4h.

When analyzing the FITC-dextran and bacterial translocation data further, Mdivi1 was found to reduce the loss of barrier function induced by *E. coli* LF82 (Fig.34C,E). One experiment was excluded which showed the same trend as the

other three experiments, but the differences between control, infected, and infected with Mdivi1 groups was much larger than the other experiments, making the 2-fold changes in the presented data appear insignificant (the excluded data are included in Fig.34B). Together the FITC-dextran and bacterial translocation data show that loss of barrier function induced by *E. coli* LF82 is dependent on mitochondrial fission by Drp1. In Fig.27 it was shown that mitochondrial fission in response to *E. coli* LF82 infection at 4h depends on Drp1 interaction with Fis1, as P110 (which targets this interaction), reduced fission. As mdivi1 targets Drp1 GTPase activity, mitochondrial fission leading to loss of barrier function may depend on the interaction of Drp1 with other adaptors other than Fis1, such as MFF. Fission overall may depend on interaction of Drp1 with all adaptors, while the fission that contributes to effects on barrier function may not rely on Fis1. Mdivi1 blocking *E. coli* LF82-induced permeability in the epithelium is unprecedented considering barrier function was not considered in other studies investigating imbalances in mitochondrial dynamics in response to infection. As barrier function is a major contributor to the etiology of inflammatory bowel disease, the discovery that mitochondrial dynamics may impact gastrointestinal epithelial barrier function is a major contribution to the field studying a role for mitochondria in inflammatory bowel disease.

Flux of FITC-dextran is most likely mediated by paracellular permeability. As Mdivi1 did not impact the loss of TER induced by *E. coli* LF82, the effect of mitochondrial fragmentation on permeability is not attributed to minute tight-

junction dependent changes due to reduced levels of energy in the cell. Larger gaps in the cell monolayer must exist to allow passage of FITC-dextran (compared to loss of TER), which are repaired by blocking mitochondrial fragmentation. This could occur through the loss of a small amount of cells by cell death, creating a wound. Although low amounts of cytochrome c release were observed at 6h post-infection with *E. coli* LF82, (average 4% of cells (Fig.32B)) small numbers of cells released from the monolayer could contribute to the translocation of FITC-dextran observed.

As wound healing is an energy demanding process, the reduction in energy production associated with mitochondrial fragmentation could impact restitution of this wound. When mdivi1 blocked mitochondrial fragmentation associated with *E. coli* LF82 infection, perhaps restitution of small wounds was restored, reducing the amount of FITC-dextran flux through the cell monolayer. The role of mitochondrial dynamics has been studied with respect to wound healing. Zhao *et al.* [399] demonstrated that in human epithelial breast cancer cell lines, inhibition of Drp1 reduced lamellipodia formation, suggesting that fission could promote wound healing through cell migrating and cell spreading. Jo *et al.* [388] presented data showing that in mouse embryonic fibroblasts, inhibition of Drp1 reduced lamellipodia formation induced by platelet-derived growth factor (PDGF), although this was thought to be unrelated to mitochondrial fragmentation as mitochondria were not localized to lamellipodia. The data from these two papers suggests that Drp1 activity could promote wound healing, which is contradictory to the hypothesis presented by my study, although Zhao *et al.* [399] also showed that depleting energy in

breast cancer cells blocked lamellipodia formation and cell migration. In my model, energy levels are reduced in *E. coli* LF82 infection, which could limit wound healing in response to a barrier defect similar to [399].

In order to investigate the role of mitochondrial fission, and Drp1, in wound healing in the context of *E. coli* LF82 infection, scratch wound assays could be carried out. As reported literature on the relationship between mitochondrial fission and wound healing is contradictory to the hypothesis that impaired wound healing due to excessive mitochondrial fission leads to loss of barrier function in my model, investigation of wound healing in the future would be necessary to clarify how Mdivi1 could contribute to barrier function. Comparing energy levels between *E. coli* LF82 infected cells and *E. coli* LF82 with Mdivi1 would also help clarify these results. Barrier function and wound healing during *E. coli* LF82 infection should also be studied in a model system utilizing genetic knockdown of Drp1 to eliminate the contribution of possible off-target effects of Mdivi1, as it has been suggested that Mdivi1 can impact electron transport chain function [400].

Cytochrome c release occurs, on average, in 40% of T84 cells within a monolayer infected with *E. coli* LF82 at 8h (Fig.31). As cytochrome c release is an early step in cell death, it is hypothesized that the cell monolayer is largely intact at 8h, however it is possible that cell death by a small number of cells could drive loss of TER. For this reason, Z-VAD, a caspase inhibitor, was used to test if cell death contributed to the reduction in TER induced by *E. coli* LF82 infection. The lack of effect by Z-VAD is consistent with the absence of caspase-3 cleavage associated with

E. coli LF82 infection (Fig.33). In order to test if TER losses are a result of caspase independent cell death (necroptosis, for example), necrostatin-1 could be used.

Mitochondrial fragmentation induced by E. coli LF82 does not impact bacterial persistence

Many intracellular pathogens are known to drive changes in mitochondrial dynamics, which ultimately alters the replication of the pathogen in some models, or the ability of the host to clear the infection [299,302,303,309,312,317]. Numbers of intracellular *E. coli* LF82 were not altered in the presence of P110 or Mdivi1, suggesting that the mitochondrial morphology induced by infection does not alter replication, internalization, or clearance of bacteria (Fig.35). Leflunomide co-treatment with *E. coli* LF82 did result in a reduced number of intracellular bacteria, which could be attributed to this agent's effect on pyrimidine metabolism, especially as the two fission inhibitors had no effect on intracellular bacteria when the outcome of all 3 agents is similar (more fused mitochondrial networks). Leflunomide inhibits the mitochondrial enzyme dihydroorotate dehydrogenase, blocking synthesis of pyrimidines [323]. As bacteria may use pyrimidines for nucleotide synthesis [401], Leflunomide could block the ability of bacteria to replicate or survive. The variability of Leflunomide in promoting mitochondrial fusion in the context of *E. coli* LF82 infection also suggests that off-target effects may be contributing to the reduction in intracellular bacteria (Fig.28). Bacterial growth curves with Leflunomide did not show an effect of the drug on extracellular

bacterial growth (Fig.26), but this does not exclude the possibility that Leflunomide impacts intracellular bacterial growth.

Interleukin-8 gene transcription, but not protein secretion is induced by E. coli LF82 in T84 cells

IL-8 gene expression was increased by *E. coli* LF82 at 4h and 8h (Fig.36). IL-8 gene transcription is induced by transcription factors targeting the NFκB and MAPK (Mitogen-activated protein kinase) pathways, which is activated by bacteria such as *E. coli* LF82 [336]. This increase in IL-8 gene expression in response to *E. coli* LF82 is consistent with many similar reports in the literature (Table 2). The dependence of IL-8 gene expression in response to *E. coli* LF82 on mitochondrial fission was measured as the production of cytokines can be heavily regulated by mitochondrial activity, highlighted by the observation that immune cells alter their metabolic profile in response to activation to favor glycolytic energy production, fueling cytokine production [402]. Mitochondrial dysfunction in intestinal epithelial cells has also been shown to promote IL-8 production [337]. Earlier in my study I showed that spent medium, which should contain any released LPS from *E. coli* LF82, did not induce mitochondrial fragmentation, but the induction of IL-8 by *E. coli* LF82 was still tested incase intracellular TLR receptors are activated by *E. coli* LF82 LPS. Although LPS-induced cytokine gene production has been shown to be impacted by mitochondrial fission in microglia [365], this observation was not recapitulated in my study at 4h post-infection (Fig.36A). At the 8h time point, P110

and Mdivi1 no longer block mitochondrial fission induced by *E. coli* LF82 (Fig.30C), allowing the conclusion to be drawn that IL-8 gene expression at 8h is independent of mitochondrial fission induced at 4h. The IL-8 gene expression that is induced by 8h could be driven by later mitochondrial fission occurring during the 6h-8h time points, which is not blocked by P110 and Mdivi1. Although T84 cells in culture had the ability to secrete IL-8 protein (Fig.37A), *E. coli* LF82 did not induce secretion of IL-8 at 4h (Fig.37B) or 8h (Fig.37C). IL-8 gene expression is increased at 4h and 8h (Fig.36), making protein translation possible at either of these time points. As reports exist in the literature of IL-8 protein being secreted by T84 cells in response to *E. coli* LF82 infection [49,88,89], these results were surprising. This discrepancy may exist due to experimental parameters such as the treatment dose and time with *E. coli* LF82, or seeding density of cells (e.g. sub-confluent vs. polarized epithelium). It is interesting to note that only 1 report compared mRNA and protein levels of IL-8 [89], therefore the protein production of IL-8 cannot be evaluated in the majority of studies that reported an increase in IL-8 transcription. My study suggests that although IL-8 transcription is increased, this mRNA is regulated to block translation of IL-8 protein. This could result from an adaptive response by *E. coli* LF82 to remain immunologically silent within epithelial cells. Manipulation of host cell cytokine production by targeting protein translation has been observed with other intracellular bacteria such as *Legionella pneumophila* [403].

Chapter 5: Conclusions

This thesis explored the novel idea that mitochondrial dynamics play a role in the development or propagation of IBD, utilizing a model of bacterial infection in the gastrointestinal epithelium.

The Crohn's disease pathobiont, adherent-invasive *E. coli* strain LF82, was observed to induce massive fragmentation of mitochondrial networks in intestinal epithelial cells, making significant headway in a new direction of AIEC pathogenesis. Mechanistic analysis of AIEC-induced mitochondrial fragmentation revealed that fission was dependent on adhesion and invasion of live *E. coli* LF82. Drp1, the presumed mediator of mitochondrial fission, was necessary in the induction of mitochondrial fission by *E. coli* LF82.

Infection of the intestinal epithelium by *E. coli* LF82 resulted in increased permeability of the epithelium, cell death, and gene expression of IL-8. It was observed that mitochondrial fragmentation induced by *E. coli* LF82 at early time points did not contribute to later cell death or IL-8 gene expression, but this study produced preliminary data on the consequences of *E. coli* LF82 induced fission. Further studies are necessary to realize the full impact of *E. coli* LF82-induced mitochondrial fragmentation on the function of the gastrointestinal epithelium *in vitro*. Stable knock-down of Drp1 and expression of non-cleavable OPA1 would allow full exploration of the role of these proteins in the mechanism of fission, and to

measure the impact that fission has on downstream events in a well-rounded manner.

Interestingly, it was observed that Mdivi1 treatment reduced *E. coli* LF82 induced barrier losses in the intestinal epithelium, suggesting for the first time that barrier losses induced by an intracellular pathogen could be dependent on mitochondrial dynamics. Although further study is necessary to determine how Mdivi1 impacted barrier function, this laid the groundwork for discovering what impact *E. coli* LF82-induced fragmentation could have in the gastrointestinal epithelium. Barrier function is a major factor contributing to the etiology of inflammatory bowel disease, and mucosal healing is the gold standard criteria for disease remission [404], leaving the provocative question: does AIEC infection in inflammatory bowel disease patients promote dysfunctional barrier processes due to mitochondrial fragmentation in the intestinal epithelium, promoting inflammation and disease? This question may be premature, but this thesis provides the preliminary data which could be used to build upon this hypothesis in future studies.

As the regulation of mitochondrial dynamics by infectious agents emerges as a common theme in the literature, this work adds to the body of literature describing how mitochondrial dynamics may act as a key aspect of the host-microbe interaction in all tissues. It is interesting to speculate if alterations in mitochondrial dynamics due to this interaction are beneficial to the host or microbial cell, as both interpretations have been presented in a variety of other infection models (Table 5).

Due to the impact of Mdivi1 on barrier function in response to *E. coli* LF82 infection, I would hypothesize that the induction of mitochondrial fission *in vivo* by *E. coli* LF82 would increase inflammation in the host by allowing entry of luminal contents into the mucosa, increasing disease severity. Increased permeability may be beneficial to *E. coli* LF82 *in vivo* if it is able to establish a niche in the mucosa inside immune cells and persist.

In order to interrogate the above hypothesis, and translate this mechanistic work into a candidate for therapeutic targeting, studies investigating the effect of adherent-invasive *E. coli* on mitochondrial dynamics *in vivo* must be carried out. Determining if mitochondrial fragmentation occurs *in vivo* with adherent-invasive *E. coli* infection has become possible with the emergence of several models allowing susceptibility to colonization of adherent-invasive *E. coli* in mice; the CEABAC10 transgenic mouse [94,101,102], antibiotic treatment [86,103], DSS treatment [68–70], or antibiotic treatment in combination with DSS treatment [85,94]. With one of these colitis models, P110 or Mdivi1 could be used to target mitochondrial fragmentation to determine the effect on inflammation and disease.

Literature emerges daily on the role of mitochondrial dynamics in a vast variety of tissues and disease states, and this study adds to this field by further expanding the possible applications of targeting excessive mitochondrial fission to the gastrointestinal system. As the role of mitochondrial dynamics in innate immunity becomes clearer, interventions to target the complex interplay between

host and microbe may become a possible avenue for treating inflammatory bowel disease.

References

1. Lewis, M. R. & Lewis, W. H. MITOCHONDRIA IN TISSUE CULTURE. *Science* **39**, 330–333 (1914).
2. Barrett, K. E. *Gastrointestinal Physiology*. (Lange Medical Books/McGraw-Hill, 2014).
3. Thompson, C. A., DeLaForest, A. & Battle, M. A. Patterning the gastrointestinal epithelium to confer regional-specific functions. *Dev. Biol.* **435**, 97–108 (2018).
4. Kalliomaki, M. A. & Walker, W. A. Physiologic and pathologic interactions of bacteria with gastrointestinal epithelium. *Gastroenterol. Clin. North Am.* **34**, 383–99, vii (2005).
5. Gribble, F. M. & Reimann, F. Enteroendocrine Cells: Chemosensors in the Intestinal Epithelium. *Annu. Rev. Physiol.* **78**, 277–299 (2016).
6. Nevo, S., Kadouri, N. & Abramson, J. Tuft cells: From the mucosa to the thymus. *Immunol. Lett.* (2019). doi:10.1016/j.imlet.2019.02.003
7. McCracken, V. J. & Lorenz, R. G. The gastrointestinal ecosystem: a precarious alliance among epithelium, immunity and microbiota. *Cell. Microbiol.* **3**, 1–11 (2001).
8. Nakamura, Y., Kimura, S. & Hase, K. M cell-dependent antigen uptake on follicle-associated epithelium for mucosal immune surveillance. *Inflamm. Regen.* **38**, 15 (2018).

9. Leung, C.-Y. & Weitz, J. S. Not by (Good) Microbes Alone: Towards Immunocommensal Therapies. *Trends Microbiol.* **27**, 294–302 (2019).

10. Sivaprakasam, S., Prasad, P. D. & Singh, N. Benefits of short-chain fatty acids and their receptors in inflammation and carcinogenesis. *Pharmacol. Ther.* **164**, 144–151 (2016).

11. Pirzer, U., Schonhaar, A., Fleischer, B., Hermann, E. & Meyer zum Buschenfelde, K. H. Reactivity of infiltrating T lymphocytes with microbial antigens in Crohn's disease. *Lancet (London, England)* **338**, 1238–1239 (1991).

12. Graff, L. A. *et al.* The relationship of inflammatory bowel disease type and activity to psychological functioning and quality of life. *Clin. Gastroenterol. Hepatol.* **4**, 1491–1501 (2006).

13. Herzer, M., Denson, L. A., Baldassano, R. N. & Hommel, K. A. Patient and parent psychosocial factors associated with health-related quality of life in pediatric inflammatory bowel disease. *J. Pediatr. Gastroenterol. Nutr.* **52**, 295–299 (2011).

14. Pearson, A. D., Eastham, E. J., Laker, M. F., Craft, A. W. & Nelson, R. Intestinal permeability in children with Crohn's disease and coeliac disease. *Br. Med. J. (Clin. Res. Ed).* **285**, 20–21 (1982).

15. Muise, A. M. *et al.* Polymorphisms in E-cadherin (CDH1) result in a mis-localised cytoplasmic protein that is associated with Crohn's disease. *Gut* **58**, 1121–1127 (2009).

16. Das, P. *et al.* Comparative tight junction protein expressions in colonic

Crohn's disease, ulcerative colitis, and tuberculosis: a new perspective. *Virchows Arch.* **460**, 261–270 (2012).

17. Mann, E. R. & Li, X. Intestinal antigen-presenting cells in mucosal immune homeostasis: crosstalk between dendritic cells, macrophages and B-cells. *World J. Gastroenterol.* **20**, 9653–9664 (2014).
18. Cadwell, K. *et al.* A key role for autophagy and the autophagy gene Atg16l1 in mouse and human intestinal Paneth cells. *Nature* **456**, 259–263 (2008).
19. Kaser, A. *et al.* XBP1 links ER stress to intestinal inflammation and confers genetic risk for human inflammatory bowel disease. *Cell* **134**, 743–756 (2008).
20. Mitsuyama, K. & Sata, M. Gut microflora: a new target for therapeutic approaches in inflammatory bowel disease. *Expert Opin. Ther. Targets* **12**, 301–312 (2008).
21. Swidsinski, A. *et al.* Mucosal flora in inflammatory bowel disease. *Gastroenterology* **122**, 44–54 (2002).
22. Bibiloni, R., Mangold, M., Madsen, K. L., Fedorak, R. N. & Tannock, G. W. The bacteriology of biopsies differs between newly diagnosed, untreated, Crohn's disease and ulcerative colitis patients. *J. Med. Microbiol.* **55**, 1141–1149 (2006).
23. Sokol, H., Lepage, P., Seksik, P., Dore, J. & Marteau, P. Temperature gradient gel electrophoresis of fecal 16S rRNA reveals active Escherichia coli in the microbiota of patients with ulcerative colitis. *J. Clin. Microbiol.* **44**, 3172–3177 (2006).

24. Manichanh, C. *et al.* Reduced diversity of faecal microbiota in Crohn's disease revealed by a metagenomic approach. *Gut* **55**, 205–211 (2006).

25. Frank, D. N. *et al.* Molecular-phylogenetic characterization of microbial community imbalances in human inflammatory bowel diseases. *Proc. Natl. Acad. Sci. U. S. A.* **104**, 13780–13785 (2007).

26. Duboc, H. *et al.* Connecting dysbiosis, bile-acid dysmetabolism and gut inflammation in inflammatory bowel diseases. *Gut* **62**, 531–539 (2013).

27. Lopez-Siles, M. *et al.* Mucosa-associated Faecalibacterium prausnitzii and Escherichia coli co-abundance can distinguish Irritable Bowel Syndrome and Inflammatory Bowel Disease phenotypes. *Int. J. Med. Microbiol.* **304**, 464–475 (2014).

28. Marchesi, J. R. *et al.* Rapid and noninvasive metabonomic characterization of inflammatory bowel disease. *J. Proteome Res.* **6**, 546–551 (2007).

29. Mow, W. S. *et al.* Association of antibody responses to microbial antigens and complications of small bowel Crohn's disease. *Gastroenterology* **126**, 414–424 (2004).

30. Hugot, J. P. *et al.* Association of NOD2 leucine-rich repeat variants with susceptibility to Crohn's disease. *Nature* **411**, 599–603 (2001).

31. Ogura, Y. *et al.* A frameshift mutation in NOD2 associated with susceptibility to Crohn's disease. *Nature* **411**, 603–606 (2001).

32. Hampe, J. *et al.* A genome-wide association scan of nonsynonymous SNPs identifies a susceptibility variant for Crohn disease in ATG16L1. *Nat. Genet.*

39, 207–211 (2007).

33. Jeong, D. Y. *et al.* Induction and maintenance treatment of inflammatory bowel disease: A comprehensive review. *Autoimmun. Rev.* (2019). doi:10.1016/j.autrev.2019.03.002

34. Darfeuille-Michaud, A. *et al.* Presence of adherent Escherichia coli strains in ileal mucosa of patients with Crohn's disease. *Gastroenterology* **115**, 1405–1413 (1998).

35. Martin, H. M. *et al.* Enhanced Escherichia coli adherence and invasion in Crohn's disease and colon cancer. *Gastroenterology* **127**, 80–93 (2004).

36. Elliott, T. R. *et al.* Quantification and characterization of mucosa-associated and intracellular Escherichia coli in inflammatory bowel disease. *Inflamm. Bowel Dis.* **19**, 2326–2338 (2013).

37. Nazareth, N. *et al.* Prevalence of Mycobacterium avium subsp. paratuberculosis and Escherichia coli in blood samples from patients with inflammatory bowel disease. *Med. Microbiol. Immunol.* **204**, 681–692 (2015).

38. Barnich, N. *et al.* CEACAM6 acts as a receptor for adherent-invasive E. coli, supporting ileal mucosa colonization in Crohn disease. *J. Clin. Invest.* **117**, 1566–1574 (2007).

39. Boudeau, J., Glasser, A. L., Masseret, E., Joly, B. & Darfeuille-Michaud, A. Invasive ability of an Escherichia coli strain isolated from the ileal mucosa of a patient with Crohn's disease. *Infect. Immun.* **67**, 4499–4509 (1999).

40. Sepehri, S. *et al.* Characterization of Escherichia coli isolated from gut

biopsies of newly diagnosed patients with inflammatory bowel disease. *Inflamm. Bowel Dis.* **17**, 1451–1463 (2011).

41. Martinez-Medina, M. *et al.* Biofilm formation as a novel phenotypic feature of adherent-invasive Escherichia coli (AIEC). *BMC Microbiol.* **9**, 202 (2009).
42. Darfeuille-Michaud, A. *et al.* High prevalence of adherent-invasive Escherichia coli associated with ileal mucosa in Crohn's disease. *Gastroenterology* **127**, 412–421 (2004).
43. Baumgart, M. *et al.* Culture independent analysis of ileal mucosa reveals a selective increase in invasive Escherichia coli of novel phylogeny relative to depletion of Clostridiales in Crohn's disease involving the ileum. *ISME J.* **1**, 403–418 (2007).
44. Dogan, B. *et al.* Multidrug resistance is common in Escherichia coli associated with ileal Crohn's disease. *Inflamm. Bowel Dis.* **19**, 141–150 (2013).
45. Lapaquette, P., Glasser, A. L., Huett, A., Xavier, R. J. & Darfeuille-Michaud, A. Crohn's disease-associated adherent-invasive E. coli are selectively favoured by impaired autophagy to replicate intracellularly. *Cell. Microbiol.* **12**, 99–113 (2010).
46. Lapaquette, P., Bringer, M. A. & Darfeuille-Michaud, A. Defects in autophagy favour adherent-invasive Escherichia coli persistence within macrophages leading to increased pro-inflammatory response. *Cell. Microbiol.* **14**, 791–807 (2012).
47. Negroni, A. *et al.* NOD2 induces autophagy to control AIEC bacteria

infectiveness in intestinal epithelial cells. *Inflamm. Res.* (2016). doi:10.1007/s00011-016-0964-8

48. Sasaki, M. *et al.* Invasive Escherichia coli are a feature of Crohn's disease. *Lab. Invest.* **87**, 1042–1054 (2007).

49. Eaves-Pyles, T. *et al.* Escherichia coli isolated from a Crohn's disease patient adheres, invades, and induces inflammatory responses in polarized intestinal epithelial cells. *Int. J. Med. Microbiol.* **298**, 397–409 (2008).

50. Raso, T. *et al.* Analysis of Escherichia coli isolated from patients affected by Crohn's disease. *Curr. Microbiol.* **63**, 131–137 (2011).

51. Schippa, S. *et al.* A potential role of Escherichia coli pathobionts in the pathogenesis of pediatric inflammatory bowel disease. *Can. J. Microbiol.* **58**, 426–432 (2012).

52. Negroni, A. *et al.* Characterization of adherent-invasive Escherichia coli isolated from pediatric patients with inflammatory bowel disease. *Inflamm. Bowel Dis.* **18**, 913–924 (2012).

53. Agus, A., Massier, S., Darfeuille-Michaud, A., Billard, E. & Barnich, N. Understanding host-adherent-invasive Escherichia coli interaction in Crohn's disease: opening up new therapeutic strategies. *Biomed Res. Int.* **2014**, 567929 (2014).

54. Sepehri, S., Kotlowski, R., Bernstein, C. N. & Krause, D. O. Phylogenetic analysis of inflammatory bowel disease associated Escherichia coli and the fimH virulence determinant. *Inflamm. Bowel Dis.* **15**, 1737–1745 (2009).

55. Nash, J. H. *et al.* Genome sequence of adherent-invasive Escherichia coli and comparative genomic analysis with other E. coli pathotypes. *BMC Genomics* **11**, 667 (2010).

56. Dreux, N. *et al.* Point mutations in FimH adhesin of Crohn's disease-associated adherent-invasive Escherichia coli enhance intestinal inflammatory response. *PLoS Pathog.* **9**, e1003141 (2013).

57. Desilets, M. *et al.* Genome-based Definition of an Inflammatory Bowel Disease-associated Adherent-Invasive Escherichia coli Pathovar. *Inflamm. Bowel Dis.* **22**, 1–12 (2016).

58. Boudeau, J., Barnich, N. & Darfeuille-Michaud, A. Type 1 pili-mediated adherence of Escherichia coli strain LF82 isolated from Crohn's disease is involved in bacterial invasion of intestinal epithelial cells. *Mol. Microbiol.* **39**, 1272–1284 (2001).

59. Chassaing, B. *et al.* Crohn disease--associated adherent-invasive E. coli bacteria target mouse and human Peyer's patches via long polar fimbriae. *J. Clin. Invest.* **121**, 966–975 (2011).

60. Barnich, N., Boudeau, J., Claret, L. & Darfeuille-Michaud, A. Regulatory and functional co-operation of flagella and type 1 pili in adhesive and invasive abilities of AIEC strain LF82 isolated from a patient with Crohn's disease. *Mol. Microbiol.* **48**, 781–794 (2003).

61. Chassaing, B., Etienne-Mesmin, L., Bonnet, R. & Darfeuille-Michaud, A. Bile salts induce long polar fimbriae expression favouring Crohn's disease-

associated adherent-invasive Escherichia coli interaction with Peyer's patches. *Environ. Microbiol.* **15**, 355–371 (2013).

62. Chan, C. H. F. & Stanners, C. P. Novel mouse model for carcinoembryonic antigen-based therapy. *Mol. Ther.* **9**, 775–785 (2004).

63. Martinez-Medina, M. *et al.* Western diet induces dysbiosis with increased E coli in CEABAC10 mice, alters host barrier function favouring AIEC colonisation. *Gut* **63**, 116–124 (2014).

64. Small, C. L., Xing, L., McPhee, J. B., Law, H. T. & Coombes, B. K. Acute Infectious Gastroenteritis Potentiates a Crohn's Disease Pathobiont to Fuel Ongoing Inflammation in the Post-Infectious Period. *PLoS Pathog.* **12**, e1005907 (2016).

65. Yakymenko, O. *et al.* Infliximab restores colonic barrier to adherent-invasive E. coli in Crohn's disease via effects on epithelial lipid rafts. *Scand. J. Gastroenterol.* 1–8 (2018). doi:10.1080/00365521.2018.1458146

66. Wine, E., Ossa, J. C., Gray-Owen, S. D. & Sherman, P. M. Adherent-invasive Escherichia coli target the epithelial barrier. *Gut Microbes* **1**, 80–84 (2010).

67. Mirsepasi-Lauridsen, H. C. *et al.* Secretion of Alpha-Hemolysin by Escherichia coli Disrupts Tight Junctions in Ulcerative Colitis Patients. *Clin. Transl. Gastroenterol.* **7**, e149 (2016).

68. Carvalho, F. A. *et al.* Crohn's disease-associated Escherichia coli LF82 aggravates colitis in injured mouse colon via signaling by flagellin. *Inflamm. Bowel Dis.* **14**, 1051–1060 (2008).

69. Low, D. *et al.* Chitin-binding domains of Escherichia coli ChiA mediate interactions with intestinal epithelial cells in mice with colitis. *Gastroenterology* **145**, 602–12.e9 (2013).

70. Tran, H. T. *et al.* Chitinase 3-like 1 synergistically activates IL6-mediated STAT3 phosphorylation in intestinal epithelial cells in murine models of infectious colitis. *Inflamm. Bowel Dis.* **20**, 835–846 (2014).

71. Rolhion, N., Barnich, N., Claret, L. & Darfeuille-Michaud, A. Strong decrease in invasive ability and outer membrane vesicle release in Crohn's disease-associated adherent-invasive Escherichia coli strain LF82 with the yfgL gene deleted. *J. Bacteriol.* **187**, 2286–2296 (2005).

72. Rolhion, N. *et al.* Abnormally expressed ER stress response chaperone Gp96 in CD favours adherent-invasive Escherichia coli invasion. *Gut* **59**, 1355–1362 (2010).

73. Rolhion, N., Carvalho, F. A. & Darfeuille-Michaud, A. OmpC and the sigma(E) regulatory pathway are involved in adhesion and invasion of the Crohn's disease-associated Escherichia coli strain LF82. *Mol. Microbiol.* **63**, 1684–1700 (2007).

74. Claret, L. *et al.* The flagellar sigma factor FliA regulates adhesion and invasion of Crohn disease-associated Escherichia coli via a cyclic dimeric GMP-dependent pathway. *J. Biol. Chem.* **282**, 33275–33283 (2007).

75. Rooks, M. G. *et al.* QseC inhibition as an antivirulence approach for colitis-associated bacteria. *Proc. Natl. Acad. Sci. U. S. A.* (2016).

doi:10.1073/pnas.1612836114

76. Bringer, M. A., Barnich, N., Glasser, A. L., Bardot, O. & Darfeuille-Michaud, A. HtrA stress protein is involved in intramacrophagic replication of adherent and invasive Escherichia coli strain LF82 isolated from a patient with Crohn's disease. *Infect. Immun.* **73**, 712–721 (2005).

77. Bringer, M. A., Rolhion, N., Glasser, A. L. & Darfeuille-Michaud, A. The oxidoreductase DsbA plays a key role in the ability of the Crohn's disease-associated adherent-invasive Escherichia coli strain LF82 to resist macrophage killing. *J. Bacteriol.* **189**, 4860–4871 (2007).

78. Bringer, M. A., Glasser, A. L., Tung, C. H., Meresse, S. & Darfeuille-Michaud, A. The Crohn's disease-associated adherent-invasive Escherichia coli strain LF82 replicates in mature phagolysosomes within J774 macrophages. *Cell. Microbiol.* **8**, 471–484 (2006).

79. Bringer, M. A., Billard, E., Glasser, A. L., Colombel, J. F. & Darfeuille-Michaud, A. Replication of Crohn's disease-associated AIEC within macrophages is dependent on TNF-alpha secretion. *Lab. Invest.* **92**, 411–419 (2012).

80. Jensen, S. R. *et al.* Distinct inflammatory and cytopathic characteristics of Escherichia coli isolates from inflammatory bowel disease patients. *Int. J. Med. Microbiol.* (2015). doi:S1438-4221(15)30012-6 [pii]

81. Chargui, A. *et al.* Subversion of autophagy in adherent invasive Escherichia coli-infected neutrophils induces inflammation and cell death. *PLoS One* **7**,

e51727 (2012).

82. Glasser, A. L. *et al.* Adherent invasive Escherichia coli strains from patients with Crohn's disease survive and replicate within macrophages without inducing host cell death. *Infect. Immun.* **69**, 5529–5537 (2001).

83. Dunne, K. A. *et al.* Increased S-nitrosylation and proteasomal degradation of caspase-3 during infection contribute to the persistence of adherent invasive Escherichia coli (AIEC) in immune cells. *PLoS One* **8**, e68386 (2013).

84. Jarry, A. *et al.* Subversion of human intestinal mucosa innate immunity by a Crohn's disease-associated E. coli. *Mucosal Immunol.* **8**, 572–581 (2015).

85. Drouet, M. *et al.* AIEC colonization and pathogenicity: influence of previous antibiotic treatment and preexisting inflammation. *Inflamm. Bowel Dis.* **18**, 1923–1931 (2012).

86. Small, C. L., Reid-Yu, S. A., McPhee, J. B. & Coombes, B. K. Persistent infection with Crohn's disease-associated adherent-invasive Escherichia coli leads to chronic inflammation and intestinal fibrosis. *Nat. Commun.* **4**, 1957 (2013).

87. Martinez-Medina, M. & Garcia-Gil, L. J. Escherichia coli in chronic inflammatory bowel diseases: An update on adherent invasive Escherichia coli pathogenicity. *World J. Gastrointest. Pathophysiol.* **5**, 213–227 (2014).

88. Vazeille, E. *et al.* Role of meprins to protect ileal mucosa of Crohn's disease patients from colonization by adherent-invasive E. coli. *PLoS One* **6**, e21199 (2011).

89. Nguyen, H. T. *et al.* Crohn's disease-associated adherent invasive Escherichia coli modulate levels of microRNAs in intestinal epithelial cells to reduce autophagy. *Gastroenterology* **146**, 508–519 (2014).

90. Bertuccini, L. *et al.* Lactoferrin prevents invasion and inflammatory response following E. coli strain LF82 infection in experimental model of Crohn's disease. *Dig. Liver Dis.* **46**, 496–504 (2014).

91. Elatrech, I. *et al.* Escherichia coli LF82 Differentially Regulates ROS Production and Mucin Expression in Intestinal Epithelial T84 Cells: Implication of NOX1. *Inflamm. Bowel Dis.* **21**, 1018–1026 (2015).

92. Costanzo, M. *et al.* Krill oil reduces intestinal inflammation by improving epithelial integrity and impairing adherent-invasive Escherichia coli pathogenicity. *Dig. Liver Dis.* **48**, 34–42 (2016).

93. Mazzarella, G. *et al.* Pathogenic Role of Associated Adherent-Invasive Escherichia coli in Crohn's Disease. *J. Cell. Physiol.* **232**, 2860–2868 (2017).

94. Carvalho, F. A. *et al.* Crohn's disease adherent-invasive Escherichia coli colonize and induce strong gut inflammation in transgenic mice expressing human CEACAM. *J. Exp. Med.* **206**, 2179–2189 (2009).

95. Zhang, H.-J. *et al.* IL-17 is a protection effector against the adherent-invasive Escherichia coli in murine colitis. *Mol. Immunol.* **93**, 166–172 (2018).

96. Lu, C. *et al.* MIR106B and MIR93 prevent removal of bacteria from epithelial cells by disrupting ATG16L1-mediated autophagy. *Gastroenterology* **146**, 188–199 (2014).

97. Brest, P. *et al.* A synonymous variant in IRGM alters a binding site for miR-196 and causes deregulation of IRGM-dependent xenophagy in Crohn's disease. *Nat. Genet.* **43**, 242–245 (2011).

98. Chassaing, B. & Darfeuille-Michaud, A. The sigmaE pathway is involved in biofilm formation by Crohn's disease-associated adherent-invasive Escherichia coli. *J. Bacteriol.* **195**, 76–84 (2013).

99. Vejborg, R. M., Hancock, V., Petersen, A. M., Krogfelt, K. A. & Klemm, P. Comparative genomics of Escherichia coli isolated from patients with inflammatory bowel disease. *BMC Genomics* **12**, 316 (2011).

100. McPhee, J. B. *et al.* Host defense peptide resistance contributes to colonization and maximal intestinal pathology by Crohn's disease-associated adherent-invasive Escherichia coli. *Infect. Immun.* **82**, 3383–3393 (2014).

101. Denizot, J. *et al.* Adherent-invasive Escherichia coli induce claudin-2 expression and barrier defect in CEABAC10 mice and Crohn's disease patients. *Inflamm. Bowel Dis.* **18**, 294–304 (2012).

102. Lashermes, A. *et al.* Adherent-Invasive E. coli enhances colonic hypersensitivity and P2X receptors expression during post-infectious period. *Gut Microbes* 0 (2017). doi:10.1080/19490976.2017.1361091

103. Oberc, A. M., Fiebig-Comyn, A. A., Tsai, C. N., Elhenawy, W. & Coombes, B. K. Antibiotics Potentiate Adherent-Invasive E. coli Infection and Expansion. *Inflamm. Bowel Dis.* (2018). doi:10.1093/ibd/izy361

104. Vyssokikh, M. Y. & Brdiczka, D. The function of complexes between the outer

mitochondrial membrane pore (VDAC) and the adenine nucleotide translocase in regulation of energy metabolism and apoptosis. *Acta Biochim. Pol.* **50**, 389–404 (2003).

105. Meisinger, C., Brix, J., Model, K., Pfanner, N. & Ryan, M. T. The preprotein translocase of the outer mitochondrial membrane: receptors and a general import pore. *Cell. Mol. Life Sci.* **56**, 817–824 (1999).
106. Soltys, B. J. & Gupta, R. S. Mitochondrial-matrix proteins at unexpected locations: are they exported? *Trends Biochem. Sci.* **24**, 174–177 (1999).
107. Vogel, F., Bornhovd, C., Neupert, W. & Reichert, A. S. Dynamic subcompartmentalization of the mitochondrial inner membrane. *J. Cell Biol.* **175**, 237–247 (2006).
108. Lambeth, J. D. NOX enzymes and the biology of reactive oxygen. *Nat. Rev.* **4**, 181–189 (2004).
109. Lopez-Armada, M. J., Riveiro-Naveira, R. R., Vaamonde-Garcia, C. & Valcarcel-Ares, M. N. Mitochondrial dysfunction and the inflammatory response. *Mitochondrion* **13**, 106–118 (2013).
110. Finkel, T. Signal transduction by reactive oxygen species. *J. Cell Biol.* **194**, 7–15 (2011).
111. Vercesi, A. E. *et al.* Mitochondrial calcium transport and the redox nature of the calcium-induced membrane permeability transition. *Free Radic. Biol. Med.* **129**, 1–24 (2018).
112. Hou, W. *et al.* Strange attractors: DAMPs and autophagy link tumor cell

death and immunity. *Cell Death Dis.* **4**, e966 (2013).

113. Chung, C. Restoring the switch for cancer cell death: Targeting the apoptosis signaling pathway. *Am. J. Health. Syst. Pharm.* **75**, 945–952 (2018).
114. Pena-Blanco, A. & Garcia-Saez, A. J. Bax, Bak and beyond - mitochondrial performance in apoptosis. *FEBS J.* **285**, 416–431 (2018).
115. Sevrioukova, I. F. Apoptosis-inducing factor: structure, function, and redox regulation. *Antioxid. Redox Signal.* **14**, 2545–2579 (2011).
116. Correia-Melo, C. & Passos, J. F. Mitochondria: Are they causal players in cellular senescence? *Biochim. Biophys. Acta* (2015). doi:S0005-2728(15)00098-5 [pii]
117. Koshiba, T. *et al.* Structural basis of mitochondrial tethering by mitofusin complexes. *Science* **305**, 858–862 (2004).
118. Brandt, T., Cavellini, L., Kuhlbrandt, W. & Cohen, M. M. A mitofusin-dependent docking ring complex triggers mitochondrial fusion. *Elife* **5**, 10.7554/eLife.14618 (2016).
119. Franco, A. *et al.* Correcting mitochondrial fusion by manipulating mitofusin conformations. *Nature* (2016). doi:10.1038/nature20156
120. Huang, P., Galloway, C. A. & Yoon, Y. Control of mitochondrial morphology through differential interactions of mitochondrial fusion and fission proteins. *PLoS One* **6**, e20655 (2011).
121. Qi, Y. *et al.* Structures of human mitofusin 1 provide insight into mitochondrial tethering. *J. Cell Biol.* **215**, 621–629 (2016).

122. Cao, Y.-L. *et al.* MFN1 structures reveal nucleotide-triggered dimerization critical for mitochondrial fusion. *Nature* (2017). doi:10.1038/nature21077

123. Mattie, S., Riemer, J., Wideman, J. G. & McBride, H. M. A new mitofusin topology places the redox-regulated C terminus in the mitochondrial intermembrane space. *J. Cell Biol.* **217**, 507–515 (2018).

124. Giacomello, M. & Scorrano, L. The INs and OUTs of mitofusins. *J. Cell Biol.* (2018). doi:10.1083/jcb.201801042

125. Tanaka, A. *et al.* Proteasome and p97 mediate mitophagy and degradation of mitofusins induced by Parkin. *J. Cell Biol.* **191**, 1367–1380 (2010).

126. de Brito, O. M. & Scorrano, L. Mitofusin 2 tethers endoplasmic reticulum to mitochondria. *Nature* **456**, 605–610 (2008).

127. Naon, D. & Scorrano, L. At the right distance: ER-mitochondria juxtaposition in cell life and death. *Biochim. Biophys. Acta* **1843**, 2184–2194 (2014).

128. Hoppins, S., Lackner, L. & Nunnari, J. The machines that divide and fuse mitochondria. *Annu. Rev. Biochem.* **76**, 751–780 (2007).

129. Liesa, M., Palacin, M. & Zorzano, A. Mitochondrial dynamics in mammalian health and disease. *Physiol. Rev.* **89**, 799–845 (2009).

130. Duvezin-Caubet, S. *et al.* Proteolytic processing of OPA1 links mitochondrial dysfunction to alterations in mitochondrial morphology. *J. Biol. Chem.* **281**, 37972–37979 (2006).

131. Ishihara, N., Fujita, Y., Oka, T. & Mihara, K. Regulation of mitochondrial morphology through proteolytic cleavage of OPA1. *EMBO J.* **25**, 2966–2977

(2006).

132. Pernas, L. & Scorrano, L. Mito-Morphosis: Mitochondrial Fusion, Fission, and Cristae Remodeling as Key Mediators of Cellular Function. *Annu. Rev. Physiol.* (2015). doi:10.1146/annurev-physiol-021115-105011 [doi]

133. Ban, T. *et al.* Molecular basis of selective mitochondrial fusion by heterotypic action between OPA1 and cardiolipin. *Nat. Cell Biol.* **19**, 856–863 (2017).

134. Ban, T., Kohno, H., Ishihara, T. & Ishihara, N. Relationship between OPA1 and cardiolipin in mitochondrial inner-membrane fusion. *Biochim. Biophys. Acta* (2018). doi:10.1016/j.bbabio.2018.05.016

135. Song, Z., Chen, H., Fiket, M., Alexander, C. & Chan, D. C. OPA1 processing controls mitochondrial fusion and is regulated by mRNA splicing, membrane potential, and Yme1L. *J. Cell Biol.* **178**, 749–755 (2007).

136. Head, B., Griparic, L., Amiri, M., Gandre-Babbe, S. & van der Bliek, A. M. Inducible proteolytic inactivation of OPA1 mediated by the OMA1 protease in mammalian cells. *J. Cell Biol.* **187**, 959–966 (2009).

137. Ehses, S. *et al.* Regulation of OPA1 processing and mitochondrial fusion by m-AAA protease isoenzymes and OMA1. *J. Cell Biol.* **187**, 1023–1036 (2009).

138. Saita, S. *et al.* Distinct types of protease systems are involved in homeostasis regulation of mitochondrial morphology via balanced fusion and fission. *Genes Cells* (2016). doi:10.1111/gtc.12351 [doi]

139. Olichon, A. *et al.* Loss of OPA1 perturbates the mitochondrial inner membrane structure and integrity, leading to cytochrome c release and

apoptosis. *J. Biol. Chem.* **278**, 7743–7746 (2003).

140. Legros, F., Lombes, A., Frachon, P. & Rojo, M. Mitochondrial fusion in human cells is efficient, requires the inner membrane potential, and is mediated by mitofusins. *Mol. Biol. Cell* **13**, 4343–4354 (2002).

141. Rambold, A. S., Cohen, S. & Lippincott-Schwartz, J. Fatty acid trafficking in starved cells: regulation by lipid droplet lipolysis, autophagy, and mitochondrial fusion dynamics. *Dev. Cell* **32**, 678–692 (2015).

142. Yang, L. *et al.* Mitochondrial fusion provides an 'initial metabolic complementation' controlled by mtDNA. *Cell. Mol. Life Sci.* **72**, 2585–2598 (2015).

143. Ono, T., Isobe, K., Nakada, K. & Hayashi, J. I. Human cells are protected from mitochondrial dysfunction by complementation of DNA products in fused mitochondria. *Nat. Genet.* **28**, 272–275 (2001).

144. Chen, H., Chomyn, A. & Chan, D. C. Disruption of fusion results in mitochondrial heterogeneity and dysfunction. *J. Biol. Chem.* **280**, 26185–26192 (2005).

145. Amchenkova, A. A., Bakeeva, L. E., Chentsov, Y. S., Skulachev, V. P. & Zorov, D. B. Coupling membranes as energy-transmitting cables. I. Filamentous mitochondria in fibroblasts and mitochondrial clusters in cardiomyocytes. *J. Cell Biol.* **107**, 481–495 (1988).

146. Parone, P. A. *et al.* Preventing mitochondrial fission impairs mitochondrial function and leads to loss of mitochondrial DNA. *PLoS One* **3**, e3257 (2008).

147. Haroon, S. & Vermulst, M. Linking mitochondrial dynamics to mitochondrial protein quality control. *Curr. Opin. Genet. Dev.* **38**, 68–74 (2016).

148. Ziegler, D. V, Wiley, C. D. & Velarde, M. C. Mitochondrial effectors of cellular senescence: beyond the free radical theory of aging. *Aging Cell* (2014). doi:10.1111/acel.12287; 10.1111/acel.12287

149. Rambold, A. S., Kostelecky, B., Elia, N. & Lippincott-Schwartz, J. Tubular network formation protects mitochondria from autophagosomal degradation during nutrient starvation. *Proc. Natl. Acad. Sci. U. S. A.* **108**, 10190–10195 (2011).

150. Smirnova, E., Griparic, L., Shurland, D. L. & van der Bliek, A. M. Dynamin-related protein Drp1 is required for mitochondrial division in mammalian cells. *Mol. Biol. Cell* **12**, 2245–2256 (2001).

151. Mears, J. A. *et al.* Conformational changes in Dnm1 support a contractile mechanism for mitochondrial fission. *Nat. Struct. Mol. Biol.* **18**, 20–26 (2011).

152. Lee, J. E., Westrate, L. M., Wu, H., Page, C. & Voeltz, G. K. Multiple dynamin family members collaborate to drive mitochondrial division. *Nature* (2016). doi:10.1038/nature20555

153. El-Hattab, A. W., Suleiman, J., Almannai, M. & Scaglia, F. Mitochondrial dynamics: Biological roles, molecular machinery, and related diseases. *Mol. Genet. Metab.* (2018). doi:10.1016/j.ymgme.2018.10.003

154. Dasgupta, A., Chen, K. H., Tian, L. & Archer, S. L. Gone fission: an asymptomatic STAT2 mutation elongates mitochondria and causes human

disease following viral infection. *Brain* **138**, 2802–2806 (2015).

155. Prudent, J. *et al.* MAPL SUMOylation of Drp1 Stabilizes an ER/Mitochondrial Platform Required for Cell Death. *Mol. Cell* **59**, 941–955 (2015).

156. Yonashiro, R. *et al.* A novel mitochondrial ubiquitin ligase plays a critical role in mitochondrial dynamics. *EMBO J.* **25**, 3618–3626 (2006).

157. Nakamura, N., Kimura, Y., Tokuda, M., Honda, S. & Hirose, S. MARCH-V is a novel mitofusin 2- and Drp1-binding protein able to change mitochondrial morphology. *EMBO Rep.* **7**, 1019–1022 (2006).

158. Karbowski, M., Neutzner, A. & Youle, R. J. The mitochondrial E3 ubiquitin ligase MARCH5 is required for Drp1 dependent mitochondrial division. *J. Cell Biol.* **178**, 71–84 (2007).

159. Park, Y.-Y. *et al.* Loss of MARCH5 mitochondrial E3 ubiquitin ligase induces cellular senescence through dynamin-related protein 1 and mitofusin 1. *J. Cell Sci.* **123**, 619–626 (2010).

160. Horn, S. R. *et al.* Regulation of mitochondrial morphology by APC/CCdh1-mediated control of Drp1 stability. *Mol. Biol. Cell* **22**, 1207–1216 (2011).

161. Loson, O. C., Song, Z., Chen, H. & Chan, D. C. Fis1, Mff, MiD49, and MiD51 mediate Drp1 recruitment in mitochondrial fission. *Mol. Biol. Cell* **24**, 659–667 (2013).

162. Otera, H. *et al.* Mff is an essential factor for mitochondrial recruitment of Drp1 during mitochondrial fission in mammalian cells. *J. Cell Biol.* **191**, 1141–1158 (2010).

163. Osellame, L. D. *et al.* Cooperative and independent roles of Drp1 adaptors Mff and MiD49/51 in mitochondrial fission. *J. Cell Sci.* (2016). doi:jcs.185165 [pii]

164. Palmer, C. S. *et al.* Adaptor proteins MiD49 and MiD51 can act independently of Mff and Fis1 in Drp1 recruitment and are specific for mitochondrial fission. *J. Biol. Chem.* **288**, 27584–27593 (2013).

165. Liu, R. & Chan, D. C. The mitochondrial fission receptor Mff selectively recruits oligomerized Drp1. *Mol. Biol. Cell* (2015). doi:mbc.E15-08-0591 [pii]

166. Clinton, R. W., Francy, C. A., Ramachandran, R., Qi, X. & Mears, J. A. Dynamin-Related Protein 1 Oligomerization in Solution Impairs Functional Interactions with Membrane-Anchored Mitochondrial Fission Factor. *J. Biol. Chem.* (2015). doi:jbc.M115.680025 [pii]

167. Kalia, R. *et al.* Structural basis of mitochondrial receptor binding and constriction by DRP1. *Nature* (2018). doi:10.1038/s41586-018-0211-2

168. De Vos, K. J., Allan, V. J., Grierson, A. J. & Sheetz, M. P. Mitochondrial function and actin regulate dynamin-related protein 1-dependent mitochondrial fission. *Curr. Biol.* **15**, 678–683 (2005).

169. Hatch, A. L., Ji, W.-K., Merrill, R. A., Strack, S. & Higgs, H. N. Actin filaments as dynamic reservoirs for Drp1 recruitment. *Mol. Biol. Cell* (2016). doi:10.1091/mbc.E16-03-0193

170. Friedman, J. R. *et al.* ER tubules mark sites of mitochondrial division. *Science* **334**, 358–362 (2011).

171. Korobova, F., Ramabhadran, V. & Higgs, H. N. An actin-dependent step in

mitochondrial fission mediated by the ER-associated formin INF2. *Science* **339**, 464–467 (2013).

172. Korobova, F., Gauvin, T. J. & Higgs, H. N. A role for myosin II in mammalian mitochondrial fission. *Curr. Biol.* **24**, 409–414 (2014).

173. Ji, W. K., Hatch, A. L., Merrill, R. A., Strack, S. & Higgs, H. N. Actin filaments target the oligomeric maturation of the dynamic GTPase Drp1 to mitochondrial fission sites. *Elife* **4**, 10.7554/eLife.11553 (2015).

174. Moore, A. S., Wong, Y. C., Simpson, C. L. & Holzbaur, E. L. F. Dynamic actin cycling through mitochondrial subpopulations locally regulates the fission-fusion balance within mitochondrial networks. *Nat. Commun.* **7**, 12886 (2016).

175. Chakrabarti, R. *et al.* INF2-mediated actin polymerization at the ER stimulates mitochondrial calcium uptake, inner membrane constriction, and division. *J. Cell Biol.* **217**, 251–268 (2018).

176. Li, H. *et al.* Mic60/Mitofilin determines MICOS assembly essential for mitochondrial dynamics and mtDNA nucleoid organization. *Cell Death Differ.* (2015). doi:10.1038/cdd.2015.102 [doi]

177. Manor, U. *et al.* A mitochondria-anchored isoform of the actin-nucleating spire protein regulates mitochondrial division. *Elife* **4**, (2015).

178. Pagliuso, A. *et al.* A role for septin 2 in Drp1-mediated mitochondrial fission. *EMBO Rep.* (2016). doi:e201541612 [pii]

179. Li, G.-B. *et al.* Mitochondrial fission and mitophagy depend on cofilin-mediated actin depolymerization activity at the mitochondrial fission site.

Oncogene (2018). doi:10.1038/s41388-017-0064-4

180. Macdonald, P. J. *et al.* A dimeric equilibrium intermediate nucleates Drp1 reassembly on mitochondrial membranes for fission. *Mol. Biol. Cell* **25**, 1905–1915 (2014).

181. Ugarte-Uribe, B., Prevost, C., Das, K. K., Bassereau, P. & Garcia-Saez, A. J. Drp1 polymerization stabilizes curved tubular membranes similar to those of constricted mitochondria. *J. Cell Sci.* (2017). doi:10.1242/jcs.208603

182. Francy, C. A., Alvarez, F. J., Zhou, L., Ramachandran, R. & Mears, J. A. The Mechanoenzymatic Core of Dynamin-Related Protein 1 Comprises the Minimal Machinery Required for Membrane Constriction. *J. Biol. Chem.* (2015). doi:jbc.M114.610881 [pii]

183. Stepanyants, N. *et al.* Cardiolipin's propensity for phase transition and its reorganization by dynamin-related protein 1 form a basis for mitochondrial membrane fission. *Mol. Biol. Cell* (2015). doi:mbc.E15-06-0330 [pii]

184. Adachi, Y. *et al.* Coincident Phosphatidic Acid Interaction Restrains Drp1 in Mitochondrial Division. *Mol. Cell* **63**, 1034–1043 (2016).

185. Matsumura, A. *et al.* Inactivation of cardiolipin synthase triggers changes in mitochondrial morphology. *FEBS letters* (2017). doi:10.1002/1873-3468.12948

186. Ishihara, N. *et al.* Mitochondrial fission factor Drp1 is essential for embryonic development and synapse formation in mice. *Nat. Cell Biol.* **11**, 958–966 (2009).

187. Cho, B. *et al.* Constriction of the mitochondrial inner compartment is a

priming event for mitochondrial division. *Nat. Commun.* **8**, 15754 (2017).

188. Anand, R. *et al.* The i-AAA protease YME1L and OMA1 cleave OPA1 to balance mitochondrial fusion and fission. *J. Cell Biol.* **204**, 919–929 (2014).

189. Otera, H., Miyata, N., Kuge, O. & Mihara, K. Drp1-dependent mitochondrial fission via MiD49/51 is essential for apoptotic cristae remodeling. *J. Cell Biol.* (2016). doi:jcb.201508099 [pii]

190. Sanderson, T. H., Raghunayakula, S. & Kumar, R. Release of mitochondrial Opa1 following oxidative stress in HT22 cells. *Mol. Cell. Neurosci.* (2015). doi:S1044-7431(14)00191-2 [pii]

191. Lee, B. *et al.* Stoichiometric expression of mtHsp40 and mtHsp70 modulates mitochondrial morphology and cristae structure via Opa1L cleavage. *Mol. Biol. Cell* **26**, 2156–2167 (2015).

192. Varadarajan, S. *et al.* Maritoclax and dinaciclib inhibit MCL-1 activity and induce apoptosis in both a MCL-1-dependent and -independent manner. *Oncotarget* **6**, 12668–12681 (2015).

193. Jones, E. *et al.* A threshold of transmembrane potential is required for mitochondrial dynamic balance mediated by DRP1 and OMA1. *Cell. Mol. Life Sci.* (2016). doi:10.1007/s00018-016-2421-9

194. Twig, G. *et al.* Fission and selective fusion govern mitochondrial segregation and elimination by autophagy. *EMBO J.* **27**, 433–446 (2008).

195. Yamaguchi, O., Murakawa, T., Nishida, K. & Otsu, K. Receptor-mediated mitophagy. *J. Mol. Cell. Cardiol.* (2016). doi:S0022-2828(16)30057-8 [pii]

196. Wang, K., Yan, R., Cooper, K. F. & Strich, R. Cyclin C mediates stress-induced mitochondrial fission and apoptosis. *Mol. Biol. Cell* (2015). doi:mbc.E14-08-1315 [pii]

197. Kiryu-Seo, S. *et al.* Mitochondrial fission is an acute and adaptive response in injured motor neurons. *Sci. Rep.* **6**, 28331 (2016).

198. Taguchi, N., Ishihara, N., Jofuku, A., Oka, T. & Mihara, K. Mitotic phosphorylation of dynamin-related GTPase Drp1 participates in mitochondrial fission. *J. Biol. Chem.* **282**, 11521–11529 (2007).

199. Katajisto, P. *et al.* Asymmetric apportioning of aged mitochondria between daughter cells is required for stemness. *Science* (2015). doi:1260384 [pii]

200. Forni, M. F., Peloggia, J., Trudeau, K., Shirihai, O. & Kowaltowski, A. J. Murine Mesenchymal Stem Cell Commitment to Differentiation Is Regulated by Mitochondrial Dynamics. *Stem Cells* **34**, 743–755 (2016).

201. Deng, H., Takashima, S., Paul, M., Guo, M. & Hartenstein, V. Mitochondrial dynamics regulates Drosophila intestinal stem cell differentiation. *Cell death Discov.* **5**, 17 (2018).

202. Frank, S. *et al.* The role of dynamin-related protein 1, a mediator of mitochondrial fission, in apoptosis. *Dev. Cell* **1**, 515–525 (2001).

203. Wakabayashi, J. *et al.* The dynamin-related GTPase Drp1 is required for embryonic and brain development in mice. *J. Cell Biol.* **186**, 805–816 (2009).

204. Oettinghaus, B. *et al.* DRP1-dependent apoptotic mitochondrial fission occurs independently of BAX, BAK and APAF1 to amplify cell death by BID and

oxidative stress. *Biochim. Biophys. Acta* (2016). doi:S0005-2728(16)30063-9 [pii]

205. Dong, Y., Undyala, V. V. R. & Przyklenk, K. Inhibition of mitochondrial fission as a molecular target for cardioprotection: critical importance of the timing of treatment. *Basic Res. Cardiol.* **111**, 59 (2016).

206. Breckenridge, D. G., Stojanovic, M., Marcellus, R. C. & Shore, G. C. Caspase cleavage product of BAP31 induces mitochondrial fission through endoplasmic reticulum calcium signals, enhancing cytochrome c release to the cytosol. *J. Cell Biol.* **160**, 1115–1127 (2003).

207. Neuspiel, M., Zunino, R., Gangaraju, S., Rippstein, P. & McBride, H. Activated mitofusin 2 signals mitochondrial fusion, interferes with Bax activation, and reduces susceptibility to radical induced depolarization. *J. Biol. Chem.* **280**, 25060–25070 (2005).

208. Kim, D. I. *et al.* Abeta-Induced Drp1 phosphorylation through Akt activation promotes excessive mitochondrial fission leading to neuronal apoptosis. *Biochim. Biophys. Acta* (2016). doi:10.1016/j.bbamcr.2016.09.003

209. Lee, Y. J., Jeong, S. Y., Karbowski, M., Smith, C. L. & Youle, R. J. Roles of the mammalian mitochondrial fission and fusion mediators Fis1, Drp1, and Opa1 in apoptosis. *Mol. Biol. Cell* **15**, 5001–5011 (2004).

210. Yu, T. *et al.* Decreasing Mitochondrial Fission Prevents Cholestatic Liver Injury. *J. Biol. Chem.* (2014). doi:10.1074/jbc.M114.588616

211. Yeon, J. Y. *et al.* Mdivi-1, mitochondrial fission inhibitor, impairs

developmental competence and mitochondrial function of embryos and cells in pigs. *J. Reprod. Dev.* (2014). doi:DN/JST.JSTAGE/jrd/2014-070 [pii]

212. Shen, T. *et al.* The Critical Role of Dynamin-Related Protein 1 in Hypoxia-Induced Pulmonary Vascular Angiogenesis. *J. Cell. Biochem.* (2015). doi:10.1002/jcb.25154 [doi]
213. Pletjushkina, O. Y. *et al.* Effect of oxidative stress on dynamics of mitochondrial reticulum. *Biochim. Biophys. Acta* **1757**, 518–524 (2006).
214. Inoue-Yamauchi, A. & Oda, H. Depletion of mitochondrial fission factor DRP1 causes increased apoptosis in human colon cancer cells. *Biochem. Biophys. Res. Commun.* **421**, 81–85 (2012).
215. Xie, Q. *et al.* Mitochondrial control by DRP1 in brain tumor initiating cells. *Nat. Neurosci.* (2015). doi:10.1038/nn.3960 [doi]
216. Wasiak, S., Zunino, R. & McBride, H. M. Bax/Bak promote sumoylation of DRP1 and its stable association with mitochondria during apoptotic cell death. *J. Cell Biol.* **177**, 439–450 (2007).
217. Xu, W. *et al.* Bax-PGAM5L-Drp1 complex is required for intrinsic apoptosis execution. *Oncotarget* (2015). doi:5013 [pii]
218. Grosse, L. *et al.* Bax assembles into large ring-like structures remodeling the mitochondrial outer membrane in apoptosis. *EMBO J.* **35**, 402–413 (2016).
219. Xie, L.-L. *et al.* Mitochondrial network structure homeostasis and cell death. *Cancer Sci.* **109**, 3686–3694 (2018).
220. Zuchner, S. *et al.* Mutations in the mitochondrial GTPase mitofusin 2 cause

Charcot-Marie-Tooth neuropathy type 2A. *Nat. Genet.* **36**, 449–451 (2004).

221. Delettre, C. *et al.* Nuclear gene OPA1, encoding a mitochondrial dynamin-related protein, is mutated in dominant optic atrophy. *Nat. Genet.* **26**, 207–210 (2000).

222. Sheffer, R. *et al.* Postnatal microcephaly and pain insensitivity due to a de novo heterozygous DNM1L mutation causing impaired mitochondrial fission and function. *Am. J. Med. Genet. A* (2016). doi:10.1002/ajmg.a.37624 [doi]

223. Fahrner, J. A., Liu, R., Perry, M. S., Klein, J. & Chan, D. C. A novel de novo dominant negative mutation in DNM1L impairs mitochondrial fission and presents as childhood epileptic encephalopathy. *Am. J. Med. Genet. A* (2016). doi:10.1002/ajmg.a.37721 [doi]

224. Gerber, S. *et al.* Mutations in DNM1L, as in OPA1, result in dominant optic atrophy despite opposite effects on mitochondrial fusion and fission. *Brain* **140**, 2586–2596 (2017).

225. Kitada, T. *et al.* Mutations in the parkin gene cause autosomal recessive juvenile parkinsonism. *Nature* **392**, 605–608 (1998).

226. Forini, F., Nicolini, G. & Iervasi, G. Mitochondria as key targets of cardioprotection in cardiac ischemic disease: role of thyroid hormone triiodothyronine. *Int. J. Mol. Sci.* **16**, 6312–6336 (2015).

227. Bousquet, J. *et al.* Indirect evidence of bronchial inflammation assessed by titration of inflammatory mediators in BAL fluid of patients with asthma. *J. Allergy Clin. Immunol.* **88**, 649–660 (1991).

228. Toyran, M., Bakirtas, A., Dogruman-Al, F. & Turktas, I. Airway inflammation and bronchial hyperreactivity in steroid naive children with intermittent and mild persistent asthma. *Pediatr. Pulmonol.* **49**, 140–147 (2014).

229. Mabalirajan, U. *et al.* Linoleic acid metabolite drives severe asthma by causing airway epithelial injury. *Sci. Rep.* **3**, 1349 (2013).

230. Liu, Q., Gao, Y. & Ci, X. Role of Nrf2 and Its Activators in Respiratory Diseases. *Oxid. Med. Cell. Longev.* **2019**, 7090534 (2019).

231. Currais, A. Ageing and inflammation - A central role for mitochondria in brain health and disease. *Ageing Res. Rev.* **21**, 30–42 (2015).

232. Wallace, D. C. A mitochondrial paradigm of metabolic and degenerative diseases, aging, and cancer: a dawn for evolutionary medicine. *Annu. Rev. Genet.* **39**, 359–407 (2005).

233. Bonomini, F., Rodella, L. F. & Rezzani, R. Metabolic syndrome, aging and involvement of oxidative stress. *Aging Dis.* **6**, 109–120 (2015).

234. Gusdon, A. M., Song, K. X. & Qu, S. Nonalcoholic Fatty liver disease: pathogenesis and therapeutics from a mitochondria-centric perspective. *Oxid. Med. Cell. Longev.* **2014**, 637027 (2014).

235. Sajic, M. Mitochondrial dynamics in peripheral neuropathies. *Antioxid. Redox Signal.* **21**, 601–620 (2014).

236. Ryan, J., Dasgupta, A., Huston, J., Chen, K. H. & Archer, S. L. Mitochondrial dynamics in pulmonary arterial hypertension. *J. Mol. Med. (Berl).* **93**, 229–242 (2015).

237. White, J. P. *et al.* IL-6 regulation on skeletal muscle mitochondrial remodeling during cancer cachexia in the ApcMin/+ mouse. *Skelet. Muscle* **2**, 14 (2012).

238. Shahni, R. *et al.* Signal transducer and activator of transcription 2 deficiency is a novel disorder of mitochondrial fission. *Brain* (2015). doi:awv182 [pii]

239. Baltrusch, S. Mitochondrial network regulation and its potential interference with inflammatory signals in pancreatic beta cells. *Diabetologia* (2016). doi:10.1007/s00125-016-3891-x [doi]

240. He, G.-W. *et al.* PGAM5-mediated programmed necrosis of hepatocytes drives acute liver injury. *Gut* **66**, 716–723 (2017).

241. Yi, C.-X. *et al.* TNFalpha drives mitochondrial stress in POMC neurons in obesity. *Nat. Commun.* **8**, 15143 (2017).

242. Nan, J. *et al.* TNFR2 Stimulation Promotes Mitochondrial Fusion via Stat3- and NF-kB-Dependent Activation of OPA1 Expression. *Circ. Res.* (2017). doi:10.1161/CIRCRESAHA.117.311143

243. Du, J. *et al.* Pro-Inflammatory CXCR3 Impairs Mitochondrial Function in Experimental Non-Alcoholic Steatohepatitis. *Theranostics* **7**, 4192–4203 (2017).

244. Joshi, A. U. *et al.* Inhibition of Drp1/Fis1 interaction slows progression of amyotrophic lateral sclerosis. *EMBO Mol. Med.* (2018). doi:10.15252/emmm.201708166

245. Rodriguez-Nuevo, A. *et al.* Mitochondrial DNA and TLR9 drive muscle inflammation upon Opa1 deficiency. *EMBO J.* (2018).

doi:10.15252/embj.201796553

246. Disatnik, M. H. *et al.* Acute inhibition of excessive mitochondrial fission after myocardial infarction prevents long-term cardiac dysfunction. *J. Am. Heart Assoc.* **2**, e000461 (2013).

247. Filichia, E., Hoffer, B., Qi, X. & Luo, Y. Inhibition of Drp1 mitochondrial translocation provides neural protection in dopaminergic system in a Parkinson's disease model induced by MPTP. *Sci. Rep.* **6**, 32656 (2016).

248. Tian, L. *et al.* Ischemia-induced Drp1 and Fis1-mediated mitochondrial fission and right ventricular dysfunction in pulmonary hypertension. *J. Mol. Med. (Berl).* (2017). doi:10.1007/s00109-017-1522-8

249. Luo, F., Herrup, K., Qi, X. & Yang, Y. Inhibition of Drp1 hyper-activation is protective in animal models of experimental multiple sclerosis. *Exp. Neurol.* **292**, 21–34 (2017).

250. Joshi, A. U., Saw, N. L., Shamloo, M. & Mochly-Rosen, D. Drp1/Fis1 interaction mediates mitochondrial dysfunction, bioenergetic failure and cognitive decline in Alzheimer's disease. *Oncotarget* **9**, 6128–6143 (2018).

251. Ong, S.-B. *et al.* Inhibiting mitochondrial fission protects the heart against ischemia/reperfusion injury. *Circulation* **121**, 2012–2022 (2010).

252. Marsboom, G. *et al.* Dynamin-related protein 1-mediated mitochondrial mitotic fission permits hyperproliferation of vascular smooth muscle cells and offers a novel therapeutic target in pulmonary hypertension. *Circ. Res.* **110**, 1484–1497 (2012).

253. Brooks, C., Wei, Q., Cho, S.-G. & Dong, Z. Regulation of mitochondrial dynamics in acute kidney injury in cell culture and rodent models. *J. Clin. Invest.* **119**, 1275–1285 (2009).

254. Lin, H.-Y. *et al.* The Causal Role of Mitochondrial Dynamics in Regulating Insulin Resistance in Diabetes: Link through Mitochondrial Reactive Oxygen Species. *Oxid. Med. Cell. Longev.* **2018**, 7514383 (2018).

255. Qi, X., Qvit, N., Su, Y. C. & Mochly-Rosen, D. A novel Drp1 inhibitor diminishes aberrant mitochondrial fission and neurotoxicity. *J. Cell Sci.* **126**, 789–802 (2013).

256. Cassidy-Stone, A. *et al.* Chemical inhibition of the mitochondrial division dynamin reveals its role in Bax/Bak-dependent mitochondrial outer membrane permeabilization. *Dev. Cell* **14**, 193–204 (2008).

257. Marzetti, E. *et al.* Altered mitochondrial quality control signaling in muscle of old gastric cancer patients with cachexia. *Exp. Gerontol.* (2016). doi:10.1016/j.exger.2016.10.003

258. De, R. *et al.* Acute mental stress induces mitochondrial bioenergetic crisis and hyper-fission along with aberrant mitophagy in the gut mucosa in rodent model of stress-related mucosal disease. *Free Radic. Biol. Med.* (2017). doi:10.1016/j.freeradbiomed.2017.10.009

259. Aung, L. H. H., Li, R., Prabhakar, B. S., Maker, A. V & Li, P. Mitochondrial protein 18 (MTP18) plays a pro-apoptotic role in chemotherapy-induced gastric cancer cell apoptosis. *Oncotarget* (2017).

doi:10.18632/oncotarget.17508

260. Cruz, M. Dela *et al.* Metabolic reprogramming of the premalignant colonic mucosa is an early event in carcinogenesis. *Oncotarget* **8**, 20543–20557 (2017).

261. Li, B. *et al.* MicroRNA-148a-3p enhances cisplatin cytotoxicity in gastric cancer through mitochondrial fission induction and cyto-protective autophagy suppression. *Cancer Lett.* **410**, 212–227 (2017).

262. Li, H. *et al.* YAP Inhibits the Apoptosis and Migration of Human Rectal Cancer Cells via Suppression of JNK-Drp1-Mitochondrial Fission-HtrA2/Omi Pathways. *Cell. Physiol. Biochem.* **44**, 2073–2089 (2017).

263. Kim, Y. Y., Yun, S.-H. & Yun, J. Downregulation of Drp1, a fission regulator, is associated with human lung and colon cancers. *Acta Biochim. Biophys. Sin. (Shanghai).* (2018). doi:10.1093/abbs/gmx137

264. Wang, S.-Q., Cui, S.-X. & Qu, X.-J. Metformin inhibited colitis and colitis-associated cancer (CAC) through protecting mitochondrial structures of colorectal epithelial cells in mice. *Cancer Biol. Ther.* 1–11 (2018). doi:10.1080/15384047.2018.1529108

265. Rademaker, G. *et al.* Human colon cancer cells highly express myoferlin to maintain a fit mitochondrial network and escape p53-driven apoptosis. *Oncogenesis* **8**, 21 (2019).

266. Ryan, J. J. *et al.* PGC1alpha-mediated mitofusin-2 deficiency in female rats and humans with pulmonary arterial hypertension. *Am. J. Respir. Crit. Care Med.* **187**, 865–878 (2013).

267. Sharp, W. W. *et al.* Dynamin-related protein 1 (Drp1)-mediated diastolic dysfunction in myocardial ischemia-reperfusion injury: therapeutic benefits of Drp1 inhibition to reduce mitochondrial fission. *FASEB J.* **28**, 316–326 (2014).

268. Hall, A. R. *et al.* Hearts deficient in both Mfn1 and Mfn2 are protected against acute myocardial infarction. *Cell Death Dis.* **7**, e2238 (2016).

269. Bach, D. *et al.* Expression of Mfn2, the Charcot-Marie-Tooth neuropathy type 2A gene, in human skeletal muscle: effects of type 2 diabetes, obesity, weight loss, and the regulatory role of tumor necrosis factor alpha and interleukin-6. *Diabetes* **54**, 2685–2693 (2005).

270. Diaz-Morales, N. *et al.* Are mitochondrial fusion and fission impaired in leukocytes of type 2 diabetic patients? *Antioxid. Redox Signal.* (2016). doi:10.1089/ars.2016.6707 [doi]

271. Ferreira-da-Silva, A. *et al.* Mitochondrial dynamics protein Drp1 is overexpressed in oncocytic thyroid tumors and regulates cancer cell migration. *PLoS One* **10**, e0122308 (2015).

272. Rehman, J. *et al.* Inhibition of mitochondrial fission prevents cell cycle progression in lung cancer. *FASEB J.* **26**, 2175–2186 (2012).

273. Bar, F. *et al.* Mitochondrial gene polymorphisms that protect mice from colitis. *Gastroenterology* **145**, 1055-1063.e3 (2013).

274. Guo, W. *et al.* Asiatic acid ameliorates dextran sulfate sodium-induced murine experimental colitis via suppressing mitochondria-mediated NLRP3 inflammasome activation. *Int. Immunopharmacol.* **24**, 232–238 (2015).

275. Amrouche-Mekkioui, I. & Djerdjouri, B. N-acetylcysteine improves redox status, mitochondrial dysfunction, mucin-depleted crypts and epithelial hyperplasia in dextran sulfate sodium-induced oxidative colitis in mice. *Eur. J. Pharmacol.* **691**, 209–217 (2012).

276. Ho, G.-T. *et al.* MDR1 deficiency impairs mitochondrial homeostasis and promotes intestinal inflammation. *Mucosal Immunol.* (2017). doi:10.1038/mi.2017.31

277. Schurmann, G. *et al.* Transepithelial transport processes at the intestinal mucosa in inflammatory bowel disease. *Int. J. Colorectal Dis.* **14**, 41–46 (1999).

278. Hsieh, S. Y. *et al.* Comparative proteomic studies on the pathogenesis of human ulcerative colitis. *Proteomics* **6**, 5322–5331 (2006).

279. Dijkstra, G. *et al.* Expression of nitric oxide synthases and formation of nitrotyrosine and reactive oxygen species in inflammatory bowel disease. *J. Pathol.* **186**, 416–421 (1998).

280. Somasundaram, S. *et al.* Uncoupling of intestinal mitochondrial oxidative phosphorylation and inhibition of cyclooxygenase are required for the development of NSAID-enteropathy in the rat. *Aliment. Pharmacol. Ther.* **14**, 639–650 (2000).

281. Soderholm, J. D. *et al.* Chronic stress induces mast cell-dependent bacterial adherence and initiates mucosal inflammation in rat intestine. *Gastroenterology* **123**, 1099–1108 (2002).

282. He, D. *et al.* Clostridium difficile toxin A triggers human colonocyte IL-8 release via mitochondrial oxygen radical generation. *Gastroenterology* **122**, 1048–1057 (2002).

283. Farhadi, A. *et al.* Heightened responses to stressors in patients with inflammatory bowel disease. *Am. J. Gastroenterol.* **100**, 1796–1804 (2005).

284. Schoultz, I. *et al.* Indomethacin-induced translocation of bacteria across enteric epithelia is reactive oxygen species-dependent and reduced by vitamin C. *Am. J. Physiol. Gastrointest. Liver Physiol.* **303**, G536-45 (2012).

285. Patel, R. *et al.* Mitochondrial neurogastrointestinal encephalopathy: a clinicopathological mimic of Crohn's disease. *BMC Gastroenterol.* **19**, 11 (2019).

286. Nazli, A. *et al.* Epithelia under metabolic stress perceive commensal bacteria as a threat. *Am. J. Pathol.* **164**, 947–957 (2004).

287. Nazli, A. *et al.* Enterocyte cytoskeleton changes are crucial for enhanced translocation of nonpathogenic Escherichia coli across metabolically stressed gut epithelia. *Infect. Immun.* **74**, 192–201 (2006).

288. Lewis, K. *et al.* Decreased epithelial barrier function evoked by exposure to metabolic stress and nonpathogenic E. coli is enhanced by TNF-alpha. *Am. J. Physiol. liver Physiol.* **294**, G669-78 (2008).

289. Lewis, K. *et al.* Enhanced translocation of bacteria across metabolically stressed epithelia is reduced by butyrate. *Inflamm. Bowel Dis.* **16**, 1138–1148 (2010).

290. Wang, A. *et al.* Targeting mitochondria-derived reactive oxygen species to reduce epithelial barrier dysfunction and colitis. *Am. J. Pathol.* **184**, 2516–2527 (2014).

291. Perse, M. & Cerar, A. Dextran sodium sulphate colitis mouse model: traps and tricks. *J. Biomed. Biotechnol.* **2012**, 718617 (2012).

292. Hansen, M. E. *et al.* Lipopolysaccharide Disrupts Mitochondrial Physiology in Skeletal Muscle via Disparate Effects on Sphingolipid Metabolism. *Shock* (2015). doi:10.1097/SHK.0000000000000468 [doi]

293. Park, J. *et al.* Anti-inflammatory effect of oleuropein on microglia through regulation of Drp1-dependent mitochondrial fission. *J. Neuroimmunol.* **306**, 46–52 (2017).

294. Cui, J. *et al.* Melatonin alleviates inflammation-induced apoptosis in human umbilical vein endothelial cells via suppression of Ca2+-XO-ROS-Drp1-mitochondrial fission axis by activation of AMPK/SERCA2a pathway. *Cell Stress Chaperones* (2017). doi:10.1007/s12192-017-0841-6

295. Ye, S. *et al.* Carboxylic Acid Fullerene (C60) Derivatives Attenuated Neuroinflammatory Responses by Modulating Mitochondrial Dynamics. *Nanoscale Res. Lett.* **10**, 953-015-0953–9. Epub 2015 May 30 (2015).

296. Stavru, F., Bouillaud, F., Sartori, A., Ricquier, D. & Cossart, P. Listeria monocytogenes transiently alters mitochondrial dynamics during infection. *Proc. Natl. Acad. Sci. U. S. A.* **108**, 3612–3617 (2011).

297. Stavru, F., Palmer, A. E., Wang, C., Youle, R. J. & Cossart, P. Atypical

mitochondrial fission upon bacterial infection. *Proc. Natl. Acad. Sci. U. S. A.* **110**, 16003–16008 (2013).

298. Lum, M. & Morona, R. Dynamin-related protein Drp1 and mitochondria are important for Shigella flexneri infection. *Int. J. Med. Microbiol.* **304**, 530–541 (2014).

299. Sirianni, A. *et al.* Mitochondria mediate septin cage assembly to promote autophagy of Shigella. *EMBO Rep.* (2016). doi:e201541832 [pii]

300. Jain, P., Luo, Z. Q. & Blanke, S. R. Helicobacter pylori vacuolating cytotoxin A (VacA) engages the mitochondrial fission machinery to induce host cell death. *Proc. Natl. Acad. Sci. U. S. A.* **108**, 16032–16037 (2011).

301. Chowdhury, S. R. *et al.* Chlamydia preserves the mitochondrial network necessary for replication via microRNA-dependent inhibition of fission. *J. Cell Biol.* (2017). doi:10.1083/jcb.201608063

302. Kurihara, Y. *et al.* Chlamydia trachomatis targets mitochondrial dynamics to promote intracellular survival and proliferation. *Cell. Microbiol.* e12962 (2018). doi:10.1111/cmi.12962

303. Escoll, P. *et al.* Legionella pneumophila Modulates Mitochondrial Dynamics to Trigger Metabolic Repurposing of Infected Macrophages. *Cell Host Microbe* (2017). doi:10.1016/j.chom.2017.07.020

304. Lobet, E. *et al.* Mitochondrial fragmentation affects neither the sensitivity to TNFalpha-induced apoptosis of Brucella-infected cells nor the intracellular replication of the bacteria. *Sci. Rep.* **8**, 5173 (2018).

305. Kim, S. J. *et al.* Hepatitis B virus disrupts mitochondrial dynamics: induces fission and mitophagy to attenuate apoptosis. *PLoS Pathog.* **9**, e1003722 (2013).

306. Fields, J. A. *et al.* HIV alters neuronal mitochondrial fission/fusion in the brain during HIV-associated neurocognitive disorders. *Neurobiol. Dis.* (2015). doi:S0969-9961(15)30095-4 [pii]

307. Teodorof-Diedrich, C. & Spector, S. A. Human Immunodeficiency Virus Type-1 gp120 and Tat Induce Mitochondrial Fragmentation and Incomplete Mitophagy in Human Neurons. *J. Virol.* (2018). doi:10.1128/JVI.00993-18

308. Li, Q. *et al.* Encapsulating Quantum Dots within HIV-1 Virions through Site-Specific Decoration of the Matrix Protein Enables Single Virus Tracking in Live Primary Macrophages. *Nano Lett.* (2018). doi:10.1021/acs.nanolett.8b02800

309. Mukherjee, A., Patra, U., Bhowmick, R. & Chawla-Sarkar, M. Rotaviral nonstructural protein 4 triggers dynamin-related protein 1-dependent mitochondrial fragmentation during infection. *Cell. Microbiol.* (2018). doi:10.1111/cmi.12831

310. Gou, H. *et al.* CSFV induced mitochondrial fission and mitophagy to inhibit apoptosis. *Oncotarget* (2017). doi:10.18632/oncotarget.17030

311. Yu, C. Y. *et al.* Dengue Virus Impairs Mitochondrial Fusion by Cleaving Mitofusins. *PLoS Pathog.* **11**, e1005350 (2015).

312. Chatel-Chaix, L. *et al.* Dengue Virus Perturbs Mitochondrial Morphodynamics

to Dampen Innate Immune Responses. *Cell Host Microbe* (2016). doi:10.1016/j.chom.2016.07.008

313. Barbier, V., Lang, D., Valois, S., Rothman, A. L. & Medin, C. L. Dengue virus induces mitochondrial elongation through impairment of Drp1-triggered mitochondrial fission. *Virology* **500**, 149–160 (2016).
314. Shi, C. S. *et al.* SARS-coronavirus open reading frame-9b suppresses innate immunity by targeting mitochondria and the MAVS/TRAF3/TRAF6 signalosome. *J. Immunol. (Baltimore, Md. 1950)* **193**, 3080–3089 (2014).
315. Chen, T. T. *et al.* Mitochondrial dynamics in the mouse liver infected by Schistosoma mansoni. *Acta Trop.* (2015). doi:S0001-706X(15)00100-X [pii]
316. Stumbo, A. C. *et al.* Mitochondrial localization of non-histone protein HMGB1 during human endothelial cell-Toxoplasma gondii infection. *Cell Biol. Int.* **32**, 235–238 (2008).
317. Pernas, L., Bean, C., Boothroyd, J. C. & Scorrano, L. Mitochondria Restrict Growth of the Intracellular Parasite Toxoplasma gondii by Limiting Its Uptake of Fatty Acids. *Cell Metab.* **27**, 886-897.e4 (2018).
318. Matisz, C. E. *et al.* Suppression of colitis by adoptive transfer of helminth antigen-treated dendritic cells requires interleukin-4 receptor-alpha signaling. *Sci. Rep.* **7**, 40631 (2017).
319. Saxena, A., Lopes, F., Poon, K. K. H. & McKay, D. M. Absence of the NOD2 protein renders epithelia more susceptible to barrier dysfunction due to mitochondrial dysfunction. *Am. J. Physiol. Gastrointest. Liver Physiol.* **313**,

G26–G38 (2017).

320. McKay, D. M. & Singh, P. K. Superantigen activation of immune cells evokes epithelial (T84) transport and barrier abnormalities via IFN-gamma and TNF alpha: inhibition of increased permeability, but not diminished secretory responses by TGF-beta2. *J. Immunol. (Baltimore, Md. 1950)* **159**, 2382–2390 (1997).

321. Smyth, D., Phan, V., Wang, A. & McKay, D. M. Interferon-gamma-induced increases in intestinal epithelial macromolecular permeability requires the Src kinase Fyn. *Lab. Invest.* **91**, 764–777 (2011).

322. Chao, Y. & Zhang, T. Optimization of fixation methods for observation of bacterial cell morphology and surface ultrastructures by atomic force microscopy. *Appl. Microbiol. Biotechnol.* **92**, 381–392 (2011).

323. Miret-Casals, L. *et al.* Identification of New Activators of Mitochondrial Fusion Reveals a Link between Mitochondrial Morphology and Pyrimidine Metabolism. *Cell Chem. Biol.* (2017). doi:10.1016/j.chembiol.2017.12.001

324. Ceponis, P. J. M., McKay, D. M., Ching, J. C. Y., Pereira, P. & Sherman, P. M. Enterohemorrhagic Escherichia coli O157:H7 disrupts Stat1-mediated gamma interferon signal transduction in epithelial cells. *Infect. Immun.* **71**, 1396–1404 (2003).

325. Toyama, E. Q. *et al.* Metabolism. AMP-activated protein kinase mediates mitochondrial fission in response to energy stress. *Science* **351**, 275–281 (2016).

326. Keita, A. V *et al.* Characterization of antigen and bacterial transport in the follicle-associated epithelium of human ileum. *Lab. Invest.* **86**, 504–516 (2006).

327. Rooney, J. P. *et al.* PCR based determination of mitochondrial DNA copy number in multiple species. *Methods Mol. Biol.* **1241**, 23–38 (2015).

328. Figueroa, D., Asaduzzaman, M. & Young, F. Real time monitoring and quantification of reactive oxygen species in breast cancer cell line MCF-7 by 2',7'-dichlorofluorescin diacetate (DCFDA) assay. *J. Pharmacol. Toxicol. Methods* **94**, 26–33 (2018).

329. Zhang, L. *et al.* Drp1-dependent mitochondrial fission mediates osteogenic dysfunction in inflammation through elevated production of reactive oxygen species. *PLoS One* **12**, e0175262 (2017).

330. Tang, H. *et al.* Doxorubicin-induced cardiomyocyte apoptosis: Role of mitofusin 2. *Int. J. Biochem. Cell Biol.* **88**, 55–59 (2017).

331. Zhao, G. *et al.* Crosstalk between Mitochondrial Fission and Oxidative Stress in Paraquat-Induced Apoptosis in Mouse Alveolar Type II Cells. *Int. J. Biol. Sci.* **13**, 888–900 (2017).

332. Hung, C. H.-L. *et al.* A reciprocal relationship between reactive oxygen species and mitochondrial dynamics in neurodegeneration. *Redox Biol.* **14**, 7–19 (2017).

333. Jang, W. B. *et al.* Cytoprotective Roles of a Novel Compound, MHY-1684, against Hyperglycemia-Induced Oxidative Stress and Mitochondrial

Dysfunction in Human Cardiac Progenitor Cells. *Oxid. Med. Cell. Longev.* **2018**, 4528184 (2018).

334. Omura, S., Asami, Y. & Crump, A. Staurosporine: new lease of life for parent compound of today's novel and highly successful anti-cancer drugs. *J. Antibiot. (Tokyo).* **71**, 688–701 (2018).

335. Klapproth, J.-M. A. & Sasaki, M. Bacterial induction of proinflammatory cytokines in inflammatory bowel disease. *Inflamm. Bowel Dis.* **16**, 2173–2179 (2010).

336. Turner, M. L., Healey, G. D. & Sheldon, I. M. Immunity and inflammation in the uterus. *Reprod. Domest. Anim.* **47 Suppl 4**, 402–409 (2012).

337. Saxena, A., Lopes, F. & McKay, D. M. Reduced intestinal epithelial mitochondrial function enhances in vitro interleukin-8 production in response to commensal Escherichia coli. *Inflamm. Res.* **67**, 829–837 (2018).

338. Anzell, A. R., Maizy, R., Przyklenk, K. & Sanderson, T. H. Mitochondrial Quality Control and Disease: Insights into Ischemia-Reperfusion Injury. *Mol. Neurobiol.* (2017). doi:10.1007/s12035-017-0503-9

339. Hu, C., Huang, Y. & Li, L. Drp1-Dependent Mitochondrial Fission Plays Critical Roles in Physiological and Pathological Progresses in Mammals. *Int. J. Mol. Sci.* **18**, (2017).

340. Coward, S. *et al.* Past and Future Burden of Inflammatory Bowel Diseases Based on Modeling of Population-Based Data. *Gastroenterology* (2019). doi:10.1053/j.gastro.2019.01.002

341. Stevens, T. W. *et al.* Systematic review: predictive biomarkers of therapeutic response in inflammatory bowel disease-personalised medicine in its infancy. *Aliment. Pharmacol. Ther.* **48**, 1213–1231 (2018).

342. Schmitt, K. *et al.* Circadian Control of DRP1 Activity Regulates Mitochondrial Dynamics and Bioenergetics. *Cell Metab.* **27**, 657-666.e5 (2018).

343. Barna, L. *et al.* Correlated confocal and super-resolution imaging by VividSTORM. *Nat. Protoc.* **11**, 163–183 (2016).

344. Kiesler, P., Fuss, I. J. & Strober, W. Experimental Models of Inflammatory Bowel Diseases. *Cell. Mol. Gastroenterol. Hepatol.* **1**, 154–170 (2015).

345. Palmela, C. *et al.* Adherent-invasive Escherichia coli in inflammatory bowel disease. *Gut* (2017). doi:10.1136/gutjnl-2017-314903

346. Saint-Georges-Chaumet, Y. & Edeas, M. Microbiota-mitochondria inter-talk: consequence for microbiota-host interaction. *Pathog. Dis.* **74**, ftv096 (2016).

347. Heinen-Weiler, J. *et al.* 3D visualization uncovers heterogenity of cardiac mitochondria and artefacts of 2D images. in (9th World Congress of Targeting Mitochondria, 2019).

348. Koopman, W. J., Distelmaier, F., Esseling, J. J., Smeitink, J. A. & Willems, P. H. Computer-assisted live cell analysis of mitochondrial membrane potential, morphology and calcium handling. *Methods* **46**, 304–311 (2008).

349. Perry, S. W., Norman, J. P., Barbieri, J., Brown, E. B. & Gelbard, H. A. Mitochondrial membrane potential probes and the proton gradient: a practical usage guide. *Biotechniques* **50**, 98–115 (2011).

350. Iannetti, E. F. *et al.* Towards high-content screening of mitochondrial morphology and membrane potential in living cells. *Int. J. Biochem. Cell Biol.* (2015). doi:S1357-2725(15)00030-8 [pii]

351. Zhao, J. *et al.* Low-dose 2-deoxyglucose and metformin synergically inhibit proliferation of human polycystic kidney cells by modulating glucose metabolism. *Cell death Discov.* **5**, 76 (2019).

352. Gleeson, L. E. *et al.* Cutting Edge: Mycobacterium tuberculosis Induces Aerobic Glycolysis in Human Alveolar Macrophages That Is Required for Control of Intracellular Bacillary Replication. *J. Immunol.* **196**, 2444–2449 (2016).

353. Czyz, D. M., Willett, J. W. & Crosson, S. Brucella abortus Induces a Warburg Shift in Host Metabolism That Is Linked to Enhanced Intracellular Survival of the Pathogen. *J. Bacteriol.* **199**, (2017).

354. Chen, Y., Zhou, Z. & Min, W. Mitochondria, Oxidative Stress and Innate Immunity. *Front. Physiol.* **9**, 1487 (2018).

355. Parsekar, S. U. *et al.* Efficient hydrolytic cleavage of DNA and antiproliferative effect on human cancer cells by two dinuclear Cu(II) complexes containing a carbohydrazone ligand and 1,10-phenanthroline as a coligand. *J. Biol. Inorg. Chem.* (2019). doi:10.1007/s00775-019-01651-8

356. Ali, S. & McStay, G. P. Regulation of Mitochondrial Dynamics by Proteolytic Processing and Protein Turnover. *Antioxidants (Basel, Switzerland)* **7**, (2018).

357. Juge, R. *et al.* Quantification and Characterization of UVB-Induced

Mitochondrial Fragmentation in Normal Primary Human Keratinocytes. *Sci. Rep.* **6**, 35065 (2016).

358. Valente, A. J., Maddalena, L. A., Robb, E. L., Moradi, F. & Stuart, J. A. A simple ImageJ macro tool for analyzing mitochondrial network morphology in mammalian cell culture. *Acta Histochem.* (2017). doi:10.1016/j.acthis.2017.03.001

359. Harwig, M. C. *et al.* Methods for imaging mammalian mitochondrial morphology: A prospective on MitoGraph. *Anal. Biochem.* (2018). doi:10.1016/j.ab.2018.02.022

360. Akira, S. & Takeda, K. Toll-like receptor signalling. *Nat. Rev. Immunol.* **4**, 499–511 (2004).

361. Yu, J. *et al.* Heme Oxygenase-1/Carbon Monoxide-regulated Mitochondrial Dynamic Equilibrium Contributes to the Attenuation of Endotoxin-induced Acute Lung Injury in Rats and in Lipopolysaccharide-activated Macrophages. *Anesthesiology* (2016). doi:10.1097/ALN.0000000000001333

362. Pan, L.-F. *et al.* The toll-like receptor 4 antagonist transforming growth factor-beta-activated kinase(TAK)-242 attenuates taurocholate-induced oxidative stress through regulating mitochondrial function in mice pancreatic acinar cells. *J. Surg. Res.* **206**, 298–306 (2016).

363. Park, J. *et al.* Peroxiredoxin 5 (Prx5) decreases LPS-induced microglial activation through regulation of Ca2+/Calcineurin-Drp1-dependent mitochondrial fission. *Free Radic. Biol. Med.* (2016).

doi:10.1016/j.freeradbiomed.2016.08.030

364. Katoh, M. *et al.* Polymorphic regulation of mitochondrial fission and fusion modifies phenotypes of microglia in neuroinflammation. *Sci. Rep.* **7**, 4942 (2017).

365. Nair, S. *et al.* Lipopolysaccharide-induced alteration of mitochondrial morphology induces a metabolic shift in microglia modulating the inflammatory response in vitro and in vivo. *Glia* (2019). doi:10.1002/glia.23587

366. Zhang, L. *et al.* Ratiometric fluorescent pH-sensitive polymers for high-throughput monitoring of extracellular pH. *RSC Adv.* **6**, 46134–46142 (2016).

367. Chen, X. H. *et al.* TNF-alpha induces mitochondrial dysfunction in 3T3-L1 adipocytes. *Mol. Cell. Endocrinol.* **328**, 63–69 (2010).

368. Jolly, C., Winfree, S., Hansen, B. & Steele-Mortimer, O. The Annexin A2/p11 complex is required for efficient invasion of Salmonella Typhimurium in epithelial cells. *Cell. Microbiol.* **16**, 64–77 (2014).

369. Wrande, M. *et al.* Genetic Determinants of Salmonella enterica Serovar Typhimurium Proliferation in the Cytosol of Epithelial Cells. *Infect. Immun.* **84**, 3517–3526 (2016).

370. Rossin, F. *et al.* Transglutaminase 2 ablation leads to mitophagy impairment associated with a metabolic shift towards aerobic glycolysis. *Cell Death Differ.* **22**, 408–418 (2015).

371. Arasaki, K. *et al.* A Role for the Ancient SNARE Syntaxin 17 in Regulating Mitochondrial Division. *Dev. Cell* (2015). doi:S1534-5807(14)00808-9 [pii]

372. Archer, S. L. Mitochondrial dynamics--mitochondrial fission and fusion in human diseases. *N. Engl. J. Med.* **369**, 2236–2251 (2013).

373. Cho, B. *et al.* CDK5-dependent inhibitory phosphorylation of Drp1 during neuronal maturation. *Exp. Mol. Med.* **46**, e105 (2014).

374. Kashatus, J. A. *et al.* Erk2 phosphorylation of Drp1 promotes mitochondrial fission and MAPK-driven tumor growth. *Mol. Cell* **57**, 537–551 (2015).

375. Kashatus, D. F. *et al.* RALA and RALBP1 regulate mitochondrial fission at mitosis. *Nat. Cell Biol.* **13**, 1108–1115 (2011).

376. Wikstrom, J. D. *et al.* AMPK regulates ER morphology and function in stressed pancreatic beta-cells via phosphorylation of DRP1. *Mol. Endocrinol.* **27**, 1706–1723 (2013).

377. Wang, Z., Jiang, H., Chen, S., Du, F. & Wang, X. The mitochondrial phosphatase PGAM5 functions at the convergence point of multiple necrotic death pathways. *Cell* **148**, 228–243 (2012).

378. Prieto, J. *et al.* Early ERK1/2 activation promotes DRP1-dependent mitochondrial fission necessary for cell reprogramming. *Nat. Commun.* **7**, 11124 (2016).

379. Shimizu, Y. *et al.* DJ-1 protects the heart against ischemia-reperfusion injury by regulating mitochondrial fission. *J. Mol. Cell. Cardiol.* (2016). doi:S0022-2828(16)30074-8 [pii]

380. Kanfer, G. & Kornmann, B. Dynamics of the mitochondrial network during mitosis. *Biochem. Soc. Trans.* **44**, 510–516 (2016).

381. Olichon, A. *et al.* OPA1 alternate splicing uncouples an evolutionary conserved function in mitochondrial fusion from a vertebrate restricted function in apoptosis. *Cell Death Differ.* **14**, 682–692 (2007).

382. Griparic, L., Kanazawa, T. & van der Bliek, A. M. Regulation of the mitochondrial dynamin-like protein Opa1 by proteolytic cleavage. *J. Cell Biol.* **178**, 757–764 (2007).

383. Baburamani, A. A. *et al.* Mitochondrial Optic Atrophy (OPA) 1 Processing Is Altered in Response to Neonatal Hypoxic-Ischemic Brain Injury. *Int. J. Mol. Sci.* **16**, 22509–22526 (2015).

384. Rosdah, A. A., K Holien, J., Delbridge, L. M. D., Dusting, G. J. & Lim, S. Y. Mitochondrial fission - a drug target for cytoprotection or cytodestruction? *Pharmacol. Res. Perspect.* **4**, e00235 (2016).

385. Sato, A. K., Viswanathan, M., Kent, R. B. & Wood, C. R. Therapeutic peptides: technological advances driving peptides into development. *Curr. Opin. Biotechnol.* **17**, 638–642 (2006).

386. Zhang, J. *et al.* Guanylate-binding protein 2 regulates Drp1-mediated mitochondrial fission to suppress breast cancer cell invasion. *Cell Death Dis.* **8**, e3151 (2017).

387. Kitamura, S. *et al.* Drp1 regulates mitochondrial morphology and cell proliferation in cutaneous squamous cell carcinoma. *J. Dermatol. Sci.* **88**, 298–307 (2017).

388. Jo, Y., Cho, H. M., Sun, W. & Ryu, J. R. Localization of dynamin-related

protein 1 and its potential role in lamellipodia formation. *Histochem. Cell Biol.* (2017). doi:10.1007/s00418-017-1554-8

389. Monian, P. & Jiang, X. Clearing the final hurdles to mitochondrial apoptosis: regulation post cytochrome C release. *Exp. Oncol.* **34**, 185–191 (2012).

390. Susin, S. A. *et al.* Molecular characterization of mitochondrial apoptosis-inducing factor. *Nature* **397**, 441–446 (1999).

391. Kroemer, G. & Martin, S. J. Caspase-independent cell death. *Nat. Med.* **11**, 725–730 (2005).

392. Galluzzi, L. *et al.* Essential versus accessory aspects of cell death: recommendations of the NCCD 2015. *Cell Death Differ.* **22**, 58–73 (2015).

393. Del Dotto, V., Fogazza, M., Carelli, V., Rugolo, M. & Zanna, C. Eight human OPA1 isoforms, long and short: What are they for? *Biochim. Biophys. Acta* **1859**, 263–269 (2018).

394. Galluzzi, L. *et al.* Molecular mechanisms of cell death: recommendations of the Nomenclature Committee on Cell Death 2018. *Cell Death Differ.* **25**, 486–541 (2018).

395. Guo, X., Sesaki, H. & Qi, X. Drp1 stabilizes p53 on the mitochondria to trigger necrosis under oxidative stress conditions in vitro and in vivo. *Biochem. J.* **461**, 137–146 (2014).

396. Choi, S.-G. *et al.* SUMO-Modified FADD Recruits Cytosolic Drp1 and Caspase-10 to Mitochondria for Regulated Necrosis. *Mol. Cell. Biol.* (2016). doi:10.1128/MCB.00254-16

397. Iannielli, A. *et al.* Pharmacological Inhibition of Necroptosis Protects from Dopaminergic Neuronal Cell Death in Parkinson's Disease Models. *Cell Rep.* **22**, 2066–2079 (2018).

398. Wen, H., Hao, J. & Li, S. K. Characterization of human sclera barrier properties for transscleral delivery of bevacizumab and ranibizumab. *J. Pharm. Sci.* **102**, 892–903 (2013).

399. Zhao, J. *et al.* Mitochondrial dynamics regulates migration and invasion of breast cancer cells. *Oncogene* **32**, 4814–4824 (2013).

400. Bordt, E. A. *et al.* The Putative Drp1 Inhibitor mdivi-1 Is a Reversible Mitochondrial Complex I Inhibitor that Modulates Reactive Oxygen Species. *Dev. Cell* **40**, 583-594.e6 (2017).

401. Turnbough, C. L. J. & Switzer, R. L. Regulation of pyrimidine biosynthetic gene expression in bacteria: repression without repressors. *Microbiol. Mol. Biol. Rev.* **72**, 266–300, table of contents (2008).

402. Chang, C.-H. *et al.* Posttranscriptional control of T cell effector function by aerobic glycolysis. *Cell* **153**, 1239–1251 (2013).

403. Fontana, M. F. *et al.* Secreted bacterial effectors that inhibit host protein synthesis are critical for induction of the innate immune response to virulent Legionella pneumophila. *PLoS Pathog.* **7**, e1001289 (2011).

404. Neurath, M. F. & Travis, S. P. L. Mucosal healing in inflammatory bowel diseases: a systematic review. *Gut* **61**, 1619–1635 (2012).

Appendix I

Systemic delivery of a selective inhibitor of mitochondrial fission to treat colitis

Nicole L. Mancini,[1†] Luke Goudie,[2†] Warren Xu,[2] Ala Al Rajabi,[1] Timothy S. Jayme,[1] Rasha Sabouny,[3] Arthur Wang,[1] José Ferraz,[4] Timothy Shutt,[3] Jane Shearer[5] and Derek M. McKay[1*]

[1]Gastrointestinal Research Group and Inflammation Research Network, Department of Physiology and Pharmacology, Calvin, Joan and Phoebe Snyder Institute for Chronic Diseases, Cumming School of Medicine, University of Calgary, Alberta, Canada

[2]Department of Biomedical Engineering, Schulich School of Engineering, University of Calgary

[3]Department of Medical Genetics, Alberta Children's Hospital Research Institute, University of Calgary

[4]Division of Gastroenterology, Cumming School of Medicine, University of Calgary

[5]Department of Biochemistry and Molecular Biology, Faculty of Kinesiology, University of Calgary

Running Title: Colitis and mitochondrial dynamics

† Authors contributed equally to the work

*Address correspondence to:
Derek M. McKay, Ph.D.
Professor, Dept. Physiology & Pharmacology
1877 HSC, University of Calgary
3330 Hospital Drive NW
Calgary, Alberta, T2N 4N1, Canada
Tel: 403-220-7362 Fax: 403-283-3029
Email: dmckay@ucalgary.ca

Disclosures: The authors declare no conflict of interest.

Funding: Funding for this study was provided by an Innovation Grant from Crohn's Colitis Canada (J. S and D.M.M) and a grant from the Canadian Institutes for Health Research (D.M.M).

ABSTRACT

Objective. Mitochondria exist in a constantly remodelling network, and excessive fragmentation (i.e. fission) can be of pathophysiological significance. Mitochondrial dysfunction can accompany enteric inflammation, but a contribution of altered mitochondrial dynamics (i.e. fission/fusion) to gut inflammation is unknown. We hypothesised that perturbed mitochondrial dynamics would contribute to colitis.

Design. qPCR for markers of mitochondrial fission was applied to human colonic biopsies and tissue from dextran sodium-sulphate (DSS) treated mice. An inhibitor of mitochondrial fission, P110, was tested in the DSS and di-nitrobenzene sulphonic acid (DNBS) models of murine colitis and the impact of DSS ± P110 on intestinal epithelial and macrophage mitochondria assessed *in vitro*.

Results. Analysis of colonic biopsies from patients with IBD or tissue from mice with DSS-colitis revealed increased mRNA expression of molecules associated with mitochondrial fission (dynamin-related protein-1) and fusion (optic atrophy 1) compared to control. Systemic delivery of P110, in prophylactic or treatment regimens, reduced DSS-or DNBS-colitis severity in mice. Microbial dysbiosis that accompanied DSS-induced colitis was unaffected by P110 co-treatment. Application of DSS to epithelia or macrophages *in vitro* evoked significant mitochondrial fragmentation. DSS-evoked perturbation of epithelial cell energetics and mitochondrial fragmentation, but not cell death, were ameliorated by *in vitro* co-treatment with P110.

Conclusion. Excessive mitochondrial fission can be a feature of intestinal inflammation, the suppression of which could be therapeutic in IBD.

SUMMARY BOX

What is already known about the subject?

Ulcerative colitis was postulated as an energy deficiency disease of the epithelium, and mitochondrial dysfunction has been shown in colonic biopsies from some patients with IBD and in models of colitis. Mitochondrial dynamics (i.e. network remodeling by fission and fusion) is a critical cellular homeostatic process. There are no data on mitochondrial dynamics in IBD or whether this process could be targeted to relieve disease symptoms and inflammation.

What are the new findings?

(1) qPCR revealed increased mRNA expression of Drp1, Fis1 and OPA1, key molecules in mitochondrial fission/fusion, in biopsies from patients with IBD. (2) Systemic delivery of a selective inhibitor of Drp1-Fis1 driven mitochondrial fission, P110, significantly reduced the severity of DSS- and DNBS-induced colitis in mice. (3) DSS-induced fragmentation of gut epithelial and macrophage mitochondria *in vitro* was blocked by P110 indicating both cell types as potential targets for the anti-colitic effect of P110.

How might it impact on clinical practice in the foreseeable future?

Mitochondrial fission may be an important overall aspect of the pathogenesis or reactivation of IBD, and the ability to pharmacologically intervene in this process could be a novel approach to disease management.

INTRODUCTION

Mitochondrial dysfunction can manifest as intestinal symptoms.[1,2] Indeed, in 1980, Roediger raised the possibility that energy deficiency in the epithelium was important in the

development of ulcerative colitis.[3] In support of the hypothesis that mitochondrial dysfunction contributes to IBD, abnormal mitochondria, reduced levels of ATP synthase, antioxidants and Kreb's cycle enzymes, as well as increased oxidative stress have been observed in colonic biopsies from patients.[4-8] Similarly, analyses of colitis in mice and epithelial cell culture models of barrier function have provided mechanistic underpinnings for how perturbed mitochondrial activity could contribute to IBD.[4,9-13] A focus on epithelial mitochondrial dysfunction is compatible with the consensus on the aetiology of IBD: disease occurs in a genetically susceptible individual by hyperactive immune responses triggered or perpetuated by environmental stimuli involving the gut microbiota.[14,15] In this context, mitochondria are important in the regulation of epithelial permeability[16] and low-grade bacterial pathogens such as *E. coli* (strain C25) and *Citrobacter rodentium* can impair mitochondrial function.[17,18]

It has emerged that mitochondria exist in a network that is constantly remodelling by the processes of fusion and fission that is critical to cellular homeostasis.[19] Fusion facilitates sub-cellular targeting of ATP and reactive oxygen species (ROS), and equalizes the distribution of proteins, metabolites, and mitochondrial DNA throughout the network.[20] Fission allows for mitochondrial partitioning during cell division and the removal of damaged segments of mitochondria by mitophagy; excessive fragmentation of the network can be a stimulus for apoptosis.[21] The dynamin family members, dynamin-related protein 1 (Drp1) and optic atrophy factor 1 (OPA1) are two of the major players in mitochondrial fission and fusion, respectively.[22] Imbalanced mitochondrial dynamics plays a role in many pathological conditions including neurodegenerative disease, heart disease, metabolic syndrome, and cancer;[23,24] all have an inflammatory component and yet mitochondrial dynamics are unstudied in the context of IBD. Furthermore, blocking excessive fission has proven beneficial in animal models of myocardial

infarction, pulmonary arterial hypertension, ischemic-reperfusion injury, multiple sclerosis and Huntington's disease.[23-25]

Consequently, we hypothesized that excessive mitochondrial fission would contribute to colitis and could be targeted as a novel approach to IBD. After uncovering evidence for increased mitochondrial fission in biopsies from some patients with IBD, systemic administration of a selective inhibitor of fission, P110,[26] was found to reduce disease severity in dextran-sodium sulphate (DSS)- or dinitrobenzene sulphonic acid (DNBS)-treated mice. Furthermore, DSS induced fragmentation of macrophage and gut epithelial mitochondria *in vitro*, and the accompanying reduction in bioenergetics in the latter, were partially abrogated by co-treatment with P110. Collectively the data herein suggest that perturbed mitochondrial dynamics in epithelia and macrophages are a component of enteric inflammatory disease, and that reducing mitochondrial dysfunction due to excessive fragmentation could promote intestinal homeostasis in patients that show evidence of enhanced mitochondrial fission.

RESULTS

qPCR indicates altered expression of mitochondrial dynamics molecules in colitis.

qPCR on biopsies from patients with IBD and controls revealed considerable heterogeneity, with no significant change in mitochondrial content as indicated by the mttRNA-leu:RPL27 ratio (not shown). However, mRNA expression for Drp1 and Fis1 was significantly increased in biopsies from patients with ulcerative colitis (figure 1A,B); Drp1 was elevated in non-inflamed colon from patients with Crohn's disease. Expression of OPA1 mRNA was significantly increased in Crohn's disease (figure 1C). Complementing these findings, Drp1, Fis1, OPA1 (figure 1D-F), MFN1 and MFN2 (suppl. figure 1) mRNA was increased in extracts of colon from mice with DSS-induced colitis. Immunoblotting revealed an increase in phospho-Ser616 Drp1

(required for Drp1 to translocate to mitochondria) in tissue extracts from mice treated with DSS for 5 days (figure 1G, H).

Systemic administration of P110 reduces disease severity in murine models of colitis.

P110 is a selective inhibitor of Drp1-Fis1 driven mitochondrial fission.[26] P110 (1 μM) activity was confirmed *in vitro* by its ability to reduce Drp1 recruitment to mitochondria and ROS generation by carbonyl cyanide m-chlorophenyl hydrazine (CCCP, 10 μM) treatment of the T84 human colon-derived epithelial cell line (data not shown; n=4). Mice treated with P110 only (figure 2) showed no signs of ill health, whereas DSS-treated mice had shortened colons, increased macroscopic disease scores, increased colonic transit time and histopathology (figure 2). Macroscopic disease scores were reduced by ~50% in the DSS+P110 group compared to DSS (figure 2B), with mice receiving P110 having a longer colon and colonic transit time not different from control mice (figure 2C,D). In contrast, colonic histopathology was not appreciably different between DSS and DSS+P110-treated mice (figure 2E). Bacterial dysbiosis occurred in DSS-treated mice and this was unaffected by co-treatment with P110 (suppl. table 1).

Treatment of Balb/c mice with DNBS resulted in severe colitis, with 27% (3/11) of mice reaching a pre-determined ill-health end-point requiring euthanasia (figure 3A,B). Systemic delivery of P110 in a prophylactic regimen resulted in less cachexia (figure 3C) with only one mouse of 15 (6.5%) requiring euthanasia (figure 3B). Similarly, the P110-treated mice had less macroscopic disease and longer colons compared to DNBS-only treated mice (figure 3D,E). Histologically, mice treated with DNBS+P110 had a degree of damage that lay between control and DNBS-only, and was not statistically different from either group (figure 3F). DNBS-colitis spontaneously resolves and by seven days post-treatment mice can display normal behaviour and

only mild colitis.[27] Using P110 in a treatment regimen (figure 4A) resulted in improved disease recovery: none of the treated animals required euthanasia (figure 4B), weight loss was reduced (figure 4C), colons were longer, and macroscopic disease and histopathology scores lower (figure 4D-F) (the latter did not reach statistical significance, likely reflecting the spontaneous resolution of colitis and the natural variability of mice in this model).

Analysis of blood smears revealed an increase in neutrophils in DSS or DNBS-treated mice and this was unaffected by P110 (data not shown, n=8).

P110 blocks DSS-induced mitochondrial changes in epithelial cells and macrophages.

Consistent with previous reports,[11,28] 2% DSS (24h) reduced viability of *in vitro* cultured epithelial cells as determined by trypan blue exclusion and this was not affected by P110 co-treatment (figure 5A). In contrast, the reduced alamarBlue metabolism in DSS-treated cells, indicating reduced NADH concentration, was abrogated by P110 co-treatment (figure 5B), suggesting that the surviving cells were healthier with increase NADH production capacity than DSS-only treated enterocytes.

DSS-treated epithelia had an increased percentage of cells with a highly fragmented mitochondrial network and P110 partially abrogated this effect resulting in a significant increase in epithelial cells with a mitochondrial network intermediate between fused and fragmented (figure 5C,D). Similarly, P110 largely abrogated the mitochondrial fragmentation in bone-marrow derived macrophages treated with 1% DSS for 24h (figure 5E,F) (with 2% DSS, macrophages lost adherence and those remaining were small and rounded).

To examine the functional impact of P110 on mitochondrial bioenergetics, the oxygen consumption rate (OCR) of saturating concentrations of specific substrates were assessed

following 24h of exposure to DSS. Analysis of basal respiration revealed DSS impaired respiration in $IEC^{4.1}$ epithelia, but restored with DSS+P110 treatment (figure 6A). Stimulation of electron transport chain (ETC) Complex I, II and IV demonstrated that co-treatment with DSS+P110 increased Complex IV activity (figure 6B-D). Trends towards reduced mitochondrial capacity in complex I and II in DSS-treated cells were also noted but less so with DSS+P110 treated cells. Epithelial fatty acid oxidation with both short (butyrate) and long chain fatty acid (palmitate) revealed impairments with DSS that were abrogated by P110 (figure 6E, 6F). These findings show significant metabolic stress in DSS-treated epithelia and that the perturbed bioenergetics were relieved, at least in part, by treatment with P110.

P110 does not affect DSS-evoked increased paracellular epithelial permeability *in vitro*

Twenty-four hours after exposure to 2% DSS, T84 monolayer transepithelial resistance was reduced by ~20% and by 48h post-treatment, TER was ~60% of pre-treatment values. This reduction in TER was unaffected by co-treatment with p110 (n=10 monolayers from 3 experiments). However, the early drop in TER was prevented by co-treatment with the pan-caspase inhibitor Z-VAD, which also reduced the barrier defect observed at 48h post-treatment (TER: DSS = 64.5 ± 5% (n=10) vs. DSS+ZVAD = 80 ± 10% (n=6) of pre-treatment values; starting TER was 1,000-2,000 $\Omega \cdot cm^2$).

Inhibitors of mitochondrial fission do not affect DSS or LPS-evoked cytokine production

Epithelia treated with DSS showed a trend towards decreased KC production, while macrophages displayed only small increases in TNFα and IL-10 upon *in vitro* exposure to DSS. These responses were not significantly affected by co-treatment with inhibitors of fission, except

for a small statistically significant increase in IL-10 output from 1% DSS+P110 treated macrophages compared to DSS alone (suppl. table 2). LPS-stimulated cytokine production was unaffected by co-treatment with P110 (suppl. table 2).

DISCUSSION

Tremendous advances have been made in the treatment of IBD, yet, as the gold standard therapy, many patients are or become refractory to biologicals:[29] hence the imperative to explore novel targets to treat IBD. A body of data illustrates perturbed mitochondrial activity (i.e. reduced ATP and antioxidants, increased ROS) in IBD[30] and mitochondrial malfunction can result in gastrointestinal symptoms.[1] Yet the role that dysfunctional mitochondria in the enteric epithelium, or other gut cells, plays in the pathophysiology of IBD is unclear: a small number of studies suggest that targeting mitochondria could be valuable in treating enteric inflammation.[11,31-33]

The 'health' of the mitochondrial network has emerged as a key aspect of cellular homeostasis, where excessive fission driven by the GTPase Drp-1 interaction with Fis1 (or other partners) or reduced fusion is implicated in many diseases.[19,24] The hypothesis that mitochondrial dynamics would be abnormal in IBD is supported by increases in Drp1, Fis1 and OPA1 mRNA in biopsies from some patients with IBD; increased Fis1-driven fission is considered pathological and a marker of disease.[26] These data from IBD-tissue are complemented by similar findings in colon from DSS-treated mice, along with evidence of increased pSer616 activated Drp1 protein, and increased MFN1 and MFN2 mRNA: thus, providing some of the first evidence for mitochondrial network remodelling in intestine from people and mice with colitis. Mitochondrial dysfunction in DSS-colitis is supported by subtle reductions in the mitochondria-specific voltage-dependent anion channel,[11] lower tissue levels of ATP and a less complex mitochondrial network, likely representing considerable fission.[13] Also, mutation in the multi-drug resistance 1 gene is an ulcerative colitis susceptibility trait, and *mdr1*$^{-/-}$ mice present with damaged epithelial mitochondria,[9] as can TNBS-treated rats.[34] These observations beg the question, would

suppression of excessive mitochondrial fission be beneficial in the treatment of enteric inflammation.

Pharmacological options to block mitochondrial fission *in vivo* are limited. Mdivi1 blocks the GTPase activity of Drp1 but may have off-target effects related to oxidative phosphorylation and the suppression of ROS.[35] The antirheumatic drug, leflunomide, blocks pyrimidine synthesis and was recently shown to antagonise mitochondrial fission by promoting fusion.[36] The small peptide P110 is conjugated to the HIV-TAT protein to facilitate transduction into cells, and was designed to bind to Fis1 to prevent docking of Drp1, thus preventing pathological fission.[26] Given increased Fis1 mRNA expression in ulcerative colitis and DSS-treated mice, P110 was a rational choice to test for putative anti-colitic efficacy in animal models of colitis.

Systemic delivery of P110 significantly reduced the severity of disease in the DSS and DNBS models of murine colitis – the mice displayed less macroscopic signs of colitis and colonic dysmotility was normalized. Notably, only 1/23 mice (4%) treated with P110+DNBS required humane euthanasia whereas 6/22 (~27%) DNBS-only treated mice developed severe illness requiring euthanasia. Analyses of colonic histopathology revealed damage that was not significantly different between DSS vs. DSS+P110 groups or DNBS vs. DNBS+P110 groups, although the latter was not statistically different from control. Complete mucosal healing is the desired goal of therapy, but it is not unusual for patients to experience symptom relief and have endoscopic or histological disease[37]: testing of novel therapies in mice can reveal macroscopic improvement concomitant with histopathology.[38] Nevertheless, while P110 has anti-colitic effects, reminiscent of its benefits in models of multiple sclerosis and cardiac dysfunction,[39-41] future studies are needed to determine if greater mucosal healing can be achieved as a standalone or adjunct therapy.

The DSS model was used to address the challenge of identifying P110's putative target cell(s). The microbiota is an important trigger for IBD[14] and dysbiosis of the colonic bacteria accompanies DSS-colitis.[42] Fis1 is not expressed in bacteria but considering the possibility of an off-target, anti-bacterial effect if P110 entered the gut lumen, assessment of the colonic microbiota was performed. DSS-treated mice were dysbiotic and this was unaffected by P110 co-treatment, ruling out the gut bacteria as a target for P1120's therapeutic effect. These data indicate that improvement in disease can occur in advance of correction or normalization of the gut microbiota. Furthermore, P110 treatment did not influence the DSS-evoked increase in circulating neutrophils, or the levels of myeloperoxidase activity in tissue extracts from colitic mice (pers. observ.) suggesting that the neutrophil was not the target for P110's anti-colitic effect.

DSS has mucolytic activity, can be cytotoxic to the epithelium, and may activate macrophages;[28,43-45] putatively concentrated by water reabsorption in the colon, these effects of DSS may combine to cause colitis. Focusing on the epithelium, we confirmed the cytotoxic effect of DSS on a murine gut-derived epithelial cell line *in vitro* and that DSS can reduce the barrier function of epithelial cell monolayers: neither effect was susceptible to P110 treatment, whereas use of a pan-caspase inhibitor did reduce the DSS-evoked drop of transepithelial resistance in human T84 cell monolayers. However, alamarBlue cleavage as an indicator of mitochondrial function suggested that the viable enterocytes in the DSS+P110 group were healthier than DSS-only treated enterocyte. In accordance, DSS evoked significant fragmentation of epithelial mitochondria with corresponding aberrations in energy metabolism (e.g. reduced β-oxidation) that were negated in part by P110 co-treatment. In this context, reduced β-oxidation (e.g. utilization of butyrate) has been described in IBD-patient samples,[46,47] and was the basis for Roediger's hypothesis on ulcerative colitis being an energy-deficient disease.[3] Our *in vitro* data support the

postulate that through the ability of P110 to block excessive mitochondrial fission, overall mitochondrial function is enhanced, which, in turn, translates to reduced severity of disease. Extrapolating to the murine models, while P110 did not prevent DSS-induced ulceration (but had some effect in DNBS-treated mice), the surrounding tissue would be healthier, contributing to improvement in the macroscopic indicators of disease.

Enteric macrophages are heterogeneous; recently recruited monocytes convert to a macrophage that can drive inflammation, while resident macrophages and those of an alternatively activated phenotype promote tissue recovery after injury.[48-50] The finding that DSS evoked mitochondrial network fragmentation in macrophages is unprecedented. The P110 suppression of DSS-induced macrophage mitochondrial fission is compatible with macrophage mitochondrial fragmentation contributing to DSS-colitis. However, suppression of mitochondrial fission in macrophages may reduce efferocytosis,[50] a component of wound healing, and so further research is necessary to determine the functional consequences of altered macrophage mitochondrial dynamics in IBD.

Immunoneutralization of TNFα in patients is therapeutic and DSS (particularly with LPS) was shown to evoke TNFα from macrophages;[47] however, here, DSS had a minimal capacity to elicit TNFα or IL-10 from macrophages and LPS-induced production of these cytokines was unaffected by P110 co-treatment. Thus, we have no data supporting P110 regulation of macrophage-derived cytokine responses as a likely component of the anti-colitic effect, with the exception of a subtle increase in IL-10 output from DSS+P110 treated macrophages *in vitro* (DSS reduced baseline KC production by IEC[4.1] and this was unaffected by P110 co-treatment). It is possible that a small local increase in IL-10 evoked by P110 aided in the suppression of the chemical-induced colitis observed here.

Another possibility is that the P110 limited the severity of colitis by affecting nerves. Indeed, the normalization of colonic motility in P110+DSS treated mice is consistent with neuronal regulation, but this could also simply reflect overall improvement in the gut because of less disease. Neuronal contributions to inflammation and anti-inflammatory reflexes are well described and given the therapeutic potential of P110 in neurological disease,[25] research efforts should analyze form, function and mitochondrial activity of neurons in DSS- or DNBS-treated mice ± P110.

Regulated by complex and coordinated processes,[19] maintaining mitochondrial homeostasis is essential to cellular health. Given this, it is not unexpected that disrupted mitochondrial dynamics (i.e. fission and fusion) is implicated in inflammation and the pathogenesis of many diseases. Despite this, there is a paucity of information on these key homeostatic processes in the normal intestine or during inflammation. Addressing this knowledge gap, data are presented to support increased mitochondrial fission as a component of enteric inflammation that can be pharmacologically targeted to reduce disease severity. Although targeting mitochondrial fission is a significant departure from the pursuit of immunomodulators to treat IBD, it may represent a novel therapeutic target for IBD management, one we believe is worthy of consideration in a personalized-medicine approach to these insidious disorders.

MATERIALS AND METHODS

Ethical consent

Animal experiments adhered to the Canadian guidelines on animal welfare as administered by the University of Calgary Animal Care Committee protocol AC13-0015. Experiments with human samples were conducted under a protocol approved by the University of Calgary Conjoint Health Research Ethics Board (REB 17-20941): healthy controls (n=15; 6M, 9F; age range 19-72), ulcerative colitis (n=10; 4M, 6F; age range 20-49), and Crohn's disease (n=12; 4M, 8F; age range 25-64) (suppl. table 3).

Real-time qPCR of human mitochondria

Human colonic pinch biopsies were placed in RNAlater (750μL, Life Technologies) and murine colonic tissue in Ribozol (VWR), RNA extracted and cDNA synthesis performed with iScript (Bio-Rad, Mississauga, ON, Canada). Assessment of Drp1, mitochondrial fission protein 1 (Fis1), OPA1, mttRNA-leu (mitochondrial tRNA) and RPL27 (ribosomal protein L27) (human tissue), mtND1 (mitochondrial NADH dehydrogenase subunit 1) and 18S rRNA (mouse tissue), mRNA expression was performed in the Realplex Eppendorf Mastercycler using iQSYBER Green Supermix (Bio-Rad) with 6.25ng of RNA and the primers shown in suppl. table 4. Resulting values were computed to SYBR green expression based on a standard curve, and normalized to RPL27 expression. Extracts of mid-mouse colon were treated similarly with qPCR performed for mitofusions 1 and 2 (MFN1, MFN2). No-template and no-reverse transcriptional negative controls were used, and melting curves performed. Assays performed in duplicate.

Murine fecal samples and cecal contents were collected and total DNA extracted from 250mg of fecal/cecal material.[51] 16S rRNA gene expression was determined with SYBR green

using 20ng/ml DNA and 0.3μM primers (suppl. table 4) and copy number calculated according to available methodology http://cels.uri.edu/gsc/cndna.html. Standard curves were normalized to 16S rRNA using reference strain genome size and 16S rRNA gene copy number values. Data are expressed as 16S rRNA gene copies/mg fecal/cecal material.[52]

Induction and assessment of colitis

Colitis was induced in 7-9 week old male BALB/c mice (Charles River Labs, QC, Canada) with DSS (5%, 40kDa (Affymetrix, Santa Clara, California) drinking water for 5 days, then three days normal water) or DNBS (3 mg, ir, 72h).[11,53] Animals were weighed and observed daily, and humanely euthanized if they lost >20% weight. At necropsy, the colon was excised, measured and a macroscopic disease score calculated.[11,53] A portion of mid-colon was fixed, paraffin-embedded, sections collected on coded slides, H&E stained and histopathology scored on a 0-12 scale.[11,53] P110 (a kind gift from Dr. D. Mochly-Rosen, Stanford Univ.) was administered daily (3mg/kg, ip.),[25] as depicted in figures 2A,3A,4A.

Peripheral Blood Cell Count

Blood smears were collected on coded slides, stained with giemsa, and mononuclear cells, neutrophils and eosinophils counted.

Colonic Motility

A 2.5-mm glass bead was inserted 2 cm into the colon in an anesthetized mouse and the time for the bead to appear at the anal verge/be expelled was recorded.[54]

Immunoblotting

Samples of mouse mid-colon were frozen, subsequently homogenized in protein lysis buffer, and protein quantified by Bradford assay (Bio-rad). Protein (60 μg) was loaded into a 12% agarose gel, transferred to a PVDF membrane (0.2μm pore size), and probed for p-Drp1 Ser616 (Cell signaling, D9A1, 1:1000), Drp1 (abcam, ab56788, 1:2000), and actin (SantaCruz, sc-1616 1:1000). Densitometric analysis was performed on inverted images on ImageJ sofeware.

Bone-marrow derived macrophages

Bone-marrow was flushed from mouse femurs with RPMI 1640 medium (Sigma-Aldrich), sieved through a 100-μm cell strainer and cultured for 7-days in 10% FBS, 2% L-glutamine, 2% penicillin-streptomycin, 1% sodium pyruvate and 20ng/ml of recombinant mouse M-CSF (R&D Systems Inc, Minneapolis, MN, USA). Cells were rinsed in Dulbecco's PBS ($MgCl_2$-, $CaCl_2$-free), and the adherent macrophages retrieved using versene and adjusted to $2.5x10^5$/ml.

Epithelial Cell Function

(1) Viability. The murine $IEC^{4.1}$ intestinal epithelial cell line was cultured under standard conditions[55] until ~70% confluent by phase-contrast microscopy, and treated with 2% DSS ± P110 (1.5 μM, 45 min pre-treatment). Twenty-four hours later, cell viability was assessed by trypan blue dye exclusion.[55]

(2) Mitochondrial Function. $IEC^{4.1}$ ($2x10^4$) were seeded into a 96-well plate, and 24h later were treated with 2% DSS ± P110 (2.5μM 45 min pre-treatment then 1.5μM). Following a 24h incubation at 37°C, alamar Blue (1/10 dilution; Sigma Chemical Co.) was added and 5.5h later

recordings were taken at 550nm (excitation) and 590nm (emission) using a SpectraMax i3 (Molecular Devices).[56]

(3) Mitochondrial dynamics. Epithelial cells ($5x10^5$) were seeded in 8-well chamber slides and stained live with MitoTracker Red CMXRos dye (ThermoFisher Scientific, 50nM), followed by Hoescht dye (ThermoFisher, 1μg/mL), then treated with P110 (45 min, 2.5μM) followed by 24h 2% DSS+P110 (1.5μM). Live cells were imaged on the Leica DMI6000B Diskovery Flex spinning disk confocal microscope. The mitochondrial network was quantified for 20 cells/monolayer as fused, intermediate, or fragmented morphology expressed as a percent mitochondrial morphology.[57]

(4) Mitochondrial bioenergetics. Real-time, continuous assessment of oxidative phosphorylation (OXPHOS) in permeabilized $IEC^{4.1}$ cells was performed using the Oxygraph-2k C-series (OROBOROS Instruments, Austria) according to the substrate inhibitor uncoupler titration protocol-002 with modifications to digitonin and carbonyl cyanide p-(trifluoro-methoxy) phenyl-hydrazone (FCCP) and glycerophosphatetitrations [http://wiki.oroboros.at/index.php/SUIT-002].[58] Cells ($1.5x10^6$) were seeded in 100x20mm culture dishes for 24h, followed by 24h exposure to 2% DSS±P110 (1.5μM). Cells ($1x10^6$/mL) were re-suspended in mitochondrial respiration medium (MiR05) containing 0.5mM EGTA, 3mM $MgCl_2.6H_2O$, 20mM taurine, 10mM KH_2P0_4, 20mM HEPES, 1 g/L BSA, 60mM potassium-lactobionate and 110mM sucrose, pH 7.1. Upon completion of the analysis, cells were collected from the chambers and counted for normalization of oxygen specific flux. Mitochondrial exclusive respiration was identified by subtracting oxygen consumption in the presence of rotenone (0.5μM) and antimycin A (2.5μM). An additional set of experiments was performed to examine butyrate oxidation in the presence ADP (5mM), sodium butyrate (2mM) and malate (400mM) (suppl. Figure 2).

(5) Permeability: monolayers of the human colonic T84 epithelial cell line were cultured on 0.4-μm porous filter supports until electrically confluent at ≥1000 Ω·cm.[2,59] Monolayers were then exposed to 2% DSS (apical side) ± P110, and 24h later epithelial barrier function was assessed by measuring transepithelial electrical resistance (TER). Other monolayers were treated with DSS+the pan-caspase inhibitor, Z-VAD (20μM; Cayman Chemical Co.).

Cytokine production

Bone-marrow derived macrophages[60] or IEC[4.1] epithelial cells (2.5 x10^5) were treated with 1 or 2% DSS or LPS (10 ng/ml) ± a 30 min pre-treatment with P110 (1.5μM), Mdivi1 (5μM)[61] or leflunomide (50 μM).[36] Twenty-four hours later culture supernatants were collected and TNFα, IL-10 (macrophages) and keratinocyte chemoattractant (KC or CXCL1) (epithelium) measured by ELISA (R&D Systems Inc).

Statistical Analysis

Data are presented as means ± SEM. For two group comparisons, Student's t-test was applied. Multiple group comparisons of parametric data were by one-way ANOVA and when $p<0.05$, this was followed by Tukey's test or Dunnett's multiple comparison test. For non-parametric data, the Kruskal-Wallis test was applied followed by Dunn's test for comparisons to one group or Tukey's multiple comparison test. A statistically significant difference was accepted when $p < 0.05$. All analyses performed with Graph-Pad Prism 6.

ACKNOWLEDGEMENTS

N. Mancini is recipient of University of Calgary Eyes High, Kiliam and Natural Sciences and Engineering Research Council of Canada (NSERC) studentships, and L. Goudie an NSERC studentship. T. Jayme was supported by a studentship from the NSERC CREATE in Host-Parasite Interactions (HPI) Program at Univ. Calgary. D.M. McKay holds a Canada Research Chair (Tier 1) in Intestinal Immunophysiology in Health and Disease. We are grateful to the Intestinal Tissue Bank facility at the University of Calgary for providing human colotic biopsies and to Ms. C. MacNaughton for instruction in the colonic motility assay.

References

1 Chapman TP, Hadley G, Fratter C, *et al.* Unexplained gastrointestinal symptoms: think mitochondrial disease. *Dig Liver Dis* 2014;46:1-8.

2 Patel R, Coulter LL, Rimmer J, *et al*. Mitochondrial neurogastrointestinal encephalopathy: a clinicopathological mimic of Crohn's disease. *BMC Gastroenterology* 2019;19:11-13.

3 Roediger WE. The colonic epithelium in ulcerative colitis: an energy-deficiency disease? *Lancet* 1980;2:712-5.

4 Nazli A, Yang PC, Jury J, *et al.* Epithelia under metabolic stress perceive commensal bacteria as a threat. *Am J Pathol* 2004;164:947-57.

5 Soderholm JD, Olaison G, Peterson KH, *et al.* Augmented increase in tight junction permeability by luminal stimuli in the non-inflamed ileum of Crohn's disease. *Gut* 2002;**50**:307-13.

6 Amrouche-Mekkioui I, Djerdjouri B. N-acetylcysteine improves redox status, mitochondrial dysfunction, mucin-depleted crypts and epithelial hyperplasia in dextran sulfate sodium-induced oxidative colitis in mice. *Eur J Pharmacol* 2012;691:209-17.

7 Schurmann G, Bruwer M, Klotz A, *et al.*. Transepithelial transport processes at the intestinal mucosa in inflammatory bowel disease. *Int J Colorectal Dis* 1999;14:41-6.

8 Santhanam S, Rajamanickam S, Motamarry A, *et al.* Mitochondrial electron transport chain complex dysfunction in the colonic mucosa in ulcerative colitis. *Inflamm Bowel Dis* 2012;18:2158-68.

9 Ho GT, Aird RE, Liu B, , *et al.* MDR1 deficiency impairs mitochondrial homeostasis and promotes intestinal inflammation. *Mucosal Immunol* 2018;11:120-30.

10 Lewis K, Caldwell J, Phan V, , *et al.* Decreased epithelial barrier function evoked by exposure to metabolic stress and nonpathogenic *E. coli* is enhanced by TNF-α. *Am J Physiol Gastrointest Liver Physiol* 2008;294:G669-78.

11 Wang A, Keita AV, Phan V, , *et al.* Targeting mitochondria-derived reactive oxygen species to reduce epithelial barrier dysfunction and colitis. *Am J Pathol* 2014;184:2516-27.

12 Rath E, Berger E, Messlik A, *et al.* Induction of dsRNA-activated protein kinase links mitochondrial unfolded protein response to the pathogenesis of intestinal inflammation. *Gut* 2012;61:1269-78.

13 Yeganeh PR, Leahy J, Spahis S, , *et al.* Apple peel polyphenols reduce mitochondrial dysfunction in mice with DSS-induced ulcerative colitis. *J Nut Biochem* 2018;57:56-66.

14 Zhu W, Winter MG, Byndloss MX, , *et al.* Precision editing of the gut microbiota ameliorates colitis. *Nature* 2018;553:208-11.

15 Chu H, Khosravi A, Kusumawardhani IP, *et al.* Gene-microbiota interactions contribute to the pathogenesis of inflammatory bowel disease. *Science* 2016;352:1116-20.

16 Schoultz I, Soderholm JD, McKay DM. Is metabolic stress a common denominator in inflammatory bowel disease? *Inflamm Bowel Dis* 2011;17:2008-18.

17 Zareie M, Riff J, Donato K, , *et al.* Novel effects of the prototype translocating *Escherichia coli*, strain C25 on intestinal epithelial structure and barrier function. *Cell Microbiol* 2005;7:1782-97.

18 Ma C, Wickham ME, Guttman JA, *et al. Citrobacter rodentium* infection causes both mitochondrial dysfunction and intestinal epithelial barrier disruption *in vivo*: role of mitochondrial associated protein (Map). *Cell Microbiol* 2006;8:1669-86.

19 Pernas L, Scorrano L. Mito-morphosis: mitochondrial fusion, fission, and cristae remodeling as key mediators of celular function. *Ann Rev Physiol* 2016;78:505-31.

20 Eisner V, Picard M, Hajnoczky G. Mitochondrial dynamics in adaptive and maladaptive cellular stress responses. *Nat Cell Biol* 2018;20:755-65.

21 Osellame LD, Singh AP, Stroud DA, *et al.* Cooperative and independent roles of the Drp1 adaptors Mff, MiD49 and MiD51 in mitochondrial fission. *J Cell Sci* 2016;129:2170-81.

22 Yu SB, Pekkurnaz G. Mechanisms orchestrating mitochondrial dynamics for energy homeostasis. *J Mol Biol* 2018;430:3922-41.

23 Ryan J, Dasgupta A, Huston J, *et al*. Mitochondrial dynamics in pulmonary arterial hypertension. *J Mol Med* 2015;93:229-42.

24 Archer SL. Mitochondrial dynamics--mitochondrial fission and fusion in human diseases. *New Engl J Med* 2013;369:2236-51.

25 Guo X, Disatnik MH, Monbureau M, *et al*. Inhibition of mitochondrial fragmentation diminishes Huntington's disease-associated neurodegeneration. *J Clin Invest* 2013;123:5371-88.

26 Qi X, Qvit N, Su YC, Mochly-Rosen D. A novel Drp1 inhibitor diminishes aberrant mitochondrial fission and neurotoxicity. *J Cell Sci* 2013;126:789-802.

27 Hunter MM, Wang A, Hirota CL, McKay DM. Neutralizing anti-IL-10 antibody blocks the protective effect of tapeworm infection in a murine model of chemically induced colitis. *J Immunol* 2005;174:7368-75.

28 Ni J, Chen SF, Hollander D. Effects of dextran sulphate sodium on intestinal epithelial cells and intestinal lymphocytes. *Gut* 1996;39:234-41.

29 Reinglas J, Gonczi L, Kurt Z, Bessissow T, Lakatos PL. Positioning of old and new biologicals and small molecules in the treatment of inflammatory bowel diseases. *World J Gastroenterol* 2018;24:3567-82.

30 Novak EA, Mollen KP. Mitochondrial dysfunction in inflammatory bowel disease. *Front Cell Dev Biol* 2015;3:62.

31 Rath E, Moschetta A, Haller D. Mitochondrial function - gatekeeper of intestinal epithelial cell homeostasis. *Nat Rev Gastroenterol & Hepatol* 2018;15:497-516.

32 Mottawea W, Chiang CK, Muhlbauer M, S, *et al.* Altered intestinal microbiota-host mitochondria crosstalk in new onset Crohn's disease. *Nat Commun* 2016;7:13419.

33 Wang SQ, Cui SX, Qu XJ. Metformin inhibited colitis and colitis-associated cancer (CAC) through protecting mitochondrial structures of colorectal epithelial cells in mice. *Cancer Biol &Ther* 2019;20:338-48.

34 Bou-Fersen AM, Anim JT, Khan I. Experimental colitis is associated with ultrastructural changes in inflamed and uninflamed regions of the gastrointestinal tract. *Med Princip Pract* 2008;17:190-6.

35 Bordt EA, Clerc P, Roelofs BA, *et al.* The putative Drp1 inhibitor mdivi-1 is a reversible mitochondrial complex I inhibitor that modulates reactive oxygen species. *Develop Cell* 2017;40:583-94.e6.

36 Miret-Casals L, Sebastian D, Brea J, *et al.* Identification of new activators of mitochondrial fusion reveals a link between mitochondrial morphology and pyrimidine metabolism. *Cell Chem Biol* 2018;25:268-78.

37 Osterman MT. Mucosal healing in inflammatory bowel disease. *J Clin Gastroenterol* 2013;47:212-21.

38 Reardon C, Sanchez A, Hogaboam CM, McKay DM. Tapeworm infection reduces epithelial ion transport abnormalities in murine dextran sulfate sodium-induced colitis. *Infect Immunity* 2001;69:4417-23.

39 Luo F, Herrup K, Qi X, Yang Y. Inhibition of Drp1 hyper-activation is protective in animal models of experimental multiple sclerosis. *Exp Neurol* 2017;292:21-34.

40 Tian L, Neuber-Hess M, Mewburn J, *et al.* Ischemia-induced Drp1 and Fis1-mediated mitochondrial fission and right ventricular dysfunction in pulmonary hypertension. J Mol Med 2017;95:381-93.

41 Disatnik MH, Ferreira JC, Campos JC, *et al.* Acute inhibition of excessive mitochondrial fission after myocardial infarction prevents long-term cardiac dysfunction. *J Am Heart Assoc* 2013;2:e000461.

42 Darnaud M, Dos Santos A, Gonzalez P, *et al.* Enteric delivery of regenerating family member 3α alters the intestinal microbiota and controls inflammation in mice with colitis. *Gastroenterology* 2018;154:1009-23.e14.

43 Johansson ME, Gustafsson JK, Sjoberg KE, *et al.* Bacteria penetrate the inner mucus layer before inflammation in the dextran sulfate colitis model. *PloS one* 2010;5:e12238.

44 Dieleman LA, Ridwan BU, Tennyson GS, *et al*. Dextran sulfate sodium-induced colitis occurs in severe combined immunodeficient mice. *Gastroenterology* 1994;107:1643-52.

45 Kono Y, Miyoshi S, Fujita T. Dextran sodium sulfate alters cytokine production in macrophages *in vitro*. *Die Pharmazie* 2016;71:619-24.

46 Chapman MA, Grahn MF, Boyle MA, *et al*. Butyrate oxidation is impaired in the colonic mucosa of sufferers of quiescent ulcerative colitis. *Gut* 1994;35:73-6.

47 Sifroni KG, Damiani CR, Stoffel C, *et al.* Mitochondrial respiratory chain in the colonic mucosal of patients with ulcerative colitis. *Mol Cell Biochem* 2010;342:111-5.

48 Rugtveit J, Nilsen EM, Bakka A, *et al*. Cytokine profiles differ in newly recruited and resident subsets of mucosal macrophages from inflammatory bowel disease. *Gastroenterology* 1997;112:1493-505.

49 Hunter MM, Wang A, Parhar KS, *et al. In vitro*-derived alternatively activated macrophages reduce colonic inflammation in mice. *Gastroenterology* 2010;138:1395-405.

50 Wang Y, Subramanian M, Yurdagul A, *et al.* Mitochondrial fission promotes the continued clearance of apoptotic cells by macrophages. *Cell* 2017;171:331-45.

51 Bomhof MR, Saha DC, Reid DT, Paul HA, Reimer RA. Combined effects of oligofructose and Bifidobacterium animalis on gut microbiota and glycemia in obese rats. *Obesity* 2014;22:763-71.

52 Stoddard SF, Smith BJ, Hein R, Roller BR, Schmidt TM. rrnDB: improved tools for interpreting rRNA gene abundance in bacteria and archaea and a new foundation for future development. *Nucleic Acids Res* 2015;43:D593-8.

53 Arai T, Lopes F, Shute A, Wang A, McKay DM. Young mice expel the tapeworm *Hymenolepis diminuta* and are protected from colitis by triggering a memory response with worm antigen. Am Physiology Gastrointest Liver Physiol 2018;314:G461-70.

54 Storr MA, Bashashati M, Hirota C, *et al.* Differential effects of CB(1) neutral antagonists and inverse agonists on gastrointestinal motility in mice. *Neurogastroenterol Motil* 2010;22:787-96, e223.

55 Lopes F, Reyes JL, Wang A, Leung G, McKay DM. Enteric epithelial cells support growth of *Hymenolepis diminuta in vitro* and trigger TH2-promoting events in a species-specific manner. *Internat J Parasitol* 2015;45:691-6.

56 O'Brien J, Wilson I, Orton T, Pognan F. Investigation of the Alamar Blue (resazurin) fluorescent dye for the assessment of mammalian cell cytotoxicity. *Eur J Biochem* 2000;267:5421-6.

57 Chatel-Chaix L, Cortese M, Romero-Brey I, *et al.* Dengue virus perturbs mitochondrial morphodynamics to dampen innate immune responses. *Cell Host & Microbe* 2016;20:342-56.

58 Doerrier C, Garcia JA, Volt H, *et al.* Identification of mitochondrial deficits and melatonin targets in liver of septic mice by high-resolution respirometry. *Life Sci* 2015;121:158-65.

59 Lopes F, Keita AV, Saxena A, *et al.* ER-stress mobilization of death-associated protein kinase-1-dependent xenophagy counteracts mitochondria stress-induced epithelial barrier dysfunction. *J Biol Chem* 2018;293:3073-87.

60 Leung G, Petri B, Reyes JL, *et al*. Cryopreserved IL-4-treated macrophages attenuate murine colitis in an integrin β7-dependent manner. J Mol Med 2016;21:924-36.

61 Smith G, Gallo G. To mdivi-1 or not to mdivi-1: Is that the question? *Develop Neurobiol* 2017;77:1260-8.

Figure Legends

Figure 1. Human inflammatory bowel disease and murine colitis tissue have increased markers of mitochondrial fission. (A-C) qPCR was performed on human intestinal biopsies (CDi and CDni, Crohn's disease involved and non-involved; UCi and UCni, ulcerative colitis involved and uninvolved) and (D-F) segments of colonic tissue from dextran sodium sulphate (DSS) treated mice for dynamin related protein-1 (Drp1) (A,D), mitochondrial fission 1 protein (Fis1) (B,E), optic atrophy factor 1 (OPA1) (C,F) and ribosomal protein L27 (RLP27) or 18S rRNA as a house-keeping gene (HSG). Expression levels in each biopsy or tissue extract was compared to the mean of the control group that was set at 1 (*$p<0.05$ compared to control, One Way ANOVA, Dunnett's multiple comparison test). Panel G shows immunoblotting for phosphorylated Drp1 (p-Drp1 Ser616), total Drp1 and actin in murinecolonic tissue extracts (Day 5, 5% DSS), with densitometric analysis provided in panel H (mean ± SEM; *, $p<0.05$, t-test) (each dot represents a patient sample or an individual mouse).

Figure 2. Systemic administration of P110 reduces the severity of DSS colitis. (A) Male Balb/c mice were given 5% DSS drinking water for 5 days, followed by a 3 day water recovery phase ± daily P110 (ip.; 3mg/kg) as shown. On necropsy, (B) macroscopic disease activity scores were calculated, (C) colon length measured, and (D) just prior to necropsy colonic motility was assessed in anesthetised animals (s, seconds). (E) Histopathology scoring was performed on H&E stained sections of mid-colon in a blinded fashion (mean ± SEM; n=8-21 mice from 2-5 experiments; * and #, $p<0.05$ compared to control and DSS, respectively; B and E, Kruksal-Wallis, then Dunn's multiple comparison test; C and D, one-way ANOVA, then Tukey's multiple comparison test).

Figure 3. Prophylactic administration of P110 reduces the severity of DNBS-induced colitis. Male Balb/c mice were treated with DNBS (3mg, ir.) ± P110 (ip., 3mg/kg) as shown in panel A. Panels B and C show numbers of mice requiring humane euthanasia due to disease severity and daily weigh change, respectively. On necropsy, colon length was measured (D), a macroscopic disease score calculated (E), and a piece of mid-colon processed for H&E staining and assessment of histopathology in a blinded fashion (F) (mean ± SEM; n=4-12 mice from 3 experiments; * and #, $p<0.05$ compared to control and DNBS, respectively; C and D, one-way ANOVA, then Tukey's multiple comparison test; E and F, Kruksal-Wallis, then Dunn's multiple comparison test).

Figure 4. P110 in a treatment protocol reduces the severity of DNBS-induced colitis. Male Balb/c mice were treated with DNBS (3mg, ir.) ± P110 (ip., 3mg/kg) as shown in panel A. Panels B and C show numbers of mice requiring humane euthanasia due to disease severity and daily weight change, respectively. On necropsy, colon length was measured (D), a macroscopic disease score calculated (E), and a piece of mid-colon processed for H&E staining and assessment of histopathology in a blinded fashion (F) (mean ± SEM; n=7-11 mice from 2 experiments; *, $p<0.05$ compared to control; C and D, one-way ANOVA, then Tukey's multiple comparison test; E and F, Kruksal-Wallis, then Dunn's multiple comparison test).

Figure 5. Treatment with P110 reduced DSS-induced epithelial and macrophage mitochondrial fragmentation. Panel A shows that DSS (2%, 24h) applied to cells of the murine $IEC^{4.1}$ epithelial cell line is cytotoxic as gauged by increased trypan blue staining that is not affected by P110 (1.5 μM) co-treatment, whereas the reduced mitochondrial activity (alamarBlue cleavage indicating NADH concentration) caused by DSS was blocked by P110 (B).

Mitochondrial networks (representative images shown in C (epithelial) & F (macrophage)) were quantified in the murine small intestinal epithelial $IEC^{4.1}$ cell line (D) and murine bone-marrow derived macrophages (E) and designated as predominantly fused, fragmented or intermediated (20 cells from each epithelial or macrophage preparation was assessed) (data are mean ± SEM; n=6 in panel D, n=4 in panel E; *$p<0.05$ compared to control, #$p<0.05$ compared to DSS, Two Way ANOVA, Tukey's Multiple Comparison Test).

Figure 6. P110 mitigates DSS-induced epithelial mitochondrial respiration defects. Oxygen specific flux in control, P110 (1.5 μM, 24h) and DSS (2%, 24h) ± P110 in $IEC^{4.1}$ cells was determined in the Oxygraph-2k. (A). Changes in oxygen flux are shown in panel A for basal respiration of intact cells following permeabilization (Basal), panels B-D for mitochondrial electron transfer chain complexes (CI, CII, CIV) and panels E-F for short (SCFA; butyrate) and long chain (LCFA; palmitate) fatty acid oxidation. Data are mean ± SEM; n=6-9, epithelial preparations from 2-3 experiments; * and #, $p<0.05$ compared to control and DSS respectively; One-Way ANOVA, then Tukey's multiple comparison test).

Mancini et al. Figure 1A-F

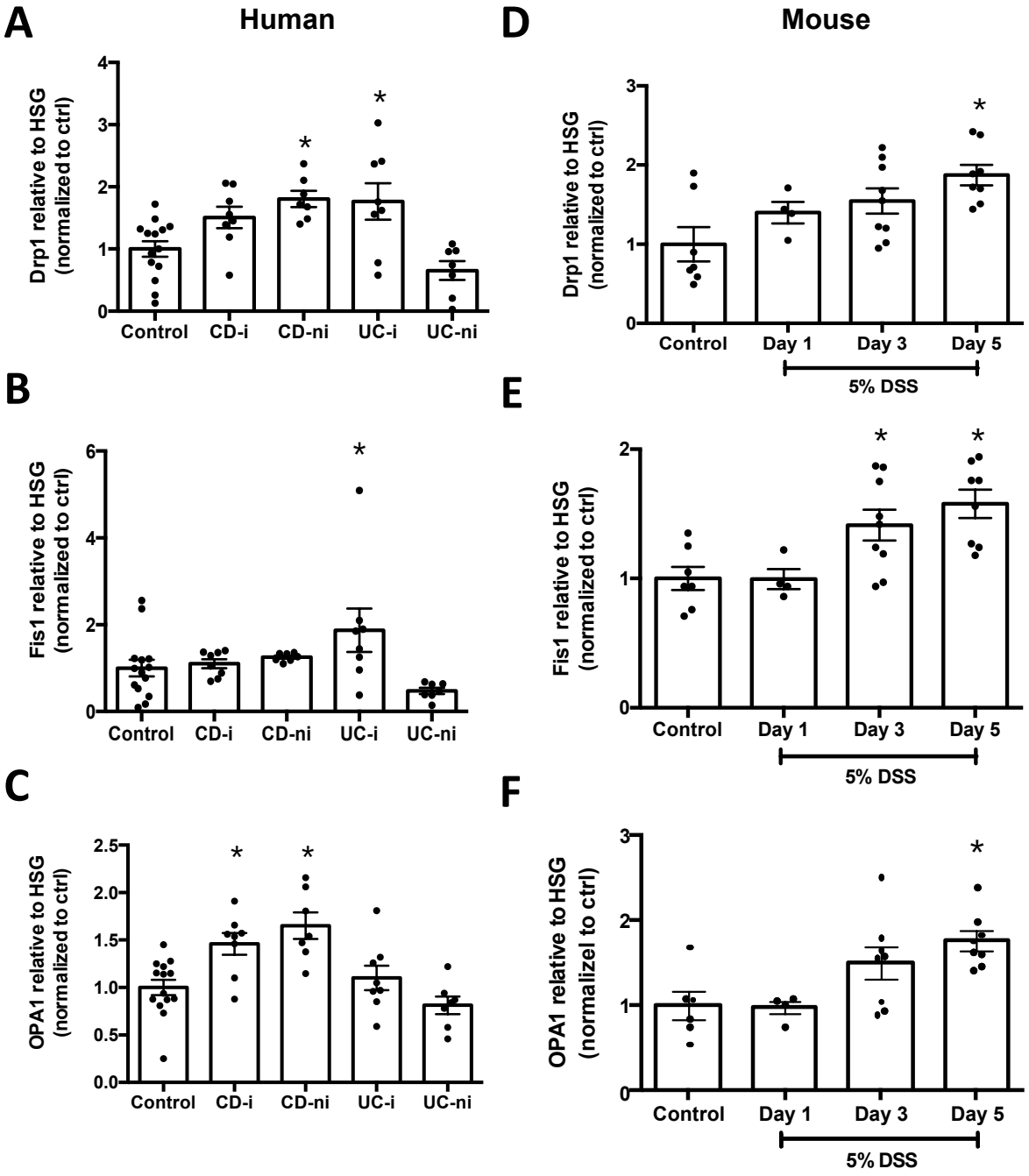

Mancini et al. Figure 1G,H

G

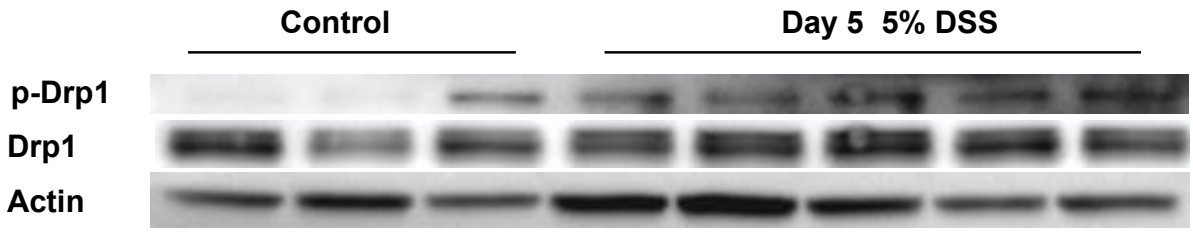

H

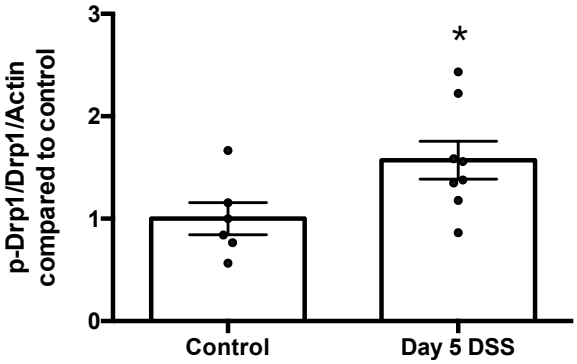

Mancini et al. Figure 2

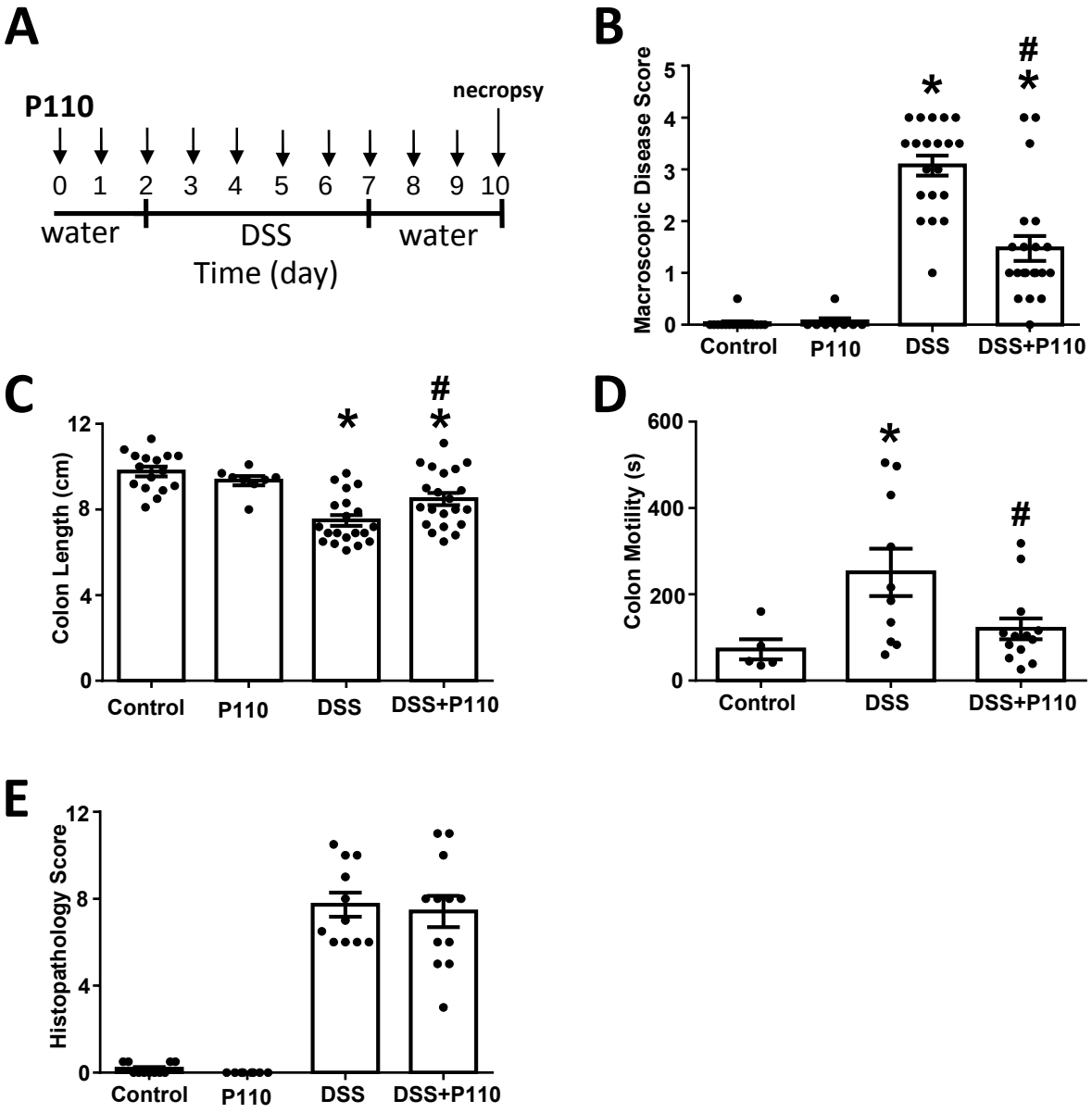

Mancini et al. Figure 3

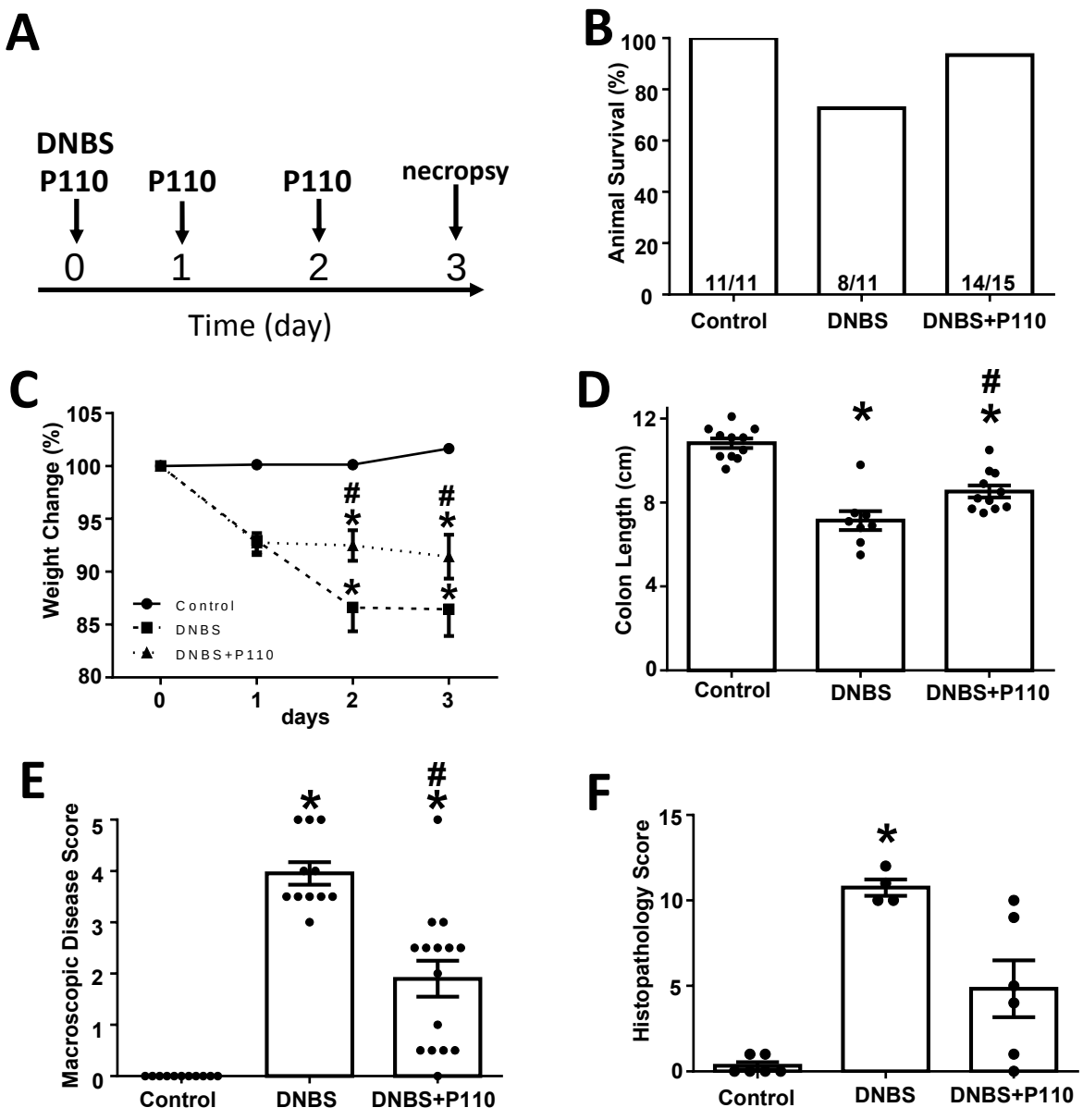

Mancini et al. Figure 4

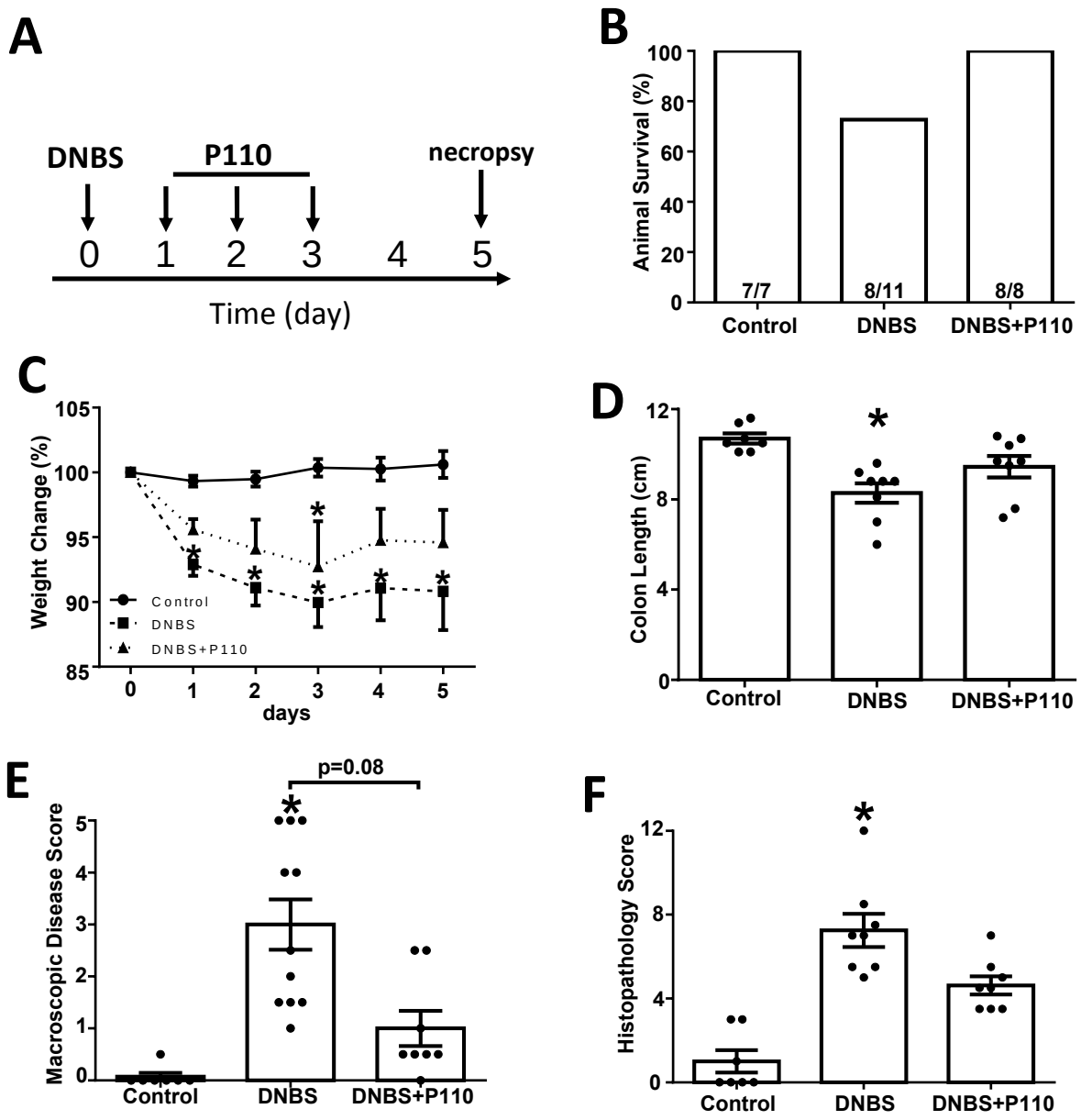

Mancini et al. Figure 5A-E

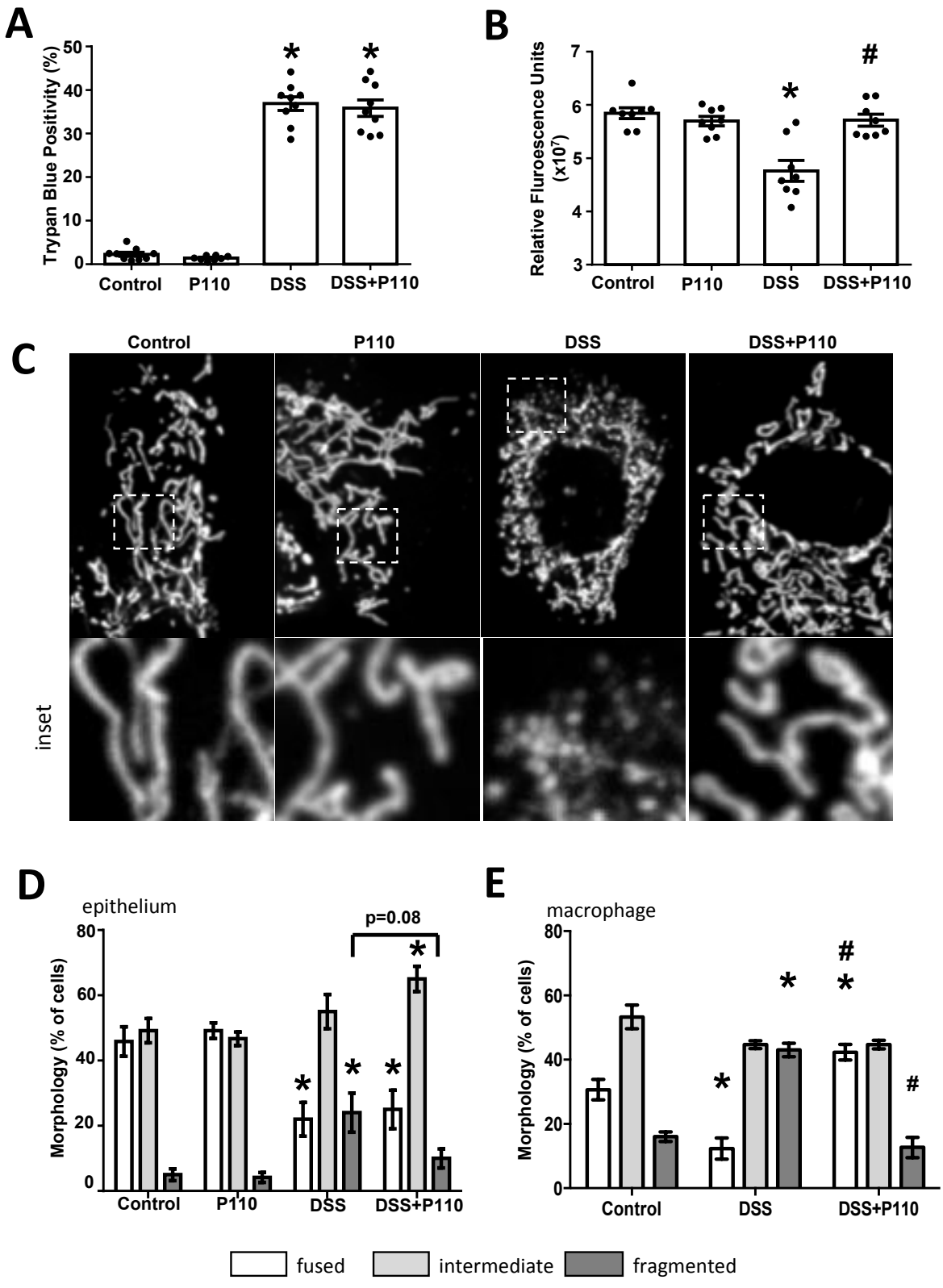

Mancini et al. Figure 5F

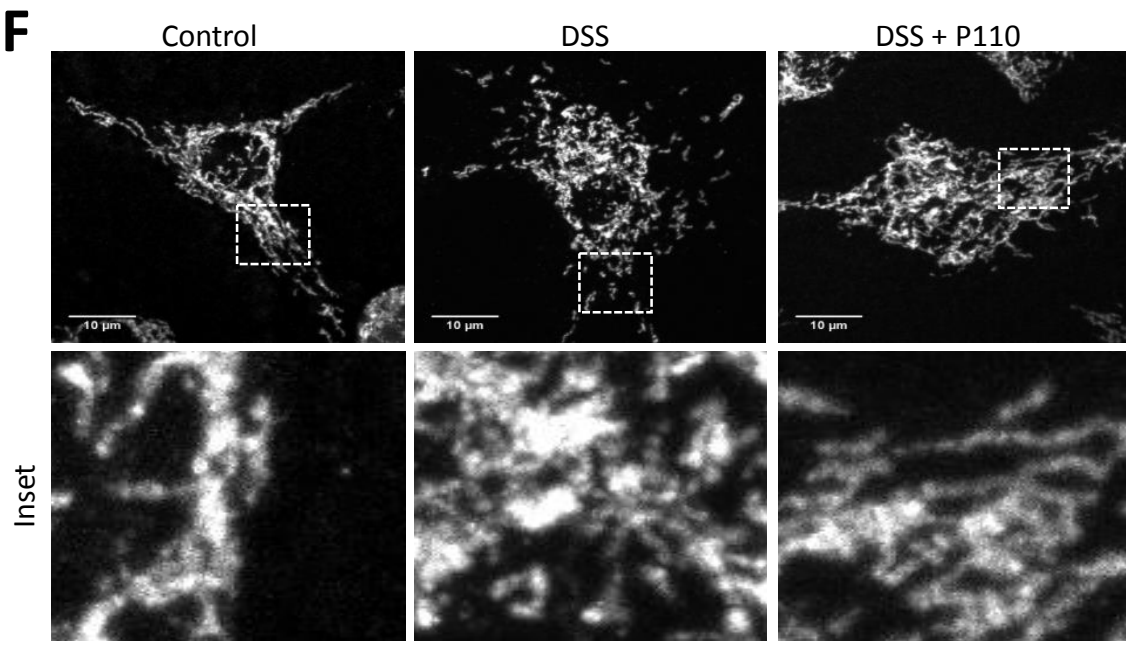

Mancini et al. Figure 6

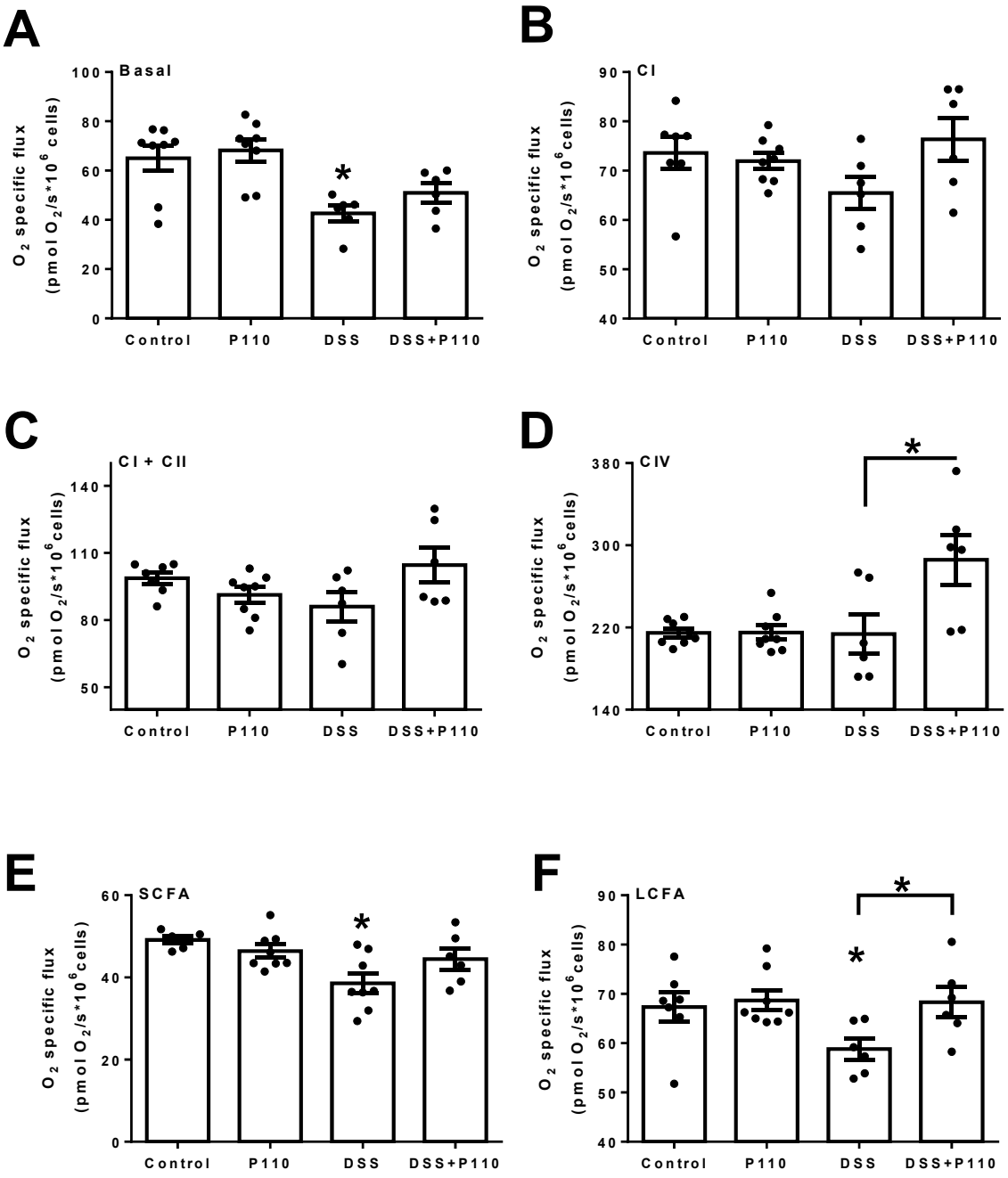

Supplementary Figure Legends

Supplementary Figure 1. Colon from mice exposed to dextran sodium sulphate (DSS) have increased expression of mitochondrial fusion markers. qPCR was performed on segments of colonic tissue from mice treated with dextran sodium sulphate (DSS) for mitofusion factor-1 (MFN1) (A) and MFN2 (B) and a house-keeping gene (HSG). Expression levels in each tissue extract was compared to the mean of the control group that was set at 1 (mean ± SEM; each dot represents an individual mouse; *, $p<0.05$, compared to control; One Way ANOVA, Dunnett's multiple comparison test).

Supplementary Figure 2. Representative tracings of modified SUIT-002 protocol for analysis of mitochondrial respiration in the murine IEC$^{4.1}$ epithelial cell line treated with DSS (2%) ± P110 (1.5 μM). Protocol begins with Panel A and continues in Panel B. Order of substrate addition and specific points of measurement when metabolic pathways are complexes were saturated with substrates are shown (see http://www.bioblast at/index.php/categories_of_SUIT_protocols for additional information)) (FAO, fatty acid oxidation; Max, maximum oxidative phosphorylation; non-mito, non-mitochondrial respiration).

Mancini et al. Supplementary Figure 1

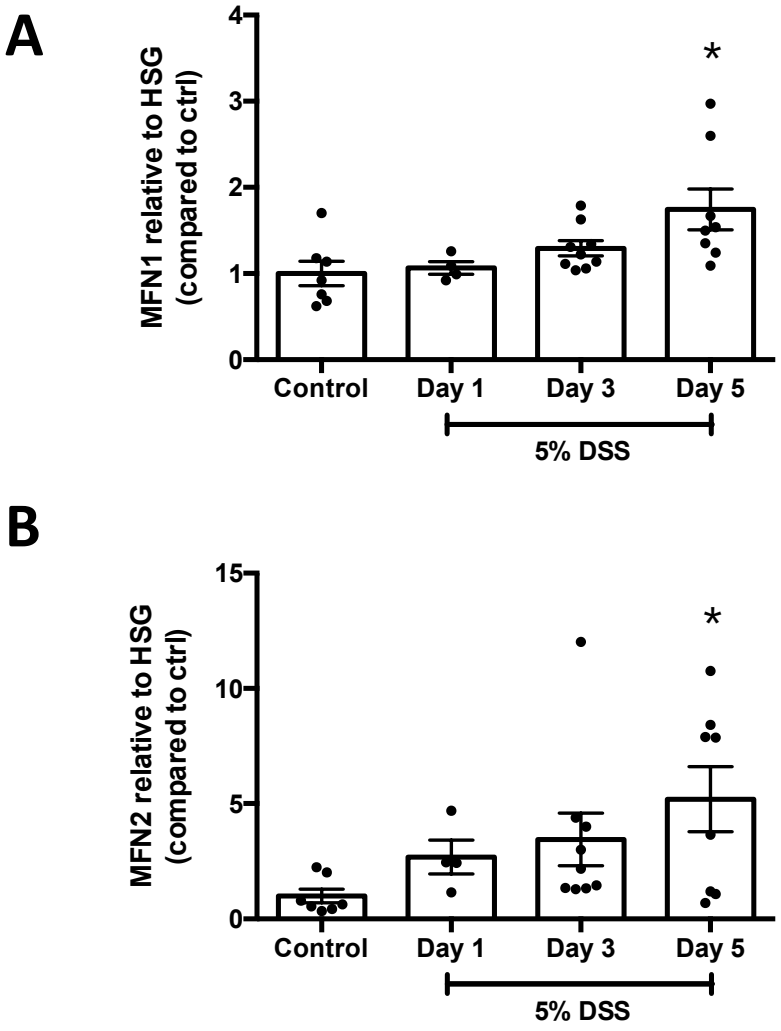

Colon from mice exposed to dextran sodium sulphate (DSS) have increased expression of mitochondrial fusion markers. qPCR was performed on sections of colonic tissue from mice treated with dextran sodium sulphate (DSS) for mitofusion factor-1 (MFN1) (A) and MFN2 (B) and HSG as a house-keeping gene. Expression levels in each tissue extract was compared to the mean of the control group that was set at 1 (mean ± SEM; each dot represents an individual mouse; *, $p<0.05$, compared to control; One Way ANOVA, Dunnett's multiple comparison test).

Mancini et al. Supplementary Figure 2

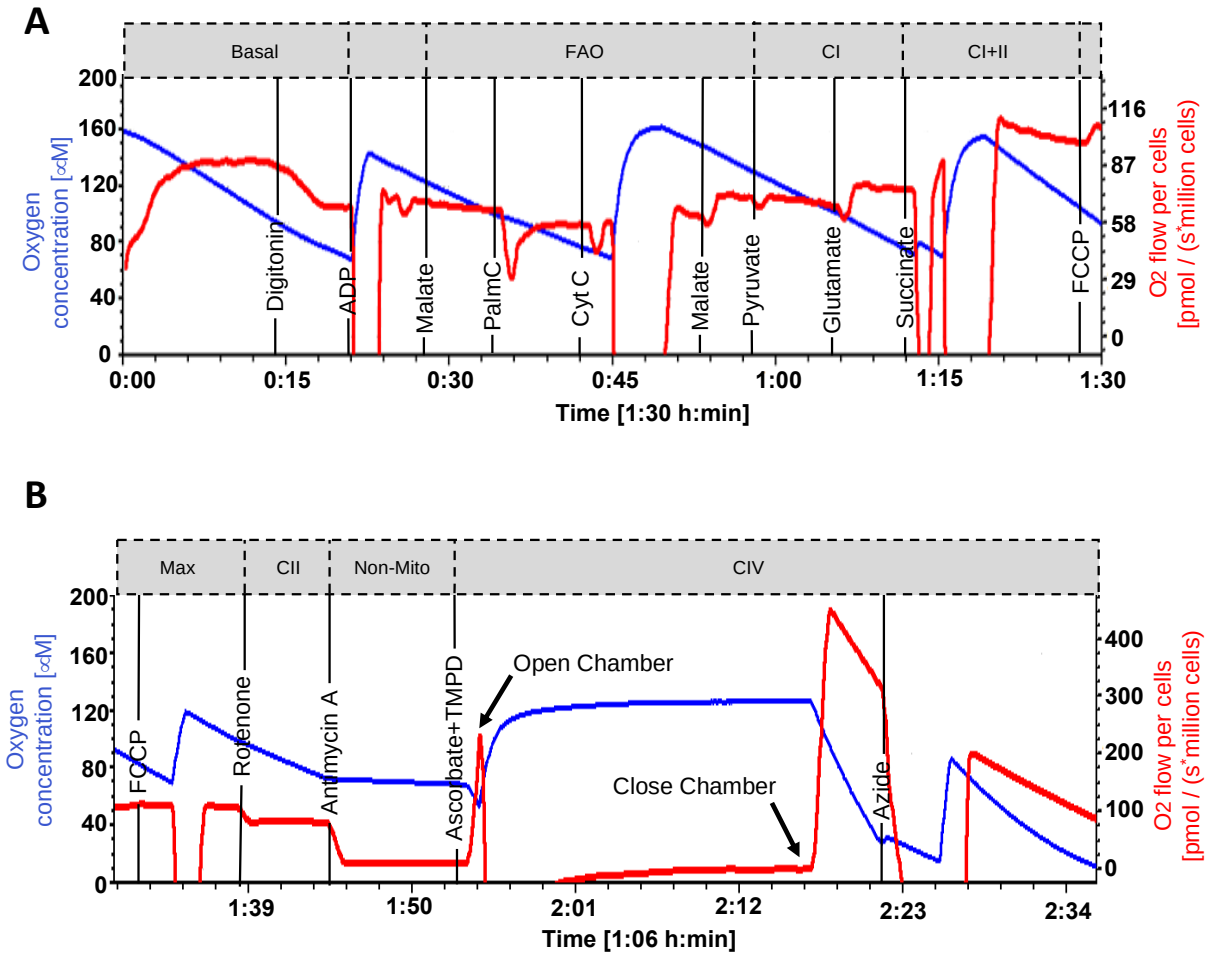

Representative tracings of modified SUIT-002 protocol for analysis of mitochondrial respiration in IEC$^{4.1}$ cells treated with DSS (2%) ± P110 (1.5 ∝M). Protocol begins with Panel A and continues in Panel B. Order of substrate addition and specific points of measurement when metabolic pathways and complexes were saturated with substrates are shown (see http://www.bioblast.at/index.php/Categories_of_SUIT_protocols for additional information) (FAO, fatty acid oxidation; Max, maximal oxidative phosphorylation; Non-mito: non-mitochondrial respiration).

Supplementary Table 1: Analysis of fecal/caecal bacterial composition in dextran sodium sulphate (DSS) treated mice ± systematic treatment with the P110 inhibitor of mitochondrial fission.

Treatment	Control	P110	DSS	DSS + P110
Bacteroides	6.54 ± 0.08	6.64 ± 0.07	6.77 ± 0.08*	6.80 ± 0.07*
Clostridium coccoides (cluster XIV)	6.50 ± 0.09	6.50 ± 0.06	6.22 ± 0.09*	6.25 ± 0.08*
Clostridium leptum (cluster IV)	5.71 ± 0.06	5.78 ± 0.80	5.22 ± 0.10*	5.23 ± 0.06*
Clostridium cluster XI	1.68 ± 0.06	1.33 ± 0.08	1.53 ± 0.08	1.50 ± 0.16
Clostridium cluster I	1.50 ± 0.11	1.51 ± 0.10	1.08 ± 0.15*	0.97 ± 0.10*
Roseburia hominis	2.75 ± 0.19	2.81 ± 0.31	1.38 ± 0.08*	1.35 ± 0.04*
Faecalibacterium prausnitzii	3.68 ± 0.19	3.87 ± 0.30	2.30 ± 0.08*	2.29 ± 0.04*
Lactobacillus spp.	1.76 ± 0.08	1.78 ± 0.12	1.51 ± 0.09*	1.56 ± 0.09*
Bifidobacterium spp.	3.63 ± 0.08	3.79 ± 0.04	3.54 ± 0.09*	3.49 ± 0.08*
Methano-brevibacter spp.	2.02 ± 0.11	1.95 ± 0.05	1.94 ± 0.08	1.88 ± 0.11
Enterobacteriacea	2.15 ± 0.11	2.17 ± 0.10	1.74 ± 0.15*	1.63 ± 0.10*
Akkermansia muciniphila	1.72 ± 0.18	2.02 ± 0.10	1.57 ± 0.25	1.41 ± 0.19

(data are mean 16s RNA gene/mg fecal-caecal material ± SEM; n=4 samples/group; *, $p<0.05$ compared to controls.)

Supplementary Table 2: Epithelial and macrophage cytokine response to dextran sodium sulphate (DSS) *in vitro* ± inhibitors of mitochondrial fragmentation

	epithelial KC	macrophage TNFα	macrophage IL-10
Control	215 ± 25	bd	8 ± 5
P110 (1.5 μM)	282 ± 15	bd	7 ± 4
Mdivi1 (5 μM)	265 ± 24	nd	nd
leflunomide (50 μM)	241 ± 33	nd	nd
1% DSS	117 ± 12	12 ± 2	58 ± 2
1% DSS + P110	99 ± 3	4 ± 2	86 ± 5*
1% DSS + Mdivi1	58 ± 3	nd	nd
1% DSS + leflunomide	79 ± 12	nd	nd
2% DSS	137 ± 53	28 ± 20	13 ± 8
2% DSS + P110	199 ± 49	33 ± 24	8 ± 5
2% DSS + Mdivi1	154 ± 63	nd	nd
2% DSS + leflunomide	59 ± 19	nd	nd
LPS (10 ng/ml)	3527 ± 187	1740 ± 354	1114 ± 112
LPS + P110	3424 ± 427	2280 ± 450	1037 ± 176

(The murine small intestinal IEC$^{4.1}$ epithelial cell line and M-CSF differentiated murine bone-marrow derived macrophages ($2.5x10^5$) were stimulated for 24h, supernatants collected and cytokines measured by ELISA; data are mean ± SEM pg/ml with n = 4 and 6 for 1% and 2 % DSS, respectively; *$p<0.05$ compared to 1% DSS only. P110 binds to Fis1 to block mitochondria fission; Mdivi1 inhibits the GTPase activity of Drp1 to block mitochondrial fission; leflunomide promotes mitochondria fusion; bd, below detection limit; nd, not done.)

Supplementary Table 3: Characteristics of patients from whom biopsies were obtained.

condition	sex	age	disease location	disease state	biopsy location
Healthy	M	50	na	control	ascending colon
Healthy	M	51	na	control	descending colon
Healthy	F	58	na	control	descending colon
Healthy	F	52	na	control	ascending colon
Healthy	M	59	na	control	ascending colon
Healthy	F	53	na	control	ascending colon
Healthy	M	65	na	control	ascending colon
Healthy	M	72	na	control	ascending colon
Healthy	F	51	na	control	ascending colon
Healthy	M	70	na	control	ascending colon
Healthy	F	44	na	control	descending colon
Healthy	F	28	na	control	descending colon
Healthy	F	19	na	control	descending colon
Healthy	F	63	na	control	ascending colon
Healthy	F	43	na	control	ascending colon
UC	F	34	rectum	inflamed	rectum
UC	F	32	unknown	non-inflamed	ascending colon
				inflamed	ascending colon
UC	F	23	unknown	non-inflamed	ascending colon
UC	M	36	pancolitis	non-inflamed	colon
				inflamed	colon
UC	M	49	rectum	non-inflamed	ascending colon
				inflamed	ascending colon
UC	F	22	pancolitis	inflamed	rectum
UC	F	34	unknown	non-inflamed	descending colon
				inflamed	descending colon
UC	M	20	unknown	inflamed	descending colon
UC	F	31	unknown	non-inflamed	ascending colon
				inflamed	ascending colon
UC	M	32	rectum	non-inflamed	descending colon
				inflamed	descending colon
CD	F	47	ileocolonic	non-inflamed	not noted
				inflamed	not noted
CD	F	25	ileocolonic	non-inflamed	not noted
CD	F	62	ileocolonic	inflamed	not noted
				non-inflamed	not noted
CD	F	39	ileocolonic	inflamed	descending colon
				non-inflamed	descending colon
CD	M	64	colonic	non-inflamed	transverse colon
CD	F	31	ileal	inflamed	neo-terminal ileum
CD	M	50	colonic	inflamed	sigmoid colon
				non-inflamed	sigmoid colon

CD	M	28	ileal	inflamed	neo-terminal ileum
CD	F	33	ileocolonic	inflamed	descending colon
CD	F	61	unknown	non-inflamed	not noted
CD	M	46	ileocolonic	inflamed	not noted
CD	F	50	ileocolonic	non-inflamed	descending colon

(CD, Crohn's disease; UC, ulcerative colitis)

Supplementary Table 4: qPCR primer sequences used in this study.

Gene	Forward sequence	Reverse sequence
Human		
RPL27	ATCGCCAAGAGATCAAAGATAA	TCTGAAGACATCCTTATTGACG
mttRNA-leu	CACCCAAGAACAGGGTTTGT	TGGCCATGGGTATGTTGTTA
Drp1	ACCCGGAGACCTCTCATTCT	TGACAACGTTGGGTGAAAAA
Fis1	GACATCCGTAAAGGCATCCGT	GAAGACGTAATCCCGCTGTT
OPA1	TCCCGCTTTATGACAGAACC	AAATAGCTGCATCCCATTGC
Mouse		
18s	ACGCGCGCTACACTGACTGG	CGATCCGAGGGCCTCACTAAACC
mtND1	AATCGCCATAGCCTTCCTAACAT	GGCGTCTGCAAATGGTTGTAA
Drp1	CTGGATCACGGGACAAGG	GTTGCCTGTTGTTGGTTCCT
Fis1	CCTGATTGATAAGGCCATGAA	ACAGCCAGTCCAATGAGTCC
OPA1	TGACAAACTTAAGGAGGCTGTG	CATTGTGCTGAATAACCCTCAA
MFN1	GTGAGCTTCACCAGTGCAAAA	CACAGTCGAGCAAAAGTAGTGG
MFN2	CATTCTTGTGGTCGGAGGAG	AAGGAGAGGGCGATGAGTCT
Enteric bacteria		
Bacteroidetes		
Bacteroides/prevotella	TCCTACGGGAGGCAGCAGT	CCGCACCCACTGTGTTGA
Firmicutes		
Clostridium Coccoides (cluster (C) XIV)	ACTCCTACGGGAGGCAGC	GCTTCTTAGTCARGTACCG
Clostridium leptum (C IV)	GCACAAGCAGTGGAGT	CTTCCTCCGTTTGTCAA
Clostridium group (C I)	ATGCAAGTCGAGCGATG	TATGCGGTATTAATCTYCCTTT
Clostridium group (C XI)	ACGCTACTTGAGGAGGA	GAGCCGTAGCCTTTCACT
Lactobacillus	GAGGCAGCAGTAGGGAATCTTC	GGCCAGTTACTACCTCTATCCTTCTT
Roseburia hominus	TACTGCATTGGAAACTGTCG	CGGCACCGAAGAGCAAT
Actinobacteria		
Bifidobacterium	CGCGTCYGGTGTGAAAG	CCCCACATCCAGCATCCA
Archaea		
Methano-brevibacter	CTCACCGTCAGAATCGTTCCAGTC	ACTTGAGATCGGGAGAGGTTAGAGG
Proteobacteria		
Enterobacteriaceae	CATTGACGTTACCCGCAGAAGC	CTCTACGAGACTCAAGCTTGC
Verrucomicrobia		
Akkermansia muciniphila	TCTTCGGAGGCGTTACACAG	AGTTGATCTGGGCAGTCTCG

Drp1, dynamin related protein-1; Fis1, mitochondrial fission protein-1; OPA1, optic atrophy factor 1; MFN, mitofusin; mtND1, mitochondrial NADH dehydrogenase subunit; RPL27, ribosomal protein L27; mttRNA-leu, mitochondrial tRNA.